



HAL
open science

Preparation and characterization of ultra porous cellulosic materials

Roxane Gavillon

► **To cite this version:**

Roxane Gavillon. Preparation and characterization of ultra porous cellulosic materials. Mechanics [physics.med-ph]. École Nationale Supérieure des Mines de Paris, 2007. English. NNT: . tel-00173409

HAL Id: tel-00173409

<https://pastel.hal.science/tel-00173409>

Submitted on 19 Sep 2007

HAL is a multi-disciplinary open access archive for the deposit and dissemination of scientific research documents, whether they are published or not. The documents may come from teaching and research institutions in France or abroad, or from public or private research centers.

L'archive ouverte pluridisciplinaire **HAL**, est destinée au dépôt et à la diffusion de documents scientifiques de niveau recherche, publiés ou non, émanant des établissements d'enseignement et de recherche français ou étrangers, des laboratoires publics ou privés.

A ma mère
A mes grand-parents

Remerciements

Ce travail a été réalisé au Centre de Mise en Forme des Matériaux (CEMEF) de l'Ecole des Mines de Paris, à Sophia-Antipolis, dans le groupe « Physico-chimie des Polymères ». Il a été réalisé dans le cadre du projet européen AEROCELL.

Je remercie en premier lieu Patrick Navard, responsable du groupe « Physico-chimie des Polymères », de m'avoir accueillie dans son équipe, et d'avoir accepté de faire partie de mon jury de thèse.

J'exprime ma gratitude à Michel Dumon, Professeur à l'université de Bordeaux et ancien maître de stage de DEA à l'INSA de Lyon d'avoir bien voulu présider mon jury de thèse.

Je remercie Madame Karin Stana-Kleinschek, Professeur à l'université de Maribor en Slovénie et Monsieur Pedro Fardim, Professeur à l'université de Abo en Finlande d'avoir accepté d'être les rapporteurs de ma thèse.

Je remercie également Hans-Peter Fink, directeur de la division des polymères naturels au Fraunhofer institut à Potsdam en Allemagne, d'avoir accepté de faire partie de mon jury de thèse.

Merci à Bernard Simon, chercheur à la SAFT à Bordeaux, avec qui j'ai collaboré sur la partie pile au lithium dans ce projet d'avoir accepté de participer à ce jury.

Je remercie chaleureusement Sandrine Berthon-Fabry et Arnaud Rigacci, chercheurs au Centre énergétique et Procédé (CEP), de l'Ecole des Mines de Paris, à Sophia-Antipolis, d'avoir collaboré à ce projet pendant trois ans et d'avoir accepté de participer à ce jury. Nos discussions scientifiques furent toujours très intéressantes et nos réunions de projet en Europe enrichissantes.

Je remercie également tous les représentants des entreprises et laboratoire partenaires du projet. Je voudrai remercier tout particulièrement Gregor Kraft de Lenzing en Autriche pour son sens de l'humour et le partage de ses compétences sur la cellulose et Manfred Pinnow pour les nombreuses analyses de porosimétrie effectuées.

Je tiens naturellement à exprimer mes profonds remerciements à Tatiana Budtova, chercheur à l'Ecole des Mines de Paris, pour avoir dirigé cette thèse avec beaucoup d'intérêt et une grande compétence scientifique. Tania, ton enthousiasme, ton optimisme et ta grande disponibilité m'ont vraiment touchée. Ce travail te doit beaucoup et moi aussi.

Je remercie sincèrement toutes les personnes dont l'aide m'a été précieuse dans la préparation et la caractérisation de ce nouveaux matériau: Michel-Yves Perrin, Monique Repoux, Gilbert Fiorucci, Suzanne Jacomet et Pierre Ilbizian.

Merci à tous les chercheurs, doctorants, techniciens et administratifs du centre de mise en forme des matériaux. Merci à Céline, Magali, Undina, Monica, Daniela, Olga, Cyril, Romain, « le fan des billes de cellulose », et aux autres membres du groupe PCP. Merci à Geneviève et Flo pour les pauses thé de l'après-midi. Merci à mon cher collègue de bureau Jérôme, « l'as des mousses » pour les pauses café matinales. Merci à Julia, Luisa et Hugues pour leur amitié. Merci aux « CEP-istes » Florent, Claire, Aude, Marilyne, Anne Lise, Alexis, Luis, Nils...

Mes pensées les plus profondes vont vers ma Mère, sans qui je ne serai pas là et qui m'a toujours soutenue au cours de mes études. Un grand merci à Baptiste pour ses encouragements tout au long de la thèse et sa précieuse aide finale.

Enfin merci à toi Lecteur qui t'apprête à lire ce manuscrit de thèse. Merci à tous et bonne lecture.

Résumé du travail de thèse	13
General introduction.....	25
Chapter I: Cellulose, its processing and preparation of porous cellulose materials.....	29
Introduction	30
1.1 Cellulose: main aspects on structure and properties	31
1.2 Generalities	31
1.3 Chemical structure of cellulose	31
1.4 Structure and organisation of micro fibrils	33
1.5 Polymorphs of cellulose	35
<i>1.5.1 Cellulose I</i>	<i>35</i>
<i>1.5.2 Cellulose II.....</i>	<i>37</i>
<i>1.5.3 Cellulose III.....</i>	<i>39</i>
<i>1.5.4 Cellulose IV.....</i>	<i>39</i>
2 Cellulose processing	40
2.1 Cellulose solvents.....	40
2.2 Main ways of cellulose processing.....	42
<i>2.2.1 Viscose process</i>	<i>42</i>
<i>2.2.2 Lyocell process.....</i>	<i>44</i>
<i>2.2.3 NaOH process</i>	<i>45</i>
2.3 Regeneration	46
3 Porosity of cellulose materials	49
3.1 Porosity of regenerated fibres	49
3.2 Porous cellulose membranes	50
3.3 Nanoporous cellulose-based materials	55
<i>3.3.1 Generalities on aerogels and supercritical drying</i>	<i>55</i>
<i>3.3.2 Cellulose-based porous materials.....</i>	<i>57</i>
Conclusions	60
References	61
Chapter II: Cellulose-NaOH solutions: preparation and rheological properties	67
Introduction	68

Table of contents

1	Bibliography: Cellulose-NaOH aqueous solutions: structure, properties and influence of additives.....	69
1.1	Effect of NaOH on cellulose fibres: the mercerisation process.....	69
1.2	Crystalline structures of Na- cellulose.....	69
1.3	Dissolution of cellulose in the aqueous 7-10%NaOH solution	71
1.4	Gelation of cellulose-NaOH aqueous solutions.....	73
1.5	Use of additives	74
2	Experimental.....	77
2.1	Materials	77
2.1.1	<i>Cellulose.....</i>	<i>77</i>
2.1.2	<i>Solvents.....</i>	<i>80</i>
2.2	Methods	80
2.2.1	<i>Preparation of cellulose/NaOH/urea/water solutions</i>	<i>80</i>
2.2.2	<i>Rheological tools.....</i>	<i>81</i>
3	Results and discussion.....	82
3.1	Steady-state flow of cellulose-NaOH solutions	83
3.2	Gelation of cellulose/NaOH/water solutions	86
3.2.1	<i>Influence of temperature on gelation time</i>	<i>86</i>
3.2.2	<i>Influence of cellulose origin and concentration on gelation temperature.....</i>	<i>90</i>
3.2.3	<i>Influence of urea concentration on gelation</i>	<i>92</i>
	Conclusions	98
	References	99
	Chapter III: Kinetics of cellulose regeneration from cellulose-NaOH-water gels and comparison with cellulose-NMMO-water solutions.....	101
	Abstract.....	101
	Introduction	102
1	Experimental section.....	103
1.1	Materials	103
1.2	Methods	104
2	Results and discussion.....	106
2.1	Analysis of experimental data: choice of the approach	106
2.2	Influence of cellulose concentration on diffusion of NaOH from Avicel-NaOH-water gels and of NMMO from Solucell-NMMO solutions	108

Table of contents

2.3	Influence of water regenerating bath temperature	115
2.4	Influence of regenerating bath type	118
	Conclusions	122
	References	123
	Chapter IV: Microstructural properties of Aerocellulose	125
	Introduction	126
1	Materials and Methods	127
1.1	Materials	127
1.1.1	<i>Cellulose solutions and gels</i>	127
1.1.2	<i>Additives</i>	127
1.1.3	<i>Regenerating bath</i>	127
1.2	Methods	128
1.2.1	<i>CO₂ supercritical drying</i>	128
1.2.2	<i>Measurements of the porosity: a brief review of methods and theoretical approaches</i>	131
1.2.3	<i>Mercury Porosimetry</i>	138
1.2.4	<i>Electron microscopy</i>	139
2	Results and discussion. Aerocellulose microstructure: influence of cellulose characteristics and preparation conditions	142
2.1	Example of Aerocellulose microstructure	143
2.2	Influence of gelation conditions	148
2.3	Influence of cellulose concentration	149
2.4	Influence of pulp properties	149
2.5	Influence of surfactant addition	150
2.6	Influence of the regenerating bath	152
2.6.1	<i>Water regenerating bath: influence of temperature</i>	152
2.6.2	<i>Influence of the nature of the regenerating bath</i>	158
	Conclusions	163
	References	165
	Chapter V: Mechanical properties of Aerocellulose	167
	Introduction	168
1	Bibliography: Mechanical properties of foams and aerogels	169

Table of contents

1.1	Mechanical properties of foams	169
1.2	Mechanical properties of aerogels	174
2	Material and Methods.....	177
2.1	Materials	177
2.1.1	<i>Aerocellulose from NaOH route</i>	<i>177</i>
2.1.2	<i>Aerocellulose from NMMO route.....</i>	<i>177</i>
2.2	Methods	178
3	Results and discussion: mechanical properties of Aerocellulose and influence of the preparation parameters	179
3.1	Examples of Aerocellulose mechanical properties	179
3.2	Effect of the displacement rate.....	182
3.3	Influence of cellulose concentration.....	183
3.4	Influence of pulp properties	186
3.5	Influence of additives	188
3.5.1	<i>Influence of surfactant concentration</i>	<i>188</i>
3.5.2	<i>Influence of fibres addition: attempts to reinforce Aerocellulose.....</i>	<i>190</i>
3.6	Influence of water regenerating bath temperature.....	192
3.7	Structure-properties correlations	193
	Conclusions	198
	References	199
	Chapter VI: Application of Aerocellulose and of its carbonised form.....	201
	Introduction	202
1	Example of Aerocellulose application	203
1.1	Preparation of Aerocellulose composite beads	203
1.2	Characterisation of Aerocellulose composite beads.....	203
1.2.1	<i>Characterisation of powders.....</i>	<i>203</i>
1.2.2	<i>Wet cellulose composite beads.....</i>	<i>205</i>
1.2.3	<i>Aerocellulose composite beads</i>	<i>206</i>
2	Carbonised Aerocellulose and its applications	209
2.1	Preparation and microstructural properties of carbonised Aerocellulose .	209
2.1.1	<i>Preparation of carbonised Aerocellulose</i>	<i>209</i>
2.2	Microstructural characterisations	212
2.2.1	<i>Comparison of organic and pyrolysed Aerocellulose.....</i>	<i>212</i>

Table of contents

2.2.2	<i>Influence of Aerocellulose preparation and pyrolysis parameters on microstructural properties of carbonised Aerocellulose</i>	215
2.3	Electrochemical applications.....	220
2.3.1	<i>Carbonised Aerocellulose for primary lithium battery Li/SOCl₂.....</i>	220
2.3.2	<i>Proton exchange membrane fuel cell application.....</i>	225
Conclusions		230
References		231
General conclusions.....		233
Perspectives.....		235

Résumé du travail de thèse

1-Contexte et objectif de l'étude

La cellulose est le polymère naturel le plus abondant sur Terre, représentant plus de 50 % de la biomasse. La cellulose est présente dans le bois, les fibres végétales comme le coton, le lin, le chanvre et dans les grandes cultures agricoles comme le blé, le maïs et la canne à sucre. Sa production annuelle créée lors de la photosynthèse des végétaux est estimée à 100 milliards de tonnes par an. Première source de la cellulose, les arbres sont de véritables « puits de carbone » car ils génèrent de l'oxygène et absorbent de grandes quantités de CO₂. De ce fait la cellulose est l'un des composants les plus prometteurs dans la réduction des émissions de gaz à effet de serre et la lutte contre le réchauffement climatique. La cellulose est un polysaccharide biodégradable, elle est facilement décomposée par des champignons et bactéries du sol. De plus, elle est renouvelable, c'est à dire qu'elle se reconstitue avec le soleil, source d'énergie inépuisable, gratuite et propre.

Ces dernières années ont été marquées par un élan des consommateurs vers des produits biodégradables et conçus selon des voies plus respectueuses de l'environnement. D'autre part, l'augmentation des prix du pétrole et sa raréfaction a permis la mise en avant de nouveaux produits d'origine naturelle. L'objectif de cette thèse qui s'inscrit dans cette perspective est de préparer et de caractériser un tout nouveau matériau ultra poreux à base de cellulose, appelé l'Aérocellulose.

La cellulose est difficile à mettre en forme du fait de son insolubilité dans de nombreux solvants. Son industrialisation a commencé au XIX^{ème} siècle avec le développement des procédés de mercerisation et viscose. Ce dernier procédé consiste à activer la cellulose dans une solution concentrée de soude (~ 20%). La cellulose est ensuite transformée chimiquement au contact du sulfure de carbone CS₂ en xanthate de cellulose. Ce dernier est par la suite solubilisé et la cellulose est mise en forme pendant régénération. Bien que très efficace, le procédé viscose est très polluant car il rejette des métaux lourds et des gaz toxiques comme le disulfure de carbone et l'hydrogène sulfuré. C'est pourquoi des alternatives à ce procédé respectant les normes environnementales ont été recherchées. A la fin des années 1980, un nouveau procédé, appelé procédé Lyocell, reposant sur la dissolution de la cellulose dans la N-méthyl-morpholine-N-oxyde (NMMO) a été développé à l'échelle industrielle et produit aujourd'hui plus de 100 000 tonnes de fibres cellulosiques. Ce procédé permet de récupérer presque 100% du solvant et est non-toxique pour l'environnement. Dans la dernière décennie, un nouveau procédé écologique de mise en forme de la cellulose basé sur la dissolution de la cellulose dans une solution aqueuse de soude concentrée à 7-10% a vu le jour.

L'Aérocellulose est un matériau ultra léger et extrêmement poreux. Son procédé de fabrication repose sur celui des aérogels. Les aérogels sont synthétisés par la voie sol-gel en milieu liquide puis séchés par extraction d'un fluide supercritique. Ces matériaux sont caractérisés par une très faible densité (0,004 à 0,2g/cm³), une grande porosité (jusqu'à 99,8%)

et une très grande surface spécifique (jusqu'à 1000 m²/g). La majorité des aérogels sont de type inorganique (SiO₂, TiO₂, ...). Des aérogels organiques du type résorcinol-formaldéhyde ou mélamine formaldéhyde ont été élaborés ces dernières années. Même si Kistler envisagea les premiers aérogels à base de cellulose et de nitrocellulose en 1932, ce n'est que très récemment que des études ont été menées sur les aérogels organiques d'origine cellulosique.

Le nouveau matériau Aérocellulose a été développé dans le cadre du projet européen AEROCELL. Deux procédés de préparation, l'un par voie chimique, l'autre par voie physique ont été considérés. Trois voies physiques de préparation du matériau ont été abordées : la voie carbamate de cellulose, la voie N-méthyl-morpholine-N-oxyde et la voie NaOH. Au cours de cette thèse, les deux dernières approches ont été examinées avec une attention particulière portée à la préparation du matériau via la voie NaOH. La mise en forme du matériau Aérocellulose par les voies NaOH et NMMO nécessite plusieurs étapes.

En premier lieu, la cellulose est dissoute soit dans une solution aqueuse d'hydroxyde de sodium, NaOH soit dans la NMMO. Les solutions cellulose/NaOH/eau gélifient dans le temps ou en température alors que les solutions cellulose/NMMO/eau cristallisent à température ambiante. L'étape suivante consiste à régénérer la cellulose dans un bain de non-solvant de la cellulose. Au cours de cette étape le solvant de la cellulose, NaOH ou NMMO, est extrait de la solution ou du gel. Il est remplacé par un non-solvant de la cellulose, généralement de l'eau. Il en résulte un gonflement de la cellulose dans le non-solvant. Par la suite, ce non-solvant est remplacé par de l'acétone en prévision du séchage du matériau humide. La cellulose gonflée dans l'acétone est séchée par extraction au CO₂ supercritique. Un matériau sec et très léger est alors obtenu, l'Aérocellulose. La figure 1.1 résume les différentes étapes de préparation de ce matériau.

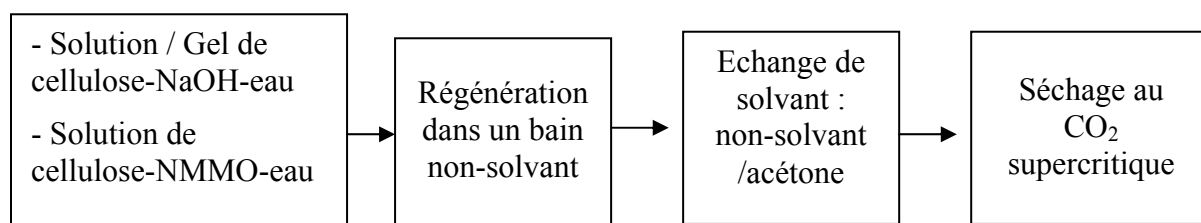


Figure 1.1: Représentation schématique des différentes étapes de préparation des Aérocelluloses

Ce nouveau matériau a des applications potentielles dans de nombreux domaines comme l'emballage écologique, l'encapsulation de cosmétiques, l'isolation thermique, les piles, les électrodes pour piles à combustibles. Certaines de ces applications sont abordées à la fin de ce manuscrit.

Le premier objectif a été de préparer le matériau Aérocellulose. Pour cela, les solutions de cellulose-NaOH-eau, les différentes étapes de régénération, les propriétés et quelques applications potentielles du matériau ont été examinées.

Le second objectif a consisté à comparer les Aérocelluloses obtenues à partir de la voie NaOH avec ceux préparés à partir des solutions cellulose-NMMO-eau.

Ce résumé présente les principaux résultats obtenus au cours de la thèse. Il est organisé selon le même plan que le manuscrit basé sur les différentes étapes de préparation du matériau Aérocellulose et ses propriétés. En premier lieu, nous évoquerons l'état de l'art relatif à la cellulose, ses procédés de fabrication et les matériaux cellulosiques poreux existants. Puis

l'étude rhéologique des solutions aqueuses de cellulose dans l'hydroxyde de sodium sera exposée. Ensuite, les cinétiques de régénération de la cellulose à partir des gels cellulose/NaOH/eau et cellulose/NMMO seront étudiées. Les deux chapitres suivants sont dédiés aux propriétés microstructurales et mécaniques des Aérocelluloses. Enfin, le dernier chapitre est consacré aux différentes applications du matériau sous sa forme initiale et carbonée, notamment ses applications électrochimiques.

2-Etat de l'art: La cellulose, ses procédés de mise en forme et la préparation de matériaux poreux à base de cellulose

La cellulose, de formule chimique $(C_6H_{10}O_5)_n$, est le matériau naturel le plus abondant sur Terre. La cellulose est un homopolymère constitué d'unités anhydroglucoses reliées entre elles par des liaisons glycosidiques β -(1 \rightarrow 4). Le degré de polymérisation dépend de l'origine de la cellulose ainsi que des traitements chimiques et mécaniques qu'elle a subis. Les nombreuses liaisons hydrogènes intra et intermoléculaires de la cellulose sont à l'origine de son insolubilité dans la plupart des solvants et de son arrangement supramoléculaire. Les chaînes de cellulose s'assemblent pour former des microfibrilles qui à leur tour s'agrègent pour former des macrofibrilles et finalement des fibres de cellulose. La cellulose est un matériau semicristallin. Quatre polymorphes de la cellulose ont été identifiés : la cellulose native ou cellulose I, et les cellulose II, III et IV. Les formes II, III et IV de la cellulose sont obtenues par traitement chimique de la cellulose I. La cellulose II est obtenue par deux voies : la mercerisation, traitement de la cellulose native avec de la soude concentrée et la dissolution de la cellulose. Ces deux procédés sont suivis par une étape de régénération. La cellulose II est la cellulose la plus décrite car elle est la structure cristalline obtenue dans la majorité des procédés industriels.

Cette étude de la littérature révèle un nombre assez restreint de solvants directs de la cellulose: liquides ioniques, complexes de cuivre, bases et acides forts, amines tertiaires. Deux grands procédés industriels conduisent à la production des fibres: le procédé viscose, qui dissout la cellulose par voie indirecte (via la derivatisation) et le procédé Lyocell, qui dissout directement la cellulose dans la N-méthyl-morpholyne-N-oxyde. Le procédé viscose, le plus employé et le plus ancien, consiste à solubiliser la cellulose pour obtenir une dispersion aqueuse de xanthate sodique, appelée viscose, puis à mettre en forme et régénérer cette cellulose. Cependant du fait de la pollution atmosphérique liée aux dégagements gazeux de sulfure de carbone et d'hydrogène sulfuré, de nouveaux procédés plus respectueux de l'environnement ont été explorés, notamment le procédé Lyocell. Ce procédé est basé sur la dissolution directe de la cellulose dans la N-méthylmorpholyne-N-oxyde, NMMO. Un nouveau procédé développé actuellement à l'échelle pilote est le procédé « soude ». Il consiste à dissoudre la cellulose dans une étroite zone de solution aqueuse de soude de concentration, 7 à 10%, à basse température. Les procédés Lyocell et soude sont particulièrement décrits car ce sont les deux procédés utilisés pour la préparation de l'Aérocellulose.

L'étape de régénération est une étape importante dans la mise en forme de la cellulose car elle influence fortement la structure et les propriétés finales des fibres obtenues. La régénération de la cellulose consiste à précipiter la cellulose dans un bain de non-solvant. Pendant la régénération, le non-solvant pénètre dans l'échantillon cellulosique alors que le solvant de la

cellulose sort vers le bain non-solvant. Les principaux paramètres influençant la régénération sont le type et la température du bain non-solvant. Ces paramètres gouvernent la diffusion du solvant de la solution ou du gel de cellulose vers le bain de régénération et donc la morphologie finale incluant la porosité de la cellulose régénérée.

Comme l'Aérocellulose est un nouveau matériau cellulosique ultra léger et microporeux, divers matériaux poreux à base de cellulose, tels les fibres régénérées, les membranes et les aérogels, sont analysés. Les fibres régénérées possèdent une nanoporosité qui est créée au cours de l'étape de régénération. Cette porosité dépend du bain non-solvant ainsi que de sa température. Les membranes cellulosiques sont créées par étalement de solution de cellulose sur une plaque de verre et immersion dans un non-solvant de la cellulose. Un échange solvant/non-solvant a lieu au sein du matériau. Il en résulte la formation d'un réseau poreux tridimensionnel. Les aérogels sont des matériaux ultra légers, nanoporeux, avec une grande surface spécifique. Ils sont principalement préparés par voie sol-gel à partir de matériaux inorganiques comme la silice. Le gel humide obtenu après polymérisation des précurseurs chimiques est séché par extraction supercritique. Ce type de séchage permet d'éviter les contraintes capillaires qui entraînent la contraction des pores et du matériau. Ces dernières années des aérogels organiques à base de mélamine-formaldéhyde ou de résorcinol-formaldéhyde ont également été développés. Très peu de publications décrivent la préparation d'aérogels à partir de matériaux cellulosiques. Par conséquent, la préparation d'une nouvelle classe d'aérogel à base de cellulose pure, au cours de cette thèse, fut un véritable défi.

3-Préparation et propriétés rhéologiques des solutions aqueuses de cellulose/NaOH

Depuis la découverte du procédé de mercerisation au XIX^{ème} siècle, le comportement de la cellulose dans les solutions aqueuses d'hydroxyde de soude a été abondamment décrit dans la littérature. En 1939, Sobue publia un diagramme de phase cellulose-NaOH-eau et il démontra que la cellulose pouvait être dissoute dans un faible domaine de concentration en soude (7-10%) et de température (-6°C - 0°C). Le traitement à la soude diminue l'ordre supramoléculaire et change la structure cristalline de la cellulose. Cinq formes cristallines appelées Na-cellulose ont été répertoriées. Les celluloses microcristallines et explosées à la vapeur de faible degré de polymérisation sont dissoutes dans la soude à 7-10% et à basse température (< 0°C). Afin d'améliorer la dissolution des fibres de cellulose possédant un grand degré de polymérisation (> 600), des additifs comme l'urée ou l'oxyde de zinc ont été ajoutés.

La préparation des solutions de cellulose-NaOH-eau, première étape de la création du matériau Aérocéllulose est décrite. Trois types de fibres : la cellulose microcristalline, Avicel, la cellulose explosée à la vapeur, Borregaard et la cellulose fibreuse, Solucell sont utilisées. La concentration en soude est fixée à 7,6%. Les concentrations en cellulose et en urée varient respectivement entre 3 et 7% et 0 et 20%. La cellulose est mélangée à l'eau et à une solution aqueuse de soude et éventuellement à une solution aqueuse d'urée. Le mélange est mixé pendant deux heures à 1000 tours par minute à -6°C.

Les solutions cellulose-NaOH-eau avec ou sans urée sont étudiées à l'aide d'un rhéomètre Gemini équipé d'outils cône plan et d'une platine Peltier. Nous avons évalué le comportement

en écoulement en mesurant la viscosité en fonction du taux de cisaillement. A basses températures (5-20°C) et faibles concentrations en cellulose ces solutions ont un comportement newtonien. Nous avons mesuré les énergies d'activation pour les systèmes cellulose-NaOH-eau et cellulose-NaOH-urée-eau. Leurs valeurs sont très proches montrant que la mobilité des chaînes de cellulose est la même dans les systèmes NaOH/eau avec ou sans ajout d'urée.

La gélification de ces solutions dans le temps ou en température est étudiée. Le point de gel est déterminé à l'intersection des courbes du module élastique, G' , et du module visqueux, G'' . Au cours de la gélification, le système se transforme d'un liquide visqueux à un réseau élastique. Les solutions de cellulose Avicel et Borregaard de 5% gélifient autour de 30°C. Un phénomène de synérèse, correspondant à la sortie du solvant hors du gel, est observé lorsque l'échantillon est chauffé longuement. Par ailleurs, les modules G' et G'' continuent d'augmenter après de longs temps d'observation montrant que le système n'a pas atteint son équilibre. Avec l'élévation de la température, le temps de gélification diminue de façon exponentielle. Avec le temps et la montée en température, les interactions cellulose-cellulose sont favorisées au détriment des interactions, cellulose-solvant, ce qui conduit à un phénomène physique irréversible de gélification des solutions due à diminution de la qualité du solvant NaOH/eau. L'augmentation de la concentration en cellulose entraîne la diminution de la température de gélification. En effet, plus la solution est concentrée en cellulose, plus les interactions entre les chaînes de cellulose sont nombreuses.

L'ajout d'urée, jusqu'à une certaine concentration, augmente la température de gélification et donc la qualité du solvant et la dissolution de la cellulose. Au-delà d'une concentration optimale d'urée, toutes les solutions gélifient. La concentration optimale permettant une meilleure dissolution dépend principalement de la cellulose utilisée. Elle est de 6% pour la cellulose explosée à la vapeur Borregaard, 12% pour la cellulose microcristalline et 16% pour la cellulose fibreuse, Solucell. L'origine de la cellulose influence donc fortement la gélification des solutions. Par ailleurs, le mécanisme de gélification des solutions de cellulose-NaOH-eau avec ou sans urée est le même, cependant l'action précise de l'urée sur la cellulose reste une question ouverte.

4-Cinétiques de régénération de la cellulose des gels cellulose-NaOH-eau et des solutions cellulose-NMMO-eau

Une fois les solutions de cellulose-NaOH-eau mises en forme et gélifiées, elles sont régénérées dans un bain de non-solvant afin de retrouver la cellulose pure. La cellulose précipite suite à l'échange solvant - non-solvant. La cellulose est alors gonflée dans un non-solvant. Les cinétiques de régénération de la cellulose des gels cellulose-NaOH-eau immergés dans un bain de non-solvant sont évaluées puis comparées à celles des solutions cellulose-NMMO-eau.

Les bains de régénération doivent être miscibles avec les solvants de la cellulose employés (NaOH ou NMMO) et être non-solvant de la cellulose. Les non-solvants de la cellulose utilisés au cours de cette étude sont l'eau et divers alcools comme l'éthanol, l'isopropanol, le butanol, le pentanol et l'hexanol. La diffusion du solvant de la solution vers le bain de régénération a été suivie par réfractométrie dans le cas de la NMMO et par titrimétrie ou

potentiométrie dans le cas de la soude. Le coefficient de diffusion a été déterminé par la loi de Fick. Trois approximations, temps court, mi-temps et temps final ont été considérées. Nous avons choisi d'utiliser l'approximation à mi-temps pour déterminer les coefficients de diffusion car elle était la plus proche des valeurs expérimentales mesurées.

Nous avons analysé l'incidence de la concentration en cellulose sur les cinétiques de régénération. Les coefficients de diffusion de NaOH et de la NMMO sont pratiquement identiques entre 5 et 7% de cellulose, ce qui signifie que la régénération des échantillons de gels de cellulose-NaOH-eau ou de solutions de cellulose-NMMO-eau, de même géométrie et dans les mêmes conditions prendra le même temps. Cependant les coefficients de diffusion de la NMMO et de la soude diffèrent à de plus basses concentrations de cellulose, le coefficient de NaOH étant plus grand que celui de NMMO.

Afin d'expliquer l'influence de la concentration de cellulose sur les coefficients de diffusions et les différences entre les deux systèmes considérés, différentes théories développées pour le transport de solutés dans les hydrogels ou dans les milieux poreux ont été utilisées. Nous avons appliqué différents modèles, notamment les modèles hydrodynamiques, d'obstruction ou la théorie du volume libre. Au cours de la régénération de la cellulose des gels cellulose-NaOH-eau immergés dans un bain non-solvant un mécanisme de séparation de phase a lieu. La cellulose se retrouve gonflée dans le non-solvant, comme une membrane, ce qui permet d'appliquer les modèles de volume libre ou hydrodynamique. La comparaison des résultats expérimentaux avec différentes théories a montré qu'une approche « milieu poreux » est préférable à une approche « hydrogel » pour décrire la régénération de la cellulose à partir des gels cellulose-NaOH-eau. L'interprétation de la diffusion de la NMMO est plus compliquée car la NMMO change d'état au cours de la régénération, elle passe d'un état cristallin à un état liquide. A faible concentration de cellulose, la concentration en NMMO dans l'échantillon est très élevée dans le système cellulose-NMMO-eau et de très nombreuses molécules de NMMO ne sont pas liées à la cellulose. Pendant la régénération, l'eau pénètre à l'intérieur de la solution et dissout les cristaux libres de NMMO. La NMMO alors fluide peut ainsi diffuser de l'échantillon vers le bain d'eau. En conséquence, pour de faibles concentrations en cellulose, la régénération de la cellulose est plus lente dans le cas des solutions de cellulose-NMMO-eau que dans le cas des gels de cellulose-NaOH-eau.

Les gels et les solutions de cellulose ont été régénérés dans de l'eau à plusieurs températures: 25°C, 50°C et 80°C. Plus la température de l'eau est élevée, plus la régénération de la cellulose est rapide. Les énergies d'activation ont été calculées en appliquant la loi d'Arrhenius à partir des coefficients de diffusion de la soude vers l'eau pour différentes températures. Elles coïncident avec celles trouvées à partir des mesures rhéologiques dans le chapitre 2. Ceci signifie que quelque soit le système: pure solution aqueuse de NaOH, solution de cellulose-NaOH-eau ou gel de cellulose-NaOH-eau, c'est l'hydrate NaOH avec ou sans la cellulose qui bouge dans le système.

Nous avons évalué l'influence de la nature du bain de régénération, principalement des alcools, sur les cinétiques de régénération. Une forte contraction des gels de cellulose-NaOH-eau a été observée. Ceci s'explique par la grande différence entre les paramètres de solubilité d'Hildebrand des alcools étudiés et de la cellulose. Dans le cas des solutions cellulose-NMMO-eau, nous constatons une baisse de la cinétique de régénération en fonction du poids moléculaire de l'alcool et donc de sa viscosité.

5-Propriétés microstructurales des Aérocelluloses

Après l'étape de régénération, la cellulose est gonflée dans un bain de non solvant. Ce non-solvant est échangé avec généralement de l'acétone en vue du séchage au CO₂ supercritique. Ce séchage consiste à placer le gel humide gonflé dans l'acétone ou l'éthanol dans un autoclave clos et à chauffer et augmenter la pression au-delà du point critique du CO₂ supercritique ($P_c = 73.8\text{bar}$, $T_c = 31.1\text{C}$). L'acétone se trouvant dans les pores du matériau est solubilisé par le solvant supercritique, qui est à son tour remplacé par de l'air. Il en résulte un matériau sec, ultraporeux et très léger ($0.06\text{-}0.25\text{ g.cm}^3$), l'Aérocellulose. Les séchages supercritiques ont été réalisés au CEP, Ecole des Mines de Paris à Sophia-Antipolis, France ou à Natex à Ternitz, Autriche.

La morphologie des Aérocelluloses est étudiée par deux techniques de microscopie : la microscopie électronique à balayage et à transmission. Ces deux techniques complémentaires permettent d'observer la porosité du matériau à différentes échelles micrométrique et nanométrique. La microstructure des Aérocelluloses a été étudiée par porosimétrie mercure et adsorption d'azote. Ces deux méthodes sont également supplémentaires car elles permettent de décrire les caractéristiques de la nano, meso et macroporosité, comme l'aire spécifique, le volume poreux ou la distribution de taille de pore. Ces tests ont été réalisés au Fraunhofer Institut de Potsdam en Allemagne.

La porosité des Aérocelluloses est ouverte avec un diamètre de pore variant de quelques nanomètres à quelques dizaines de micron. Le diamètre moyen des pores est de l'ordre de quelques centaines de nanomètres. La porosité est supérieure à 90%. La surface spécifique est principalement due aux micropores et elle varie entre 200 et 500 m².g⁻¹. Presque tous les échantillons ont une peau en surface. Cette peau est créée par une rapide diminution de la quantité de solvant en surface, ce qui conduit à une augmentation de la concentration de la cellulose en surface.

Nous avons considéré l'éventuelle influence des différents paramètres de préparation sur la microstructure des Aérocelluloses. Les conclusions suivantes peuvent être faites :

- Les conditions de gélification des solutions de cellulose-NaOH-eau ainsi que l'origine des pulpes de cellulose étudiées ont peu d'effet sur la microstructure des Aérocelluloses.
- Plus la concentration en cellulose est élevée, plus le rayon moyen du pore diminue.
- La température du bain d'eau de régénération a une grande influence sur la morphologie et la structure finale du matériau aussi bien pour les Aérocelluloses obtenues à partir des gels de cellulose-NaOH-eau que pour les solutions de cellulose-NMMO-eau. L'augmentation de la température de l'eau rend la structure plus «nuageuse», augmente le volume poreux et donc allège le matériau.
- La nature du bain de régénération modifie la microstructure des Aérocelluloses. Par exemple pour les Aérocelluloses obtenues à partir de la voie NaOH, régénérées dans l'acide sulfurique, le diamètre des pores décroît. Dans le cas des Aérocelluloses préparées via la voie NMMO et régénérées dans différents alcools, plus le poids moléculaire de l'alcool est élevé, plus la structure de l'échantillon est dense.

Il apparaît que la concentration en cellulose, la nature du bain non-solvant et sa température influencent grandement la microstructure du matériau.

Par ailleurs l'état dans lequel est la solution de cellulose, i.e, solide ou liquide pour les solutions de cellulose-NMMO-eau et gélifié ou liquide pour les solutions de cellulose-NaOH-eau conduit à différentes morphologies des Aérocelluloses. Par exemple, des sphères connectées de taille inférieure au micron apparaissent dans le cas des solutions liquides de cellulose-NMMO-eau directement régénérées dans un bain non-solvant. Ceci est caractéristique d'un mécanisme de séparation de phase par décomposition spinodale.

Un réseau tridimensionnel poreux avec une large distribution de pore est créé quand les Aérocelluloses sont préparées à partir d'échantillons ayant déjà connu une première séparation de phase, c'est le cas des solutions cristallisées de cellulose-NMMO-eau et des solutions gélifiées de cellulose-NaOH-eau. La formation de grands pores est due à la sortie rapide du solvant non lié à la cellulose, cristaux de NMMO libres ou solutions aqueuses de soude, au cours de la régénération. Les pores plus petits sont formés suite à la deuxième séparation de phase lorsque le solvant est complètement détaché de la cellulose.

6-Propriétés mécaniques des Aérocelluloses

L'Aérocellulose est un nouveau type de matériau ultra-léger à base de cellulose. Ce n'est pas une mousse polymère conventionnelle puisque ce matériau est extrêmement poreux (porosité > 90%) avec une taille de pore de l'ordre de quelques centaines de nanomètres et qu'il possède une porosité ouverte.

Nous avons examiné les propriétés mécaniques en compression uniaxiale des matériaux Aérocellulose obtenus par la voie soude et la voie NMMO. Les échantillons cylindriques ont été sollicités en compression jusqu'à 70% de déformation avec un taux de déplacement de 0,1 mm.s⁻¹. Leur comportement en compression est caractéristique des matériaux cellulaires. Les courbes contrainte-déformation sont caractérisées par une région élastique aux faibles déformations, suivie d'un long plateau quasi horizontal correspondant à l'effondrement progressif des cellules et enfin une montée abrupte de la contrainte qui correspond à la densification du matériau due au contact des parois cellulaires. A partir des courbes de compression, nous avons déterminé les principales caractéristiques mécaniques comme le module d'Young, la contrainte au plateau et l'énergie d'absorption. Les Aérocelluloses ont un comportement plastique en compression, aucune recouvrance du matériau n'a été observée après compression.

L'influence des paramètres de préparation sur les propriétés mécaniques des Aérocelluloses a été étudiée. Nous pouvons en conclure les points suivants :

- Le type de cellulose influence les propriétés mécaniques des Aérocelluloses. Plus le degré de polymérisation de la cellulose est élevé, plus le module d'Young et la contrainte au plateau sont élevés.
- Plus la concentration en cellulose augmente et donc plus la porosité du matériau diminue, plus la hauteur du plateau et l'énergie d'absorption augmentent et plus la contrainte à laquelle la densification du matériau commence, diminue. Les propriétés mécaniques du matériau poreux sont fortement reliées à sa densité.

- L'addition de fibres de renfort à de faibles concentrations, 1 et 2%, améliore les propriétés mécaniques des Aérocelluloses.
- L'ajout de surfactant lors de la préparation des solutions de cellulose-NaOH-eau suivie d'une gélification immédiate permet de créer des bulles d'air et donc d'augmenter la proportion de macropores. Le matériau est allégé. En conséquence, les propriétés mécaniques des Aérocelluloses obtenues diminuent.
- Lorsque les gels de cellulose-NaOH-eau sont régénérés dans des bains d'eau chaude, des macropores sont créés, la densité des Aérocelluloses diminue, le matériau est fragilisé et se fracture plus rapidement. La présence de macropores influence donc fortement les propriétés mécaniques des Aérocelluloses.

Le lien entre les propriétés microstructurales et mécaniques a été réalisé en utilisant les modèles développés pour les mousses polymères, plus particulièrement le modèle d'Ashby et Gibson et les modèles développés pour les aérogels. Ces modèles reposent sur des lois puissance entre le module d'Young et la contrainte au plateau en fonction de la densité. Ils diffèrent par la valeur du coefficient de puissance trouvée, proche de 2 dans le cas des mousses polymères et de 3-4 pour les aérogels. Nous avons trouvé de bonnes corrélations avec le modèle d'Ashby et Gibson. Nous avons déterminé des coefficients de puissance de l'ordre de 2. Il en résulte que les Aérocelluloses obtenues par les deux voies soude et NMMO se comportent d'un point de vue mécanique plus comme des mousses que comme des aérogels. Ceci peut s'expliquer par le fait que la taille moyenne des pores est de l'ordre de quelques centaines de nanomètres soit assez loin de celle des aérogels, qui est de l'ordre de quelques dizaines de nanomètres. En outre, les Aérocelluloses obtenues par la voie NMMO sont plus résistantes et ils absorbent plus d'énergie que les Aérocelluloses obtenues par la voie soude, ceci peut s'interpréter par la différence entre les degrés de polymérisation des fibres de cellulose utilisées, qui est plus important dans le cas des Aérocelluloses obtenues par la voie NMMO.

7-Applications des matériaux Aérocelluloses et des Aérocelluloses carbonées

Le matériau Aérocellulose constitué de cellulose pure a été utilisé sous forme de billes pour encapsuler des particules insolubles inorganiques. Des particules de fer, de cuivre, de magnésium, d'oxyde de titane, de noir de carbone et des pigments ont été employés. Les billes sont obtenues en faisant goutter à l'aide d'une micropipette les solutions de cellulose-NaOH-eau+ particules dans un bain d'eau chaude. Nous avons observé que ces particules inorganiques sont soit piégées à l'intérieur de la structure poreuse, comme les particules de fer, soit piégées le long des fibres de cellulose : c'est le cas des particules d'oxyde de titane. Nous n'avons pas constaté de libération des particules excepté dans le cas des noirs de carbone.

Afin d'obtenir une texture poreuse à base de carbone, des échantillons d'Aérocellulose ont été pyrolysés, au CEP, Ecole des Mines, Sophia-Antipolis, France. Différents cycles de pyrolyse ont été envisagés, le cycle le plus long conduit à une plus grande quantité de carbone dans le matériau. La perte de masse obtenue est de l'ordre de $83 \pm 3\%$. Suite à la pyrolyse, nous observons une densification du matériau et une diminution de la taille des pores (< 100 nm). L'action des paramètres de préparation comme le gaz utilisé lors de pyrolyse, la concentration

en cellulose ou la température de l'eau dans le bain de régénération sur les propriétés microstructurales des Aérocelluloses pyrolysés a été examinée. En faisant varier ces paramètres, nous pouvons ajuster la porosité des Aérocelluloses pyrolysés. Les Aérocelluloses carbonées ont été testés sous forme de pile primaire Lithium - chlorure de thionyle à la SAFT, Bordeaux, France et en support catalytique pour les électrodes des piles à membrane échangeuse de protons (PEMFC), au LEPMI, Grenoble, France. Les résultats électrochimiques obtenus pour ces deux applications sont très prometteurs.

8-Conclusions

L'objectif de cette thèse était d'élaborer de nouveaux matériaux ultra poreux à base de cellulose, les Aérocelluloses, et de comprendre les relations liant leurs structures, leurs propriétés et les modes de préparation. Les matériaux obtenus par la voie « soude » ont été comparés à ceux obtenus par la voie NMMO.

Nous avons employé le procédé « soude » pour dissoudre la cellulose dans une solution aqueuse d'hydroxyde de sodium à une concentration de 7.6% et à basse température, -6°C. Les propriétés rhéologiques des solutions cellulose-NaOH-eau préparées ont été étudiées. Le temps, la température et l'augmentation de la concentration de cellulose favorisent les interactions cellulose-cellulose, au détriment des interactions cellulose-solvant, diminuant la qualité du solvant et conduisant à la formation d'un gel irréversible. L'ajout d'urée permet de retarder la gélification et d'améliorer la qualité du solvant. Cependant le comportement rhéologique des solutions diffère selon la quantité d'urée ajoutée et l'origine de la cellulose. Les raisons de telles différences demeurent à ce jour une question ouverte.

Nous avons étudié les cinétiques de régénération de la cellulose des gels physiques de cellulose et nous les avons comparées à celle des solutions de cellulose-NMMO-eau. Différents modèles relatifs au transport de solutés dans les hydrogels ou dans les milieux poreux ont été utilisés. Le modèle poreux est le mieux adapté pour décrire la diffusion des solvants de la cellulose, NaOH et NMMO, vers le bain dans de régénération car une séparation de phase se produit au cours de la régénération de la cellulose placée dans un bain non-solvant. D'autre part, plus la température du bain de régénération est élevée plus la régénération de la cellulose est rapide. Ceci nous permet en utilisant la loi d'Arrhenius, de calculer la valeur du coefficient de diffusion du solvant, NaOH ou NMMO vers le bain d'eau, à toute température. Enfin, nous avons observé que plus la viscosité de l'alcool utilisé comme bain de régénération était élevée, plus la régénération de la cellulose était lente.

L'analyse des morphologies des Aérocelluloses démontre que l'étape de régénération est primordiale pour la structure finale du matériau. La température et la nature du bain de régénération, la concentration en cellulose ont un réel impact sur les propriétés microstructurales des Aérocelluloses. Par exemple, les structures obtenues par régénération dans un bain d'eau chaude sont « nuageuses » et le matériau est allégé par la création de macropores. L'état de la solution, fondue ou cristallisée dans le cas des solutions cellulose-NMMO-eau, liquide ou gélifié dans le cas des solutions cellulose-NaOH-eau joue également un grand rôle sur la morphologie des Aérocelluloses. Nous observons des structures poreuses ou des structures de forme granulaire selon que la solution de cellulose-NMMO-eau est cristallisée ou fondue avant régénération. Tous les Aérocelluloses ont une porosité ouverte,

supérieure à 90%, avec un diamètre de pores variant de quelques nanomètres à quelques dizaines de micron. Leur surface spécifique varie entre 200 et 500 m².g⁻¹.

L'influence des paramètres de préparation de l'Aérocélulose joue un rôle également sur les propriétés mécaniques du matériau. Le degré de polymérisation de la cellulose influence les propriétés mécaniques des Aérocéluloses. Plus il est élevé, plus les caractéristiques mécaniques du matériau sont élevées. D'autre part plus la concentration et donc la densité sont élevées, plus les propriétés mécaniques sont importantes. La formation de macropores obtenue, soit par une élévation de la température du bain de régénération soit par ajout de surfactant, diminue la densité du matériau et les caractéristiques mécaniques du matériau. Nous avons analysé les propriétés mécaniques des Aérocéluloses en utilisant les modèles des mousses et des aérogels. Il apparaît que l'Aérocélulose se comporte plus comme une mousse que comme un aérogel. Ceci provient peut être de la taille de ses pores qui sont de l'ordre de quelques centaines de nanomètres alors que les pores des aérogels sont de l'ordre de quelques nanomètres.

Enfin, le matériau Aérocélulose a été évalué dans diverses applications. Des structures composites, sous forme de billes, cellulose-particules inorganiques ont été créées, démontrant l'utilisation de la cellulose comme une matrice biodégradable permettant par exemple de stabiliser les particules insolubles en solution. Nous avons pyrolysés les Aérocéluloses afin d'obtenir des structures carbonées poreuses. Les pertes de masse sont importantes, 83±3%. Les structures poreuses carbonées diffèrent de celle de l'Aérocélulose initiale, des particules de types plus ou moins granulaires sont créées au cours de la pyrolyse. Les Aérocéluloses carbonées utilisées dans les piles primaires au lithium ainsi que les Aérocéluloses carbonées platinées testées comme électrode dans les piles à combustibles conduisent à des résultats prometteurs.

En conclusion, nous avons démontré que la biomasse et notamment son principal constituant, la cellulose, pouvait être valorisée autrement que dans les applications traditionnelles comme les fibres et le papier. A terme la cellulose est capable de se substituer aux polymères synthétiques et être transformée en de nouveaux matériaux à haute valeur ajoutée, comme nous venons de le démontrer avec l'Aérocélulose, ceci d'autant plus que les caractéristiques de ce matériau répondent aux nouvelles exigences environnementales, il est naturel, propre, et biodégradable.

9-Perspectives

L'Aérocélulose étant un tout nouveau matériau, de nombreux points notamment les liens structures - propriétés restent à approfondir. En effet, nous avons observé que de nombreux paramètres de préparation de l'Aérocélulose modifient les propriétés finales du matériau. Une étude à partir des solutions liquides cellulose-NaOH-eau directement régénérées dans un bain de non-solvant est à mener, notamment pour observer l'influence de l'état de la solution sur la morphologie des Aérocéluloses. De plus, l'influence des solutions acides sur les cinétiques de régénération et la morphologie finale serait à développer.

Concernant les propriétés rhéologiques des solutions de cellulose-NaOH-eau avec ou sans urée, une étude plus approfondie du comportement des solutions est à réaliser, notamment en

variant les degrés de polymérisation et l'origine des celluloses. Nous pouvons également envisager la création d'un diagramme de phase cellulose-NaOH-urée-eau. De plus, la compréhension des phénomènes physiques comme l'action exacte de l'urée sur la gélification des solutions de cellulose nous permettrait de connaître précisément le rôle de l'urée et d'optimiser la dissolution de la cellulose dans ces systèmes.

Les premiers tests réalisés sur les Aérocelluloses carbonées comme électrodes dans les piles primaires au lithium et dans les piles à combustibles sont prometteurs. Cependant la préparation des Aérocelluloses pyrolysées et les relations liant leurs structures-propriétés doivent être approfondies et améliorées afin d'optimiser ces nouveaux matériaux carbonés d'origine « verte ».

General introduction

Cellulose is the most abundant natural polymer on Earth. This polysaccharide is the major component of wood, of plant fibres like cotton, flax and hemp and it is found in most of agricultural cultures like wheat, corn and sugarcane. Its annual natural “production” is estimated as 100 billions tons per year. Trees, the major source of cellulose, are a giant carbon “collector” since via photosynthesis they generate oxygen and absorb high amounts of carbon dioxide. Thus, cellulose is one of the most promising components to reduce greenhouse gas emission and to contribute to the prevention of global warming targeted by the Kyoto protocol. Cellulose is a biodegradable polysaccharide; it is decomposed easily by fungi and soil bacteria. Furthermore, it is a renewable natural resource, reproducing itself through natural cycle by using sunlight, which is an infinite, free and clean source of energy.

In the recent years, a strong consumer demand for biodegradable and eco-friendly products has appeared in order to increase health and life quality. On the other hand, oil price increase and its scarcity in the future are accelerating the development of new biodegradable products emerging from the research on biomaterials. The annual natural polysaccharide production is a thousand times more important than synthetic polymer production based on oil resource. Therefore, polysaccharides and especially cellulose are a very appealing alternative for substituting synthetic polymers. Biopolymers produced from the largest chemical reactor, Nature, are one of the most promising materials of tomorrow.

However, cellulose cannot be melted or dissolved in ordinary solvents because of strong intramolecular hydrogen bonds. The oldest technology for manufacturing regenerated cellulose fibres is the viscose process, which was developed more than 100 years ago. It is based on the xanthogenate derivatisation of cellulose. Despite its efficiency, it is very harmful for environment as it rejects heavy metals and toxic gases like carbon disulphide and hydrogen sulphide. Considerable efforts have thus been made to explore new environmentally friendly processes. In the late 1980s, a new process called Lyocell process, based on cellulose direct dissolution in N-methyl-morpholine-N-oxide (NMMO), was launched in an industrial scale and this technology currently produces more than 100.000 tons of cellulose fibres. Nearly all solvent is recovered, which makes this process non-toxic. Since the last decade, a new eco-friendly process to form cellulose based on dissolution of cellulose in 7-10% sodium hydroxide (NaOH) has also appeared. Due to its low cost and non-polluting way of cellulose dissolution, NaOH is also a promising solvent.

The goal of the thesis is to prepare a totally new ultra light and highly porous material based on cellulose, called Aerocellulose. The main idea in the preparation of this material is taken from aerogel area. Aerogels are synthesised via sol-gel phase transition in a liquid media and then dried by supercritical extraction. These materials are characterised by a very low density (0.004 to 0.2g/cm³), a high porosity (up to 99.8%) and a very large specific surface (up to 1000 m²/g). Most aerogels are inorganic (SiO₂, TiO₂, etc.). Organic aerogels such as resorcinol-formaldehyde or melamine formaldehyde have appeared in the recent years. Although Kistler first considered aerogels from cellulose and nitrocellulose in 1932, research on organic aerogels from cellulose origin has only been conducted very recently.

Aerocellulose was developed in the frame of European project AEROCELL. Two preparation processes, either chemical or physical way, were considered. Three physical methods to prepare this material were explored: from cellulose carbamate, from cellulose-NMMO solutions and from cellulose-sodium hydroxide solutions. In the thesis, the two latter approaches have been studied with a particular attention to the material preparation via NaOH route. Forming of Aerocellulose material through NaOH and NMMO is a multi-step procedure.

First cellulose is dissolved either in aqueous sodium hydroxide solution or in NMMO. Cellulose-NaOH-water solutions gel in time or when heated while cellulose-NMMO-water solutions crystallise at ambient temperature. Next step is cellulose regeneration in a non-solvent bath. During this step, NaOH or NMMO are released out of the solution or gel, and the non-solvent, usually water, penetrates inside the sample. As a result, cellulose is swollen in non-solvent. Subsequently, this non-solvent is exchanged with acetone. Cellulose samples are dried in CO₂ supercritical condition. A dry ultra-light pure cellulose material is obtained, Aerocellulose. Figure 1.1 summarizes the different steps of Aerocellulose preparation.

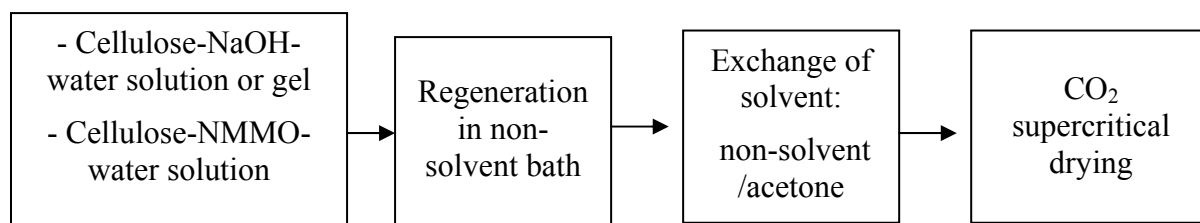


Figure 1.1: Schematic presentation of multi-step preparation of Aerocellulose

This new type of material has potential applications in various fields such as biopackaging, batteries, electrodes for fuel cells, encapsulation for cosmetics, thermal insulation and much more. Some of these applications are presented at the end of the manuscript.

This work has two objectives: the first is the preparation of Aerocellulose from cellulose-NaOH route and a comparison with Aerocellulose prepared from NMMO route, and the second is to understand the structure-properties relationships of the material.

Our first objective was to use cellulose-NaOH-water solutions for making Aerocellulose, to study the different preparation steps, like rheological behaviour of cellulose solution, cellulose regeneration and formation of the porous structure. At each step, we have compared the materials obtained from NaOH route with the ones prepared from NMMO route.

The second objective was to evaluate the properties of Aerocellulose such as microstructural, mechanical and electrochemical properties and to link the structure to the properties and applications of this new material.

The preparation and characterisation of Aerocellulose material were carried out in a close collaboration with research institutions. It includes French laboratories Centre Energétique et Procédé, CEP, of Ecole des Mines and Laboratoire d'électrochimie et de physico-chimie des matériaux et des interfaces, LEPMI; Fraunhofer Institute for Applied Polymer Research, FHG-IAP, from Germany and industrial partners as Austrian companies Lenzing and Natex, German company Genialab, French company Saft and Italian company Novamont.

The manuscript is divided into six chapters.

The first chapter deals with the literature review on cellulose, its processing and the preparation of porous cellulose materials. First the chemical structure of cellulose, its organisation in microfibrils and its crystalline form are presented. Then the cellulose processing, namely the viscose, Lyocell and NaOH are described. The last part illustrates the preparation of porous cellulosic materials as regenerated fibres, membrane or aerogel.

The second chapter presents the preparation and the rheological properties of cellulose-NaOH-water solutions with or without additives. A brief review of literature describes the structure and the properties of cellulose-NaOH-water solution and the influence of additives on their gelation. Then the experimental results obtained are presented and discussed. The steady state flow of the cellulose-NaOH-water solution under shear stress is examined. Gelation of the solution with or without urea is studied. The influence of cellulose type and concentration and of urea concentration as well as of experimental conditions like temperature and time on gelation of solutions was investigated.

Chapter III, in the form of scientific article (accepted in *Biomacromolecules*), is devoted to the kinetics of cellulose regeneration from cellulose-NaOH-water gels immersed in a non-solvent bath. The results are compared with the ones found for cellulose-NMMO-water solutions. The influence of cellulose concentration, of the nature of the non solvent bath and its temperature is examined. Different theoretical models are applied to better understand and interpret cellulose regeneration from cellulose-NaOH-water gels and from cellulose-NMMO-water solutions.

Chapter IV is dedicated to the microstructural properties of Aerocellulose. CO₂ supercritical drying method, porosimetry experiments and electron microscopy techniques are briefly presented. In order to better understand the morphology and microstructure of Aerocellulose, a special attention is paid on the influence of preparation parameters like cellulose concentration, pulp origin, surfactant concentration, regenerating bath temperature and nature.

Chapter V focuses on the mechanical properties of Aerocellulose. First, a short bibliography on the mechanical properties of foams and aerogels is presented. Afterwards, the experimental results obtained from uniaxial compression tests performed on Aerocellulose prepared from NaOH and NMMO routes are described. The influence of parameters of Aerocellulose preparation like cellulose concentration, pulp origin, bath regenerating temperature, presence of additives on the mechanical properties is investigated. Finally, the mechanical and microstructural relationships are studied using the deformation compressive models.

Chapter VI presents three examples of Aerocellulose applications. The first one is the preparation of Aerocellulose-inorganic particles composite by encapsulating insoluble powders inside the Aerocellulose. The possibility to use carbonised Aerocellulose obtained from the pyrolysis of Aerocellulose for electrochemical purposes was investigated. Two applications of carbonised Aerocellulose are presented: as an electrode material for primary lithium battery and catalyse support in Proton Exchange Membrane Fuel Cell electrodes.

Finally, conclusions are drawn and suggestions for further investigation are proposed.

Chapter I: Cellulose, its processing and preparation of porous cellulose materials

Introduction

Cellulose is a natural polymer of particular interest due to its abundant availability and biodegradability. It has been studied and formed for many years, to yield various useful products. It represents thus a considerable economic investment and is of a great interest from an industrial point of view. Moreover, with the growing emphasis on producing environmentally friendly products, there has been a significant scientific and technological interest in the development of non-polluting processes for cellulose forming and in making new cellulose-based products with a high added value for new applications.

As it was already mentioned in the Introduction, the principal objective of my thesis is to develop a new material called “Aerocellulose”. Aerocellulose is a new ultra light, nano or micron-size porous multifunctional material with a high specific surface area. It can be used in numerous applications as biopackaging, as a matrix for encapsulation in cosmetics and pharmacology, batteries, electrodes for fuel cells and much more. This material is obtained from solutions or gels of cellulose, which are regenerated in successive baths of non-solvent. The latter is eliminated by CO₂ supercritical extraction to obtain an ultra porous cellulose material. The goal of this first chapter is to review the state of art about the structure and morphology of cellulose, the processes of cellulose forming and the preparation of porous objects based on cellulose in order to prepare and optimise the structure and properties of Aerocellulose.

The first part of this chapter deals with generalities concerning cellulose: it is the basic material of this work and thus the understanding of its structure, micro and macro organization and its different crystalline forms from native to regenerated fibres is important.

The second part focuses on the forming of cellulose and especially on the existing industrial processes. The study and the comprehension of the regeneration methods are of primary importance because it controls the final properties of the material. Three main cellulose processes are studied: the “old” viscose process and the “new” environmentally friendly processes, Lyocell and NaOH process. The ability of processing cellulose via dissolution in dilute aqueous NaOH solutions is discussed, as it is the process involved in the Aerocellulose preparation.

In the third part we will examine some existing porous cellulose-based products such as regenerated fibres, membranes or aerogels that are micro-porous materials. The mechanisms of formation of membranes and aerogels will be discussed.

1.1 Cellulose: main aspects on structure and properties

1.2 Generalities

Cellulose is the major component of wood; it represents 40-45% of broad-leaved trees and 38-50% of coniferous wood. It also represents more than 50 % of the biomass and it is the most abundant organic compound on earth. Cellulose is produced by green plants on a 100–150 billion-ton scale each year. Every tree produces, on average, approximately 13 to 14 grams of cellulose per day. This natural polymer is present in many types of vegetation with a content varying from 15% to 99%. It provides a frame and support to the cell walls in plant cells. This polysaccharide is also biosynthesised by some bacteria such as the acetobacter xyloium and is present in a highly crystalline form in some seaweed like valonia or the microdycon. Cellulose is also present in the fibres of stem such as cereals straw, sugar cane and reeds, grain fibres such as coconut or cotton and other fibres such as flax, hemp or jute (Table I.1).

Plant material	Cellulose content (dried material, %)
Corn	17-20
Bamboo, Straw, Sugar Cane	40-50
Flax, Hemp, Ramie	70-75
Cotton	95-99

Table I.1: Cellulose content in common vegetation [Klemm et al, 1998]

Wood is the principal source of cellulose. It represents 86% of the total production of pulp, 51% of this pulp coming from softwood and 35% from broad-leaved trees. Almost 80% worldwide production of chemical cellulose pulp is used for the fabrication of paper and cardboard. The remaining 20% are used for the fabrication of regenerated cellulose for textile fibres and cellulosic derivatives [Klemm et al, 1998].

1.3 Chemical structure of cellulose

The elemental composition of cellulose was determined in the XIX century by the French chemist Anselme Payen: 44% carbon, 6% hydrogen and the remaining being oxygen. However, it was only 50 years later that Weillstatter and Zechmeister wrote down the chemical formula of cellulose, $(C_6H_{10}O_5)_n$ while Polyani determined the volume of the crystalline unit in 1921. The following research established the primary structure of cellulose: a linear homopolymer composed of β (1 \rightarrow 4)-D-anhydroglucopyranose units with a 4C_1 chair conformation. The cellulose chains are rotated by 180° around their longitudinal axis (Figure I.1).

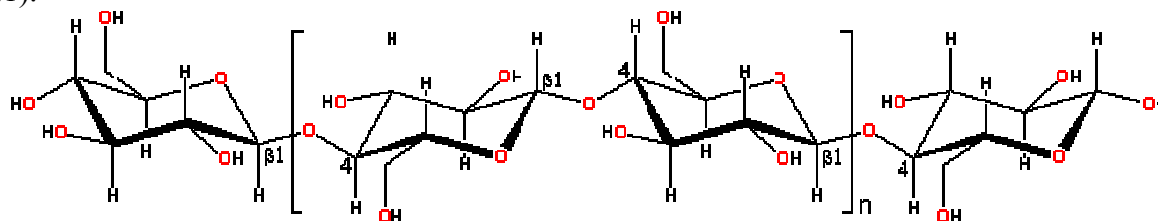


Figure I.1: Schematic representation of cellulose chain

Hydroxyl groups, located at C2 and C3, and CH₂OH group located at C6 are in equatorial positions while hydrogen atoms are in axial positions. This configuration makes them suitable for the formation of hydrogen bond, particularly with water molecules, which can be thoroughly linked to cellulose.

Hydrogen intermolecular bonds between oxygen atoms O3' and O5 (O3'...O5 = 2.5Å) as well as O2 and O6' atoms are responsible for the considerable stiffness of the cellulose chain.

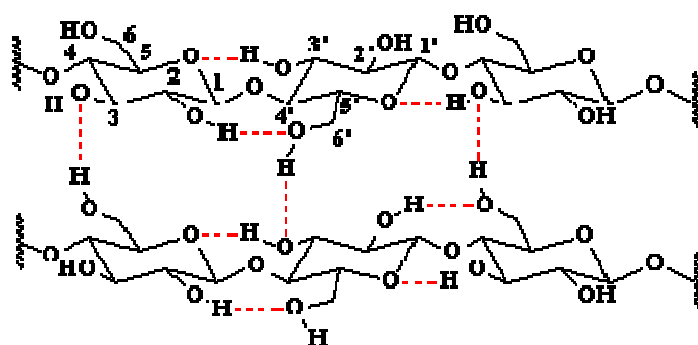


Figure I.2: Intra and intermolecular hydrogen links within cellulose

The formation of hydrogen intra and inter chains bonds leads to various ways to form a stable three-dimensional structure. Intramolecular hydrogen bonds give to cellulose its stiffness and rigidity and its insolubility in most solvents. Hydroxyl groups are liable to react chemically as primary or secondary alcohols [Krassig, 1996].

The degree of polymerisation, DP, which is the number of monomer units in a polymer chain, is closely linked to the cellulose origin and pre-treatment. Its value varies from 100 to several thousands depending of the vegetal specie, as shown in Table I.2. The DP of native cotton fibre can be over 12 000 whereas the DP of wood pulp is generally between 500 and 1000 [GFP, 2000].

Vegetal species	DP
Algae Valonia	26 000
Cotton	10 000
Flax, Hemp	9 000
Spruce	8 000
Wood pulp	500 - 1000

Table I.2: Polymerization degree of different vegetal species [Klemm et al, 1998]

Moreover, purification and solubilisation processes generally cause the scission of cellulose chains. This is the reason why the degree of polymerisation of cellulose in its natural state is not established. Cellulose properties depend on the celluloses origin, the process used to obtain it and its subsequent treatment.

1.4 Structure and organisation of micro fibrils

The intra and inter molecular hydrogen bonds are responsible for the supramolecular structure of cellulose. It consists of micro fibrils of various sizes depending of the cellulose origin. Their aggregations form fibrils and rigid and resistant fibres. The network of hydrogen bonds between the cellulose chains makes cellulose partially crystalline. Moreover, the space regularity of these connections generates a great interchain cohesion. Although the chemical structure of cellulose is well known, its crystalline and fibrous structure is not yet completely elucidated. Cellulose is a semi crystalline fibrillar material. Crystalline domains and very organised solid states coexist with disordered amorphous regions (Figure I.3).

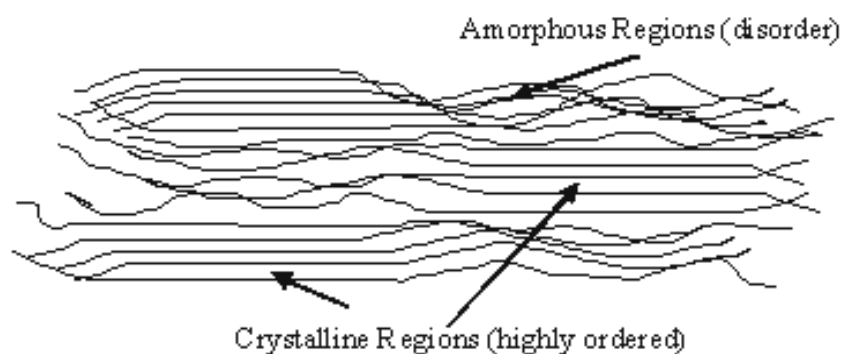


Figure I.3: Cellulose microfibril presentation [web site 1]

The crystalline parts have a structural role whereas the amorphous parts have viscoelastic properties. X-rays diffraction studies have enlightened the crystallographic structure of cellulose. However, the determination of the three-dimensional orientation of the cellulose chains has been and remains one major open question in the study of cellulose.

A cellulose fibre is made up of an assembly of crystallites having a common axis but random orientation. The absence in the diffractograms of reflexion (0,0,1) informs us of a helical symmetry of the polymeric chain. The variations of conformation depend mainly on glycosidic rotations around the bonds. The cellulose structure is a double helix with a periodicity of 10.36 Å. This conformation has a minimal energy due to the Van der Waal interactions and optimal anomeric effects.

The transmission electronic microscopy reveals that the microfibril is the basic crystalline element of native cellulose. According to their origin, the cellulose microfibrils have a diameter from 20 to 200 Å. They join to form larger fibres of ordered structure. Microfibrils composing fibres are organised in a helix. An example of a fibre structure (cotton and wood) is represented in Figure I.4.

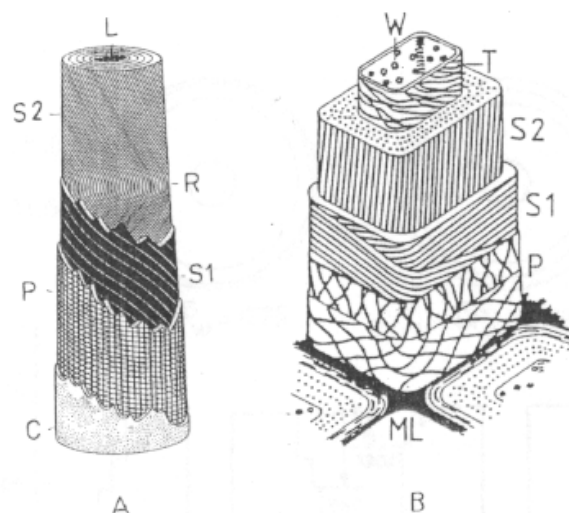


Figure I.4: Schematic representation of the structure of a cotton fibre (A) and wood fibre (B): C-cuticle (rich in pectins and waxes), L-lumen, ML-middle lamella (mainly lignin), P-primary wall, R-reversal of the fibril spiral, S1-secondary wall ('winding layer'), S2-secondary wall (main body), T-tertiary wall, W-wart layer [Krassig, 1996]

During the period of growth, the cotton fibres make only a thin cell wall, the so-called primary wall, which is only a few tenths of a micron thick and contains only approximately 5% of the cellulose matter constituting the fibre. The primary wall consists mainly of pectins and waxes. After completion of the growth in length, the thickness of the fibres' wall increases by the deposition of cellulose fibrils in a second relatively thick layer, the secondary wall, on the inner side of the primary wall. The central channel of the cell, the lumen, is narrowed but not completely filled. In trees, the second layer, S2, contains from 80 to 85% of the cellulose matter of the total wood fibre. The cellulose fibrils are positioned in an extended helix oriented in the direction of the fibre axis.

The wood fibres measure between 1 to 2 mm in length and 30 to 60 microns in diameter. These fibres are made up of microfibrils from 1 to 10 microns length and approximately 35 Å diameter. These microfibrils count themselves from 30 to 40 cellulose chains. The supramolecular organisation of cellulose in wood is represented in Figure I.5.

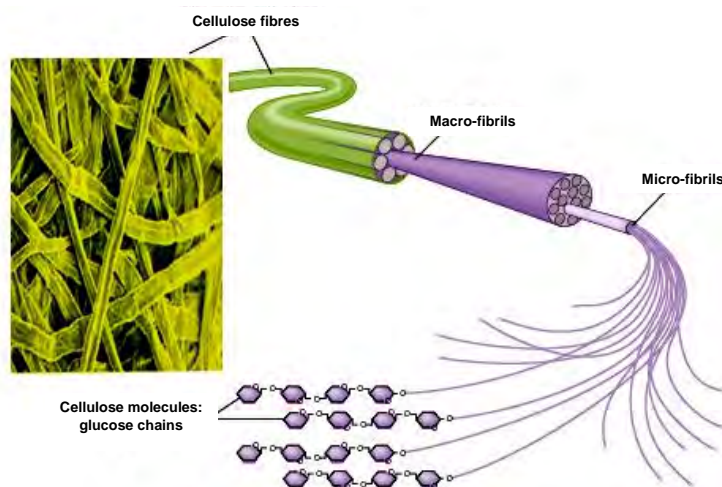


Figure I.5: Supramolecular organisation of cellulose [web site 2]

1.5 Polymorphs of cellulose

Four principal polymorphs of cellulose have been identified: I, II, III and IV [Atalla, 1985]. Under families exist within these allomorphs. Each one of these forms can be identified by its X-rays diffraction characteristics.

1.5.1 Cellulose I

Native cellulose commonly called cellulose I is the most abundant form of cellulose in nature. In 1928, Meyer et al proposed from X-rays diffraction data of ramie fibre a monoclinic unit cell of native cellulose with dimensions of 8.35Å for the a-axis, 7.0Å for the b-axis, 10.3Å for the c-axis and 84° for the γ -angle. The studies performed by Gardner [Gardner et al, 1974] showed that the native cellulose unit proposed by Meyer was satisfactory. However, in 1974 Gardner refutes the assumption of Meyer concerning the antiparallelism of the chains and concludes that the native cellulose chains are arranged parallel to one another, which was confirmed by Sarko and Muggli the same year [Sarko et al, 1974]. Herbert and Muller indicate that according to cellulose various origins, the native celluloses crystallise in different arrangements with different dimensions [Herbert et al, 1974].

In 1984, Vanderhaart and Atalla analysed the NMR spectra of carbon atom in the solid state (Figure I.6), and discovered the existence of two families constituting the native celluloses, named I_α and I_β .

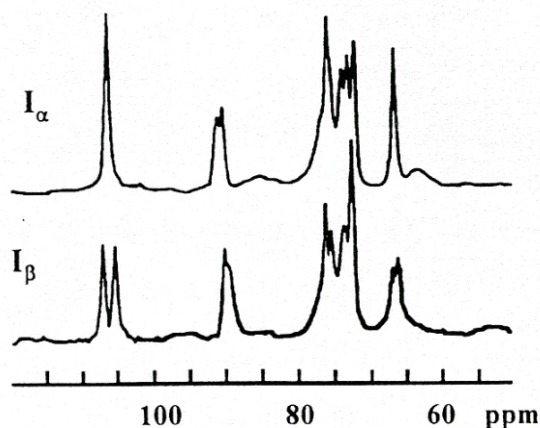


Figure I.6: NMR spectra of celluloses I_α and I_β . [Vanderhaart et al, 1984]

The molecular models of Sternberg et al (Figure I.7) established that crystalline arrangements correspond to two architectures with the lower energy resulting from the parallel association of the cellulose chains [Sternberg et al, 2003].

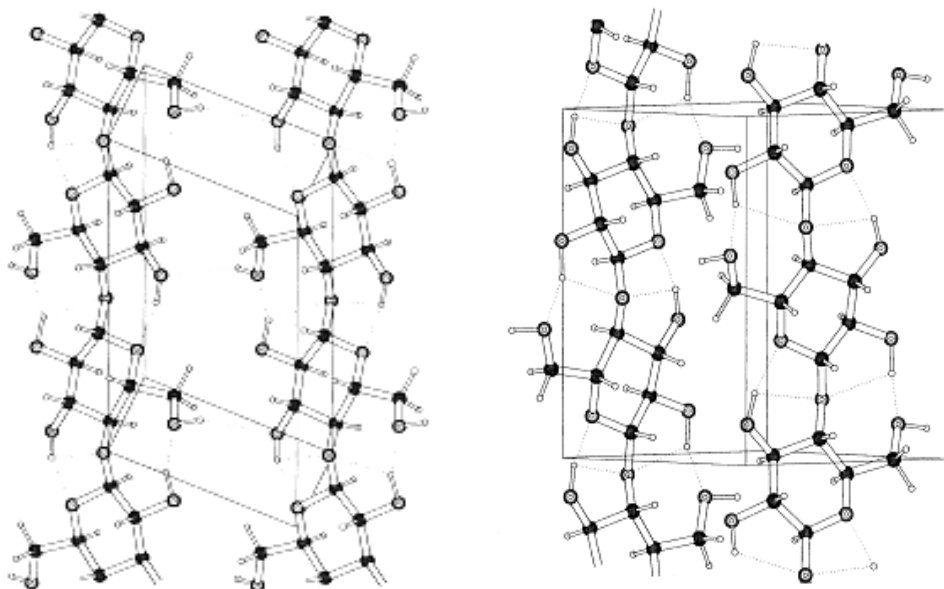


Figure I.7: Molecular models of cellulose I_{α} and I_{β} [Sternberg et al, 2003]

The wood and cotton celluloses as well as the shells of certain marine animals are made up mainly of allomorph I_{β} , whereas the primitive organisms, such as bacteria, are rich in I_{α} cellulose. The crystalline phases I_{α} and I_{β} are in various proportions depending of the origin of the cellulose [Atalla, 1999].

Allomorph I_{β} is thermodynamically more stable than I_{α} . Moreover, the crystalline transformation of the I_{α} phase into I_{β} is irreversible. The two forms I_{α} and I_{β} are arranged in a parallel way. According to Zugenmaier the cell crystalline parameters of allomorphic I_{β} are $a=7.85 \text{ \AA}$, $b=8.27 \text{ \AA}$, $c=10.38 \text{ \AA}$ and $\gamma=96.3^{\circ}$; the unit cell is a monocyclic group of P_{21} space. The unit cell of allomorph I_{α} is triclinic, of P_1 group space, its dimensions are $a=6.74 \text{ \AA}$, $b=8.93 \text{ \AA}$, $c=10.36 \text{ \AA}$ $\alpha=117^{\circ}$, $\beta=113^{\circ}$ and $\gamma=81^{\circ}$ (Figure I.8) [Zugenmaier, 2001].

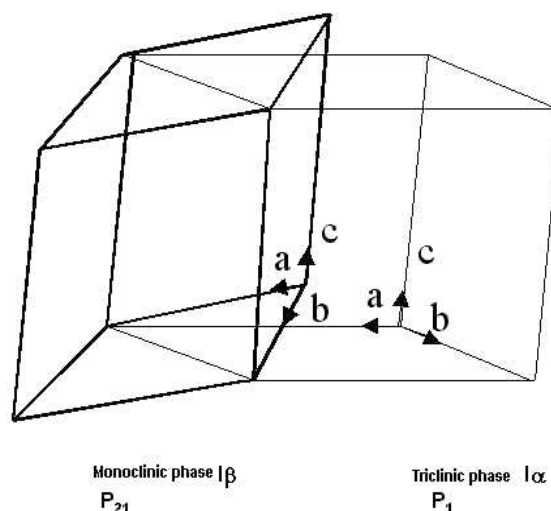


Figure I.8: Representation of monoclinic phase I_{β} and triclinic phase I_{α} [Zugenmaier, 2001]

1.5.2 Cellulose II

Cellulose II is obtained by two distinct processes: mercerisation (treatment with concentrated aqueous NaOH) or dissolution, both followed by regeneration. The different steps of mercerisation will be studied in the Chapter II. In order to obtain cellulose II from its native form, a soluble derivative should be prepared followed by regeneration; this is the case of viscose. The use of direct solvents of cellulose also allows the preparation of cellulose II: this is the case, for instance, of the processes using N-methyl morpholine oxide, NMMO, a direct solvent of cellulose, generally called Lyocell procedure.

Structure of cellulose II

The studies of Sarko et al [Sarko et al, 1974] and Kolpak et al [Kolpak et al, 1976] propose a model where the chains of cellulose II have a helicoidal symmetry of order 2, compatible with the existence of two intra and intermolecular hydrogen bonds (OH3' - O5 and OH2-O6' [2.5Å]). These bonds ensure the formation of layers composed of cellulose chains in the crystalline phase. This three-dimensional arrangement is characterised by the anti parallel orientation in the monoclinic unit cell with two chains whatever the transformation process of cellulose I to cellulose II. This arrangement was confirmed recently by the studies of neutron diffraction by Langan et al [Langan et al, 1999] and by Nishiyama and co-workers [Nishiyama et al, 2002]. Although cellulose II is very rare in nature, Kuga et al proposed a structure of type II in the case of native cellulose for a mutant strain of acetobacter xylinium [Kuga et al, 1993]. The crystalline model of cellulose II structure is presented in Figure I.9.

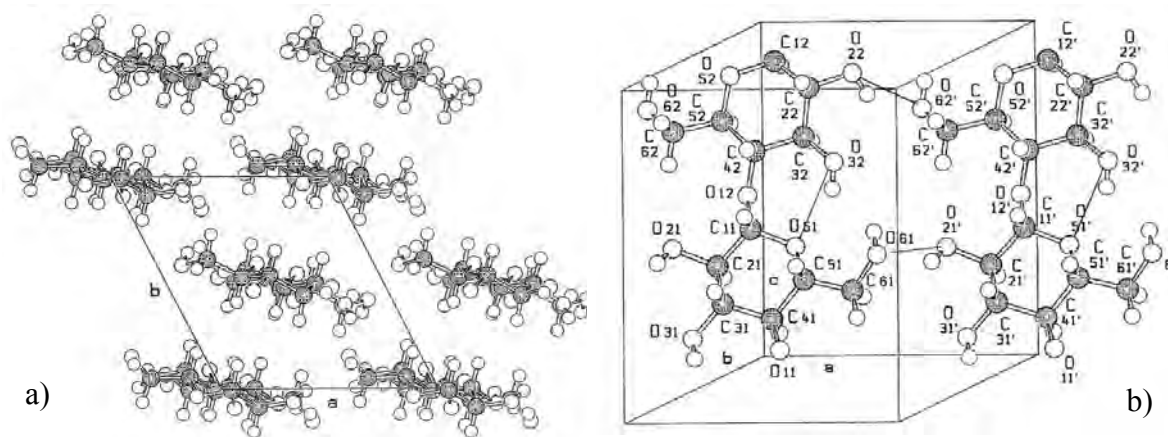


Figure I.9: Model of cellulose II: a) perpendicular projection to the (ab) plane and b) molecules in the crystallographic plane (010) [Zugenmaier, 2001]

Chanzy et al [GFP, 2000], through X-ray and neutrons diffraction methods, established the network of intermolecular and intramolecular hydrogen bonds in cellulose II. The structural model of cellulose II is presented in Figure I.10.

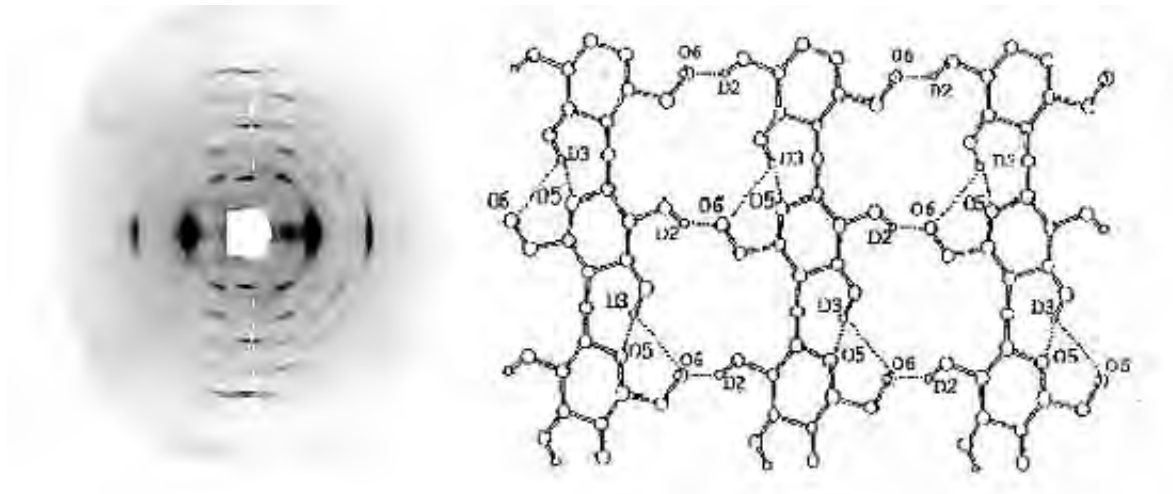


Figure I.10: X-ray diffraction diagram of cellulose II and its 3D structure. [Langan, 1999]

Polymorph II is energetically more stable than polymorph I. This is the reason why it is possible to convert cellulose I into cellulose II but not the contrary. The fibrillar arrangement of regenerated cellulose differs somewhat from the one of native cellulose, as arrangement in distinct layers does not exist. In the same way, the helicoidal structure, which exists in the cellular walls of native cellulose, does not exist in precipitated or regenerated cellulose fibres.

The structure of cellulose I chains differs from the one of cellulose II. Whereas the chains of cellulose I are all parallel, those of mercerised or regenerated celluloses are antiparallel. The X-rays diffractograms of the two polymorphs of cellulose (cellulose I and cellulose II) are represented in Figure I.11.

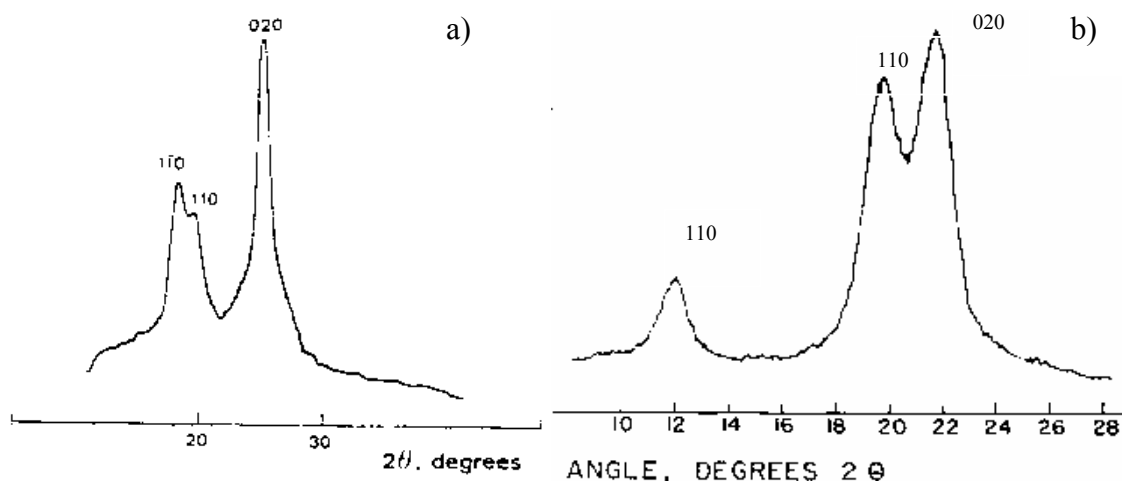


Figure I.11: X-ray diffractograms of two polymorphs of cellulose: a) cellulose I [Chanzy et al, 1983] and b) cellulose II [Nelson et al, 1964]

In the case of cellulose precipitated from solutions, the cellulose crystals are relatively small and are randomly distributed in a semi-amorphous matrix. In man-made cellulose fibres, the crystallites are always aligned in their longitudinal axis along the direction of stretch, i.e.

along the length and the axis of fibre. The degree of orientation depends mainly on the degree of stretch applied in the post-treatment during fibre processing [Krassig, 1996].

1.5.3 Cellulose III

A treatment with ammonia or with certain amines as the ethylene diamine EDA allows the preparation of cellulose III either from the cellulose I (which leads to cellulose III₁) or from the cellulose II (which leads to cellulose III₂). Sarko et al proposed a model of structure in which the cellulose chains do not have symmetry exactly of order 2 [Sarko et al, 1976].

1.5.4 Cellulose IV

Cellulose III, heated at high temperatures in glycerol, is transformed into cellulose IV. There are two forms: cellulose IV₁ and cellulose IV₂ obtained from cellulose III₁ and III₂, respectively. Cellulose IV is a disordered form of cellulose I, which explains why it can be found in X-ray diffractions for native cellulose of some plants. Gardiner and Sarko [Gardiner et al, 1985] have established by X-rays diffraction the crystalline unit cell of these two polymers: for allomorph IV₁ a= 8.03 Å, b = 8.13 Å, c = 10.34 Å and for allomorph IV₂ a= 7.99 Å, b = 8.10 Å, c = 10.34 Å. These authors suggest a space group of type P1.

The Table I.3 presents the dimensions of elementary unit for principal polymorphs of cellulose.

Type	Unit (Å, °)					
	α	β	γ	a	b	c
I _{α}	117	113	81	6.74	5.93	10.36
I _{β}	90	90	96.3	7.85	8.27	10.38
II merc.	90	90	117.1	8.10	9.05	10.31
III ₁	90	90	122.4	10.25	7.78	10.34
IV ₁	90	90	90	8.03	8.13	10.34
IV ₂	90	90	90	7.99	8.10	10.34

Table I.3: Unit cell dimensions of cellulose polymorphs [Zugenmaier, 2001]

The relations between these different polymorphs are schematically summarised in Figure I.12.

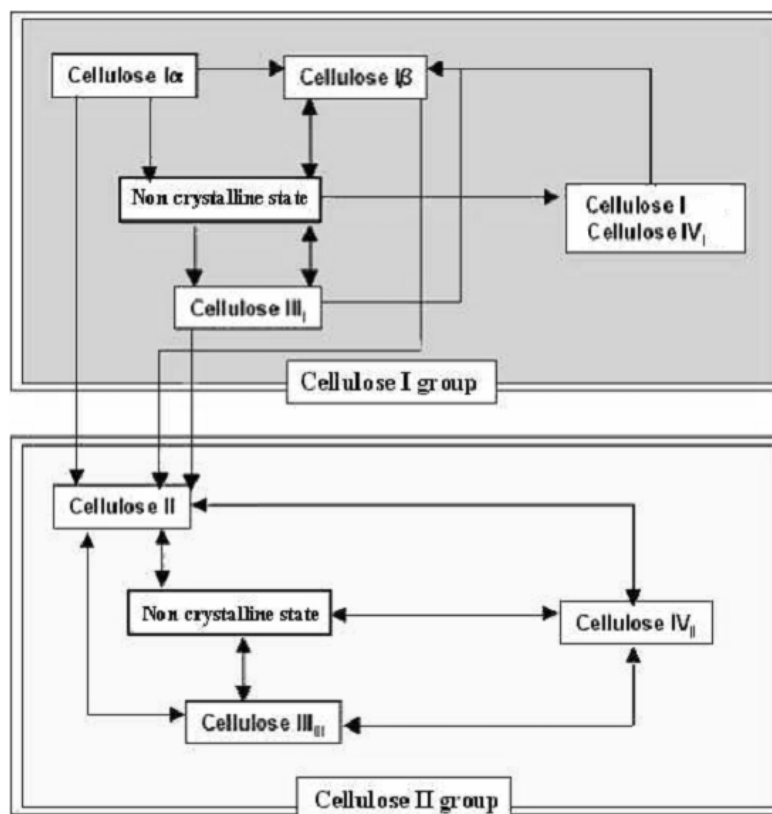


Figure I.12: Schematic representation of relations that link cellulose polymorphs [GFP, 2000].

The free hydroxyl groups of cellulose forming intra and inter molecular hydrogen bonds explain the various crystalline arrangements. The density of the crystalline phase is of 1.59 g.cm^{-3} but, when determined for natural samples, is of the order of 1.55 g.cm^{-3} , meaning that 70% of the sample is composed of crystalline phase.

The degree of crystallinity depends on the origin and the treatment applied to cellulose. It can be estimated by infrared spectrometry according to the relative intensity of certain bands. The various crystalline states of cellulose thus vary according to the arrangement of the intermolecular hydrogen bonds, the parallel or antiparallel position of the cellulose chains and the parameters of crystalline unit.

2 Cellulose processing

2.1 Cellulose solvents

Due to its strong intramolecular hydrogen bonds, cellulose is insoluble in most common solvents. A literature study reveals a rather restricted number of solvents for cellulose:

- Solvents containing a lithium halide like lithium chloride or lithium bromide used in the presence of N, N-dimethylacetamide (DMA). The lithium chloride can be associated with various solvents (DMSO, 1-methyl-2-pyrrolidone (NMP), 1,3-dimethyl-2-imidazolidinone (DMI)). To decrease the energy contribution necessary to rupture the intra- and intermolecular bonds, it is possible to pre-treat the cellulose by solvent exchange water/methanol and later with methanol/DMA. It is necessary to use

methanol as intermediate solvent between water and the DMA because cellulose is linked to water molecules by hydrogen bonds. The exchange allows not to exceed temperatures of 80°C during the dissolution phase [Dupont, 2003].

- Copper complexes like cuprammonium hydroxide and cupriethylenediamine and the cadmium complexes such as cadoxene can be employed as solvents of cellulose. Cellulose forms a complex with the metal ion [Jayme, 1971].
- Aqueous solvents: very concentrated aqueous solutions of acids (sulphuric, nitric, phosphoric, etc [Fadeeva et al, 2003]), or bases (potassium, hydrazine, etc). The action of the strong mineral bases such as lithium or sodium hydroxide in aqueous solution on the cellulose (mercerisation) leads to the formation of alkali-cellulose. Very strong salt compounds like sodium iodides or zinc chlorides are also solvents of cellulose. In 1939 Sobue built a phase diagram of cellulose dissolution in NaOH [Sobue et al, 1939] showing that cellulose can be dissolved in 7-10% aqueous NaOH. Recently, in 1998, Isogai and Atalla have taken up again the dissolution in this alkali conditions and developed a dissolution process based on aqueous NaOH distinctive for its simplicity and low-cost energy requirement [Isogai and Atalla, 1998]. The NaOH process is described in Section II.2.3.
- Tertiary amines oxides are also solvents known to dissolve cellulose. They have the property of not causing degradation of cellulose. Moreover, they have a strong power of solvation and are not very toxic. Chanzy et al [Chanzy et al, 1983] have studied the swelling and the dissolution of cellulose fibres in N-methylmorpholine-N-oxide (NMMO)-water system. Authors have demonstrated that according to the water concentration, cellulose fibres can be dissolved or can only swell. They defined water concentration areas in which interactions with native cellulose are irreversible (A et B), reversible (C) or non-existent (D) (Figure I.13). Cellulose can be dissolved in aqueous NMMO without swelling above 70°C in a narrow range of water concentration [12%-18%] (A).

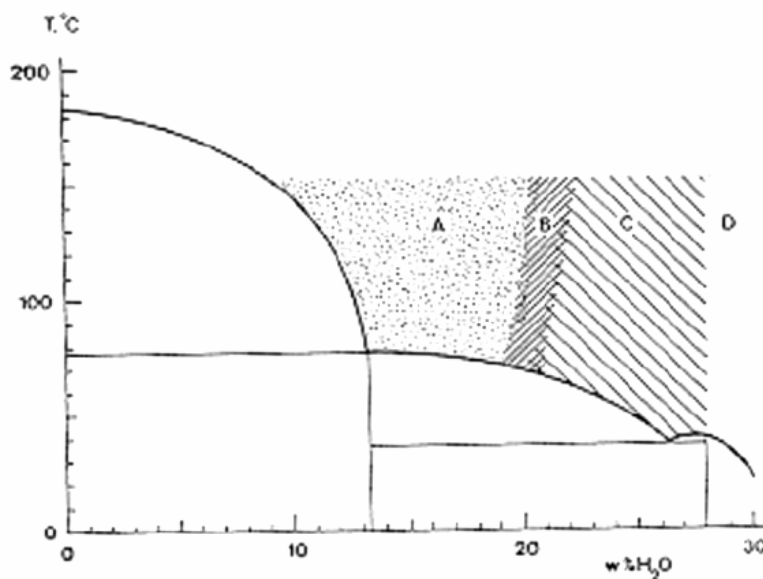


Figure I.13: Phase diagram of cellulose-NMMO aqueous system for different water concentrations and temperatures, dissolution without swelling (A), irreversible swelling (B), reversible swelling (C) non activated zone (D) [Chanzy et al, 1983]

The system NMMO-cellulose is solid at ambient temperature; it becomes liquid when it is heated above 70°C. The fibres obtained by the Lyocell processes are obtained by using N-MMO which is a recyclable organic solvent [Rosenau et al, 2003]. The Lyocell process is described in Section I.2.2.2.

- Ionic liquids are a new class of “green” cellulose solvents. Most of these organic salts are liquid at temperature lower than 100°C. They have a good thermal and chemical stability, a low toxicity and they are non volatile solvents. Cellulose can be directly dissolved in some hydrophilic ionic liquids, such as 1-butyl-3-methylimidazolium chloride (BMIMCl) and 1-alkyl-3-methylimidazolium chloride (AMIMCl) [Swatloski, 2003]. The ability of the ionic liquids to dissolve cellulose varies significantly with the size and the polarization of the anions present and also with the nature of the cation. Chloride-containing ionic liquids appear to be the most effective solvents, presumably solubilizing cellulose through hydrogen-bonding from hydroxyl functions to the anions of the solvent. Zhu et al, [Zhu et al, 2006] have prepared solutions containing up to 25 wt % cellulose in BMIMCl under microwaves heating that accelerates the dissolution process. The higher the chloride concentration, the faster the dissolution and the higher the solubility. Ionic liquid is a new emerging class of cellulose solvents. However, one of the drawbacks of these solvents is their expensive price.

The majority of the solvents cited above cause an important decomposition of cellulose. Moreover, to be used at an industrial scale, cellulose solutions should be prepared under moderate temperatures conditions (<100°C), must be non toxic and non polluting, recyclable, must not degrade cellulose and allow regeneration, and finally it must be of low cost. Among the solvents listed, ionic liquids, NMMO and sodium hydroxide in aqueous solution fulfil the desired industrial requirements.

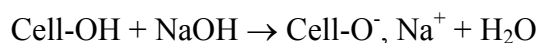
2.2 Main ways of cellulose processing

The viscose process is one of the most industrially used processes nowadays but it is very polluting. Therefore, research on new direct solvents of cellulose is continuously ongoing. In the recent years, the Lyocell process based on NMMO was developed. Aqueous sodium hydroxide solution is another direct cellulose solvent; it was recently considered as a prospective one. Cellulose processing using the two last solvents are described below in details because they are the ones used in the preparation of Aerocellulose.

2.2.1 Viscose process

The viscose process was discovered by the English chemists Croos, Bevan and Beadley in 1892. It is a batch processing.

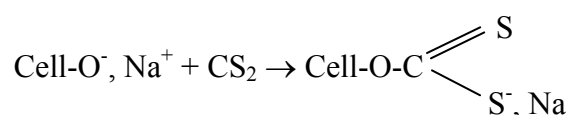
At the beginning, cellulose pulp is immersed in 17-24% aqueous sodium hydroxide (NaOH) solution at a temperature in the range of 18 to 25°C in order to swell the cellulose fibres and to convert cellulose to alkali cellulose. This is the mercerisation step.



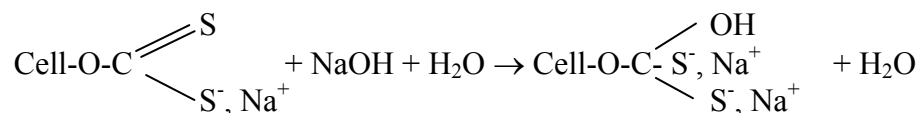
This step is necessary to break down the crystalline sections in the cellulose fibrils and realise the ensuing reaction to form cellulose xanthate. This step and the influence of sodium hydroxide on cellulose will be discussed further in the chapter II.

Then, the swollen alkali cellulose is squeezed and shredded mechanically to remove the excess of caustic soda solution and to yield finely divided, fluffy particles called "crumbs". This step provides increased surface area of the alkali cellulose, thereby increasing its ability to react in the next steps. The alkali cellulose is aged in order to depolymerise cellulose macromolecule to the desired degree of polymerisation. The crumb in contact with the oxygen is partially oxidised and degraded to lower molecular weights.

Then the aged crumb is placed into a mixing vessel and treated with gaseous carbon disulfide (CS₂). The alkali cellulose reacts with the CS₂ to form cellulose xanthate; the degree of substitution depends on the crystal form of the starting material.



The carbon disulfide also reacts with the alkaline medium to form inorganic impurities, which give the cellulose mixture a characteristic orange colour. The orange crumb is then dissolved in aqueous caustic solution.



Because the cellulose xanthate solution has a very high viscosity, it has been termed "viscose". The reversible xanthation reaction allows some of the xanthate groups to revert to cellulosic hydroxyls and free CS₂. This free CS₂ can then escape or react with other hydroxyl groups on other parts of the cellulose chain. In this way, the ordered or crystalline regions are gradually broken down and a more complete dissolution is achieved.

The next step is the spinning of the viscose solution, which is pressed through a spinneret into a spin bath containing aqueous sulphuric acid, sodium sulphate and zinc sulphate. Once the cellulose xanthate is acidified and neutralised, rapid coagulation of the rayon (fibres obtained from viscose process) occurs. This transformation of cellulose xanthate leads to regenerated cellulose. The freshly regenerated rayon includes many salts and other water-soluble impurities, which are removed during various purification baths. Then the filaments are dried. The result is the formation of fine filaments of cellulose, or rayon.

Stretching and decomposition are crucial for getting the desired tenacity and other properties of rayon. Slow regeneration of cellulose and stretching of rayon will lead to greater areas of crystallinity within the fibres, as is done with high-tenacity rayons.

The production of viscose causes significant environmental and economical problems because of the considerable air and soil pollution by carbon disulfide and by-products, hydrogen sulphide and heavy metals.

2.2.2 Lyocell process

To mitigate the environmental problems encountered with the viscose process, an alternative process has been developed to find another direct solvent of cellulose. Tertiary amine oxides were the ones of the most promising approaches to dissolve cellulose. It turned out that the N-methylmorpholine-N-oxide (NMMO, Figure I.14) was the most interesting among amine oxides from the economical as well as ecological points of view. NMMO is produced by the oxidation of the ternary amine *N*-methylmorpholine (NMM) with hydrogen peroxide at 150°C.

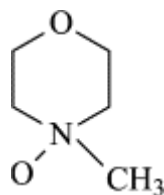


Figure I.14: Schematic structure of the NMMO (N-methylmorpholine N-oxide) solvent

Due to the high polarity of the N–O bond, the oxygen of this group is able to form one or two hydrogen bonds with hydroxylated substances such as cellulose. NMMO leads to a very good solubilisation of cellulose without prior derivatisation [Rosenau et al, 2003].

The Lyocell process was studied at the beginning of the 1980s and has been developed on large industrial scale for cellulosic fibres production in the last decade of the 20th century. There are three types of cellulose fibres obtained starting from NMMO: the Lenzing Lyocell fibres (produced by Lenzing AG), Newcell (produced by Akzo Nobel) and Tencel (produced by Courtaulds). Lyocell is an appropriate generic name for these manufactured fibres from regenerated cellulose since the NMMO solvent systems exhibits some of the characteristics of a lyotropic (solution concentration dependant) liquid crystalline solution. Today, the annual production of Lyocell fibres is approximately 100 000 tons.

The Lyocell process is a dry jet-wet spinning process. It takes place at elevated temperature between 80°C and 120°C. The following steps characterise the manufacture of cellulose-regenerated fibres by NMMO-route:

First, the wood pulp is dissolved in water-NMMO mixture. The solutions have composition of 8-20% cellulose, 75-80% NMMO and 5-12% water. Then the highly viscous solution is extruded through an air gap into a precipitation bath, which is usually water or aqueous NMMO. The next step is the regeneration of cellulose fibres in the precipitation bath. Then fibres are washed, dried, cut and packed. The NMMO is recovered from the precipitation and washing baths. The process is represented schematically in Figure I.15. Each of these production steps allows variation of the final structure of fibres and their properties. Depending on the spinning conditions applied, difference in density, crystallites size, crystallite and fibrillar and pores number can be observed.

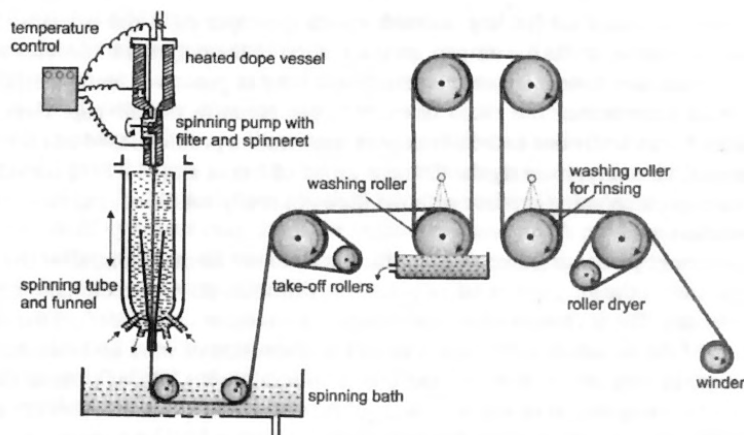


Figure I.15: Diagram of the spinning process of fibres from the cellulose NMMO solutions [Fink et al, 2001]

The cost of the Lyocell solvent is offset by the greater than 99% recovery and reuse, causing the production cost of Lyocell fibres to be similar to that of producing viscose rayon fibres. Moreover, NMMO is completely biodegradable by ubiquitous soil bacteria. In relation to the traditional viscose production, the Lyocell process consists in a lower number of process steps.

Lyocell process is an environmentally friendly process, which opens up new perspectives for the production of cellulose fibres, films, and other cellulose materials. Compared to viscose fibres spun from derivatised cellulose, the fibres produced from cellulose–NMMO solutions have a different structure; they are characterised by high dry and wet strength, dimensional stability, with high fibrillation, good dye ability and excellent processing properties. However, some environmental issues remain unsolved, for example, the presence of undesired (explosive) by-products and some problems with efficient recovery of the expensive solvent [Rosenau et al, 2001].

2.2.3 NaOH process

In 1992, a new type of cellulose fibres for textile applications has been developed by using aqueous caustic soda as a solvent [Yamashiki et al, 1992]. The new class of fibres was prepared using the 7-10% NaOH as cellulose solvent, by wet spinning method with aqueous H_2SO_4 as a coagulation bath. In most cases the temperature of the cellulose–NaOH–water solution is lower than $15^\circ C$ because higher temperature induces gelation of these solutions. The mechanical properties of new fibres are almost of the same range as the viscose rayon. The advantages of aqueous sodium hydroxide are that it clears up the environmental issues. It is one of the cheapest solvents of cellulose. In comparison with the viscose process, it reduces the cost induced by the purchase of chemical product necessary to the transformation of native cellulose into cellulose II, it avoids the recovery of released gas and strongly decreases the cost of water treatment.

Chen et al [Chen et al, 2006] have prepared regenerated cellulose fibres by dissolution of cotton linter pulp in NaOH (9.5 wt %) and thiourea (4.5 wt %) aqueous solution followed by wet-spinning and multiroller drawing. The schematic diagram of the pilot scale spinning machine is presented below:

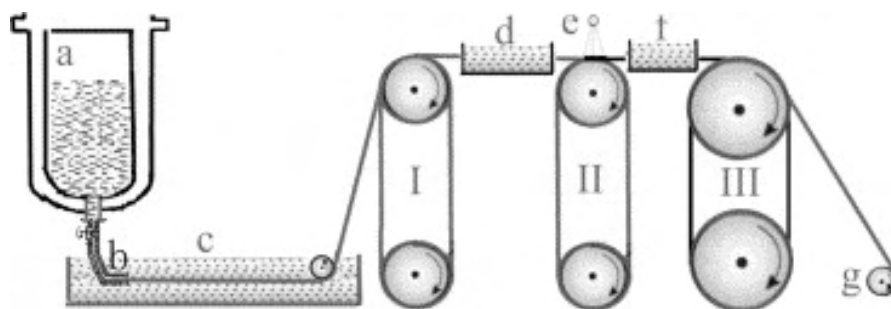


Figure I.16: Schematic diagram of the pilot scale spinning machine: (a) a pressure extruder with a stainless cylinder having a cooling jacket; (b) filter and spinneret; (c) first coagulation bath; (d) second coagulation bath; (e) hot water washing; (f) third post-treatment bath (plasticizing bath); (g) take-up device; (I) and (II) Nelson-type rollers; (III) heated roller [Chen et al, 2006]

The first coagulation bath contains 10 wt% NH_4Cl and 4 wt% H_2SO_4 in aqueous solution; the second coagulation bath contains 5 wt% H_2SO_4 in aqueous solution. The wet spinning process was coupled with drawing stages after treatments in three different baths: coagulation (I), (II) and post-treatment (III).

Rom et al [Rom et al, 2006] have also prepared new cellulose fibres, called Biocelsol, based on direct cellulose solubilisation in sodium hydroxide solutions. In this process, the original pulp was mechanically shredded and thereafter treated by commercial enzymes. The enzyme-treated cellulose was dissolved in 7.6 wt % NaOH water solution and then extruded in acidic coagulation bath. Enzyme-treated cellulose fibres were first regenerated in 5-20% H_2SO_4 - 10-15% Na_2SO_4 and then in cold and hot water baths. Biocelsol fibres present the same characteristics as viscose ones, except that their tenacity is slightly lower than the one of typical cellulose man-made viscose fibres.

As far as the properties of aqueous cellulose- NaOH solutions are not well understood yet, its wet spinning process has still not been fully optimised; some improvements concerning the low chain orientation and the tenacity of cellulose fibres should be performed. In general, the lower cost and toxicity of this alkali solvent system and its relative ease for wet spinning exhibited some prospectives for the development of a new more economical and environmental friendly process of the production of cellulose fibres.

2.3 Regeneration

As it was mentioned in the previous section, the regeneration of cellulose is an important stage in the formation of cellulose structure. “The regeneration of cellulose” means precipitation or coagulation of the cellulose when introducing cellulose solution into a non-solvent liquid. During cellulose coagulation in a non-solvent bath, the non-solvent penetrates into the cellulose meanwhile the solvent of cellulose is released outside the cellulosic sample into the regenerating bath. Following the solvent/non-solvent exchange, the cellulose is in a swollen state. It is expected that the regeneration of cellulose-NMMO or NaOH -water solutions follows the well-known principle of phase separation in polymer solutions valid in such a shaping process as membrane formation. This point is explained in section I.3.2. We will focus here on the regeneration of cellulose-NMMO-water solutions because there are

very few publications on the regeneration process for objects made from cellulose-NaOH solutions.

Fink et al have represented the phase diagram at 100°C of the system cellulose-NMMO-water (Figure I.17).

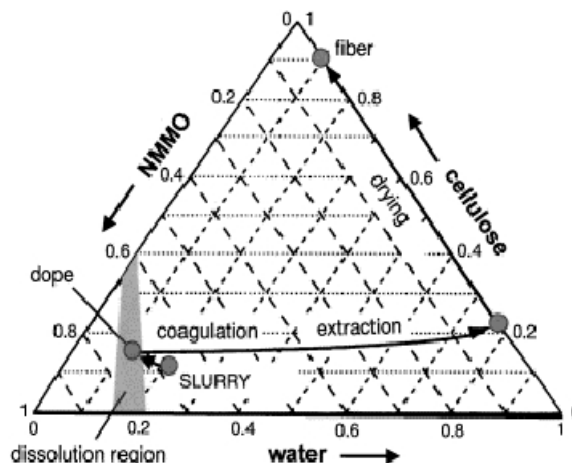


Figure I.17: Phase diagram of cellulose–NMMO–water system [Fink et al, 2001]

The composition changes are presented in the form of a pathway through the phase diagram, in Figure I.17. The small region in grey indicates where cellulose is completely dissolved in the highly concentrated NMMO. The exchange of solvent against non-solvent, e.g. water, in the spinning ray leads to a desolvation of the cellulose molecules and to a re-formation of intra and intermolecular hydrogen bonds. Polar liquids, like water, cause the removal of the solvent. During the coagulation of the cellulose solution, the NMMO molecules attract the precipitant molecules and the desolvation of the cellulose molecules occurs. These processes lead finally to the formation of a highly swollen cellulose in fibrillar or two-dimensional form [Fink et al, 2001].

Laity et al [Laity et al, 2002] have followed the coagulation of cellulose from NMMO-cellulose-water solution into water regenerating bath using NMR. Coagulation occurs in several stages. The first stage of coagulation involves diffusive exchange of water and NMMO, in the cellulose. This process occurs relatively quickly, near the cellulose/water interface, and a large composition change is indicated within the first 30s. However, deeper within the cellulose sample, the exchange takes place more slowly and the rise in water content appears to precede the decrease in NMMO content. Laity et al have observed that the NMMO diffusion coefficients towards the regenerating bath and of water towards cellulose-NMMO are identical: about $(0.135 \pm 0.01) \cdot 10^{-3} \text{ mm}^2/\text{s}$. Authors suggested a spinodal decomposition mechanism of phase separation.

The thesis of O.Biganska [Biganska, 2002] corroborates these results. She had demonstrated that the higher the initial cellulose concentration in cellulose+NMMO solution, the weaker the NMMO diffusion coefficient from cellulose-NMMO solution towards the water bath. The non-solvent diffusion coefficient from the regenerating bath towards the cellulose+NMMO samples does not depend on the cellulose concentration. She had established that the diffusion coefficient of the non-solvent is higher than the diffusion coefficient of the solvent (NMMO). Non-solvent thus penetrates into the cellulose+NMMO more quickly than the solvent is

leaving. It appears that the higher the NMMO concentration in the regenerating bath, the lower both diffusion coefficients [Biganska et al, 2005].

In 1983, Dube et al. estimated the time of phase separation during the regeneration of Lyocell fibres at 150 ms [Dube et al, 1983]. Mortimer gives a value of 1-2s for the complete coagulation of a fibre of 50 μm [Mortimer et al, 1996].

Zhang et al described the coagulation process of cellulose/NaOH/urea system in aqueous sulphuric acid solution from 1 to 15 wt% [Zhang et al, 2005]. According to them, when cellulose solution contacts the coagulant, a counter diffusion and chemical neutralisation process occurs between solvent in the cellulose solution and non-solvent in the coagulant bath. The coagulant penetrates into the cellulose solution, leading to a physical cross-linking network caused by a self-association of cellulose macromolecules, in which its hydroxyl groups act as junction. The authors suggested that the mechanism of coagulation is based on a two phases separation, namely a cellulose rich phase in the swollen cellulose and a poor cellulose phase in solution.

3 Porosity of cellulose materials

3.1 Porosity of regenerated fibres

In 1983, Dube et al described the structure of regenerated fibres from the Lyocell process as being fibrillar and porous [Dube et al, 1983]. Schurz and Lenz proposed a model of the structure of an elementary unit of regenerated fibre produced by Lyocell process [Schurz et al, 1994]. The structure of the fibre consists in five different zones (Figure I.18): crystallites (A), amorphous zones (B), zones connecting the amorphous zones laterally (C), crystallite aggregates (D) and pores (E).

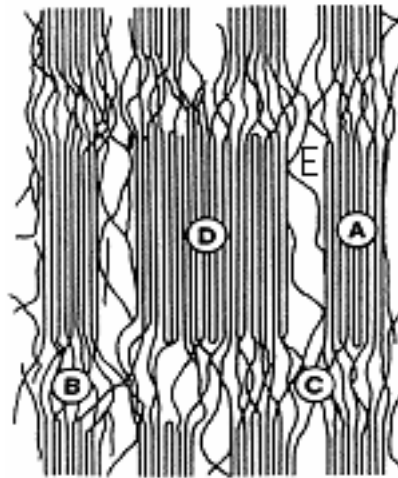


Figure I.18: Structure of a Lyocell fibre: crystallites (A), amorphous zones (B), zones connecting the amorphous zones laterally (C), crystallite aggregates (D) and pores (E) [Schurz et al, 1994]

Schurtz pointed out that the pores volume fraction in a fibre spun by NMMO process has an approximate order of 10^{-4} - 10^{-3} . He noted that extended pores between the elementary microfibrils are responsible of the great tenacity of regenerated fibres produced by the Lyocell process.

In 1988, Romanov et al also described the existence of a porous structure in cellulose fibres prepared from Lyocell process but the cellulose-NMMO-water solutions were coagulated in isopropanol bath [Romanov et al, 1988]. They noticed that an increase of temperature from 25°C to 35°C reduces the viscosity of the polymeric system and increases the cellulose fibres porosity. The formation of macrovoids was also detected in regenerated cellulose. Authors observed that the kinetics of macrovoids growths depends on the temperature of the regenerating bath.

Fink [Fink et al, 2001] characterised the structure of fibres obtained from the Lyocell process precipitated in water as dense and crystalline, having strongly oriented amorphous chain segments. The voids present in the microfibrils have a size, which varies between 5 and 100 nm. The structure of Lyocell fibres is uniform throughout the cross-section, except for a small boundary layer with highly densified material. It was noticed that an increase in coagulation bath temperature increases the size of the pores. Textile viscose fibres have a skin-core

structure with larger voids (around 25-150 nm) in the core region and a densified skin layer which is about 1.5-2.5 μ m thick with pores of about 2-25 nm.

Fink used several liquids for the regenerating baths, in particular several alcohols, in order to compare the structure of fibres regenerated in alcohols with the ones regenerated in water (Figure I.19).

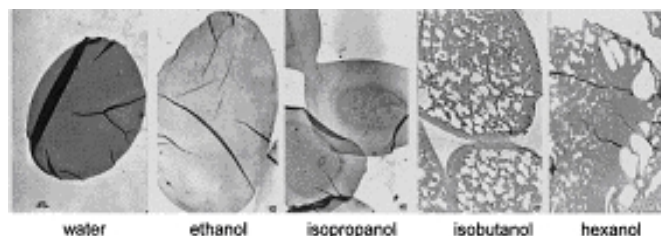


Figure I.19. Transmission electron microscopy images of cross-section of NMMO-type fibres precipitated in different alcohol media [Fink et al, 2001]

It appears that fibres precipitated in ethanol have a structure similar to the ones precipitated in water. As a small morphological difference, authors found only a slightly decreasing network density towards the centre of ethanol-precipitated fibre. As compared to the precipitation media water and ethanol, isopropanol leads to a distinct skin-core structure of the fibre. The core structure is less compact and contains pores up to the range of microns. The more densely structured outer zone contains smaller pores of about 15-60 nm and is surrounded by a thin layer of further increased density. In the case of regeneration in isobutanol, the interior of fibres is characterised by the presence of large pores of diameter reaching 300 nm. For fibres precipitated in hexanol the structure is a very loose and uneven, void exist with diameter up to the micron scale. The more the molecular weight of alcohols increases, the more the orientation of fibres and the breaking strength decreases. However, an increase of the alcohols molecular weight lowers the fibrillation tendency, particularly in the cases of pentanol and hexanol. Therefore, the conditions of precipitation are of a great importance for controlling the porosity and structure of the fibres.

3.2 Porous cellulose membranes

In the last 30 years, cellulose membranes have attracted a lot of research and practical interest because of their chemical stability, low cost, good biological compatibility, good mechanical performance and their remarkable hydrophilic properties. Commercial applications of these biodegradable membranes are mainly in the separation field, dialysis technologies, medical application, food processing, etc. In the separation field, cellulose membranes are more and more developed and used as column packing in liquid chromatography, such as gel filtration, ion-exchange or affinity chromatograph. These membranes are also used for the purification of organic solvents, concentrated alcohols and for the contamination inspection of such solutions. They are also used in enzymology, in hydrochemistry and for dust measurements.

Each application demands specific requirements on the morphology and structure of the membrane. The micro porous structure is important as it is related to trans-membrane flow of water and sieving properties for macromolecules. For microfiltration and ultrafiltration membranes, the porosity and pore sizes of the membrane determine the efficiency of

filtration. For gas separation, the selectivity and the permeability of the membrane material determine the efficiency of the gas separation.

During the last three decades, different techniques have been proposed to generate selective permeable membrane. The most used are called phase inversion techniques based on the phase separation of polymer solutions, producing porous polymer membranes. In general, three components are necessary for the phase inversion process: a polymer (P) (in our case cellulose), a solvent (S) and a non-solvent (NS).

The phase separation mechanisms can generally be subdivided in three main categories depending on the parameters that induce demixing:

- Temperature induced phase separation (or TIPS): when changing the temperature at the interface of the polymer solution, heat is exchanged and demixing is induced.
- Reaction induced phase separation (RIPS): the phase separation occurs when the polymer solution is subjected to a reaction.
- Diffusion induced phase separation (DIPS), which is the most used technique. Three types of techniques were developed to achieve DIPS:

- a) Precipitation with non-solvent vapour,
- b) Evaporation of solvent and
- c) Immersion precipitation into a non-solvent bath.

When contacting a polymer solution with a vapour or liquid, the mass exchange due to diffusion leads to a change in the local composition of the polymer solution and demixing can be induced.

Most of the samples described in this thesis are based on ternary solvent/non-solvent/cellulose system and have been prepared by immersion precipitation. For this reason the phase separation process by immersion precipitation is discussed thereafter in more details.

A polymer solution is immersed in a (polymer) non-solvent bath and a mass transfer process involving interchange of solvent/non-solvent occurs. The ternary phase diagram non-solvent/solvent/polymer (Figure I.20) describes the possible composition paths. The latter are determined by mass transfer models used to describe the diffusion process. During the process of immersion precipitation, a polymer solution will start on the polymer-solvent axis and when it is immersed in a non-solvent bath it will follow a specific composition path from its original point on the ternary diagram non-solvent/solvent/polymer to its final composition.

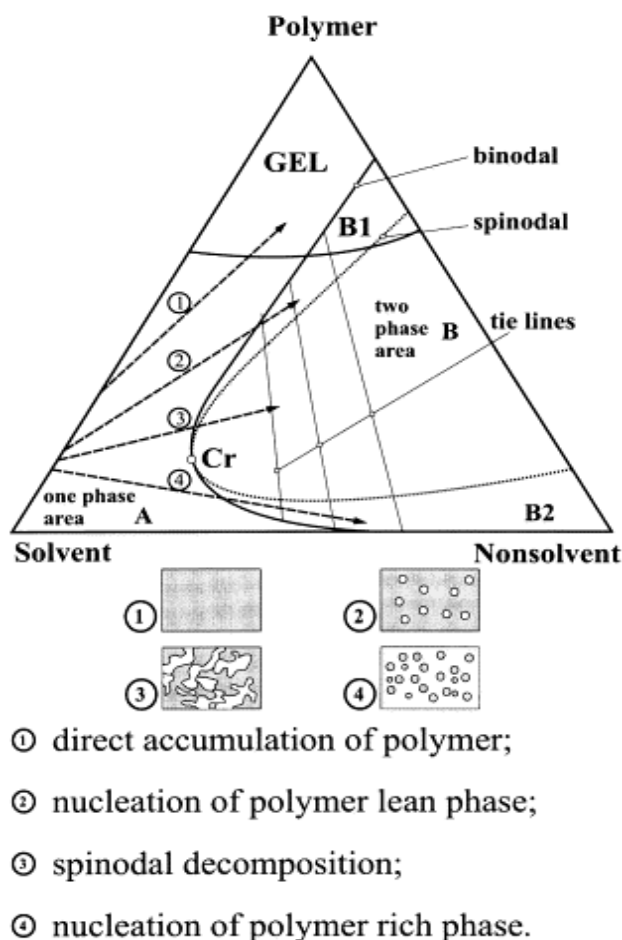


Figure I.20: Ternary phase diagram of a polymer/solvent/non-solvent system with various composition paths indicated by arrows and numbers; membrane structures, composition paths and modes of phase separation are correlated [Stropnik et al, 2000]

The binodal curve separates the two-phase region from the one phase region, with rich and lean polymer phases, which have their compositions given by the tie lines. It corresponds to the liquid–liquid demixing gap. The spinodal curve represents the line where all possible fluctuations lead to instability. The region between binodal and spinodal corresponds to metastable compositions where phase separation by nucleation and growth takes place. The point where binodal and spinodal coincide is called the critical point (Cr). For a monodisperse polymer this point is located at the maximum of binodal. Depending on the polymer concentration, liquid-liquid demixing proceeds according to different mechanisms.

At high polymer concentrations (1), phenomena such as vitrification, crystallisation or gelation can occur in the polymer solution and lead to a direct accumulation of the polymer. “Direct accumulation of polymer” is the first mode of primary mass transport. In the very first moment of the cast solution–coagulation bath contact, the non-solvent/polymer interaction causes a retreat of the coiled polymer molecules from the contact area into the interior of the cast solution. The retreatment of further polymer molecules leads to the accumulation of polymer. When accumulation exceeds a certain concentration, the solidification of the accumulated polymer takes place. This results in a dense morphology with little or no porosity. Compositions between the binodal and spinodal curves (B1 and B2) are metastable; the solution is stable with respect to small fluctuation in the composition. If the precipitation path crosses the binodal above the critical point (2), nucleation of the polymer lean phase may

occur, which results in the formation of liquid-filled pores in the continuous polymer matrix. On the other hand, if the precipitation path crosses the binodal below the critical point (4), nucleation of a polymer rich phase may initiate the phase separation process. If the phase separation occurs in the unstable region of the phase diagram bounded by the spinodal line (3), the solutions demix immediately by spinodal decomposition via the formation of a bicontinuous interwoven network of polymer and non-solvent.

Two types of demixing processes exist: instantaneous demixing, which occurs in less than one second, and delayed demixing. This difference in demixing ultimately leads to a difference in membrane morphology. In the case of instantaneous demixing, the top layer of the membrane often consists of nodular structures with a certain degree of porosity. During delayed demixing, the coalescence of the nodules can proceed, resulting in membranes with a non-porous top layer. Thus instantaneous demixing results in porous membranes suitable for ultrafiltration or microfiltration, while delayed demixing results in membranes with a dense skin layer suitable for reverse osmosis, gas separation or pervaporation [Van de Witte et al, 1996].

Let us review the preparation of cellulose membranes and their properties.

Generally, a cellulose solution is cast on a glass plate to obtain a certain membrane thickness and then the cast solution is immersed into a coagulation bath and dried by evaporation. The membrane properties are related to their structures and morphologies, which are mainly controlled by the type of solvent and non solvent, the polymer concentration in the casting solution, the temperature of the coagulation bath, the coagulation mechanism and the drying conditions.

Hongo et al have developed regenerated cellulose membranes from cupramonium hydroxide solution by acid coagulation [Hongo et al, 1999]. The morphology of the membranes changed drastically as a function of both cellulose concentration in the original cellulose solution and the concentration of sulphuric acid as coagulant. The increase of sulphuric acid concentration creates a skin structure and thus lowers the membrane porosity. The decrease of cellulose concentration from 8% to 5% leads to a greater porosity with practically no distinct skin structure and hence a higher flux.

In 1980, Kuga developed a cellulose membrane for column packing in liquid chromatography. He dissolved cellulose of various DP in aqueous solution of calcium thiocyanate at 120°C and then regenerated and dispersed cellulose in methanol forming cellulose beads. He found that the mean pore size increases with decrease of the cellulose concentration and of the polymerisation degree. At the same concentration, cotton linter of DP 1620 gave a smaller pore size than microcrystalline cellulose of DP 180. Kuga suggested that longer cellulose molecules cause greater shrinking of the gel structure when cellulose is regenerated, which leads to small pores. Author observed that an increase of microcrystalline cellulose concentration from 3% to 9% leads to a decrease of the mean pore size from 100 nm to 10 nm [Kuga, 1980].

As it was already mentioned, NMMO can be used as a powerful cellulose solvent. Laity et al have studied cellulose membranes prepared from the cellulose/NMMO/H₂O system, reporting a mutually continuous, interwoven network structure of polymer domains and pores on a scale of few nanometres, which indicates spinodal decomposition [Laity et al, 2002].

Recently, cheap cellulose membranes from a non-polluting process have been prepared: from cellulose-NaOH-additive solutions.

Zhang et al [Zhang et al, 2005] have described the preparation of regenerated cellulose membranes made from cellulose dissolved in 7.5 wt% NaOH/ 11wt% urea aqueous solution and regenerated in H₂SO₄ aqueous solution and other organic solvents and finally air-dried at ambient temperature. The thickness of the membrane is around 250 μm. They observed that the membranes coagulated in relatively low temperatures show better mechanical properties as compared to those regenerated at relatively high temperature. Zhang et al proposed that higher temperature accelerates the mobility of all components in the coagulation system and increases the coagulation rate. This rapid precipitation gives to cellulose chains less time to pack themselves into an ordered structure, resulting in a drop of the mechanical properties.

Mao et al [Mao et al, 2006] prepared the same membranes as described above. Authors observed that dried membrane have a pore size lower, around a factor of 2, than the wet membrane, probably due to the contraction of the membrane walls during the drying process. They noted that the pore size distribution shows a typical Gaussian distribution and that different distribution width depends on the used coagulant. The membranes coagulated in acidic coagulants exhibit smaller pores sizes than those coagulated from salt and pure water. Authors observed from scanning electron microscope images that the pore size of membrane core was of a range from 173 to 266 nm while pores at the free surface were from 265 to 730 nm. They suggest that this phenomenon is due to the phase separation that proceeds from the free surface to the core of cellulose membrane. Authors proposed that the mechanism of nucleation and growth of the cellulose-lean phase during the cellulose solution coagulation results in the formation of porous cellulose membrane.

Kuo et al described a new method of creating semi-permeable cellulose membranes based on cellulose regeneration and neutralisation reaction of cellulose-NaOH-water solutions [Kuo et al, 2005]. Microcrystalline cellulose was dissolved in aqueous NaOH at concentration from 1.6M to 2.6M. Cellulose solutions were cast on a glass plate and immersed in 2.1M hydrochloric acid, then washed by deionised water. The generated wet membranes are proved to be able of sieving molecules with a molecular weight above 50.000. Kuo has observed that an increase of cellulose concentration results in the decrease of pore size as well as in increase of wall thickness of the cellulose porous network. He also observed that the higher the acid concentration, the smaller are the pore size of cellulose membrane and hence the more and more compact aggregation of cellulose can be formed. Another point is that higher is acid concentration in the regenerating solution, more cellulose can be regenerated and precipitated on the membrane surface rather than at its bottom, leading to a thick skin on the membrane surface.

The influence of the preparation conditions on the pores size and morphology of cellulose membranes prepared by different authors are summarised in Table I.4.

Authors	Membrane Preparation	Pore size
[Hongo et al, 1999]	Cupramonium hydroxide cellulose solution regenerated in 10 wt% H ₂ SO ₄ .	/
[Kuga, 1980]	Calcium thiocyanate cellulose solution regenerated in methanol	100 nm to 1 μm
[Laity at al, 2002]	cellulose/NMMO/H ₂ O solutions regenerated in water	few nanometres
[Zhang et al; 2005]	Cellulose dissolved in 7.5-wt % NaOH/11wt% urea aqueous solution and regenerated in H ₂ SO ₄ aqueous solution	~1 μm
[Mao et al, 2006]	Cellulose dissolved in 7.5-wt % NaOH/11wt% urea aqueous solution and regenerated in H ₂ SO ₄ aqueous solution	173 to 730 nm
[Kuo et al, 2005]	Cellulose-NaOH solution regenerated in 2.1M HCl	/

Table I.4: Authors studied, membrane preparation and its pore size

The influence of various parameters of regeneration, such as the nature of the bath or its temperature on microstructural and mechanical properties of Aerocellulose, will be studied in chapters IV and V.

3.3 Nanoporous cellulose-based materials

3.3.1 Generalities on aerogels and supercritical drying

Aerogel is one of the most attractive solid materials existing. It is a highly porous solid material (90-99.8 % air) with extremely low densities (0.004-0.15g/cm³), open pores and high specific surface areas. The first inorganic silica aerogels were prepared by Kistler in 1931; these aerogels were prepared by the acidic condensation of aqueous sodium silicate. Kistler also described the formation of aerogels of alumina, ferric oxide, stannic oxide, nickel oxide, etc. Nowadays, silica aerogel is the most common type of aerogel and the most extensively studied and used.

The first organic aerogels based on nitrocellulose were prepared by Kistler in 1932, but active research in organic aerogel did not start until about 1970. The most extensive work in this area has been performed by Pekala and co-workers mainly on resorcinol/formaldehyde and melamine/formaldehyde systems. These organic aerogels have been suggested as an alternative insulator to opacified silica aerogels. In general, organic aerogels are less fragile than inorganic aerogels, and they can be converted into carbon aerogels through pyrolysis.

The main aerogels properties are as follows: a low thermal conductivity and low sound velocity, combined with a high surface area. Aerogels can be obtained as monoliths, granulates, or powders. Aerogels have many applications in different fields of science and

industry. One of the most captivating applications is the one practiced by NASA (USA) on Stardust mission where silica aerogels are used to collect comet particles and later return those samples to the Earth.

Aerogels are prepared by the so called “sol-gel process” involving a cross-linking reaction of chemical precursors. The sol is made of colloidal suspension or solution of solid particles with diameter in the range of 1-1000 nm in a liquid. In a typical sol-gel process, the precursor is subjected to a series of hydrolysis and polymerisation reactions, which leads to the formation of a gel. This gel is formed when attractive dispersion forces cause particles of sol to bond together. The pores of the three-dimensional solid network created are filled with liquid typically water or alcohol. If the liquid in a wet gel is removed under supercritical condition, the solvent in the gel is replaced with air without altering the network structure or the volume of the gel body and a highly porous and extremely low-density material called aerogel is obtained. If drying the gel by means of low temperature treatments (25-100°C), it is possible to obtain porous solid matrices called xerogels. Another way to remove the pore liquid is to perform “freeze drying”: the liquid in the pores is frozen and then sublimated in vacuum. The material obtained is called “cryogel” [Brinker et al, 1990].

Direct drying of gels usually results in partial or total collapse of the nanopores due to the capillary forces. In the pores, capillary forces are created when the adhesive intermolecular forces between the liquid and the solid are stronger than the cohesive intermolecular forces within the liquid. The liquid rises in the pore because of the difference in the specific energy of the solid-vapour interface (γ_{SV}) and the solid-liquid interface (γ_{SL}). The effect causes a concave meniscus that is formed when the liquid is in contact with a vertical surface. The energy gained by this process is:

$$\Delta E_c = 2 \pi r h (\gamma_{SV} - \gamma_{SL})$$

where r is the capillary radius, h is the height to which the liquid rises .

The work performed by the liquid to move against gravity is equal to the product of the capillary pressure P_c and the volume of liquid moved, $\Delta V = \pi h r^2$. Taking into account the equation of energy gained during capillary process, the capillary pressure can be expressed by:

$$P_c = -2 \pi h (\gamma_{SV} - \gamma_{SL})/r = -2\gamma_{LV} \cos (\theta)/r$$

where γ_{LV} is the specific energy of the liquid -vapour interface and θ the contact angle formed between solid and liquid (Figure I.21).

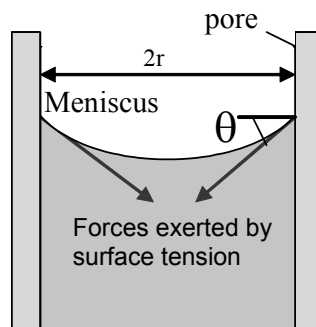


Figure I.21: Illustration of the capillary forces in the meniscus

The significant stresses generated by the meniscus in the pores results in their contraction. As our goal was to prepare porous cellulose material from a wet gel, the principles used in aerogel science were used in order to conserve the porous network structure of cellulose gels while evaporation solvent. To avoid this shrinkage of cellulose gels we have used a special drying, the supercritical drying. Practically, supercritical drying consists of heating the wet gel in an autoclave, so that the pressure and the temperature exceed the critical temperature (T_{cr}) and critical pressure (P_{cr}) of the liquid entrapped in the pores inside the gel. Above the critical point there is no liquid-vapour interface and thus no capillary pressure [Brinker, 1990].

The supercritical fluid (a fluid in the supercritical state) has properties midway between a gas and a liquid (Figure I.22). It expands like a gas, but with a density close to the one of a liquid. Supercritical fluids have also lower surface tension than liquids. Supercritical drying leaves the porous structure intact by preventing pores collapse due to the capillary action.

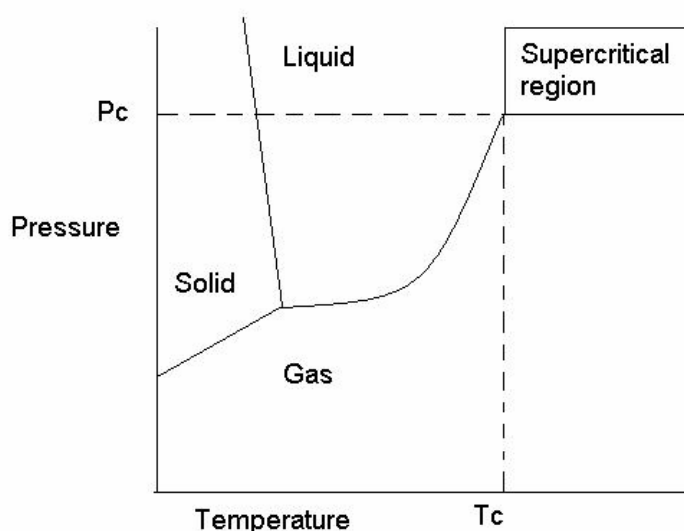


Figure I.22: State phase diagram showing the area of supercritical conditions

The supercritical fluid used in our study is carbon dioxide, CO_2 . CO_2 has the following properties: it is fireproof, cheap and it is chemically inert. It has a good solvation power and its critical point is rather easily obtained as compared with other liquids: at $P=73.8$ bar and $T = 31.1^\circ C$.

In the following paragraphs we will briefly describe the few results reported in literature on the preparation of porous cellulose-based materials via drying of physical cellulose-based gels and the elaboration of a new class of aerogels prepared from cellulose derivatives.

3.3.2 Cellulose-based porous materials

In 1971, Weatherwax and Caulfield prepared porous cellulose from cellulose pulp by the following technique [Weatherwax et al, 1971]. First, water contained in the wet cellulose pulp was exchanged with ethanol which was exchanged with liquid carbon dioxide. Carbon dioxide was removed by heating up to $35^\circ C$ and pressurised up to 75 atmospheres which is

above its critical point (31.1°C- 73.8 atm). The gas was allowed to escape slowly to prevent its temperature decreasing below 34°C. Cellulose with a specific surface area of 206 m²/g was obtained, which is close to those of wet sulphite pulps, 200 m²/g, suggesting the conservation of cellulose porosity owing to the supercritical drying.

Tan et al [Tan et al, 2001] have developed an organic aerogel based on cellulose acetate crosslinked with tolylene-2,4-diisocyanate (TDI) using pyridine as a catalyst. Using CO₂ supercritical drying, authors obtained cellulose acetate aerogel. The characteristics of this material are the following: a density of 0.15 g/cm³, a Brunauer-Emmett-Teller (BET) surface of 300 m²/g and pore radii of 7 nm.

Pimenov et al [Pimenov et al, 2003] produced a physical cellulose acetate gel using thermally induced phase separation of the ternary chloroform/methanol/cellulose acetate system. To prepare porous samples, a hot solution of cellulose acetate in chloroform-methanol was prepared and gelled. Via supercritical CO₂ drying, the liquid phase was removed from the gel. Cellulose acetate aerogels were obtained with a density of 1.5-9 mg/cm³ and average pore size of 2.33-19.7 μm.

Jin et al [Jin et al, 2004] have developed highly porous cellulose aerogels consisting of cellulose nanofibrils. They were prepared by dissolution of cellulose in aqueous calcium thiocyanate followed by regeneration in methanol bath and then drying by freeze drying using liquid nitrogen. The surface area ranged 160-190 m²/g. Figure I.23 presents the aerogel structure obtained by this procedure. The approximate pore size is around 500 nm and 2 μm for porous cellulose materials obtained respectively from cellulose concentrations 3% and 1%.

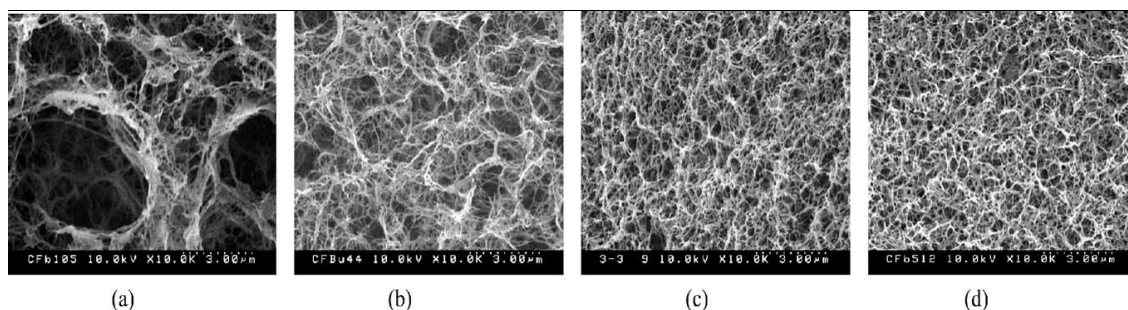


Figure I.23: Scanning electron microscope images of cellulose aerogel obtained by freeze drying of solutions of cellulose of different concentrations: (a) 0.5%, (b) 1%, (c) 2%, (d) 3% [Jin et al, 2004]

In 2006, Fischer et al [Fischer et al, 2006] have developed in the framework of AEROCELL project a new organic aerogel using cellulose derivatives as precursors. Cellulose acetate was crosslinked with a non-toxic isocyanate in acetone *via* sol-gel route, using tin-based catalyst. Low-density materials (from 0.25 cm³/g to 0.85 cm³/g) were obtained after supercritical carbon dioxide drying (see cellulose-acetate aerogel structure in Figure 1.24). Their specific surface areas and characteristic pore sizes vary between 140 and 250 m²/g and 13 to 25 nm, respectively (see Figure I.24).

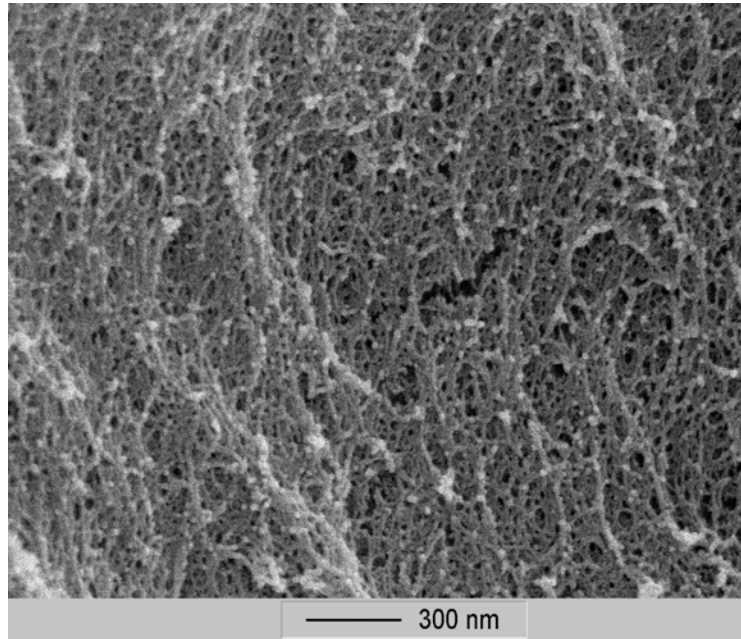


Figure I.24: Scanning electron microscopy of cellulose acetate aerogel [Fischer et al, 2006]

It has been demonstrated that the crosslinker content has an important impact on both gelation and aerogels properties, whatever cellulose acetate DP and concentration. The variation of the cross-linker concentration in solution induced the modifications in bulk density, porous volume and pore size distribution of the final materials. These divided cellulose based aerogels were studied as “green” materials for thermal insulation application. They have shown low thermal conductivity at atmospheric pressure (inferior to 0.030 W/m. K) and are comparable with typical insulating foams (like polyurethane). However, the first tests showed that thermal conductivities are higher than super insulating materials like silica aerogels.

As we can see from the review of existing articles on organic aerogels, very few works have been done in the area of preparation of cellulose-based aerogels. Real aerogels were obtained only from a cellulose derivative, cellulose acetate. Porous cellulose materials were obtained from physical cellulose gels via freeze-drying. No article refers to the preparation of a pure cellulose aerogel or aerogel-like material. Consequently, the way to obtain such a material was a total novelty and thus a challenge.

Conclusions

The described above state of the art on the structure and processing of cellulose and the preparation of porous cellulose-based materials is a basis for the development of a new light ultra porous pure cellulose material: Aerocellulose. It will be obtained starting from cellulose solution or gel that is regenerated in a non-solvent of cellulose and then dried with CO₂ in supercritical conditions in order to extract the liquid from regenerated cellulose and get a dry porous material. The desirable size of pores should be in the range from nano- to micrometres.

In order to prepare porous cellulose material it is very important to understand the changes that the cellulose undergoes during dissolution, regeneration and drying. The analysis of the articles and data describing the structure and molecular organisation of the native and regenerated cellulose and also cellulose processing allows making the following general conclusions:

- There are four main types of cellulose, one being natural, cellulose I; the others are celluloses having undergone some treatment. Cellulose II is the most current and the most studied because it is the end product of the majority of the industrial processes.
- The structure, chains organisation and elementary units are well understood for celluloses I and II.
- Two major industrial processes lead to the production of cellulose II: the viscose process (by derivatisation of cellulose) and Lyocell process (by cellulose dissolution in the direct solvent water-NMMO), both followed by regeneration in a non-solvent. A new process appears on the laboratory and pilot scale: cellulose processing via dissolution in 7-10% aqueous NaOH solution. The two last processes are much less polluting than viscose process thus being very promising.
- However, because Lyocell and NaOH processes are rather new ones, a better comprehension of the correlations between the properties of final materials, their morphology and the way of preparation including regeneration is needed.

Cellulose regeneration is one of the important steps in the preparation of cellulose objects. The principal parameters of regeneration are the type and temperature of the non-solvent. These parameters govern the diffusion of solvent outside cellulose solution or gel and of the non-solvent inside cellulose and thus the final morphology of regenerated cellulose including porosity. There are articles examining the kinetics of regeneration, the mechanisms of phase separation and the influence of regeneration parameters on the final morphology of cellulose obtained with Lyocell process. However, very little is known about parameters influencing and controlling regeneration kinetics and the final morphology of regenerated cellulose obtained from NaOH process. The study of cellulose regeneration kinetics from cellulose-NaOH gels and comparison with regeneration from cellulose-NMMO solutions will be an important step in the development of the new material Aerocellulose.

Another important step in the preparation of a porous cellulose material is drying of the wet gel. The supercritical drying will be used in order to avoid the collapse of cellulose pores and to obtain pure cellulose aerogel-like material. This review of literature shows that very few articles exist on cellulose-based aerogels. Subsequently, the way of preparation of pure cellulose aerogel was an opened question before our work started and thus the elaboration of a new class of aerogel was a challenge.

References

[Atalla, 1984]	Atalla, R.H.; Native cellulose: a composite of two distinct crystalline forms Science, (1984), pp 223-283
[Atalla, 1985]	Atalla, R.H.; Studies of polymorphy in native cellulose Papermaking raw materials, (1985), pp 59-75
[Atalla et al, 1999]	Atalla, R. H.; Vanderhart, D.L.; The role of solid state ^{13}C NMR spectroscopy in studies of the nature of native celluloses, Solid State Nuclear Magnetic Resonance, 15, 1, (1999), pp 1-19
[Biganska, 2002]	Biganska, O.; Thèse : Etude physico-chimique des solutions de cellulose dans la N-methylmorpholine-N-Oxyde; (2002)
[Biganska et al, 2005]	Biganska, O.; Navard, P.; Kinetics of precipitation of cellulose from cellulose-NMMO-water solutions Biomacromolecules, 6, (2005), pp 1949-1953
[Brinker et al, 1990]	Brinker, C.J.; Scherer, G.W. ; Sol-gel science The physics and chemistry of sol-gel processing Academic press, San Diego, (1990)
[Chanzy et al, 1983]	Chanzy, H.; Noe, P.; Paillet, M.; Smith, P.; Swelling and dissolution of cellulose in amine oxide/water system Journal of Applied Polymer Science : Applied Polymer Symposium, 37, (1983), pp 239-259
[Chen et al, 2006]	Chen, X.; Burger, C.; Dufei, F.; Ruan, D.; Zhang, L.; Hsiao, B. S.; Chu, B.; X-ray studies of regenerated cellulose fibers wet spun from cotton linter pulp in NaOH/thiourea aqueous solutions Polymer, 47, 8, (2006), pp 2839-2848
[Dube et al, 1983]	Dube, M.; Blackwell, R.H.; Precipitation and crystallisation of cellulose from amine oxyde solutions Proceeding of the International dissolving and speciality pulps conference, Boston, USA: Tappi press, 111, (1983)

[Dupont, 2003]	Dupont, A.L; Cellulose in lithium chloride <i>N,N</i> -dimethylacetamide, optimisation of a dissolution method using paper substrates and stability of the solutions Polymer, 44, 15, (2003), pp 4117-4126
[Fadeeva et al, 2003]	Fadeeva, J.; Shmukler, L.; Safonova, L.; Investigation of the phosphoric acid - <i>N,N</i> -dimethylformamide system as potential solvent for cellulose Journal of Molecular Liquids, 103-104, (2003), pp 339-347
[Fink et al, 2001]	Fink, H.; Weigel, P.; Purz, HJ.; Ganster, J.; Structure formation of regenerated cellulose materials from NMMO-solutions Progress in Polymer Science, 26, 9, (2001), pp 1473-1524
[Fischer et al, 2006]	Fischer, F.; Rigacci, A.; Pirard, R.; Berthon-Fabry, S.; Achard, P.; Cellulose based aerogels Polymer, 47, (2006), pp 7636-7645
[Gardner et al, 1974]	Gardner, K.H.; Blackwell, J.; The structure of native cellulose Biopolymers, 13, (1974); pp 1974-2001
[Gardiner et al, 1985]	Gardiner, E.S., Sarko, A. The crystal structures of celluloses IV ₁ and IV ₂ Canadian Journal of Chemistry, 63, (1985), pp173-80
[GFP, 2000]	Initiation à la chimie et à la physico chimie macromoléculaires. Groupe Français d'étude et d'application des Polymères (GFP) Vol 13, Les polymères naturels: structure, modifications, applications. Chapter 1, Edition Strasbourg, (2000), pp 1-39
[Herbert et al, 1974]	Herbert, J.J.; Muller, L.L.; An electron diffraction study of the crystal structure of native cells Journal Applied Polymer Science, 18, (1974), pp 3373-3377
[Hongo et al, 1999]	Hongo, T.; Inamoto, M.; Iwata, M.; Matsui, T.; Okakima, K.; Morphological and structural formation of the regenerated cellulose membranes recovered from its cuprammonium solution using aqueous sulphuric acid Journal of Applied Polymer Science, 72, 13, (1999), pp 1669-1678

[Isogai et al, 1998]	Isogai, A.; Atalla, R.H.; Dissolution of cellulose in aqueous NaOH solutions Cellulose, 5, (1998), pp 309-319
[Jayme, 1971]	Jayme, G.; Cellulose and Cellulose Derivatives N.M. Bikales et L. Segal, Eds., Interscience, New-York, (1971)
[Jin et al, 2004]	Jin, H.; Nishiyama, Y.; Wada, M.; Kuga, S.; Nanofibrillar cellulose aerogels Colloids and Surface A: Physicochemical Engineering., 240, (2004), pp 63-67
[Klemm et al, 1998]	Klemm, D.; Philipp, B.; Heinze, T.; Heinze, U.; Wagenknecht W.; Comprehensive Cellulose Chemistry. Volume 1, Fundamentals and analytical Methods Edition Weinheim: Wiley (1998)
[Kolpak et al, 1976]	Kolpak F.J.; Blackwell J.; Determination of the structure of cellulose II Macromolecules 9, 2, (1976); p 273
[Krassig, 1996]	Krassig, H.; Polymer monographs volume 11 Cellulose: structure, accessibility and reactivity, Gordon and Breach Science publishers, Amsterdam, (1996)
[Kuga, 1980]	Kuga, S.; New cellulose gel for chromatography Journal of Chromatography, 195, (1980), pp 221-230
[Kuga et al, 1993]	Kuga, S.; Takagi, S.; Brown R.M.; Native folded-chain cellulose II Polymer Journal, 34, 15, (1993), pp 3293-3297
[Kuo et al, 2005]	Kuo, Y.; Hong, J.; A new method for cellulose membrane fabrication and the determination of its characteristics Journal of Colloid and Interface Science, 285, 1, (2005), pp 232- 238
[Laity at al, 2002]	Laity, P.R.; Glover, P.M.; Hay, J.N.; Composition and phase changes observed by magnetic resonance imaging during non-solvent induced coagulation of cellulose Polymer, 43, 22, (2002), pp 5827-5837

[Langan et al, 1999]	Langan, P. ; Nishiyama, Y. ; Chanzy, H.; A Revised Structure and Hydrogen-Bonding System in Cellulose II from a Neutron Fiber Diffraction Analysis Journal of American Chemical Society, 121, (1999), pp 9940-9946
[Mao et al, 2006]	Mao, Y.; Zhou, J.; Cai, J.; Zhang, L.; Effects of coagulants on porous structure of membranes prepared from cellulose in NaOH/urea aqueous solution Journal of Membrane Science, 279, (2006), pp 246-255
[Mortimer et al, 1996]	Mortimer, S.A.; Peguy, A.A.; The Formation of Structure in the Spinning and Coagulation of Lyocell Fibers Cellulose Chemistry and Technology, 30, (1996), pp 117-132
[Nelson et al, 1964]	Nelson, M.L.; O'Connor, R.T.; Relation of certain infrared bands to cellulose crystallinity and crystal lattice type. Part II. A new infrared ratio for estimation of crystallinity in celluloses I and II Journal of Applied Polymer Science, 8, (1964), pp 1325-1341
[Nishiyama et al, 2002]	Nishiyama, Y. ; Chanzy, H.; Langan, P.; Neutron and synchrotron X-ray fiber diffraction studies of cellulose polymorphs Polymer Preprints, 43, (2002), p 175
[Pimenov et al, 2003]	Pimenov, V.G.; Drozhlin, V.S.; Sakharov, A.M.; Ultra-low density microcellular aerogels based on cellulose acetate Polymer Science series B, 45, 1-2, (2003), pp 4-6
[Romanov et al, 1988]	Romanov, V.V.; Sokira, A.N.; Lumina, O.B.; Iovleva, M.M.; Morphological features of the structure of fibres prepared from solutions of cellulose in NMMO Translated from Khimicheskie Volokna, vol 2, (1988), pp 24-25
[Rom et al, 2006]	Rom, M.; Janicki, J., Rabiej, S.; Slusarczyk, C.; Vehvillainen, M.; The supermolecular structure of newly developed Biocelsol cellulose fibres Polymer Fibres Conference: Manchester United Kingdom, 12 th -14 th July 2006.

[Roseneau et al, 2001]	Roseneau, T.; Potthast, A.; Sixta, H.; Kosma, P.; The chemistry of side reactions and by-product formation in the system NMMO/cellulose (Lyocell process) Progress in Polymer Science, 26, 9, (2001), pp 1763-1837
[Roseneau et al, 2003]	Roseneau, T.; Hofinger, A.; Potthast, A.; Kosma, P.; On the conformation of the cellulose solvent N-methylmorpholine-N-oxide (NMMO) in solution Polymer, 44, (2003), pp 6153–6158
[Sarko et al, 1974]	Sarko, A.; Muggli, R.; Packing analysis of carbohydrates and polysaccharides. III. Valonia Cellulose and cellulose II Macromolecules, 7, (1974), pp 486- 487
[Sarko et al, 1976)	Sarko, A.; Southwick, J.; Hayashi, J.; Packing analysis of carbohydrates and polysaccharides. 7. Crystal structure of cellulose III ₁ and its relationship to other cellulose polymorphs Macromolecules, 9, (1976); pp 857-863
[Schurz et al, 1994]	Schurz, J.; Lenz, J.; Investigations on the Structure of Regenerated Cellulose Fibres Die Makromolekulare Chemie- Macromolecular symposia, 83, (1994), pp 273-89
[Sternberg et al, 2003].	Sternberg, U.; Koch, F.T.; Priß, W.; Witter, R.; Crystal structure refinements of cellulose polymorphs using solid state ¹³ C chemical shift Cellulose, 10, (2003), pp 189-199
[Stropnik et al, 2000]	Stropnik, C.; Musil, V.; Brumen, M.; Polymeric membrane formation by wet-phase separation; turbidity and shrinkage phenomena as evidence for the elementary processes Polymer, 41, 26, (2000), pp 9227-9237
[Tan et al, 2001]	Tan, C.; Fung, B.M.; Newmann, J.K.; Vu, C.; Organic aerogels with very high impact strength Advanced materials, 13, 9, (2001), pp 644-646
[Swatloski et al, 2003]	Swatloski, R. P.; Holbrey, J. D.; Spear, S. K.; Rogers, R. D. ; dissolution and processing of cellulose using ionic liquids Patent WO03/029329 A2, (2003)

[Van de Witte et al, 1996]	Van de Witte, P., Dijkstra, P. J.; Van den Berg, J. W. A.; Feijen, J.; Phase separation processes in polymer solutions in relation to membrane formation Journal of Membrane Science, 117, 1-2, (1996), pp 1-31
[Weatherwax et al, 1971]	Weatherwax, R.C.; Caulfield, D.F.; Cellulose aerogels: an improved method for preparing a highly expanded form of dry cellulose Tappi, 54, 6, (1971), pp 985-986
[Web site 1]	http://www.cfr.ncsu.edu/wps/k12activities/ppts/forest/
[Web site 2]	http://ici.cegep-ste-foi.qc.ca/profs/gbourbonnais/pascal/fya/chimcell/notesmolecules/glucides_3.htm
[Yamashiki et al, 1992]	Yamashiki, T.; Matsui, T; Kowsaka, K.; Saitoh, M.; Okajima, K.; Kamide, K.; New class of cellulose fiber spun from the novel solution of cellulose by wet spinning method Journal of Applied Polymer Science, 44, 4, (1992), pp 691-698
[Zhang et al, 2005]	Zhang, L.; Mao, Y.; Zhou, J.; Cai, J.; Effects of coagulation conditions on the properties of regenerated cellulose films prepared in NaOH/Urea Aqueous Solution Ind. Eng. Chem. Res 44, (2005), pp 522-529
[Zhu et al, 2006]	Zhu, S.; Wu, Y.; Chen, Q.; Dissolution of cellulose with ionic liquids and its application: a mini-review The Royal Society of Chemistry, (2006), pp325-327
[Zugenmaier, 2001]	Zugenmaier, P.; Conformation and packing of various crystalline cellulose fibers Progress in Polymer Science, 26, 9, (2001), pp 1341-1417

Chapter II: Cellulose-NaOH solutions: preparation and rheological properties

Introduction

To find a route alternative to polluting viscose process, new solvents of cellulose were searched. NMMO is one of the solvents that responds to this request. Another direct solvent of cellulose, aqueous solution of sodium hydroxide of 7-10% NaOH is rediscovered nowadays. Due to its low cost and non-polluting way of cellulose dissolution, NaOH is also a promising solvent.

The behaviour of cellulose in aqueous alkali solutions has been studied for a long time since the discovery of the mercerisation process at the end of the XIX century. In 1939, Sobue showed that cellulose could be dissolved in a narrow interval of NaOH concentrations (7% to 10%) and temperatures (from -5°C to 0°C). Recently, the production of regenerated fibres from NaOH plus additives has been developed at a pilot scale. Because dissolution of cellulose in 7-10% NaOH is rather poor, urea and thiourea are used to improve cellulose dissolution. Despite a large amount of publications that appeared the past decade on cellulose-NaOH aqueous solutions with or without additives, the understanding of the structure and properties of these systems is far from being complete.

To create Aerocellulose material, the first step is the preparation of cellulose-NaOH solution and then their gelation. Gelation is needed to pre-form Aerocellulose precursors. Cellulose will be then regenerated from cellulose-NaOH gels and dried using CO_2 supercritical extraction technique (Chapters 3 and 4). Thus in order to prepare Aerocellulose precursor it is necessary to study gelation properties of cellulose solutions with or without additives, and the influence of cellulose and additives concentration on gelation time, gelation temperature and gel strength.

The goal of this chapter is to describe gelation of cellulose-NaOH aqueous solutions, with or without additives. First, the state of the art on the properties of these solutions will be reviewed. Then materials and methods used in this study will be described including the preparation of cellulose/NaOH aqueous solutions. These solutions will be the basis of future Aerocellulose. The third part considers time and temperature behaviour of cellulose-NaOH solutions. The studies are performed using rheological tools in continuous and dynamic mode. The influence of cellulose concentration, its origin and of the presence of additives like urea on solution gelation will be investigated.

1 Bibliography: Cellulose-NaOH aqueous solutions: structure, properties and influence of additives

1.1 Effect of NaOH on cellulose fibres: the mercerisation process

In 1844, John Mercer discovered the mercerisation process. It consists of a treatment of cotton with a concentrated caustic alkaline solution. Though other strong alkaline solution such as lithium hydroxide or potassium hydroxide can be used for cellulose mercerisation, in practice caustic soda is generally used, with NaOH concentration varying between 20% and 25%. When cellulose is dipped into a strong alkaline solution such as caustic soda or lithium hydroxide, the cellulose fibre swells to various extents depending on the type and the concentration of alkali, and also on the temperature. In the mercerisation process, while being in this swollen state, the cotton fibres are treated in a stretched condition and then rinsed with water, afterwards the alkali is removed and a permanent silk-like lustre is obtained. The mercerisation process increases the ability to absorb dye, improves the reactions with a variety of chemicals, the smoothness, the strength and elongation of the fibres and also enhances the dimensional stability of fibres.

Mercerisation induces the irreversible transformation of the crystalline structure of native cellulose or cellulose I into cellulose II. During this transformation, the original parallel-chains crystal structure of cellulose I changes to the one of cellulose II, which is based, as it was shown in the first chapter, on the antiparallel organisation of chains. Stable ternary complexes cellulose/NaOH/water called “soda celluloses” are formed. According to the conditions like temperature and concentration, various soda celluloses (or “Na-cell”) are produced. The swelling of crystalline parts of fibres in NaOH involves a modification of the crystalline structure, which can be detected by X-rays.

1.2 Crystalline structures of Na- cellulose

In 1939, Sobue has studied the influence of the temperature on sodium hydroxide solution action on native ramie cellulose fibres. When cellulose fibres are soaked in aqueous NaOH of various concentrations, a series of crystalline alkali-celluloses are produced. On the basis of X-Ray diffraction, Sobue has classified these structures as Na-cellulose I, II, III, IV, V and Q and has represented a diagram (Figure II.1) showing the formation of these various soda-celluloses as a function of the sodium hydroxide concentration (0% to 45%) and temperature (-20°C to +100°C). The boundaries in which the various types of alkali cellulose exist are defined more or less distinctly.

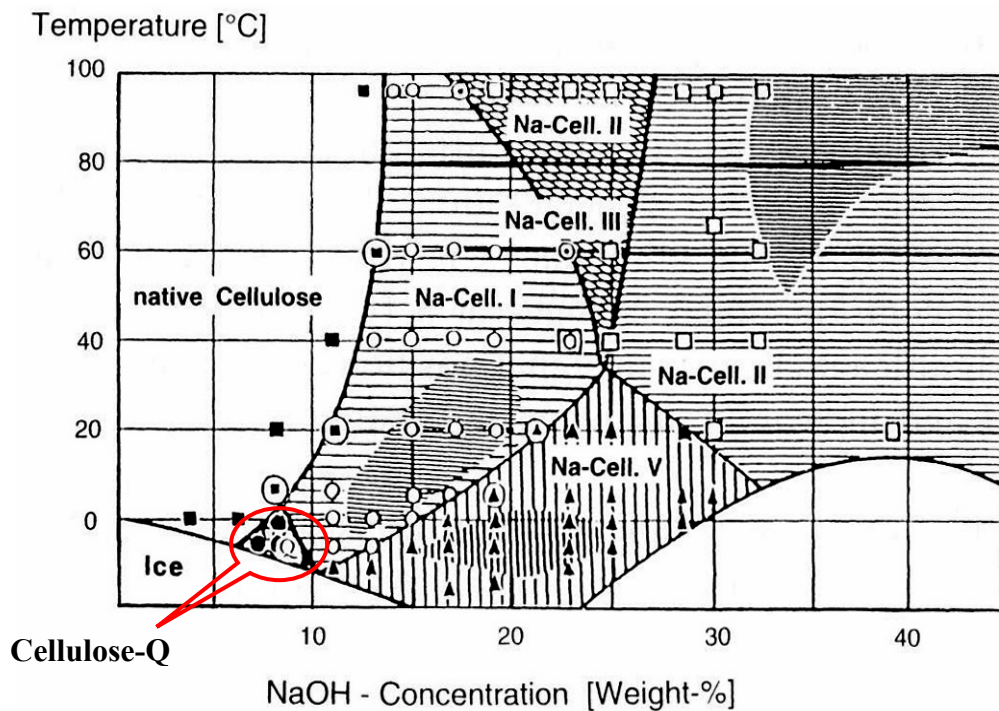


Figure II.1: Phase diagram of cellulose-NaOH aqueous system (different types of Na-Cell compounds) for different NaOH concentrations and temperatures [Sobue et al, 1939]

Sobue paid a special attention on the Na-cell V and Na-cell Q crystalline structure formed below 0°C. The Na-Cell V is close to Na-Cell II. Na-Cell Q occurs in a small region of NaOH concentrations (7 to 10% NaOH) and temperatures (-6°C to +1°C) (see marked area in Figure II.1). In this region fibres have a glassy transparency appearance and swell considerably; thus they were named Na-Cell Q from the word “Quellung” meaning “swelling” in German. The X-ray diffraction pattern of Na-cell Q differs distinctly from the other types of Na-cellulose showing a highly disordered lattice state.

Sarko and Okano [Okano et al, 1985] have intensively investigated cellulose transformations during mercerisation process at a molecular level. They studied the crystalline structures of the Na-celluloses by X-rays and proposed a possible mechanism of mercerisation (Figure II.2). During the first step of this transformation, NaOH penetrates into cellulose amorphous areas, which coexist with crystallites. This results in the formation of Na-cellulose I without important movements of chains and a light effect on the crystalline zones. Gradually, the crystalline areas of cellulose I decreases to the benefit of the formation of soda celluloses I crystallite.

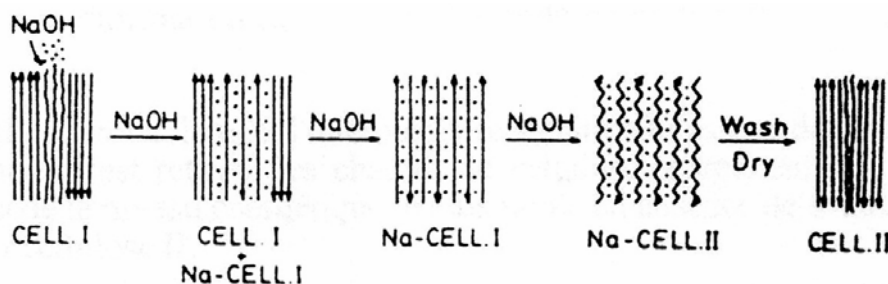


Figure II.2: Possible mercerisation mechanism [Okano et al, 1985].

The treatment with sodium hydroxide reduces the supramolecular order and changes the cellulose crystal structure. The alkali celluloses formed are an activated form of cellulose and are used as the reactive initial stage in many derivatising routes like xanthate or carbamate cellulose. Table II.1 summaries the characteristics of the various alkali celluloses.

Soda cellulose	Parameter a (Å)	Parameter b (Å)	Parameter c (Å)	γ (degrees)	Number of chains by unit cell	Type of crystalline unit
Na cell I	8.83	25.28	10.29	90	4	rhombohedral
Na cell II	14.94	14.94	15.39	120	2	hexagonal
Na cell III	12.54	26.40	10.28	115	4	monoclinic
Na cell IV	9.57	8.72	10.35	122	2	monoclinic
Na cell V	13.95	13.95	15.3	120	2	rhombohedral

Table II.1: Crystalline units of alkali celluloses [Sarko et al, 1987]

Takahashi and co-workers [Takahashi et al, 1991] have analysed the alkali cellulose structure using ^{13}C solid state NMR (CP/Mass) spectroscopy and suggested that Na^+ is coordinated to the hydroxyl group at C_2 of the α glucopyranose ring. The small cations Na^+ ($\text{Na}^+=0.276\text{nm}$) occupy the cellulose porous structure. By selective coordination of Na^+ to the hydroxyl group at C_2 , the $\text{O}_2\text{-H}\cdots\text{O}_6'$ intermolecular hydrogen bond is broken. Above 25 wt % aqueous NaOH, the $\text{O}_3\text{-H}\cdots\text{O}_5'$ intramolecular hydrogen bond is broken by selective coordination of Na^+ to O_3 at C_3 . During intensive washing, the linked Na-ions are removed and another lattice is formed, the cellulose II lattice.

Nishiyama et al [Nishiyama et al, 2000] have studied the crystalline conversion of cellulose fibres from cellulose I to cellulose II via mercerisation process by X-ray diffraction. It appears that the most important alkali cellulose types obtained during mercerisation, Na-cellulose I formed by 3-5 N NaOH at room temperature and Na-cellulose II formed by more than 7N NaOH at higher temperature (60-100°C) are stable and did not inter-convert to each other when increasing the NaOH concentration. The stability of these crystal structures indicates that the parallel to antiparallel rearrangement of cellulose chains is not likely to occur in the crystalline region of Na-cellulose.

1.3 Dissolution of cellulose in the aqueous 7-10%NaOH solution

Kamide and his co-workers [Kamide et al, 1984] demonstrated that cellulose regenerated from cuprammonium solutions in aqueous sulphuric acid, after partially and slowly evaporating ammonia from the cast solution in the air, can be completely dissolved in 8-10 wt% aqueous NaOH solution at 4°C. They correlated the solubility of cellulose in aqueous alkali solution with the degree of breakdown of an intramolecular hydrogen bond ($\text{O}_3\cdots\text{O}_5'$) of cellulose as determined by CP/MAS ^{13}C NMR method.

Yamashiki et al succeed in dissolving steam-exploded cellulose in 8 and 9 wt% NaOH at 4°C. They assumed that the steam explosion process (pressurising cellulose fibres with a high steam pressure for a certain period of time) results in the partial cleavage of the intramolecular hydrogen bonds between the hydroxyls groups on C₃ of pyranose rings and the ring oxygen atoms of adjacent anhydroglucose units. This cleavage may be the key factor in increasing the solubility of steam-exploded pulp in aqueous NaOH.

Yokota et al [Yokota et al, 1990] also investigated the dissolution of cellulose in aqueous NaOH solutions. Rayon is almost converted into alkali cellulose in a 9% aqueous NaOH solution. It appears that the conversion of cellulose to Na-cell takes place at lower aqueous NaOH solutions concentration for rayon than for linter fibres. Such an easy conversion of rayon to Na-cell I compared to the one of linter fibres may be attributed to the weakness of hydrogen bonding network, poorly ordered crystalline regions and the low degree of polymerisation of this sample.

Yamada et al [Yamada et al, 1991] proposed a dissolving mechanism of alkali soluble celluloses into aqueous NaOH solutions of concentration varying from 8 to 11% at low temperature: hydrated hydroxyl and sodium ions of aqueous NaOH completely destroy the amorphous region consisting of cellulose molecules with weak intramolecular hydrogen bonds, resulting in the activation of the molecular mobility. Further, the alkali penetrates into the neighbouring crystalline part unzipping the crystalline plane, finally destroying crystalline zones. This results in the total destruction of the crystalline part and finally the cellulose sample dissolves completely into aqueous NaOH without forming Na-cell I.

Isogai and Atalla [Isogai et al, 1998] have examined the dissolution of cellulose samples in aqueous NaOH. The optimum conditions involved swelling cellulose in 8-9 wt% NaOH. The dissolution of cellulose was obtained by a freezing-thawing process. Authors found that the presence of lignin, contrary to the presence of hemicellulose, reduces the level of solubility. The original linter cellulose, its mercerised form and cellulose III samples had limited solubility values of only up 36%, meanwhile microcrystalline, amorphous linter cellulose and Kraft pulps were essentially dissolved. The authors concluded that the disruption of long range order present in solid cellulose was the basis of cellulose dissolution in NaOH. For the low DP cellulose, the domains of coherent order are likely to have an upper limit of the order of 100 nm, corresponding to the approximate length of a cellulose chain consisting of 200 anhydroglucose units. They suggested that crystallisation of water in domains of this magnitude is sufficient to cause complete disruption of intermolecular association, so that dissolution in the caustic solution becomes possible. Fibrous celluloses having dimensions higher than 100 nm do not have their order disrupted by freezing to allow their dissolution in the aqueous NaOH system by the freezing process. If, however, their long range order is first disrupted by dissolution and regeneration from one of other stronger solvent systems, they do become susceptible to dissolution by freezing followed by the dissolution process.

Recently, Cuissinat et al [Cuissinat et al, 2006] have observed the dissolution mechanism of native cotton and wood cellulose fibres in aqueous NaOH solution at various concentrations and temperatures by optical microscopy. It appears that the cellulose fibres exhibit a heterogeneous swelling by ballooning in the best dissolving conditions (-5°C, 7.6% of NaOH). The balloons are growing until they reach a maximum diameter after which a certain equilibrium is attained. Three different zones within one fibre (see Figure II.3) can be distinguished. These various zones are unswollen fibre parts (A), balloons (B) surrounded by

a membrane (C) and unswollen sections (D). An unswollen fibre (A) is the part of one fibre, or a full fibre, that did not start yet the swelling process, but that will swell later with balloons.

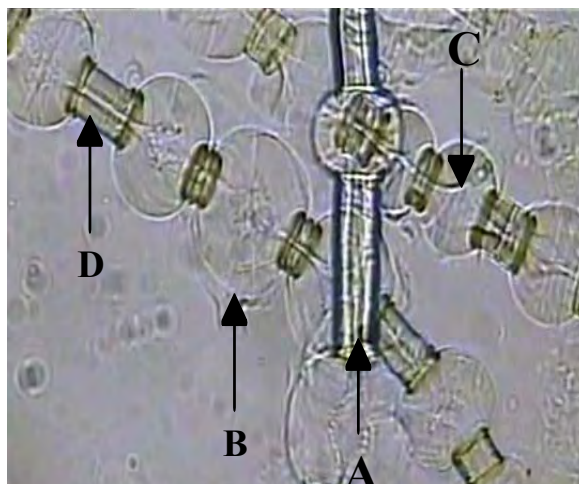


Figure II.3. Swelling of a Borregaard fibre by ballooning in 7.6%NaOH–water solutions (optical microscopy in transmitted light): an unswollen fibre (A), a balloon (B) surrounded by a membrane (C) and an unswollen section (D) [Cuissinat et al, 2006]

Only cellulose present inside the balloons is dissolved. The membrane and the unswollen sections cannot dissolve in 7.6%NaOH solution without a mechanical action. Without mixing, the fibres stay as they are which means that a mechanical action is necessary to obtain the dissolution of cellulose in 7-10%NaOH. However, cellulose solutions prepared even with intensive mixing present a lot of insoluble particles [Cuissinat et al, 2006]. Cellulose of a low DP like microcrystalline cellulose can be nearly fully dissolved in 7-10%NaOH-water, with very few insoluble particles present.

Finally, Egal et al [Egal et al, 2006] have studied by DSC the binary 0-20%NaOH-water and ternary cellulose–NaOH-water solutions in the area of cellulose dissolution (7-10%NaOH below 0°C). Investigating the binary phase diagram of NaOH-water, which has a simple eutectic behaviour, they have studied the influence of the addition of cellulose. They have found that a minimum of four NaOH molecules should be linked to one anhydroglucose unit to provide cellulose dissolution. This corresponds to equal cellulose and NaOH proportion taken in weight. If cellulose concentration is higher, it will not dissolve. As the cellulose can be dissolved only in a narrow range of sodium hydroxide concentrations, from 7 to 10%, this means that maximal amount of cellulose that can be dissolved in NaOH-water solutions is 10%.

1.4 Gelation of cellulose–NaOH aqueous solutions

Roy et al [Roy et al, 2003] have studied the rheological properties and gelation of aqueous cellulose-9 wt% NaOH solution. Within cellulose concentration interval where no gelation was noticed (dilute systems), they calculated the flow index, n , which is determined as:

$$\eta = (\dot{\gamma})^n$$

where η is viscosity and $\dot{\gamma}$ is shear rate. For «classical» polymers solutions, n is equal to 0.6 or 0.7, while for suspensions n is inferior to 0.5. Depending on temperature, cellulose

concentration and DP, n varies between 0.07 and 0.19. The flow index is similar to the one of suspension and not to that of polymer solutions, thus authors concluded that cellulose solution in NaOH behaves as a suspension and that cellulose-NaOH solution is formed of cellulose aggregates. The formation of cellulose aggregates is favoured when temperature is increased. In the semi-dilute regime, an irreversible aggregate-based gelation occurs, being faster with temperature increase. Roy et al made a hypothesis that the increasing role of inter- and intra-chain hydrophobic interaction with temperature increase, above 20°C, leads to aggregate compactisation in dilute regime and to gelation in semi-dilute regime.

Egal et al [Egal et al, 2005] observed a similar behaviour for aqueous cellulose-7.6% NaOH solutions with 0.7% ZnO or 4% urea added. The flow index varies between 0.09 and 0.21. It appears that additives used – 0.7% ZnO and 4% urea – do not modify the structure of cellulose-NaOH system which behaves as a suspension.

1.5 Use of additives

During the last decade, additives were used to improve the dissolution of cellulose in 7-10% sodium hydroxide solution, particularly for the pulp with a high DP.

Laszkiewicz [Laszkiewicz, 1997] demonstrated that when 1% of urea is added to a 8.5% NaOH solution at a temperature of -5°C, the solubility of cellulose increases. In this solvent bacterial cellulose may be dissolved as far as its polymerisation degree is below 560.

Zhou and Zhang [Zhou, 2000] have studied the influence of urea concentration on cellulose dissolution in aqueous NaOH. They calculated the solubility, S , of different cellulose in NaOH/urea aqueous solution by measuring the amount of dissolved and insoluble cellulose. They changed the weight rate of NaOH to urea such as 6:0, 6:2, 6:4, 6:6, 8:0, 8:2, 8:4, 8:6 (Table II.2).

Cellulose	S (%)									
	6:0	6:2	6:4	6:6	6:8	8:0	8:2	8:4	8:6	8:8
Linter	44.7	50.5	48.4	43.3	36.1	40.6	48.5	40.5	28.3	23.7
Bagasse	56	61.7	74.3	68.6	54	62.8	64	62.7	58.1	56.1
Steam exploded spruce pulp	Gel	100	100	100	100	100	100	100	100	100
Bemliese®	Gel	100	100	100	100	100	100	100	100	100

Table II.2: Solubility of cellulose in NaOH/urea aqueous solution [Zhou, 2000]

The addition of 2-4 wt% urea to 6-8 wt% NaOH aqueous solution significantly improves the solubility of cellulose. The solubility of cotton linter and bagasse at 0-4°C increased with urea concentration and reached maximum in NaOH: urea = 6:4 and 8:2 aqueous solution. With continued addition of urea, the solubility of cellulose decreased. Steam exploded pulp and Bemliese® exhibited excellent solubility in all NaOH/urea and were stable at least 3 months at

4°C. Cellulose can be dissolved at 6 wt% NaOH aqueous solutions at 0°C but turns into a gel with increasing temperature. The addition of moderate urea avoids the formation of gel.

Kunze and Fink [Kunze et al, 2005] have demonstrated that cellulose dissolution can be optimised using activating effect of urea on cellulose. Activation of cellulose is a treatment of cellulose in the aim to increase the accessibility and the reactivity of cellulose for subsequent reactions by structural changes on the various structural levels. The alkali celluloses produced by caustic soda treatment are activated forms of cellulose and are applied as the reactive initial stage in many derivatisation routes. In their study, cellulose pulps were treated with lye in the range of concentration from 0 to 8% NaOH and 15% to 40% urea at ambient temperature during one hour or at -25°C during 12 hours. It appears that a decrease of temperature acts similar to an increase in NaOH concentration on cellulose dissolution. By analysing the ^{13}C - CP/MAS- NMR spectrum of cellulose samples steeped with NaOH/urea aqueous solutions, authors revealed the formation of a special urea-NaOH-cellulose complex, different from the spectra of cellulose I and cellulose II. The activating effect of a treatment with urea containing caustic soda was investigated for the synthesis of cellulose carbamate. Authors observed that the combined 7% NaOH/ 30% urea treatments results in a superior degree of substitution as compared with the single 18% NaOH treatments. These results were used to improve the synthesis of cellulose carbamate.

Recently, Zhang et al [Zhang et al, 2006] have added thiourea into the NaOH solution to improve the dissolution of native cellulose. The presence of thiourea enhanced the solubility of cellulose in NaOH aqueous solution and reduced gelation. Authors measured the dependence of the intrinsic viscosity on the thiourea content in 1.5M NaOH aqueous solution. The intrinsic viscosity hardly changed with increasing thiourea content in 1.5M NaOH aqueous solution until 0.75M thiourea. The higher intrinsic viscosity of the polymer solution reflects the larger expansion of the coil, namely, stronger solvation of polymer molecules. Their results indicate that 1.5M NaOH/0.65M thiourea have a stronger solvation power on cellulose molecules than pure NaOH or NaOH/urea preventing the self-association of cellulose molecules.

Weng et al, [Weng et al, 2004] investigated the thermal gelation of cellulose in this 6wt% NaOH/5%wt thiourea aqueous solution. The temperature of the gel point found at the crossover of the storage modulus (G') and the loss modulus (G'') decreased from 36.8°C to 20.1°C with an increase of cellulose concentration from 4 to 6 wt %. It appears also that the higher the cellulose concentration, the faster is the gelation, implying that the gelation process relates closely to an increasing chance for “collision” of cellulose chain. After gelation occurs, authors do not observe a plateau for G' , suggesting that the gelation process does not result from a chemical cross-links but probably is caused by the formation of a condensed network, accompanied with a micro-phase separation. They suggested a schematically gelation process (Figure II.4): at temperature below 20°C, sodium ions, water and thiourea molecule surrounding the cellulose chain form an “overcoat” preventing the self-association of cellulose chain. At higher temperature this layer is broken leading to a physical cross-linking network and the turbidity of the solution is caused by the self-association of macromolecules where the exposed hydroxyl serves as junction. At temperature higher than 50°C, more junctions of cellulose chains are formed leading to the formation of a gel network.

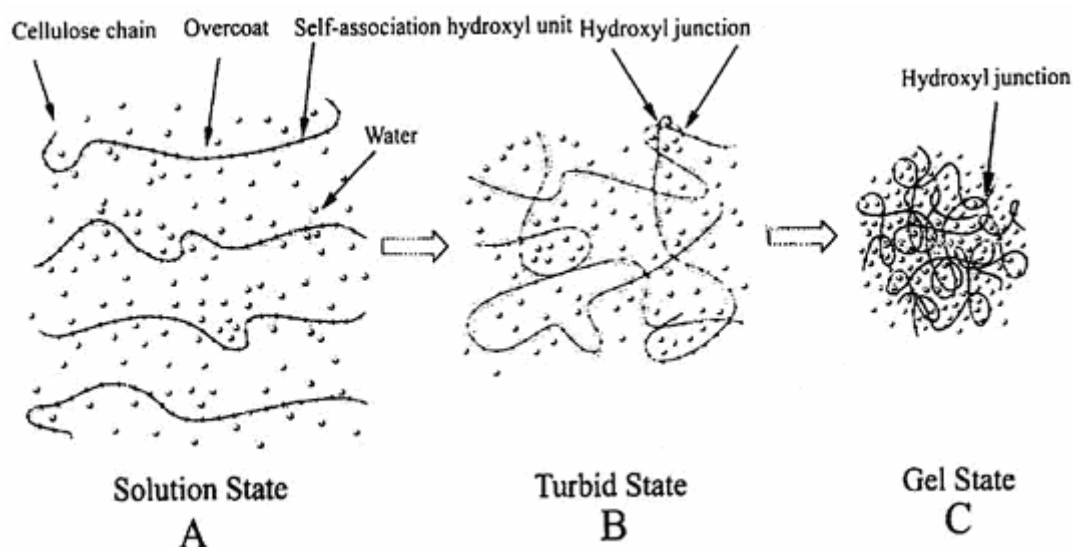


Figure II.4: Schematic gelation process of the cellulose solution below 20°C (A), at 25-40°C (B) and above 50°C (C) [Weng et al, 2004]

Finally, in 2006, Cai et al [Cai et al, 2006] investigated the gelation behaviour of cellulose in 7-wt% NaOH/12 wt% urea aqueous solution using dynamic viscoelastic measurements. The gelation point was determined as the point when elastic and viscous moduli are equal. Authors observed that the gelation temperature of the cellulose solution having a viscosity-average molecular weight (M_{η}) of $11.4 \cdot 10^4$ decreased from 60.3 to 30.5°C with an increase of cellulose concentration from 3 to 5 wt%. They also noted that the gelation temperature of a 5 wt% cellulose solution dropped from 59.4 to 30.5°C as the M_{η} value was increased from $4.5 \cdot 10^4$ to $11.4 \cdot 10^4$. Gels can be formed at either higher temperature (above 30°C), or lower temperature (below -3°C), or for longer gelation time. However the cellulose solution remains a liquid state for a long time in the temperature range from 0 to 5°C. The gelation of the cellulose/7 wt% NaOH/12 wt% urea aqueous solution is an irreversible process; the gel could not be broken by heating or cooling cycles.

Conclusions

As it has been seen in this brief review of literature, the effect of sodium hydroxide on cellulose fibres has been studied for more than 100 years with the industrialisation of the mercerisation process. In 1939, Sobue discovered that cellulose can be dissolved in a narrow range of temperatures and NaOH concentrations. The solubility of cellulose in sodium hydroxide is correlated to the degree of breakdown of weak intramolecular hydrogen bond. It appears that steam exploded cellulose and cellulose with low DP as microcrystalline cellulose are essentially dissolved in 8% NaOH. The last decade, additives as urea or thiourea were used to improve the cellulose dissolution particularly for cellulose with high DP. In this work we will investigate the role of cellulose origin and of urea addition on gelation of cellulose NaOH aqueous solutions.

2 Experimental

2.1 Materials

2.1.1 Cellulose

2.1.1.1 *Microcrystalline cellulose*

Microcrystalline cellulose was purchased from FMC Biopolymer Corporation (Philadelphia, USA). The trade name is Avicel PH101[®], called Avicel in the following. It is purified partially de-polymerised alpha cellulose, free of other polysaccharide like hemicellulose or lignin with a mean degree of polymerisation of 170 as given by the manufacturer.

The raw material for Avicel is purified plant fibres, or alpha cellulose, and it is composed of millions of microfibrils. Each microfibril is composed of two areas: the paracrystalline region, which is an amorphous flexible mass of cellulose chains and the crystalline region, which is composed of tight bundles of microfibrils in a linear arrangement. During processing, the fibrous material is hydrolysed with a diluted mineral acid solution, at 100°C, to remove the amorphous regions, leaving only the crystalline bundles. Cellulose is depolymerised to a degree of polymerisation lower than 200. The resulting cellulose is then purified by filtration and dried to obtain powdered microcrystalline Avicel. The mean size of microcrystalline cellulose is from about 15 to 50 microns.

Microcrystalline cellulose is used in the food domain. As it is virtually inert, it does not interfere with nutrients, such as vitamins or minerals. Avicel is a good suspending agent and can provide stable suspension of even very heavy minerals particulates. Avicel is a good source of dietary fibres, which contributes with very little calories in the food systems. It is also used, for instance, as foam stabiliser or fats and oil replacer.

Avicel is largely employed in the pharmaceutical industry to produce tablets. As it promotes rapid disintegration it is used in the drug release systems.

Figure II.5 presents a scanning electron microscopy (SEM) image of microcrystalline cellulose:

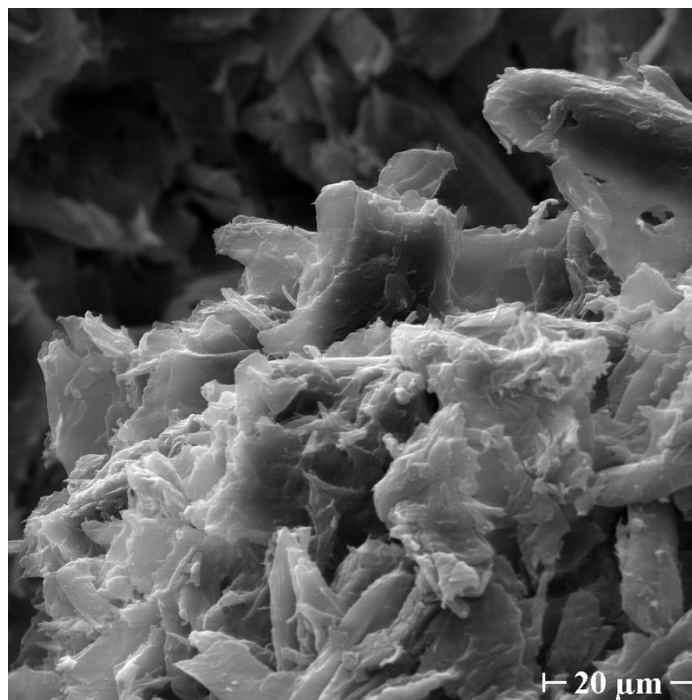


Figure II.5: SEM image of microcrystalline cellulose

2.1.1.2 Steam exploded Borregaard

Borregaard, which is cellulose I, was provided by Innovia Films Ltd, UK. Spruce and pine softwoods were submitted to the steam explosion process. In this process cellulose is pressurised with high steam pressure for a certain period of time, followed by sudden decompression. In the reactor, steam under high pressure penetrates by diffusion into the softwood structures. The steam condenses under the high pressure thereby “wetting” the material. The moisture in the biomass hydrolyses the acetyl groups of the hemicellulose fractions, forming organic acids such as acetic and uronic acids. Under high pressure steam, the amorphous regions of cellulose are hydrolysed to some degree. The “wet” biomass is “exploded” when the pressure within the reactor is released. The expansion of the water vapour exerts a shear force on the surrounding structure. If this shear force is high enough, the vapour will cause the mechanical breakdown of the lignocellulosic structures. The steam explosion treatment enables to activate cellulose fibres by decreasing the DP of cellulose and thus improves the dissolution of this type of fibres. The DP of Borregaard steam exploded pulps used is 500.

2.1.1.3 Fibrous cellulose Solucell

Fibrous cellulose Solucell 400 called Solucell in the following was provided by Lenzing AG, Austria. The samples were prepared from the eucalyptus pulp Solucell 1175 with initial DP_v = 412 using two types of treatment:

- By degradation using electron beam (60kGy) leading to a cellulose I with a DP of 307 which will be called in the following “Solucell 307”

- Or by alkali treatment leading to cellulose II with DP=198 which will be called in the following “Solucell (II) 198”

The molar mass distribution of Solucell 307, determined by chromatography GPC at Lenzing, is presented on Figure II.6.

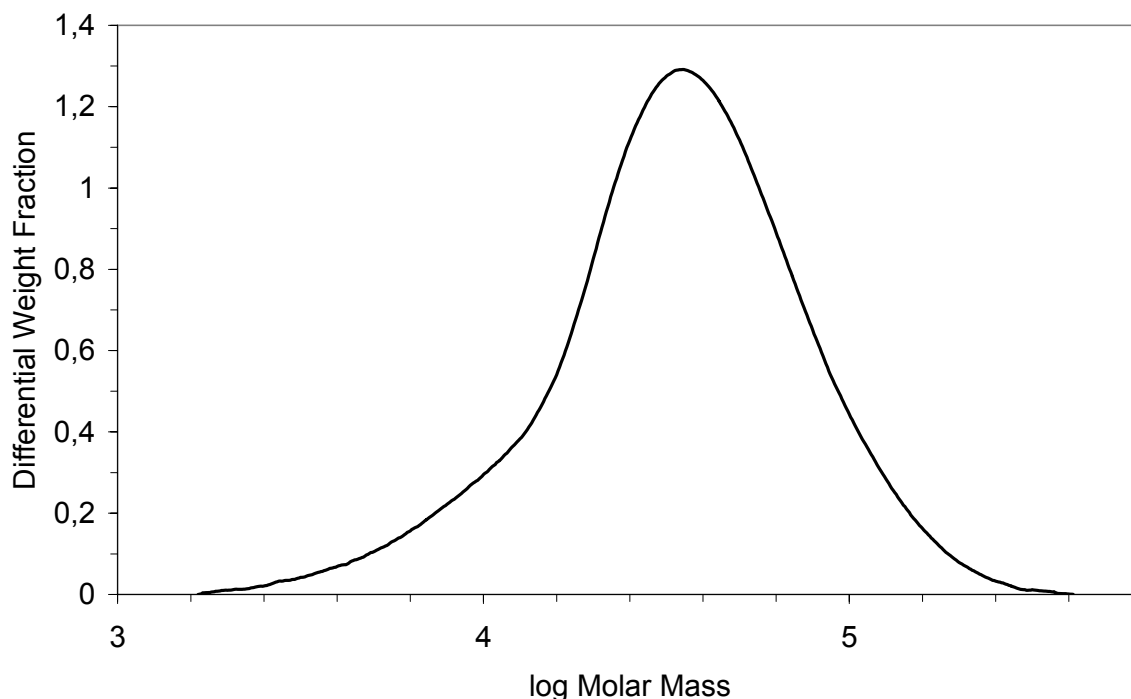


Figure II.6: Molar mass distribution of cellulose Solucell 307

Table II.3 summarises the characteristics of the different pulps used for cellulose-NaOH solutions preparation:

Samples	Origin	DP	Crystalline structure
Avicel, microcrystalline cellulose	Various	170	Cellulose I
Borregaard	Spruce and pine softwood	500	Cellulose I
Solucell 307	Eucalyptus	307	Cellulose I
Solucell (II) 198	Eucalyptus	198	Cellulose II

Table II.3: Characteristics of celluloses used in the study

Before preparing solutions, cellulose was dried in an oven at 60°C in order to remove the remaining water.

2.1.2 Solvents

2.1.2.1 NaOH

Sodium hydroxide, NaOH, with a purity superior to 98% was purchased from VWR. NaOH powder was dissolved in distilled water. NaOH weight in solution was always fixed to 7.6g for 100g of solution.

2.1.2.2 Urea

Urea was used as an additive to improve cellulose dissolution in aqueous NaOH. Urea of purity superior to 99% was purchased from Merck. It was dissolved in distilled water; urea weight in solution was between 0 to 20g for 100g of solution.

Distilled water was used to prepare the aqueous solutions.

Because cellulose solvents are often multi-component, like NaOH/urea/water, in order to avoid confusions in determination and notation of “concentrations”, we used and will note in the following the weight (in grams) of the component in 100 g of total solution. For example, Xcellulose/YNaOH/Zurea/water means that the components in 100 grams of solution are in the following quantities: X g of cellulose, Y g of NaOH, Z g of urea and (100-X-Y-Z) of water.

It can be noted that weight per cent concentration determined as $C_i \% = \frac{M_i}{M_i + M_{water}} 100\%$ (where M_i and M_{water} are the weights of component “i” and water, respectively) coincides with the shown amount of grams only for binary systems, and “%” will be used only for such cases.

2.2 Methods

2.2.1 Preparation of cellulose/NaOH/urea/water solutions

As it can be seen from literature, cellulose can be dissolved in NaOH/water solutions in a certain interval of NaOH concentrations (7%-10%) and temperatures (-7°C – -0°C) without chemical derivatisation [Sobue et al, 1939].

The preparation of cellulose+NaOH water solutions is described bellow:

Cellulose was placed in a drying oven at 60°C (~12h) to dry from the remaining humidity. Sodium hydroxide was dissolved in water at a concentration of 12 wt% and cooled down to -6°C. When urea was used as an additive, urea aqueous solution of 50 % was cooled down to +5°C. Water was added to cellulose pulp for cellulose swelling and cellulose+water system

was left at +5°C for about 2 hours. Cold aqueous NaOH and urea solution were added to swollen-in-water cellulose. The amount of cellulose in the 100 g of final solution varied from 3g to 7g, of NaOH was always 7.6g and of urea from 0 to 20 g. Cellulose solutions in NaOH/water with or without additives (urea) were placed in a thermobath at -6°C and stirred during two hours at 1000 revolutions.min⁻¹ and then stored at +5°C to avoid aging.

2.2.2 Rheological tools

Steady and dynamic shear tests were carried out at different temperatures using cone-plate geometry (cone angle 2°, plate diameter 60 mm) on a stress-controlled Bohlin Gemini[®] rheometer from Malvern Instruments equipped with a Peltier temperature control system.

We studied gelation using the method developed by Winter and Chambon [Winter et al, 1986] who have studied the gelation of chemical gels and more particularly the determination of gel point. They described two experimental methods suitable for the characterisation of gelation:

The first one consists to measure the viscosity η as a function of time t at a fixed shear rate $\dot{\gamma}$ (Figure II.7). During the crosslinking reaction, the viscosity increases until the stress is reaching the apparatus limit or the sample break. Close to the gel point viscosity is tending towards the infinity. Beyond the gel point (solid state), the modulus G is measured in time. However, this method does not give precisely the time and temperature of the gel point.

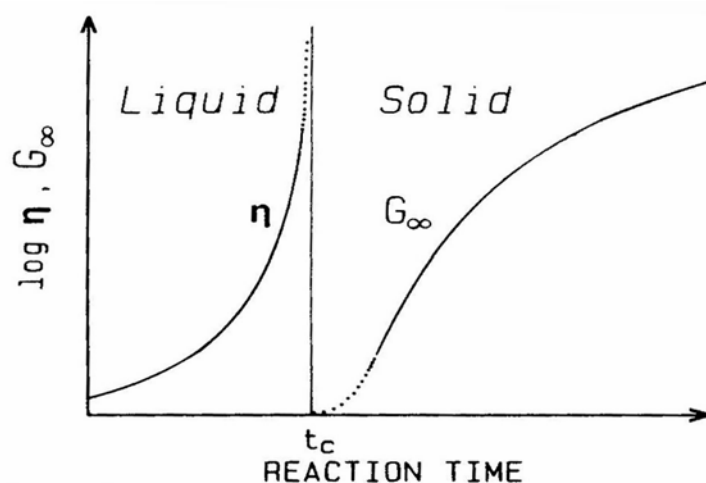


Figure II.7: Evolution of viscosity η and modulus G during gelation [Winter et al, 1986]

In the second method, the evolution of storage G' and loss G'' moduli as a function of time at a fixed frequency and stress are recorded. Figure II.8 shows the evolution of G' and G'' in time at a fixed frequency (0.5 rad/s) for a polydimethylsiloxane (PDMS) polymer.

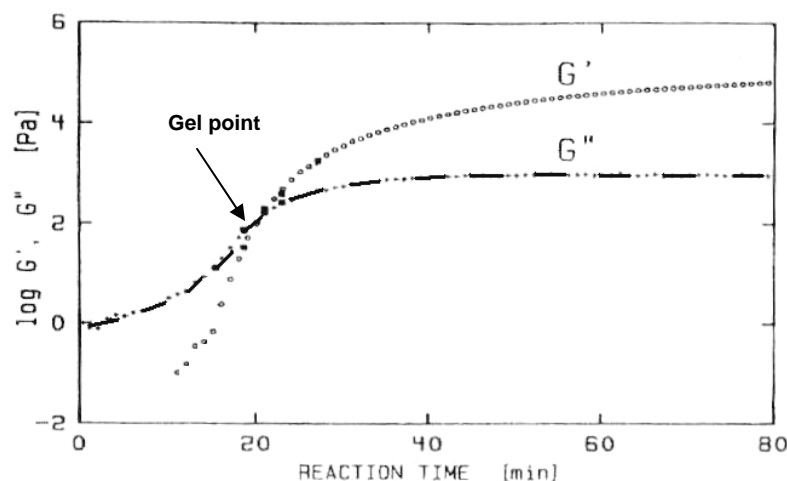


Figure II.8: Evolution of G' and G'' as a function of time for a PDMS polymer (polydimethylsiloxan) $f = \text{cst} = 0.5 \text{ rad/s}$ [Winter et al, 1986]

Initially, the system is in a liquid state, the viscous component G'' is high while the elastic component G' is negligible. During cross-linking, G'' is progressively increasing whereas G' is dramatically increasing until the two moduli are joining. G'' becomes constant whereas G' is still increasing before reaching a plateau. When the crosslinking reaction is terminated, the two components G' and G'' are constant. The advantage of this method is that it shows the evolution of viscoelastic properties during the gelation phenomenon.

In our investigation, the moduli were measured as a function of time and the gelation time was determined following Winter procedure at fixed frequency, 1Hz and stress, 0.01Pa (linear regime). Another procedure was used to determine the gelation temperature. The gel point was determined as an intersection of elastic, G' , and viscous, G'' , moduli as a function of temperature. From this measurement gelation temperature and gel strength when $G' = G''$ can be obtained. This test is not very precise but allows the acquisition of relative information on gelation temperature.

The steady-state viscosity measurements were performed at fixed temperature with shear rate varying from 0.1 to 100 s^{-1} .

3 Results and discussion

In this section, the results of the flow and gelation of cellulose/NaOH aqueous solutions with or without urea are presented. The influence of cellulose origin and concentration, of urea concentration on gelation characteristics such as gelation time, temperature and gel strength at the gel point were investigated. The goal of this work was to determine the conditions for the preparation of gels for further making of Aerocellulose samples and to get some indications on the influence of urea on gelation characteristics.

3.1 Steady-state flow of cellulose-NaOH solutions

Viscosity as a function of shear rate for 5Avicel/7.6NaOH/H₂O solution at different temperatures was measured (Figure II.9).

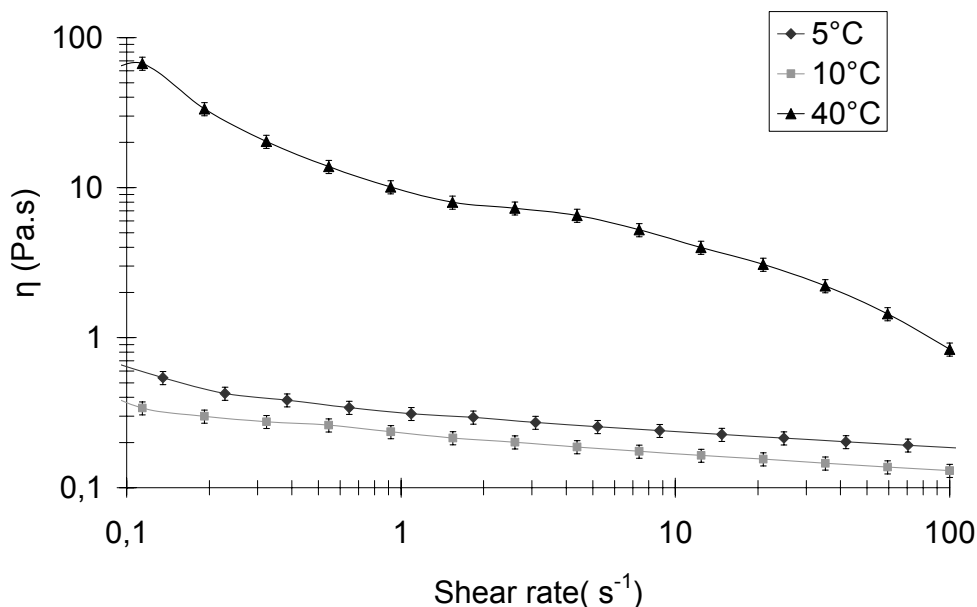


Figure II.9: Viscosity as a function of shear rate at 5°, 10° and 40°C for a 5Avicel/7.6 NaOH/H₂O solution. Lines are given to guide the eye.

From this graph, two trends can be observed. First, solutions at 5° and 10°C are slightly shear thinning. Viscosity decreases with the shear rate increases; this shear-thinning effect is typical for many polymer solutions and melts due to chains orientation in the flow. As it will be shown in the following, the solution at 40°C starts to gel, thus the “shear thinning” can be most probably breaking of the weak gel.

Second, with temperature increase from 5°C to 10°C the viscosity decreases, as it should be for most of solutions due to the thermal motion of macromolecules. But from 10°C to 40°C the viscosity strongly increases. This large viscosity increase together with the more pronounced shear thinning is related with the formation of a physical network: solution is gelling with temperature increase and the gel is breaking under shear.

The flow of cellulose solutions in NaOH/water in the presence of urea was also studied at temperatures far enough from gelation. Viscosity as a function of shear rate for 5cellulose/7.6NaOH/12urea/water solution was measured at 10°, 20° and 30°C. The results are presented in Figure II.10:

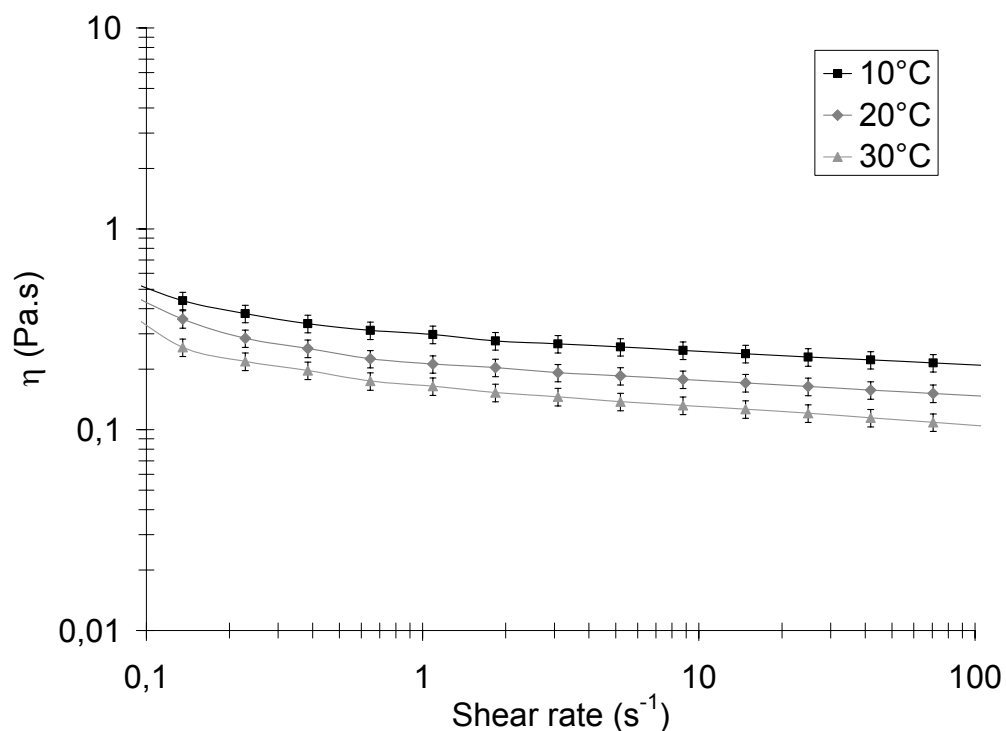


Figure II.10: Viscosity as a function of shear rate at 10°, 20 and 30°C for a 5Avicel/7.6 NaOH/12Urea/H₂O solution. Lines are given to guide the eye.

It appears that 5cellulose/7.6NaOH/12urea/water solution shows a Newtonian behaviour at the chosen temperatures and shear rates.

The viscosity decreases with temperature increase from 10°C to 30°C, which is typical for “normal” solutions. For this cellulose solution it means that in this temperature interval the solution is far from its gelation, thus it is behaving as a “normal” polymer solution.

The same trend was observed for cellulose/NaOH/water solutions far enough from gelation in the temperature range from 5°C to 20°C. The addition of urea only changes the gelation temperature, as we will see latter.

Figure II.11 shows the viscosity versus shear rate for 5Avicel in 7.6NaOH/water and in 7.6NaOH/12urea/water at 10°C, temperature where no gelation was noticed, the flow index “n” was calculated in the shear thinning zone. It was determined as follow:

$$\eta = (\dot{\gamma})^n$$

where η is viscosity, $\dot{\gamma}$ is shear rate and n the flow index

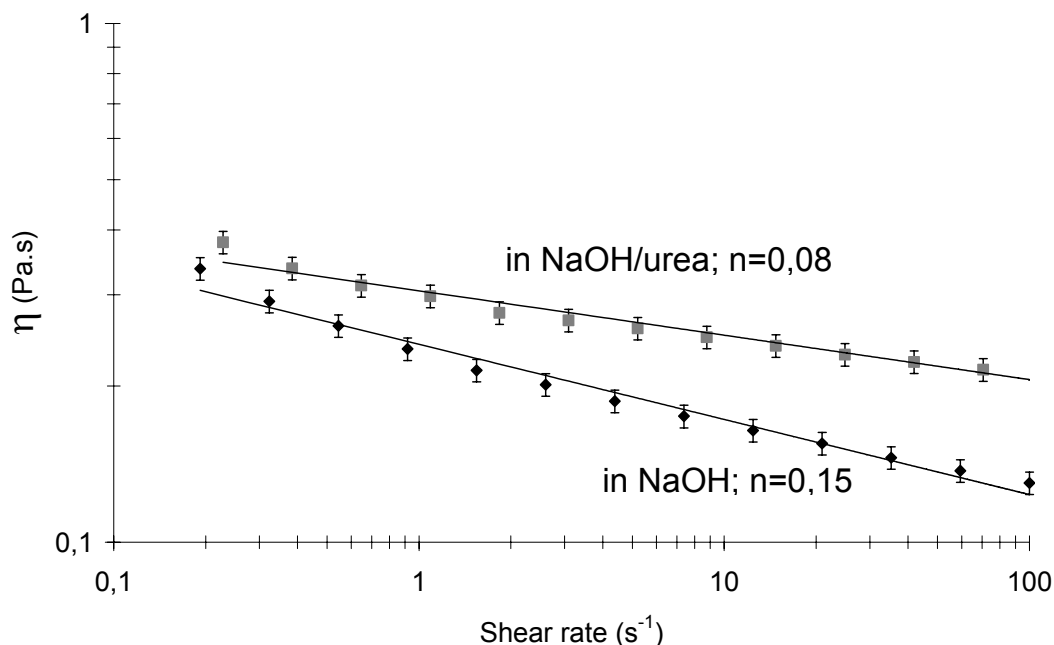


Figure II.11: Viscosity as a function of shear rate at 10°C for 5 Avicel cellulose in 7.6NaOH/H₂O and in 7.6NaOH/12Urea/H₂O

We observe that under shear cellulose/NaOH/urea aqueous solution has a more Newtonian behaviour than cellulose/NaOH aqueous solution as far as the flow index for cellulose/NaOH/water solution is higher than for cellulose/NaOH/urea water. Another point to note is that the viscosity of solution in NaOH/water is lower than the one in the presence of urea. It is thus possible to conclude that NaOH/urea/water is thermodynamically a better cellulose solvent than NaOH/water and that in NaOH/water solution is more structured (this structure being destroyed under flow) due to more “intensive” cellulose-cellulose interaction in NaOH/water than in cellulose/NaOH/urea/water solution.

For the two systems, with or without urea, we observe that in a certain interval of temperature far from gelation, higher the temperature, lower the viscosity. This could be explained by an increase of the mobility of cellulose chains. The calculation of the activation energy allows quantifying this phenomenon. The activation energy is determined by the Arrhenius law:

$$E_a = RT \ln(\eta)$$

where E_a is the activation energy (J/mol), R is the constant of perfect gas (8.314 J/mol/°K), T is the temperature (°K) and η is zero shear rate viscosity (Pa.s).

If we plot the logarithm of the viscosity versus the inverse temperature, we obtain from the slope the activation energy. Figure II.12 shows the curves obtained for the cellulose solution with or without urea.

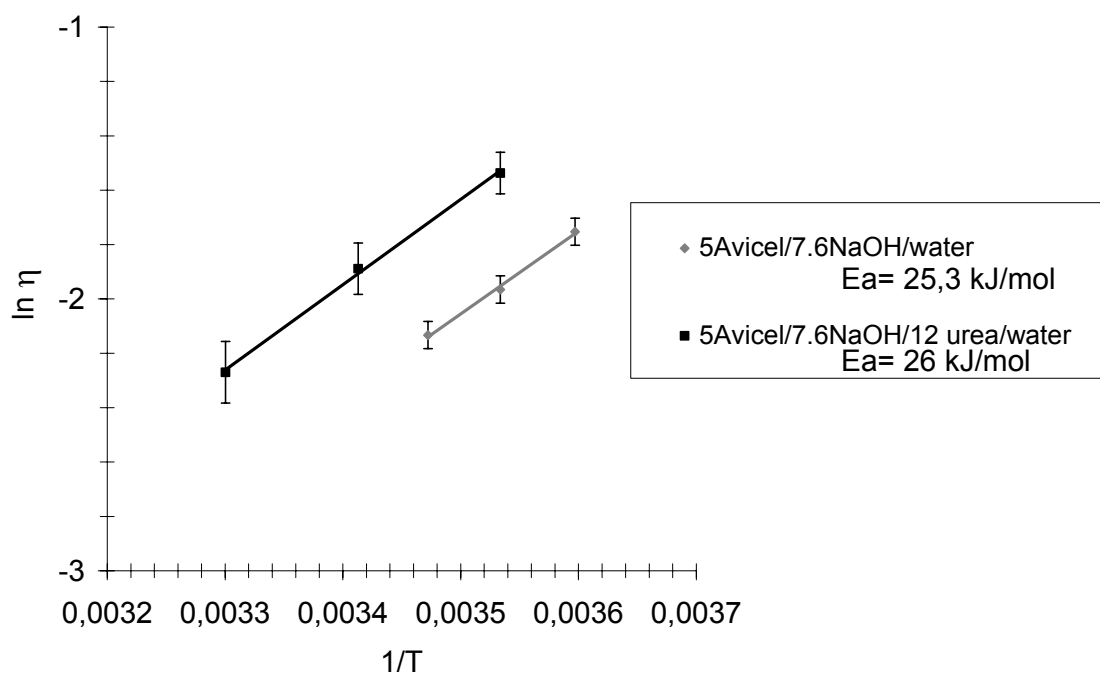


Figure II.12: $\ln \eta$ as a function $1/T$ for 5Avicel cellulose in 7.6 NaOH/H₂O and in 7.6NaOH/12urea/H₂O and values of the corresponding activation energy (kJ/mol)

The values of activation energy for the two systems are very close, around 25.6 ± 0.4 kJ/mol. The mobility of cellulose chain in 7.6NaOH/water with or without urea added is the same.

3.2 Gelation of cellulose/NaOH/water solutions

3.2.1 Influence of temperature on gelation time

Gelation time as a function of temperature was determined from the measurement of the evolution of G' and G'' as a function of time for different fixed temperatures. Figure II.13 is an example of one of such a measurement.

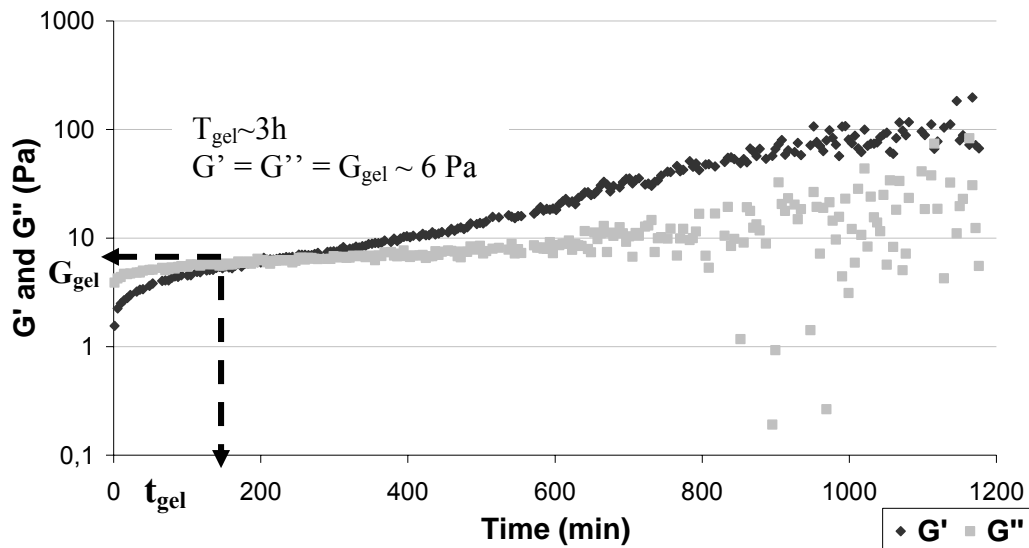


Figure II.13: G' and G'' as a function of time for a 5 Borregaard DP500/7.6NaOH/H₂O solution at 20°C. Gelation time t_{gel} and gel strength G_{gel} at gel point are shown with the arrows

At time $t=0$ min, viscous modulus G'' is superior to elastic modulus G' , the system is in a solution state; the sample behaves like a viscous liquid. With time G' increases more rapidly than G'' : it crosses G'' at a certain gelation time t_{gel} and becomes larger than G'' . The system gradually transforms from a viscous liquid into an elastic network. Similar results were obtained for other temperatures.

One can notice that the formed gel has certain opacity: this means that a micro-phase separation takes place. In about ten hours, points become very scattered. We observed a phenomenon of syneresis: solvent is released from the gel and the sample slides leading to bad reproducibility of the rheological measurements. The syneresis can be clearly observed if heating the system for several hours at higher temperatures, around 50°C (Figure II.14): up to 17% of volume can be released in a few days. The high amount of liquid released can be explained either by thermal degradation of cellulose and/or phase separation evolving in time. Aside of general reasoning that phase separation occurs due to the decrease of solvent (NaOH/water) thermodynamic quality at temperatures above zero, the particular mechanism of this phenomenon is not very clear yet.

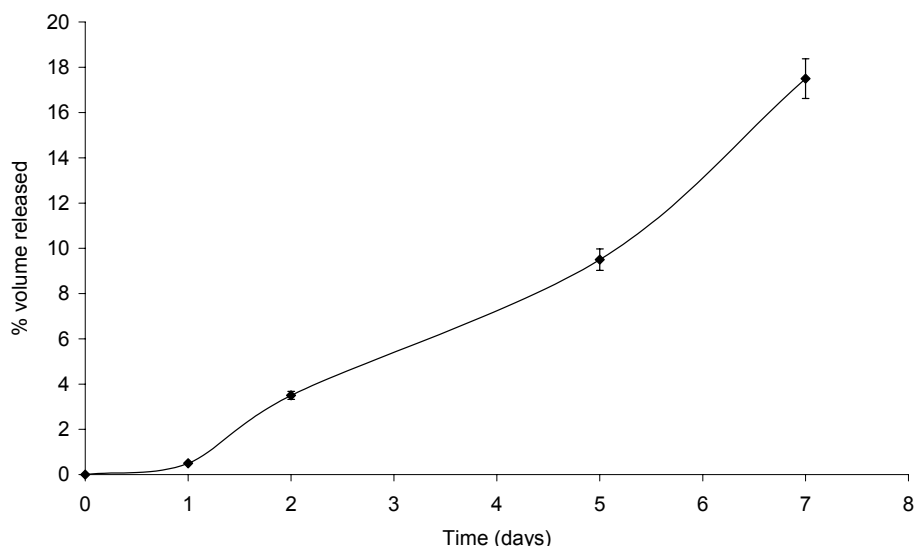


Figure II.14: Phenomenon of syneresis: percentage of volume loss as a function of time for a 5Avicel/7.6NaOH/H₂O gel at 50°C

With time both moduli G' and G'' increase but do not reach any plateau. For classical gelling systems, moduli reach a constant value. In our case moduli increase even at very long observation times. This means that the system does not reach an equilibrium state and that the gel still evolves becoming stronger with time. At least two reasons of moduli increase with time can be given. On one hand, the amount of “cross-linking junctions” may increase because of cellulose-cellulose chains preferential interactions caused by the decrease of solvent quality. On the other hand, such an evolution can be a sort of artefact simply linked to syneresis: the continuous increase of cellulose concentration inside the gel leads to the increase of gel moduli. The second assumption is not valid because the increase of moduli values in time are much higher than it could be due to cellulose concentration increase; this was checked by comparing G' and G'' values of gels with different cellulose concentrations. We can thus conclude that the amount of cellulose-cellulose bonding increases in time.

The influence of the temperature on gelation of 5Avicel/7.6NaOH/water solutions is shown in Table II.4.

Temperature	Avicel cellulose of DP = 170	
	Gelation Time	G_{gel} (Pa)
10°C	~ 50 hours	1.8
20°C	~ 40 min	1.3
30°C	< 1 min	1.5
40°C	Few seconds	≈ 2.3

Table II.4: Time of gelation and gel strength for 5Avicel/7.6NaOH/H₂O solution

Figure II.15 shows the dependence of gelation time as a function of temperature for 5Avicel/7.6NaOH/H₂O solution studied plus the experimental result obtained by C. Roy for 5Avicel/9NaOH/H₂O solution [Roy et al, 2003].

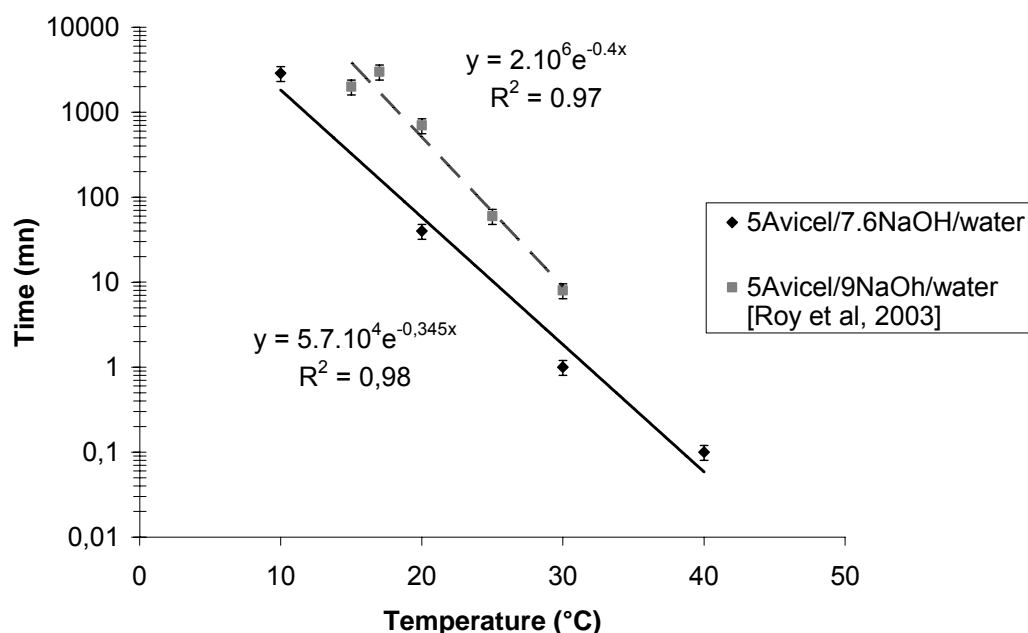


Figure II.15: Time of gelation as a function of temperature of 5Avicel cellulose in 7.6NaOH/H₂O and in 9NaOH/H₂O solutions [Roy et al, 2003]

The time of gelation decreases in an exponential way $t_{\text{gel}} (\text{min}) = 5.7 \cdot 10^4 \exp(-0.345T^{\circ}\text{C})$ with temperature increase. If we compare our results with the ones obtained by C.Roy [Roy et al, 2002] for 5Avicel/9NaOH/H₂O, we observe a same exponential trend. It should be noted that the increase of sodium hydroxide concentration from 7.6 to 9% delays the gelation time of cellulose/NaOH/H₂O solutions.

As shown in the previous section, phase separation followed by syneresis occurs in time. It is thus possible to assume that time and temperature are acting on cellulose/NaOH/water solutions in the same “destabilising” way. Indeed, NaOH/water is not a very good cellulose solvent (see results on cellulose dissolution, [Cuissinat et al, 2006]). The thermodynamic quality of NaOH/water decreases with temperature increase (decrease of the intrinsic viscosity with temperature increase observed in [Roy et al, 2003] thus leading to the preferential cellulose-cellulose interactions. That is why in semi-dilute solutions these interactions induce gelation that is faster at higher temperatures.

Moreover, we have observed that gelation at ambient temperature, 20°C, is faster for the microcrystalline Avicel cellulose solutions (40 minutes) than for the Borregaard cellulose solutions (3 hours; see Figure II.13). This surprising result ($DP_{\text{Avicel}} = 170$ and $DP_{\text{Borregaard}} = 500$) can be explained by a better dissolution of the micro-crystalline cellulose in 7.6NaOH/water solution: Borregaard fibres that remain undissolved or are partly dissolved do not participate to solution gelation and thus the real cellulose concentration in solution of Borregaard cellulose is slightly decreased. As it will be shown in Section II.3.2.2, the decrease of cellulose concentration “delays” gelation, i.e. leads to the increase of gelation temperature and, in the same way, increase gelation time.

3.2.2 Influence of cellulose origin and concentration on gelation temperature

In order to check the influence of cellulose type (origin, DP and treatment) and concentration on gelation temperature, G' and G'' of cellulose/7.6NaOH/water solutions for three types of cellulose of different concentrations were studied as a function of temperature. Microcrystalline Avicel, steam-exploded Borregaard and Solucell I with a DP = 170, 500, 307 respectively, were compared. Cellulose content in 100 g solution was varied from 3 to 7g; the temperature interval was from 10°C to 100°C. Gelation temperature T_{gel} and gel strength at gelation point $G_{gel} = G' = G''$ was determined at the intersection of the two moduli. An example for 5Avicel/7.6NaOH/H₂O solution is shown in Figure II.16.

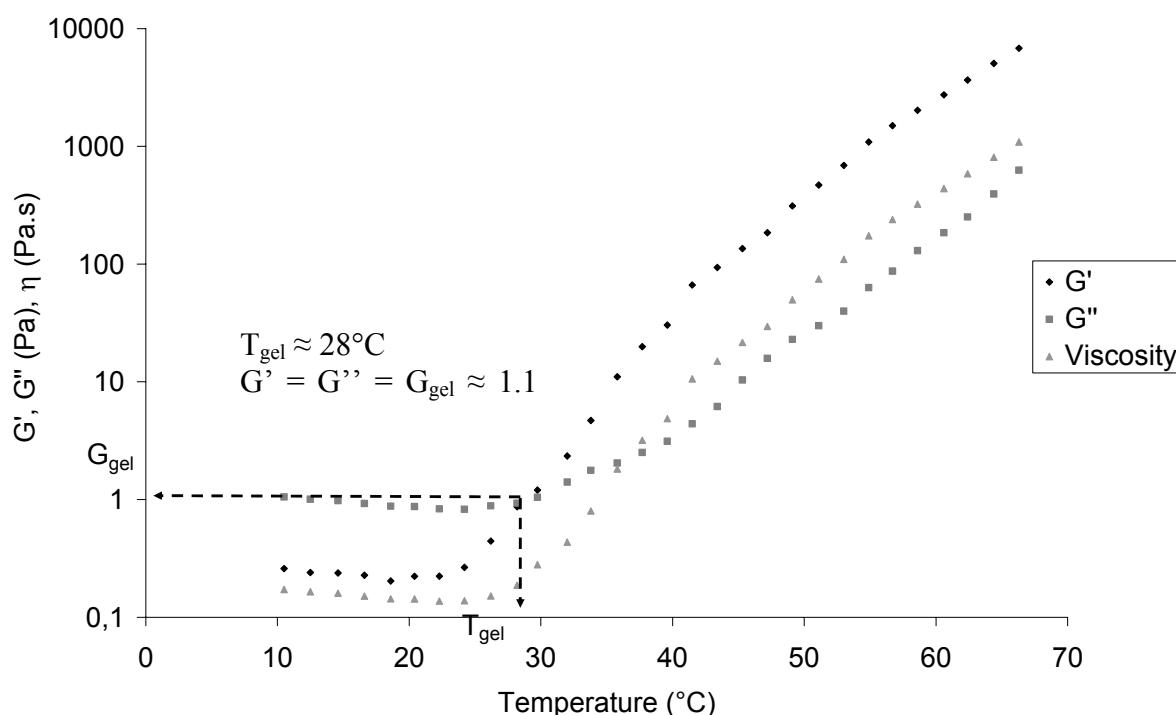


Figure II.16: G' , G'' and η^* as a function of temperature for 5Avicel/7.6NaOH/H₂O solution. Gelation temperature T_{gel} and gel strength G_{gel} at gel point are shown with the arrows

Below 25°C, G' and G'' slightly decrease with temperature increase. G'' value is about one decade higher than G' : it is a typical liquid-like behaviour. Above 25°C gelation starts and visco-elastic characteristics go through a minimum: both moduli increase with temperature, G' strongly increases and overcomes G'' around 28°C. Similar trends were obtained for other systems. The results are summarised in Figures II.17 and II.18 for gelation temperature and gel strength at the gel point, respectively.

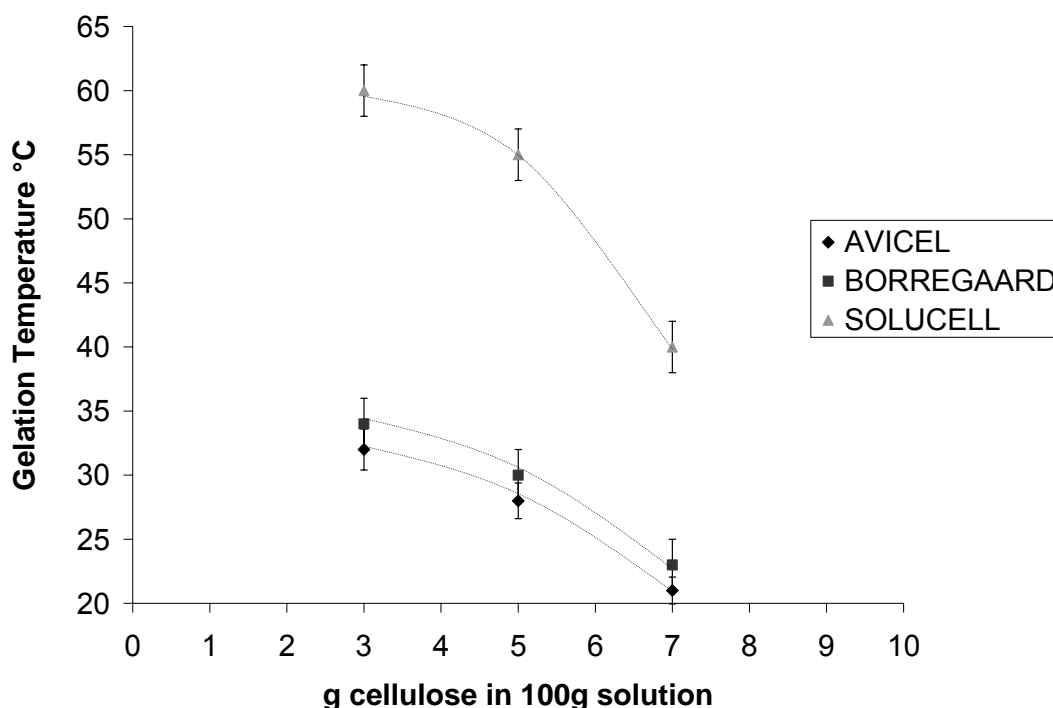


Figure II.17: Gelation temperature as a function of cellulose content for Avicel (DP 170), Borregaard (DP 500) and Solucell I (DP 307) in 7.6NaOH/H₂O solution

The increase of cellulose concentration leads to a decrease of gelation temperature. Indeed, the more concentrated the solution is, the more numerous the chains interactions are. Thus less energy is needed to start gelation in higher concentrated solutions.

While gelation temperature of Avicel and Borregaard solutions for studied cellulose concentrations is practically the same, T_{gel} of Solucell I solution is 20-25°C higher. Obviously, it is not DP but the way of cellulose preparation and probably of cellulose origin that plays an important role in cellulose-cellulose interactions in NaOH/water solutions. It should be noted that Solucell II with DP 198 does not dissolve in 7.6%NaOH aqueous solution. A similar observation for cellulose II has been reported by Isogai and Atalla who noted the insolubility of mercerized linter cellulose in 8%NaOH [Isogai et al, 1998].

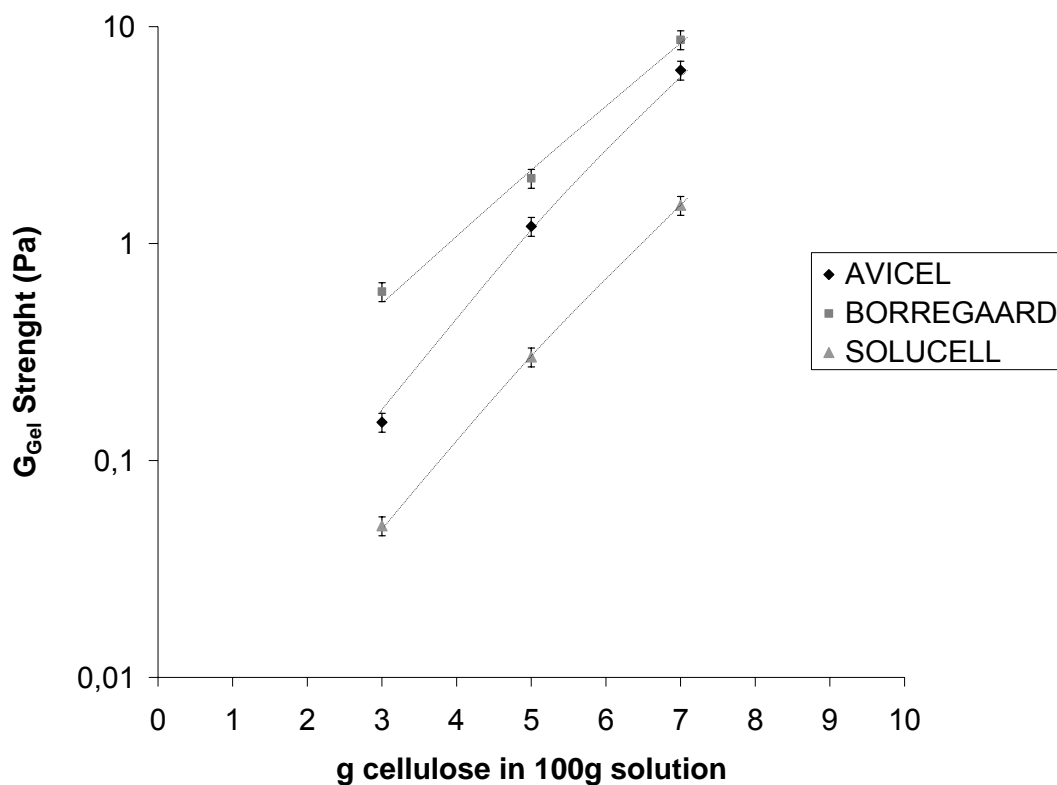


Figure II.18: G_{gel} strength as a function of cellulose content for Avicel, Borregaard and Solucell I in 7.6NaOH/H₂O solution

The increase of cellulose concentration leads to an increase of gel strength (Figure II.18). It is due to the progressive increase of cellulose chains interactions leading to a stronger network structure. The value of G_{gel} for Borregaard solution is higher than the one of Avicel solution and one decade higher the one of Solucell I. This can be explained by the influence of DP. The origin of cellulose also may influence the strength of the gel as well as gelation temperature, as demonstrated in the previous paragraph. The fact that Borregaard gel is stronger than Avicel or Solucell I gel could also be explained by the presence of undissolved parts of the Borregaard pulp that could reinforce the gel. In order to choose what the main parameter responsible for gel strength is, more experiments are needed where cellulose DP and origin are varied in the systematic way.

3.2.3 Influence of urea concentration on gelation

The influence of additives such as urea on cellulose/NaOH/water solution gelation was investigated. Figure II.19 represents an example of the evolution of viscous and elastic moduli and of dynamic viscosity as a function of temperature for the 5Avicel/7.6NaOH/12urea/water solution. Gelation temperature and gel strength at the gel point were determined as previously.

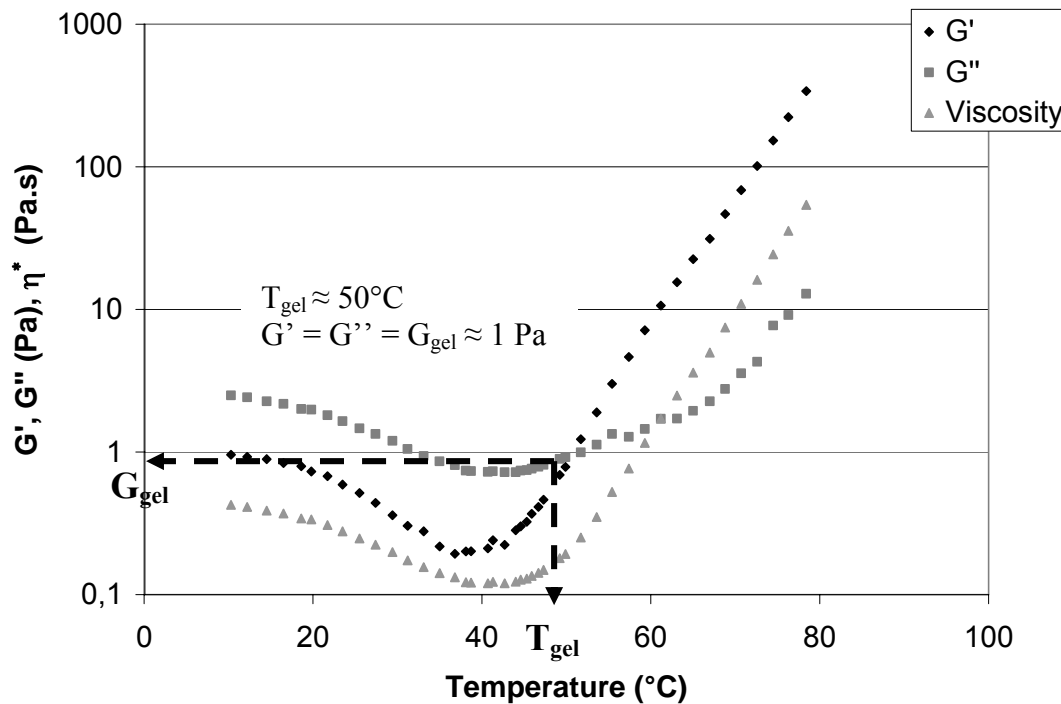


Figure II.19: G' , G'' , η^* as a function of temperature for 5Avicel/7.6NaOH/12urea/water solution

As in Avicel/7.6NaOH/water solutions, all visco-elastic characteristics of 5Avicel/7.6NaOH/12urea/water solution decrease with temperature increase, up to 40°C, G'' being higher than G' by one decade. At 40°C gelation starts and G' , G'' and η^* show a minimum: all characteristics increase with temperature increase, G' having the fastest rate of increase and crossing G'' at about 50°C. In order to conclude on the influence of urea on gelation of cellulose/NaOH aqueous solutions, let us compare the evolution of G' as a function of temperature with and without urea. An example of such a comparison is shown in Figure II.20 for 0, 6 and 12 g of urea in 100 g solution. It is clear that higher is urea content, more the minimum on the G' curve is shifted towards higher temperatures.

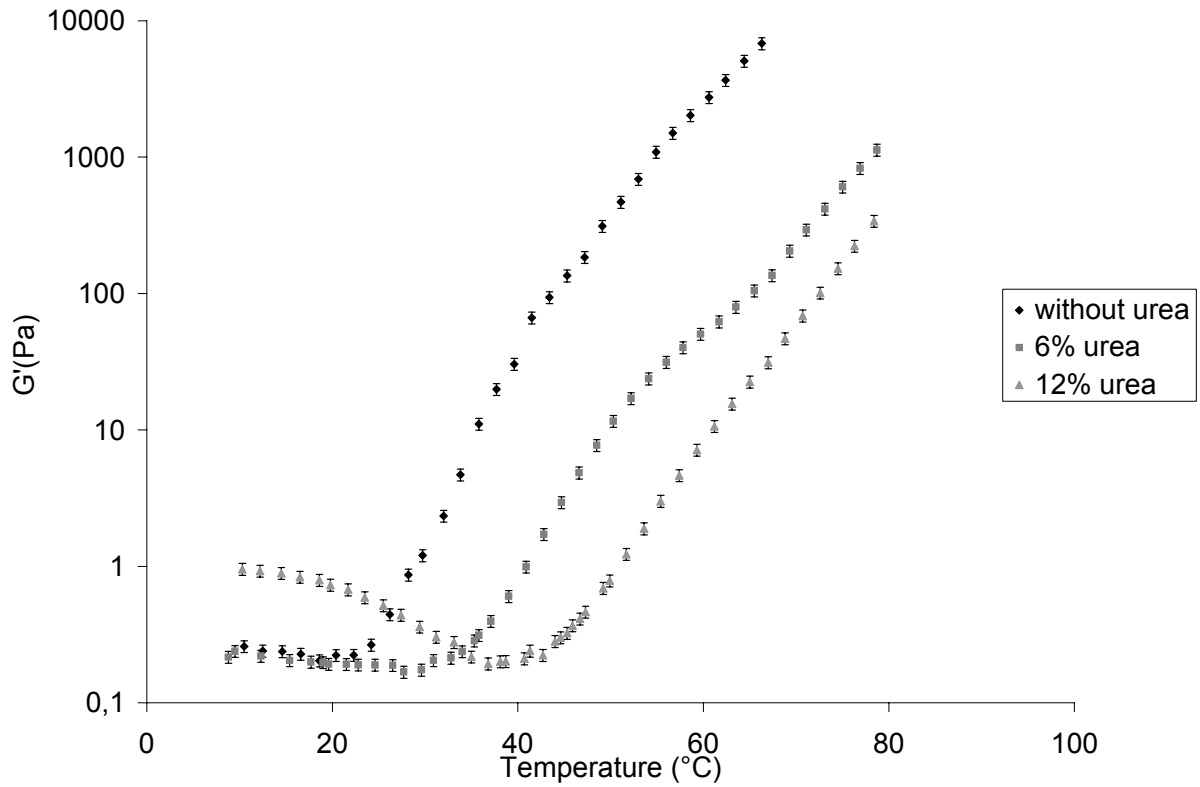


Figure II.20: G' as a function of temperature for 5Avicel/7.6NaOH/water solution without and with 6% and 12 % urea

Figure II.21 shows the same data as in Figure II.20 but with 6% and 12% urea shifted by (-12.5°C) or (-23°C), respectively, which corresponds to the difference of gelation temperature between 5Avicel/7.6NaOH/water solution and 5Avicel/7.6NaOH/Zurea/water solution with $Z=6$ or 12.

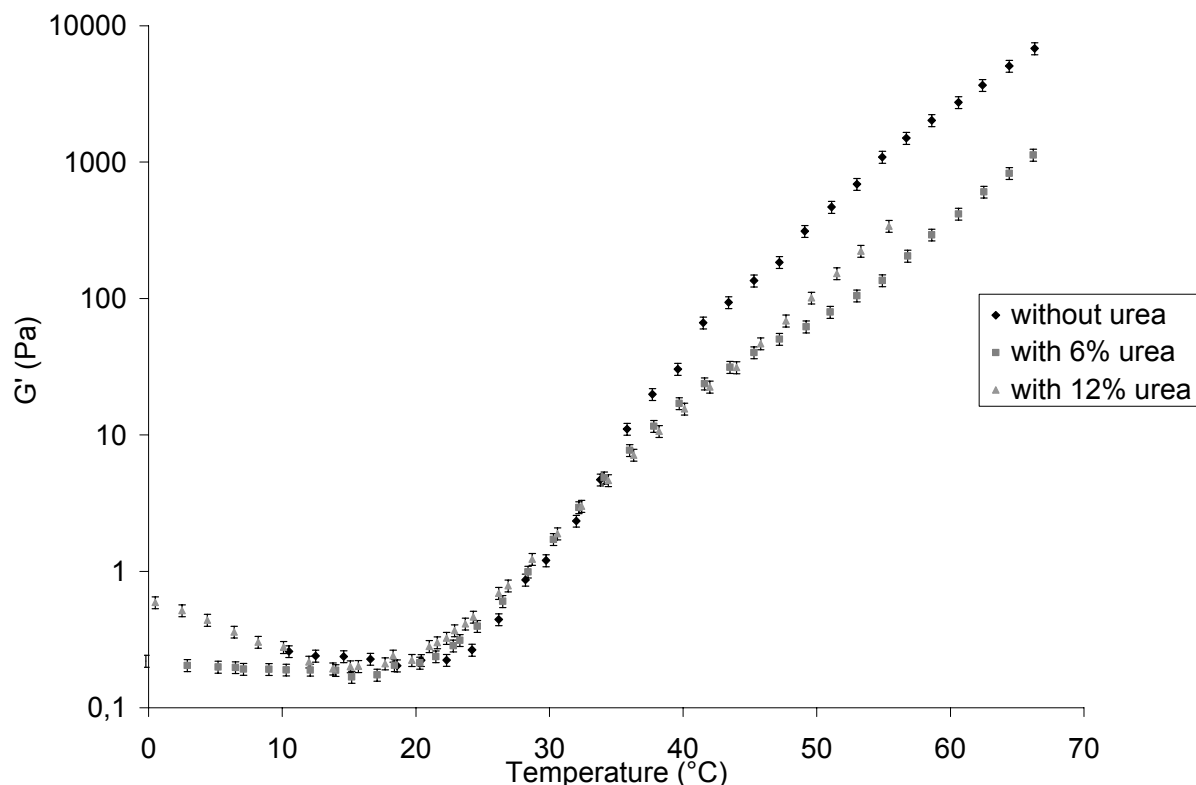


Figure II.21: G' as a function of temperature for 5Avicel/7.6NaOH/Zurea/water with G' shift by -12.5°C and -23°C respectively for $Z= 6$ and 12

With the temperature shift, it appears that the three curves coincide at the minimum of elastic modulus. After gelation occurs, the elastic modulus increases with temperature increase. At high temperature, above 50°C the strength of 5Avicel/7.6NaOH/6urea/water gel is lower than the one of 5Avicel/7.6NaOH/water gel. For instance at 60°C we observe one order decade between gel without urea and gel with 6urea. The elastic modulus for cellulose/NaOH/water with 6 and 12 urea coincides and the general trend is the same as without urea. It is thus possible to conclude that the gelation mechanism remains the same whatever is the urea concentration.

The measurements of G' and G'' as a function of temperature were performed for other urea concentrations keeping the content of cellulose and NaOH constant: 5cellulose/7.6NaOH/Zurea/water with $Z= 6, 12, 16$ and 20 g in 100 g solution and for different cellulose types (Avicel, Borregaard and Solucell I and II of DP = 170, 307 and 500, respectively). Figure II.22 presents gelation temperature as a function of the content of urea for different types of cellulose. In some cases gelation was observed during solution preparation; this gelation temperature is noted as occurring at -6°C .

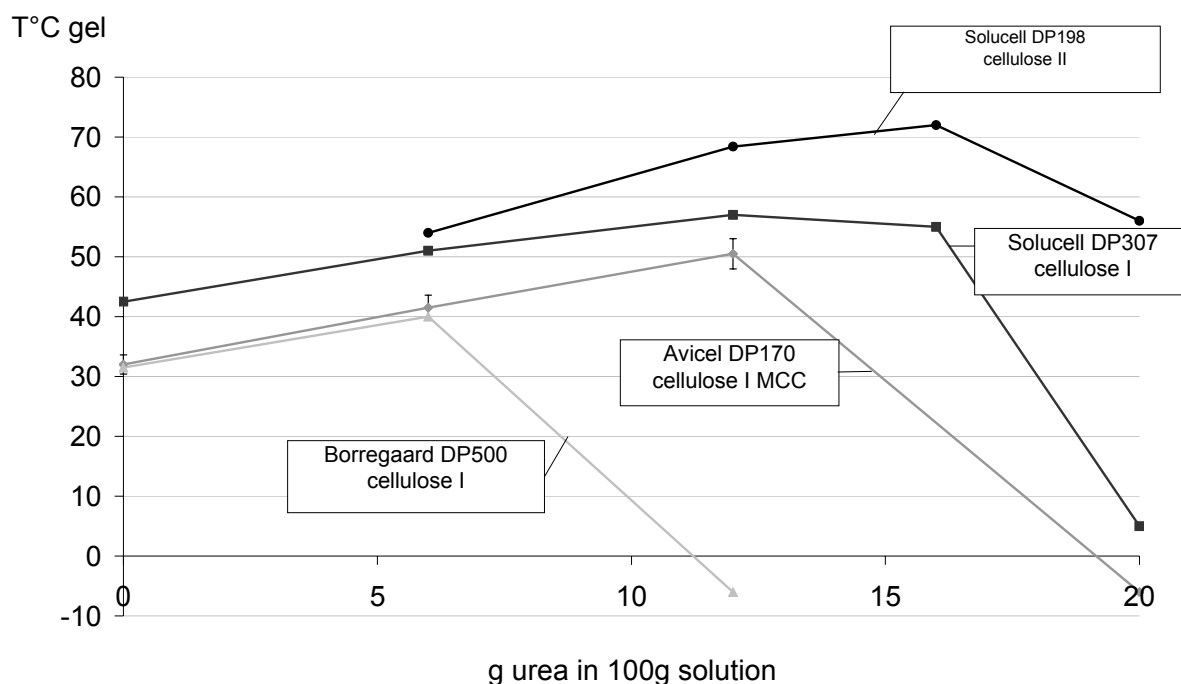


Figure II.22: Gelation temperature of aqueous 5cellulose/7.6NaOH/Zurea/water solutions of different cellulose types (DP, origin) as a function of urea content Z, Z = 6, 12, 16 and 20 g in 100 g solution

Figure II.22 shows that the addition of urea is increasing gelation temperature up to a certain urea concentration, thus improving solvent quality and cellulose dissolution. Above this value (at higher urea concentrations), gelation temperature strongly decreases and cellulose solution is gelling immediately after the preparation, below 0°C. For each cellulose type, there is an optimal urea content, Z, in terms of highest gelation temperature. For Avicel Z=12 g in 100 g solution, for Borregaard Z=6 g, for Solucell I of DP=307 Z=12 g and for Solucell II of DP=198 Z=16. Maximal gelation temperature was observed for Solucell cellulose II of DP=198: 72°C, but this cellulose is not dissolved in 7.6NaOH/water. In average, gelation temperature in the presence of urea is shifted by 10-20°C towards higher values as compared with cellulose/7.6NaOH/water solution depending on cellulose origin, treatment and DP.

Compared to the optimal ratios of 2% urea-8%NaOH obtained in ref. [Zhou et al, 2000] to improve the dissolution of cellulose, we found higher values of urea content, Z=6 to 16 g in 100 g solution increasing gelation temperature and thus the quality of the solvent. At Z >16 g, all cellulose solutions are gelling showing that the increase of urea content above a certain optimal value decrease solvent quality, as observed by Zhou et al who described a decrease of cellulose solubility with continued addition of urea. The optimal urea content clearly depends on cellulose used.

If we consider the gel strength G_{gel} at $G' = G''$ of each cellulose for different urea content from 0 to 20 g in 100 g solution, we observe the same value of G_{gel} for a given cellulose whatever the urea proportion is (Table II.5). There is no effect of urea content on the gel strength, but it depends on cellulose type.

Cellulose	Solucell II DP 200	Solucell DP307	Avicel DP170	Borregaard DP500
Gel strength $G' = G''$ (Pa)	0.2 ± 0.1	0.22 ± 0.02	1.1 ± 0.2	3.9 ± 0.1

Table II.5: Gel strength at gel point for various celluloses at urea content from 6 to 16 g in 100 g solution

It is not clear why the optimal proportion urea/cellulose is different for different cellulose types and there is no direct correlation with cellulose DP. Cellulose treatment and origin seems to play an important role in solution gelation. The common point for all celluloses studied is that the addition of urea first improves solvent quality and shifts gelation temperature towards higher values and high urea concentrations lead to a strong decrease in solvent quality. A precise action of urea on cellulose remains an open question; a detailed phase diagram cellulose/NaOH/urea should be built and more studies of the influence of cellulose DP and treatment on solution gelation should be performed in order to answer this question. However, whatever are the characteristics of the systems studied gelation mechanism remains the same with or without urea.

Conclusions

Gelation of cellulose-NaOH-aqueous solutions with and without additives (urea) was studied in order to use this knowledge for the preparation of Aerocellulose precursors. The influence of the characteristics of materials used like cellulose type and concentration and of urea concentration as well as of experimental conditions like temperature and time on gelation of solutions was investigated. The parameters studied were time needed for gel formation, gelation temperature and gel strength. The results obtained are as following:

- An irreversible physical gelation of cellulose (7-9%NaOH) aqueous solutions occurs with time and temperature increase whatever is cellulose origin and DP. Long heating times lead to the phase separation followed by syneresis.
- Avicel and steam exploded Borregaard (DP = 170 and 500) cellulose solutions of around 5% are gelling within 30-40 minutes around 20°C; Solucell (prepared via electron beam irradiation, DP=300) 5% cellulose solution is gelling at higher temperatures, around 55°C.
- Gelation time of Avicel/7.6NaOH/water solution exponentially decrease with time:
$$t_{\text{gel}} = 5.7 \cdot 10^4 \exp(-0.345T^{\circ\text{C}})$$
- The increase of cellulose concentration leads to a decrease in gelation temperature.
- The gelation of cellulose/NaOH aqueous solutions is due to the cellulose-cellulose interactions that are favoured by a temperature increase that induces the decrease of solvent quality.
- The addition of urea shifts time and temperature of gelation towards higher values due to the increase of solvent quality. An optimal urea concentration to delay cellulose gelation depends on the nature of cellulose: it is between 6 g in 100 g solution for steam exploded Borregaard (DP = 500) and 16 g for Solucell cellulose I (DP = 307) and Solucell cellulose II (DP = 198).
- The gelation mechanism of cellulose/(7-9) NaOH/water solutions with or without urea is the same; however, the exact action of urea on cellulose is still an open question.

For the preparation of Aerocellulose precursors, cellulose solutions will be made as described in Section II.2.1; cellulose concentration will be varied from 3 to 7%. Knowing the course of gelation for different celluloses as a function of its concentration and of the presence of urea, of temperature and time, different gels will be prepared.

The next step of the preparation of Aerocellulose is the regeneration of cellulose from the gels obtained. The kinetics of regeneration and the influence of bath parameters will be studied in the next chapter.

References

[Cai et al, 2006]	Cai, J.; Zhang, L.; Unique gelation behaviour of cellulose in NaOH/urea aqueous solution. Biomacromolecules, 7, (2006), pp 183-189
[Chambon et al, 1985]	Chambon, F.; Winter, H.H.; Stopping of crosslinking reaction in a PDMS polymer at the gel point Polymer Bulletin 13, (1985), pp 499-503
[Cuissinat et al, 2006]	Cuissinat, C.; Navard, P.; Swelling and dissolution of cellulose Part II: free floating cotton and wood fibres in NaOH – water – additives systems Macromolecular Symposia, 244, (2006), pp 19-30
[Egal et al, 2005]	Egal, M.; Gavillon, R.; Budtova, T.; Navard, P.; Propriétés rhéologiques et gélification de solutions aqueuses de cellulose dans NaOH en présence d'additifs Proceeding in 40 th annual conference of GFR (Groupe Français de Rhéologie), Nice, France, October 2005, pp 300-304
[Egal et al, 2006]	Egal, M.; Budtova, T.; Navard, P.; Structure of cellulose-sodium hydroxide aqueous solutions below 0°C Biomacromolecules, (2006), accepted
[Isogai et al, 1998]	Isogai, A.; Atalla, R.H.; Dissolution of cellulose in aqueous NaOH solutions Cellulose, 5, (1998), pp 309-319
[Kamide et al, 1984]	Kamide, K.; Okajima, K.; Matsui, K.; Kowasaka, K.; Study on the solubility of cellulose in aqueous alkali solution by deuterium IR and ¹³ C NMR Polymer Journal, 16, (1984), pp 857-866
[Kunze et al, 2005]	Kunze, J.; Fink, H.P.; Structural changes and activation of cellulose by Caustic soda solution with urea Macromolecular Symposia, 223, (2005), pp 175-187
[Laszkiewicz, 1997]	Laszkiewicz, B.; Solubility of bacterial cellulose and its structural properties Journal of Applied Polymer Science, 67, (1997), pp 1871-1876
[Nishiyama et al, 2000]	Nishiyama, Y.; Kuga, S.; Mechanism of mercerization revealed by X-ray diffraction Journal of Wood Science, 46, (2000), pp 452-457

[Okano et al, 1985]	Okano, T.; Sarko, A.; Mercerization of cellulose. II. Alkali-cellulose intermediates and a possible mercerization mechanism Journal of Applied Polymer Science, 30, (1985), pp 325-332
[Roy et al, 2003]	Roy, C.; Budtova, T.; Navard, P.; Rheological properties and gelation of aqueous cellulose-NaOH Biomacromolecules, 4, (2003), pp 259-264
[Sarko et al, 1987]	Sarko, A.; Nishimura, H.; Okano, T.; Journal of American Chemical Society, 97, (1987), pp 170-176
[Sobue et al, 1939]	Sobue, H.; Kiessig, H.; Hess, K.; The cellulose-sodium hydroxide-water system as a function of the temperature Z.Physik.Chem., 43, (1939), pp 309-328
[Takahashi et al, 1991]	Takahashi, M. ; Ookubo, M ; Takenaka, H.; Solid state of ¹³ C spectra analysis of alkalicellulose Polymer Journal, 23, (1991), pp 1009-1014
[Weng et al, 2004]	Weng, L.; Zhang, L.; Ruand, D.; Shi, L.; Xu, J.; Thermal gelation of cellulose in a NaOH/Thiourea aqueous solution Langmuir, 20, (2004), pp 2086- 2093
[Yamashiki et al, 1992]	Yamashiki, T.; Matsui, T.; Kowsaka, K.; Saitoh, M.; Okajima, K.; Kamide, T.; New class of cellulose fibers spun from the novel solution of cellulose by wet spinning process Journal of Applied Polymer Science, 44, (1992), pp 691-698
[Yokota et al, 1990]	Yokota, H.; Sei, T.; ¹³ CP/MAS NMR study on alkali cellulose Journal of Applied Polymer Science, 41, (1990), pp 783-791
[Zhang et al, 2006]	Zhang, L.; Ruan, D.; Gao, S.; Dissolution and regeneration of cellulose of cellulose in NaOH/Thiourea aqueous solution Journal of Polymer Science: Part B: Polymer Physics, 40, (2002), pp 1521-1529
[Zhou et al, 2000]	Zhou, J.; Zhang, L.; Solubility of cellulose in NaOH/urea aqueous solution Polymer Journal, 32,10, (2000), pp 866- 870

Chapter III: Kinetics of cellulose regeneration from cellulose- NaOH-water gels and comparison with cellulose- NMMO-water solutions

Article published in *Biomacromolecules*, January 2007, volume 8, pp 424-432
Authors: Roxane Gavillon and Tatiana Budtova

Abstract

The regeneration kinetics of cellulose from cellulose-NaOH-water gels immersed in a non-solvent bath is studied in detail. Cellulose concentration, bath type and temperature were varied and diffusion coefficients were determined. The results were compared with measured and taken from literature data on regeneration kinetics of cellulose from cellulose-NMMO monohydrate solutions.

Different theories developed for the transport behaviour of solutes in hydrogels or in porous media were tested on the systems studied. While the diffusion of NaOH from cellulose-NaOH-water gels into water has to be described with “porous media” approaches, the interpretation of NMMO diffusion is complicated because of the change of NMMO state during regeneration (from solid crystalline to liquid) and high concentration of NMMO in the sample. The activation energies were calculated from diffusion coefficient dependence on temperature for both systems and compared with the ones obtained from the rheological measurements. The activation energy of cellulose-NaOH-water systems does not depend on cellulose concentration or the way of measurement. This result shows that whatever the system is – pure NaOH-water solution, cellulose-NaOH-water solution or cellulose-NaOH-water gel, it is NaOH hydrate with or without cellulose in solution, which is moving in the system. The swelling of cellulose in different non-solvent liquids like water or different alcohols during regeneration was investigated and interpreted using Hildebrand parameter.

Introduction

Processing of cellulose is more than 100-years old, but it still attracts attention of research and industry because of search of less polluting, simpler and lower energy consuming methods than the existing ones. Therefore, cellulose dissolution in aqueous solutions of sodium hydroxide is a topic of intensive research. Since the publication of cellulose-NaOH-water phase diagram in the paper of H.Sobue¹, it is known that it is possible to dissolve cellulose in a narrow range of low temperatures and concentrations of NaOH (from 7% to 10% NaOH in water at -6°C). From that time there has been an ongoing research in the understanding of the structure and properties of cellulose-NaOH-water solutions (see, for example, refs. 2-5). Several papers report that cellulose dissolution in NaOH-water may be improved if substances like urea or thiourea are added⁶⁻¹⁰, still NaOH concentration range remaining the same as shown in ref.1.

Fibres and membranes from cellulose-NaOH-water or cellulose-NaOH-additive solutions can be made by so called regeneration or coagulation technique^{8, 11-18} that is used to make shaped cellulose objects from viscose or cellulose-N-methylmorpholine-N-oxide (NMMO) solutions¹⁹. Regeneration of cellulose from either cellulose-NaOH or cellulose-NMMO solutions should occur in a more or less similar way because in both cases cellulose is not initially derivatised but directly dissolved and then regenerated due to phase separation. In the case under consideration, solvent (NaOH-water or NaOH-additive-water) is replaced by cellulose non-solvent, the latter usually being water, or aqueous acid or salt solutions^{15, 16}, or some organic liquid combinations like ethanol and acetone¹⁶. The main principle is that the regenerating liquid must be miscible with the aqueous NaOH solution and be a non-solvent for cellulose. As well as for cellulose-NMMO solutions, the type of regenerating liquid is shown to strongly influence the structure, morphology and properties of cellulose fibres and membranes made from cellulose-NaOH solutions (see, for example, for cellulose materials regenerated from cellulose-NMMO ref. 19; for cellulose-NaOH membranes refs. 13-17). However, there is no publication giving any insight on the kinetic aspects of the regeneration process for objects made from cellulose-NaOH solutions. The kinetics of cellulose regeneration should be controlled by the diffusion of NaOH from the cellulose-NaOH solution into the regenerating bath and of the non-solvent from the bath into the cellulose solution. Is regeneration kinetics of cellulose from cellulose-NaOH solutions comparable to the one of cellulose-NMMO solutions? What is the influence of cellulose concentration, of the non-solvent power, bath type and temperature on regeneration of cellulose from cellulose-NaOH solutions? These questions are important for the understanding and controlling the process of cellulose shaping from NaOH-water solutions.

The goal of this work is to describe the regeneration kinetics of cellulose-NaOH-water gels. The fact that cellulose-NaOH-water solutions are gelling with time and temperature⁵ was used to prepare samples with a well defined shape and volume that were placed in a regenerating bath. To have a defined shape is required for the adequate calculation of diffusion coefficients using Fick theory and for the analysis of results obtained with different diffusion approaches developed for membranes and hydrogels. The influence of cellulose concentration, bath type and temperature on regeneration kinetics of cellulose-NaOH-water gels was investigated and compared with the regeneration of cellulose-NMMO solutions in the same conditions.

1 Experimental section

1.1 Materials

Cellulose

Two types of native cellulose were used: Avicel PH-101, DP = 180, purchased from FMC (Avicel in the following) and Solucell 400, mean DP 950, kindly provided by Lenzing AG (Solucell in the following). Avicel was used for the regeneration studies of cellulose-7.6%NaOH-water gels and Solucell - for cellulose-(NMMO monohydrate) solutions.

Solvents

NaOH and NMMO were of 97% purity, purchased from VWR and Aldrich, respectively. Distilled water was used to prepare the solutions and the regenerating bath. Different alcohols were used for the regenerating bath as non-solvents of cellulose: ethanol (Bioblock, 99.9% purity), isopropanol, butanol, pentanol and hexanol (all from Aldrich, 98-99% purity). The concentrations are given in wt%.

Sample preparation

Avicel-NaOH-water solutions were prepared as follows: Avicel was mixed with 7.6%NaOH-water solution, at -6°C , for 2 hours, with a stirring rate of 1000 min^{-1} ; Avicel concentration was varied from 3 to 7%. Solutions were poured into the mould of $22\text{mm} \times 18\text{mm} \times h\text{ mm}$ dimensions, h being the sample thickness which varied from 1.2 to 2 mm, and kept at room temperature for 15 hours. In these conditions cellulose-7.6%NaOH-water solutions are gelling irreversibly⁵. As a result, rectangular gels slabs were ready for diffusion experiments. Gel dimensions were chosen as a compromise between easiness of sample handling and infinite plane approximation (see Analysis of experimental data section).

Solucell-NMMO solutions were prepared in Lenzing AG. The proportions between Solucell/NMMO/water components in solutions are listed in Table III.1.

Solucell, wt %	NMMO, wt %	H ₂ O, wt %
0.3	80.4	19.3
1.09	80.21	18.7
2.28	80.54	17.18
3.0	82.0	15.0

Table III.1: Weight concentrations of Solucell, NMMO and water in Solucell-NMMO solutions, as given by Lenzing AG

Solucell-NMMO solutions are in a crystalline state at room temperature; they were melted at 80°C and the hot solution was poured into the same mould as used for Avicel-NaOH-water solutions. The solutions cooled down to room temperature and, as a result, solid rectangular samples of the same shape as Avicel-NaOH-water gels were obtained.

Avicel-NaOH-water gels or Solucell-NMMO solutions were placed into regenerating bath and the diffusion coefficient of NaOH or NMMO was measured using various methods (see next section). When regeneration was completed, the morphology of the swollen cellulose was investigated with Environmental Scanning Electron Microscope (ESEM). The pictures of regenerated cellulose swollen in water are shown in Figure III.1. Both samples (regenerated from Avicel-NaOH-water gels or Solucell-NMMO solutions) show a porous structure; the one regenerated from Avicel-NaOH-water gels (Figure III.1a) is denser and with smaller pores than regenerated from Solucell-NMMO solution (Figure III.1b).

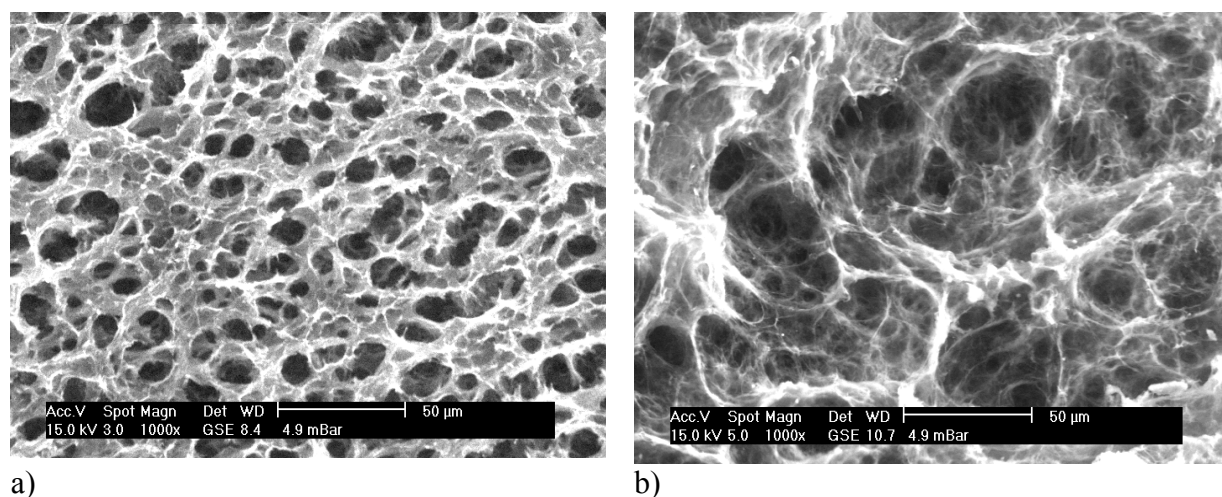


Figure III.1: ESEM images of regenerated cellulose from a) 5% Avicel-NaOH-water gels and b) 3% Solucell-NMMO solutions, both regenerated in water bath at 25°C

1.2 Methods

Regeneration of cellulose was performed in a bath of cellulose non-solvent, water or alcohol, with a controlled volume and temperature. The diffusion coefficient of cellulose solvent (either NaOH or NMMO) from a sample towards the regenerating bath was studied as follows. A sample of Avicel-NaOH-water gel or Solucell-NMMO solution of a given weight and volume was placed in the regenerating bath at a fixed temperature. The proportion between sample/bath weights was kept constant and equal to ten. Magnetic stirrer was used to gently mix liquids in regenerating bath during NaOH or NMMO release, for homogenisation. The amount of NaOH or NMMO released into the bath was measured as a function of time using methods described in the following paragraphs (refractometry for NMMO and potentiometry and titration for NaOH). Each experiment was repeated 3 to 5 times and the mean value of the diffusion coefficient (see details on diffusion coefficient determination in Results section) was calculated.

Refractometry

The concentration of NMMO in regenerating bath was measured using Abbe refractometer. First, calibration dependence was obtained by measuring the refractive index of NMMO-water or NMMO-alcohol solutions as a function of known NMMO concentration. During regenerating experiments, small amounts of regenerating bath liquids were taken in time and

their refractive index was measured. NMMO concentration in the bath was determined with the help of the calibration dependence. These data were used to describe the kinetics of NMMO release from the sample.

Titration and potentiométrie

The evolution of NaOH concentration in the regenerating bath as a function of time was measured using titration with acetic acid in the presence of an indicator. The amount of NaOH released from the sample in time was calculated knowing the initial sample and bath weight.

In order to double check the values of the NaOH diffusion coefficients obtained with titration, NaOH concentration during cellulose regeneration in the bath at room temperature was measured using ion (Na^+) selective electrode (Mettler Toledo) coupled with pH-meter from Denver Instruments. The electrode was inserted in the bath. First, a calibration curve of conductivity (mV) vs known NaOH concentration was built. This calibration was then used to follow the kinetics of NaOH release. The diffusion coefficient obtained with this method coincided with the ones obtained with titration within experimental error.

The experimental errors on concentration measurements were less than 10%.

Rheological measurements

The viscosity of 7.6%NaOH-water, of NMMO monohydrate and of 1% and 3%Solucell-NMMO solutions was measured as a function of the shear rate at different temperatures with a cone-plate geometry using a Bohlin Gemini[®] rheometer equipped with a Peltier temperature control system. The temperature intervals were as follows: from 10°C to 25°C for 7.6%NaOH-water solution and from 70°C to 90°C for NMMO monohydrate and Solucell-NMMO solutions, with the temperature increment of 5°C. All solutions studied showed a Newtonian behaviour in the 1 to 100 s⁻¹ shear rate range. A viscosity value (Pa s) corresponding to each temperature was taken for plotting viscosity vs temperature dependence for the further calculation of the activation energy.

Scanning electron microscopy

The morphology of wet cellulose-NaOH-water gels was characterised by Philips XL Environmental Scanning Electron Microscopy (ESEM). ESEM works under controlled environmental conditions and requires no conductive coating of the specimen. The Peltier cooling stage PW6750 was used to control the temperature. Images were acquired at a temperature of 2°C and the chamber pressure was maintained at 5 mbar.

2 Results and discussion

2.1 Analysis of experimental data: choice of the approach

The experimental data, i.e. the increase of NaOH or NMMO amount in the regenerating bath as a function of time and in different conditions (various cellulose concentration, regenerating bath liquid, bath temperature), was analysed using Fick approach. It is widely applied in drug release field and formation of membranes due to phase separation, and was already used to describe the kinetics of cellulose regeneration from cellulose-NMMO-water solutions¹⁸. The applicability of Fick approach was checked by plotting the cumulative amount of substance $M(t)$ (here - NaOH or NMMO) released in time t as a function of \sqrt{t} . The experimental data were approximated with a straight line, within 10% experimental error, up to $\sim 80\%$ of $M(t)$, which indicates a diffusion-controlled process. All samples, except cellulose-NaOH-water gels placed in alcohol baths, practically did not change their volume during regeneration (within 10% error) allowing the application of Fick approach.

The amount of a substance released in time from a semi-infinite plane can be described as follows²⁰:

$$\frac{M(t)}{M} = 1 - \sum_{n=0}^{\infty} \frac{8}{(2n+1)^2 \pi^2} \exp\left(\frac{-D\pi^2 t(2n+1)^2}{l^2}\right) \quad (1)$$

where M is the amount of substance released at $t = \infty$ (in our case M coincides with the amount of substance in the initial sample), D is diffusion coefficient and l is half sample thickness because diffusion takes place from its both sides.

If the diffusion coefficient is constant, several simplifications are used to determine D from the slope of $\frac{M(t)}{M} = f\left(\sqrt{\frac{t}{l^2}}\right)$ curves:

a) Early time approximation ($0 \leq \frac{M(t)}{M} \leq 0.4$):

$$\frac{M(t)}{M} = 4\left(\frac{Dt}{\pi l^2}\right)^{\frac{1}{2}}, \quad (2)$$

b) Late time approximation ($0.4 \leq \frac{M(t)}{M} \leq 1$):

$$\frac{M(t)}{M} = 1 - \frac{8}{\pi^2} \exp\left(\frac{-\pi^2 Dt}{l^2}\right) \quad (3)$$

c) Half time ($\frac{M(t)}{M} = 1/2$) approximation: here the diffusion coefficient is calculated at the point where $\frac{M(t)}{M} = 1/2$; it is equal to $D = \frac{0.049}{(t/l^2)_{1/2}}$ where $(t/l^2)_{1/2}$ is the abscissa when $\frac{M(t)}{M} = 1/2$. The experimental data can be then fitted with formula 1 with $n = 0$.

In order to select the approximation for the calculation of the diffusion coefficient, the experimental data $\frac{M_{NaOH}(t)}{M} = f(\sqrt{\frac{t}{l^2}})$ were fitted with early, half and late time approaches (Figure III.2). The best fit gives half-time approximation; it will be used to determine all diffusion coefficients in the following.

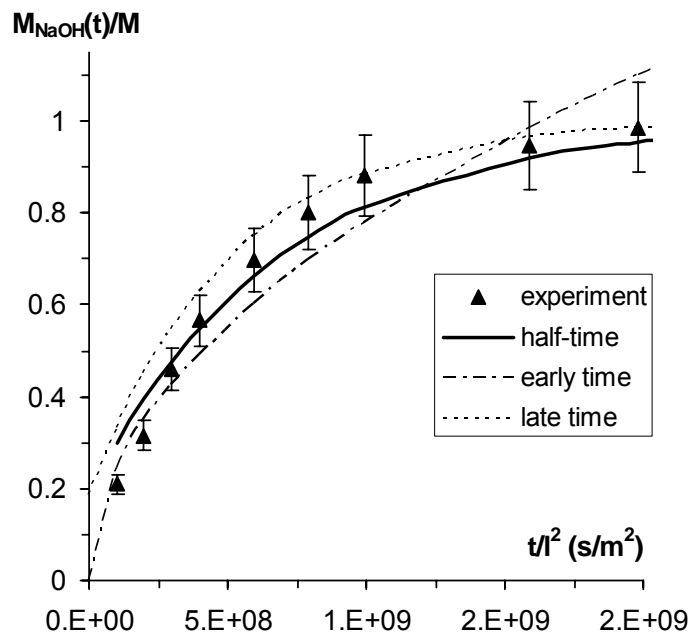


Figure III.2: Illustration of the choice of approximation. Experimental data: regeneration of 6%Avicel-NaOH-water gel in water bath at 25°C

The regeneration of cellulose from Avicel-NaOH-water gels into water bath was performed in different conditions: at different temperatures (25°C, 50°C and 80°C, $C_{cell} = 5\%$) and with different cellulose concentration C_{cell} (3%, 5%, 6% and 7%, all in water bath at 25°C).

$\frac{M_{NaOH}(t)}{M} = f(\sqrt{\frac{t}{l^2}})$ was plotted for each case and D_{NaOH} was calculated using half-time approximation.

The same procedure was performed for solid Solucell-NMMO samples¹ in the part that concerns the influence of bath temperature (25°C, 50°C and 80°C); Solucell concentration in this case was 3%. As for the influence of cellulose concentration on NMMO diffusion, the values of D_{NMMO} were partly taken from ref. 18 for $C_{cell} = 3-12\%$ and partly measured using refractometry for low cellulose concentrations, $C_{cell} = 0.5-3.0\%$. It was possible to combine all data because cellulose molecular weight does not affect the diffusion of NMMO during cellulose regeneration¹⁸ and our samples and the ones in ref.18 were prepared in the same way, by Lenzing AG. Indeed, we measured D_{NMMO} at $C_{cell} = 3\%$ and it coincided with the value from ref.18 for this cellulose concentration within the experimental error.

Because the concentration of the released substance (NaOH or NMMO), in the bath was always low, lower than 0.8% for NaOH and 8% for NMMO, the dependence of the diffusion coefficient on NaOH or NMMO concentration in the bath was neglected. For cellulose-NMMO solutions it was shown¹⁸ that D_{NMMO} decrease starts to be noticeable when NMMO content in the bath is higher than 10% which was never our case.

The influence of the bath type on the kinetics of cellulose regeneration was also studied. Because Avicel-7.6%NaOH-water gels were strongly contracting in alcohol baths, it was not possible to use Fick approach and D_{NaOH} were not calculated. The correlation between sample contraction and the solubility parameter will be discussed. On the contrary, Solucell-NMMO samples were practically not contracting, thus D_{NMMO} were obtained using refractometry. These results will be correlated with the viscosity of each alcohol used.

2.2 Influence of cellulose concentration on diffusion of NaOH from Avicel-NaOH-water gels and of NMMO from Solucell-NMMO solutions

The values of diffusion coefficients of NaOH and NMMO during regeneration of cellulose in a water bath at 25°C are presented in Table III.2. D_{NaOH} and D_{NMMO} at zero cellulose concentration, $D_{NaOH}(C_{cell} = 0)$ and $D_{NMMO}(C_{cell} = 0)$, respectively, are added for comparison and will be used in the following when considering different theoretical models. The value of $D_{NaOH}(C_{cell} = 0) = 1.5 \cdot 10^{-9} \text{ m}^2/\text{s}$ was taken from ref.22. The value of $D_{NMMO}(C_{cell} = 0)$ was calculated using Stoke-Einstein formula which relates the diffusion coefficient and hydrodynamic size R of the solute (here – NMMO):

$$D(C_{cell} = 0) = \frac{k_B T}{6\pi\eta R} \quad (4)$$

where k_B is Boltzmann constant, T is temperature and η is the viscosity of bath liquid (here - water or alcohol in Section III.2.4) at temperature T . The size $R_{NMMO} = 3.1 \cdot 10^{-10} \text{ m}$ was kindly calculated by T.Rosenau, BOKU, Austria, using Density functional theory. It should be noted that Stoke-Einstein approach is developed to describe the motion of a solid sphere in a dilute suspension. In order to fulfill this condition (i.e. to use formula 4 for the calculation of the

¹ Using NMR²¹ it was shown that NMMO diffusion coefficient varies as a function of the position inside the cellulose sample. However, this was not detectable with our technique, thus the diffusion coefficient measured is a mean value.

diffusion coefficient at $C_{cell} = 0$), the concentration of the solute, NaOH or NMMO, should be low. While this is more or less the case for NaOH (7.6% in water), it is not at all the case of NMMO (80% in water), but there is no theory allowing calculation of the diffusion coefficient at high solute concentration. Thus the value of $D_{NMMO}(C_{cell} = 0)$ calculated in the approximation of dilute suspension (i.e. one NMMO moving in a pure water) will be, by definition, higher than what could be obtained in reality for the diffusion of NMMO during the dissolution of a solid NMMO monohydrate. Unfortunately, it was not possible to directly measure this specific D_{NMMO} because of extremely high sample hygroscopicity. As it will be shown in the following paragraphs, the value of D_{NMMO} at $C_{cell} = 0$ calculated with formula 4 is indeed higher than what can be deduced from the experiment.

Cellulose concentration, wt%	0	3	5	6	7
$D_{NaOH}, \times 10^{-10} \text{ m}^2/\text{s}$	15.1 ^{a)}	2.09	1.42	1.21	1.10

Cellulose concentration, wt%	0	0.3	1.1	2.3	3	6 ^{c)}	8 ^{c)}	10 ^{c)}	12 ^{c)}
$D_{NMMO}, \times 10^{-10} \text{ m}^2/\text{s}$	7.04 ^{b)}	1.42	1.31	1.20	1.25	1.10	0.98	0.81	0.50

Table III.2: Diffusion coefficients of NaOH and NMMO during regeneration of Avicel-NaOH-water gels and Solucell-NMMO solutions in a water bath of 25°C a) Taken from ref. 22. b) Calculated from the size of NMMO, using Stoke-Einstein formula 4 and c) Taken from ref.18

The values of NaOH and NMMO diffusion coefficients at 5-7% cellulose concentration are very close (Table III.2 and Figure III.3) which means that regeneration of cellulose from the samples (cellulose-NaOH-water gel or solid cellulose-NMMO solution) of the same geometry in the same conditions will take about the same time. However, the trend of the diffusion coefficient decrease with the increase of cellulose concentration is not the same for NaOH and NMMO (Figure III.3). The analysis of diffusion data with theoretical models and of the difference between D_{NaOH} and D_{NMMO} evolution as a function of cellulose concentration is discussed below.

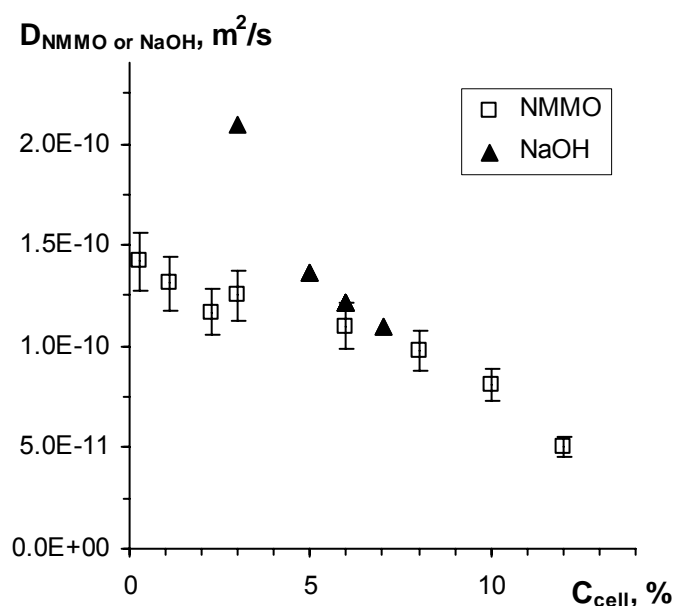


Figure III.3: NaOH and NMMO diffusion coefficients measured during regeneration of Avicel-7.6%NaOH-water gels and Solucell-NMMO solutions, as a function of cellulose weight concentration. Regenerating bath: water at 25°C

The initial state of the Avicel-NaOH-water samples is a gel and the final state is regenerated (or precipitated) swollen cellulose. During regeneration, the state of cellulose changes: a phase separation takes place. Different types of models explaining the transport behaviour of solutes in hydrogels or in porous media can be thus tested. These models mainly include free volume theory, hydrodynamic and obstruction approaches and their combinations as well. A review of these models and their applicability towards experimental data obtained for different types of hydrogels (homogeneous or not, charged or not) and solutes (polymers, micelles and low molecular weight compounds) is given in ref. 23. Free volume model was strongly criticised when being applied to hydrogels with high water content²³ despite it is widely used in the field of controlled drug release. Initially, the free volume model was developed for homogeneous membranes in which the pores are fixed neither in size nor in location²⁴. The hydrodynamic models seem to provide a reasonable description of solute diffusion in homogeneous hydrogels, while the models containing obstruction effect are more consistent with the diffusion behaviour in heterogeneous gels.

Nothing is known about the structure of cellulose-NaOH-water gels. What we know is that gelation of cellulose-NaOH-water solution occurs in time and with temperature increase due to the decrease of solvent quality and increase of cellulose-cellulose macromolecular interactions⁵. On one hand, cellulose-NaOH-water gels should be considered as heterogeneous, as most of polysaccharide hydrogels. The main difference between approaches used for heterogeneous and homogeneous gels is that the first one takes into account the size of the polymer chain and the other does not. On the other hand, during regeneration process cellulose coagulates due to phase separation, leading to cellulose-swollen-in-water “membrane” (Figure III.1a). The latter can be seen as a porous medium, and thus free volume or hydrodynamic approach could be applied to describe NaOH diffusion.

Before applying different approaches to our experimental data, several system parameters had to be determined. First of all, cellulose volume fraction f_{cell} must be calculated. It is related with the cellulose weight concentration C_{cell} as follows:

$$f_{cell} = \frac{C_{cell} / d_{cell}}{C_{solution} / d_{solution} + C_{cell} / d_{cell}} \quad (5)$$

where $d_{cell} = 1.52 \cdot 10^{-3} \text{ kg/m}^3$ (from FMC data sheet) and $d_{solution} = 1.0813 \cdot 10^{-3} \text{ kg/m}^3$ ²⁵ are the densities of Avicell and 7.6%NaOH-water solution, respectively. The approaches used to describe diffusion in heterogeneous gels require solute and polymer chain radii: $R_{NaOH} = 1.4 \cdot 10^{-10} \text{ m}$ was calculated from formula 4 knowing $D_{NaOH}(C_{cell} = 0)$ from ref.22 and cellulose mean chain radius $R_{cell} = 5.1 \cdot 10^{-10} \text{ m}$ was calculated from the crystalline structure of cellulose²⁶.

The diffusion models that were used to approximate the dependence of NaOH diffusion coefficient as a function of cellulose concentration are listed in Table III.3 and shown in Figure III.4, together with experimental data. The results are presented in semi-logarithmic coordinates: reduced NaOH diffusion coefficient as a function of cellulose volume fraction f_{cell} in the gel.

Gel type	Model	Expression	reference
heterogeneous	obstruction	$\frac{D}{D_0} = \left[1 + \frac{2}{3} \left(\frac{R_{cell} + R}{R_{cell}} \right)^2 f_{cell} \right]^{-1}$	27
heterogeneous	hydrodynamic	$\frac{D}{D_0} = \left[1 + k^{0.5} + \frac{1}{3}k \right]^{-1}$; $k = \frac{f_{cell}^{1.17}}{0.31} \left(\frac{R}{R_{cell}} \right)^2$	28
heterogeneous	combined obstruction and hydrodynamic	$\frac{D}{D_0} = \left[1 + \frac{2}{3} \left(\frac{R + R_{cell}}{R_{cell}} \right)^2 f_{cell} \right]^{-1} \times$ $\times \exp(-\pi f_{cell}^{0.174 \ln(59.6 R_{cell} / R)})$	29
heterogeneous	obstruction	$\frac{D}{D_0} = \exp \left[- \frac{(R_{cell} + R)}{R_{cell}} \sqrt{f_{cell}} \right]$	30
heterogeneous	obstruction	$\frac{D}{D_0} = \exp \left(-\pi \left[\frac{R_{cell} + R}{a f_{cell}^{-0.5} + 2R_{cell}} \right]^2 \right)$, a is a scaling constant depending on the flexibility of the polymer chain	23
homogeneous (curve 1 in Figure III.4)	hydrodynamic	$\frac{D}{D_0} = \exp(-bRf_{cell}^{0.75})$, b is a constant	32
homogeneous (curve 2 in Figure III.4)	free volume for hydrogels	$\frac{D}{D_0} = \exp \left[-cR^2 \frac{f_{cell}}{(1 - f_{cell})} \right]$, c is a constant	23, 33

Table III.3: Summary of diffusion models tested.

Here D and D_0 are solute diffusion coefficients in the sample and in water, respectively, R is solute radius

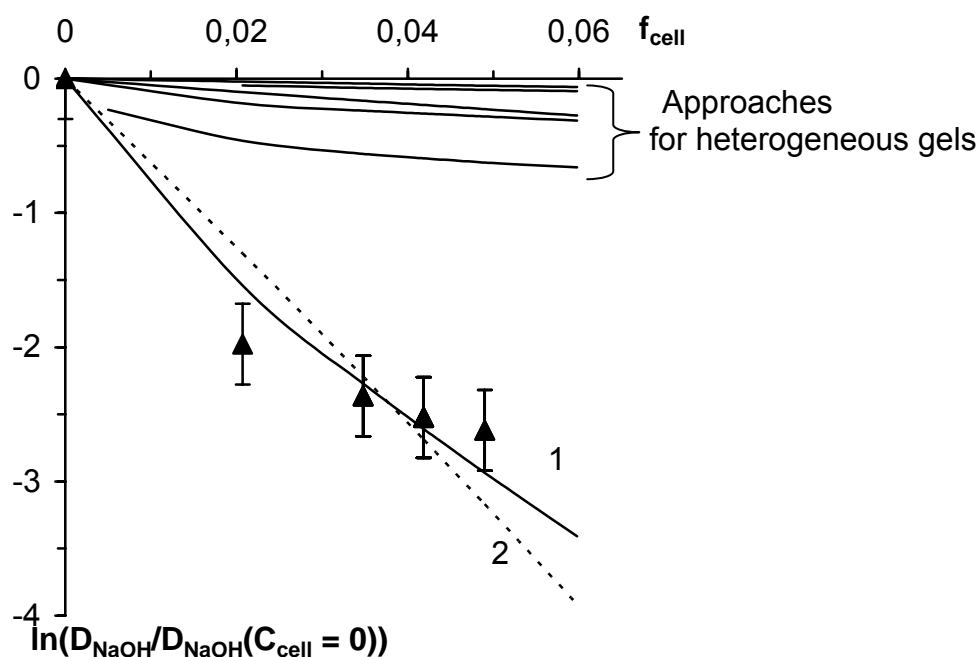


Figure III.4: Reduced NaOH diffusion coefficient as a function of cellulose volume fraction in the gel during regeneration at 25°C. Curve 1 corresponds to hydrodynamic and curve 2 – to free volume approaches. For details see Table III.3

Figure III.4 shows that approaches developed for heterogeneous and homogeneous gels split into two parts, respectively. Five approaches that take into account the influence of polymer chain radius on solute diffusion are far from experimental data (the sequence of these five curves from top to bottom is the same as the sequence of approaches/equations listed in Table III. 3). On the contrary, free volume and hydrodynamic models seem to better describe the diffusion of NaOH in cellulose-NaOH-water gel during cellulose regeneration in water. Another way to treat experimental data with a free volume approach is shown in Figure III.5. The theory predicts a linear dependence of the logarithm of the reduced diffusion coefficient as a function of water volume fraction f_{water} in the sample as follows: $\ln(D_{NaOH}/D(C_{cell} = 0)) \sim (1/f_{water} - 1)^{24}$. Figure III.5 shows that experimental data are well approximated by a straight line. This means that “membrane” and not “hydrogel” approaches should be used to describe the diffusion of NaOH during regeneration cellulose-NaOH-water gels.

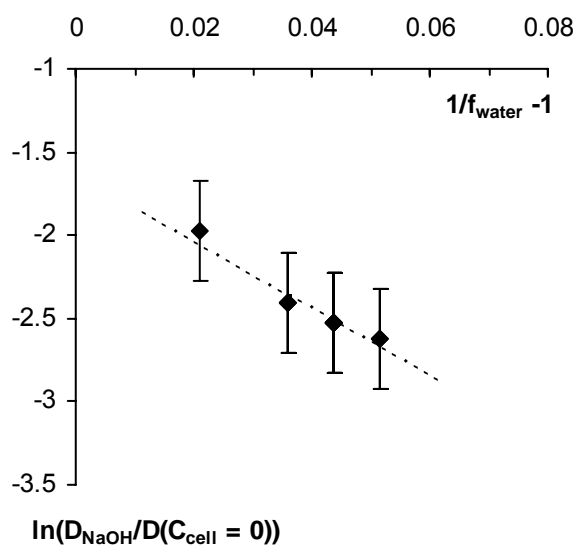


Figure III.5: Reduced NaOH diffusion coefficient as a function of water volume fraction in Avicel-7.6%NaOH-water gel during regeneration at 25°C; free volume theory approximation. Line is the best fit with $R^2 = 0.94$

The influence of cellulose concentration on the diffusion coefficient of NMMO during regeneration of Solucell-NMMO solutions in water was revised in the same way as described for diffusion of NaOH. The dependences calculated for NMMO according to the approaches developed for heterogeneous gels fall far away from experimental data and thus will not be shown. The reduced diffusion coefficients of NMMO are presented in Figure III.6 together with the ones of NaOH; the curves corresponding to hydrodynamic and free volume approaches are shown for each solvent. For the calculation of cellulose volume fraction in the sample according to expression 5, the density of NMMO monohydrate solution was taken as $d_{\text{solution}} = 1.2 \cdot 10^{-3} \text{ kg/m}^3$.

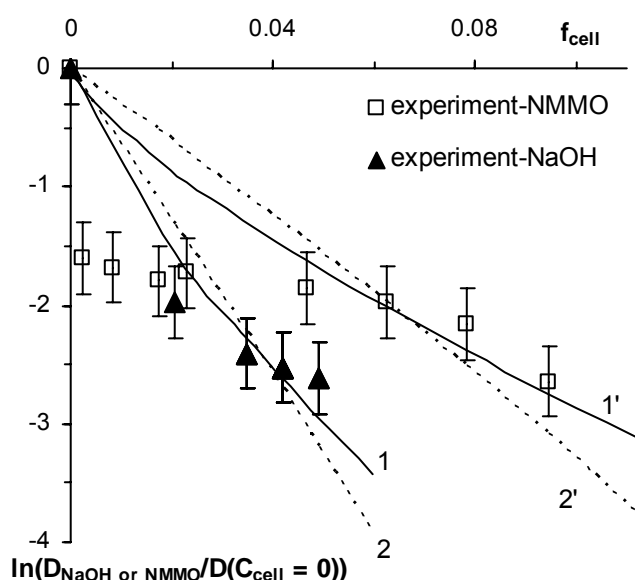


Figure III.6: Comparison of NaOH and NMMO reduced diffusion coefficients during cellulose regeneration in water at 25°C. Curves 1, 1' and 2, 2' correspond to hydrodynamic and free volume models for NaOH (1 and 2) and NMMO (1' and 2'), respectively (see formulas in Table III.3)

It is clear that the trend of D_{NaOH} and D_{NMMO} decrease with the increase of cellulose volume fraction is different (Figure III.6). D_{NaOH} smoothly decreases from $D_{NaOH}(C_{cell} = 0)$ with the increase of f_{cell} . On the contrary, D_{NMMO} shows saturation at low cellulose concentrations. The saturation of D_{NMMO} at low cellulose concentrations was predicted in ref. 18 and our experimental data confirm it. The reason of this saturation was proposed in ref. 18. At low cellulose concentrations, the sample contains a lot of crystallised NMMO monohydrates that are not bound to cellulose. During regeneration, water enters solid cellulose-NMMO sample, dilutes free NMMO monohydrates to the state when NMMO becomes fluid and then it can diffuse from the sample into the water bath. At low cellulose concentrations NMMO behaves almost as if there are no cellulose chains around. The increase of cellulose concentration decreases the amount of free NMMO molecules and NMMO “detachment” from cellulose chains becomes noticeable. This is reflected by the decrease of D_{NMMO} at $C_{cell} > 5\text{-}6\%$ (or $f_{cell} > 0.04$).

As suggested in ref. 18, the extrapolation of the plateau to $f_{cell} = 0$ should give the value of D_{NMMO} in a dissolving in water NMMO monohydrate: it is around $1.4 \cdot 10^{-10} \text{ m}^2/\text{s}$. This value is five times smaller as compared with the calculated one according to formula 4 at $C_{cell} = 0$ (see Table III.2). This difference in $D_{NMMO}(C_{cell} = 0)$ obtained experimentally and calculated with Einstein approach was expected and is explained by the high NMMO concentration in the sample (see discussion of the applicability of formula 4 to the case of pure NMMO solution). Some other reasons complicating the interpretation of NMMO diffusion can be also given. First, NMMO forms different types of hydrates, depending on its concentration in water, and thus NMMO is dragging water molecules during diffusion. This is not taken into account in the calculation of NMMO size and thus in the calculation of the diffusion coefficient at $C_{cell} = 0$. Second, the initial states of NMMO – calculated or real – is different: formula 4 takes into account only the size of the solute free moving in water, while real NMMO has to change the phase state during regeneration, from solid to liquid, which slows down calculated diffusion coefficient values.

2.3 Influence of water regenerating bath temperature

The influence of bath temperature on regeneration kinetics of 5%Avicel-NaOH-water gels and 3%Solucell-NMMO solutions was studied. An example of NaOH release from 5%Avicel-NaOH-water gels into water bath at 25°C, 50°C and 80°C is shown in Figure III.7.

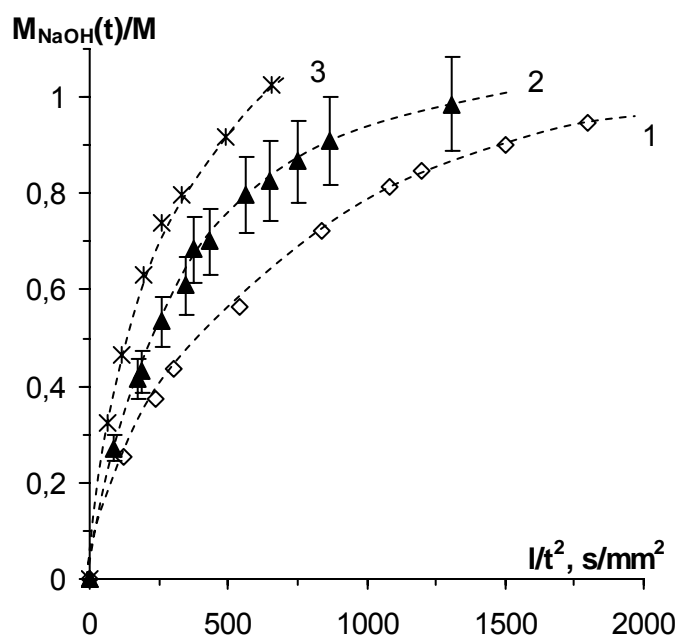


Figure III.7: Diffusion of NaOH from 5%Avicel-7.6%NaOH-water gels into water regenerating bath of 25°C (1), 50°C (2) and 80°C (3). The lines are shown to guide the eye

As expected, higher is bath temperature, quicker is NaOH release from cellulose gels, and thus quicker is cellulose regeneration. The same occurs for regeneration of 3%Solucell-NMMO solutions in water baths of different temperatures. The diffusion coefficients D_{NaOH} and D_{NMMO} were calculated for 25°C, 50°C and 80°C and Arrhenius law was applied to obtain the activation energy for each system. Figure III.8 shows that the values of D_{NaOH} and D_{NMMO} at the same temperature T practically coincide, and so do the values of the activation energy: $E_{\text{NaOH}} = 21 \pm 2 \text{ kJ/M}$ and $E_{\text{NMMO}} = 19 \pm 2 \text{ kJ/M}$.

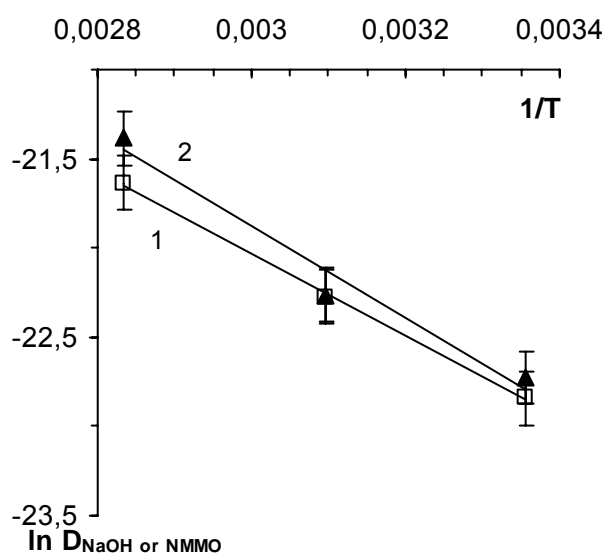


Figure III.8: Arrhenius plot for NMMO (1) and NaOH (2) diffusion coefficients for samples 3%Solucell-NMMO solutions and 5%Avicel-7.6%NaOH-water gels, respectively. Lines are least square linear approximations

The value of E_{NaOH} obtained for 5%Avicel-7.6%NaOH-water gels was compared with two other NaOH activation energy values that were obtained with rheological measurements: of pure 7.6%NaOH-water solutions and of Avicel-NaOH-water solutions. For 7.6%NaOH-water solutions, measurements of solution viscosity at different temperatures were performed and Arrhenius law was applied, which gave 19 kJ/M. As for cellulose-NaOH-water solutions (at cellulose concentrations and solution temperatures far from gelation), the activation energy is known for Avicel dissolved in 9%NaOH-water⁵. It is equal to 21 kJ/M and does not depend on cellulose concentration which means that cellulose-NaOH-water solutions are not real solutions but suspensions⁵. The value of E_{NaOH} obtained with the measurements of NaOH diffusion during Avicel regeneration in water is the same as compared with the previously found values of the activation energy with rheological measurements⁵. This means that whatever the system is – pure NaOH solution, cellulose-NaOH-water solution or cellulose-NaOH-water gel, it is NaOH hydrate with or without cellulose, which is moving in the system. The presence of cellulose, either in solution or in gel state, does not change the motion mechanics.

The same comparison of the activation energy obtained from diffusion and rheological experiments was performed for Solucell-NMMO system. The viscosities of NMMO monohydrate and of 1% and 3% Solucell-NMMO solutions in the temperature interval of 70°C-90°C were measured; the Arrhenius plot is shown in Figure III.9. The activation energy varies from 46 and 57 kJ/mole, correspondingly. For more concentrated solutions, for example, 15% cellulose-NMMO³⁴, the activation energy is 90-100 kJ/mole. The increase of the activation energy with the increase of cellulose concentration is a normal trend for polymer solutions (Figure III.10).

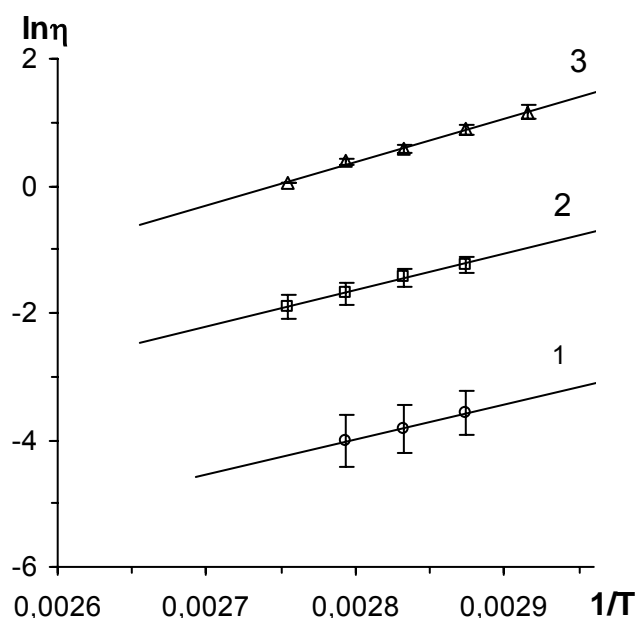


Figure III.9: Viscosity vs inverse temperature for NMMO monohydrate (1) and Solucell-NMMO solutions of 1% (2) and 3% (3) cellulose concentrations. Lines are least square approximations

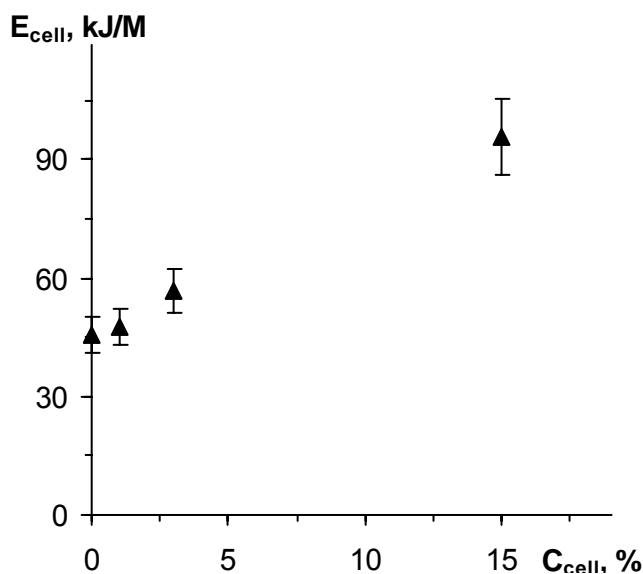


Figure III.10: Activation energy of Solucell-NMMO solutions as a function of cellulose concentration

There is a large difference in the activation energy values obtained from the rheological and diffusion coefficient (19 kJ/M) measurements. This discrepancy should be expected and, in fact, the “rheological” and “diffusion” activation energies correspond to very different moving entities. In the rheological measurements we are dealing with real solutions of cellulose in NMMO, and the activation energy corresponds to the motion of cellulose chains. During cellulose regeneration, the initial state of the sample is a crystallized cellulose-NMMO solution, and in the course of regeneration a two-phase system appear: a swollen-in-water cellulose and a dissolving-in-water NMMO. The mechanics of the moving entities in the rheological and regeneration experiments is very different and the only prediction that could be made is that “rheological” activation energy should be higher than the “diffusion” one. This is what was obtained in the experiments. What is much more surprising is that NaOH activation energy obtained from the rheological and diffusion coefficient measurements coincide and do not depend on cellulose concentration. This means, as said above and suggested in ref.5, that NaOH solution is a suspension of NaOH hydrates in water and cellulose-NaOH-water is not a real solution.

2.4 Influence of regenerating bath type

In the previous sections the regenerating (or non-solvent) bath was water. The type of non-solvent used for cellulose regeneration strongly influences the structure and morphology of regenerated cellulose fibres or membranes and, as a consequence, their properties (see, for example, refs. 19, 35, 36). Here we investigate the influence of the bath type on the behaviour of Avicel-NaOH-water gels and on NMMO diffusion coefficient.

Figure III.11 shows the kinetics of 5%Avicel-7.6%NaOH-water gel contraction in regenerating baths of different alcohols and in water. The smallest volume reduction occurs in water: $V(t)/V_0 > 85\%$, where V_0 and $V(t)$ are initial sample volume and in the course of

regeneration, respectively. In alcohol baths, Avicel-7.6%NaOH-water gels are contracting more than twice. In most of the cases, the fastest contraction occurs during the first ten/twenty hours after sample immersion into regenerating bath; during the following thirty/forty hours the sample slowly approaches its equilibrium size.

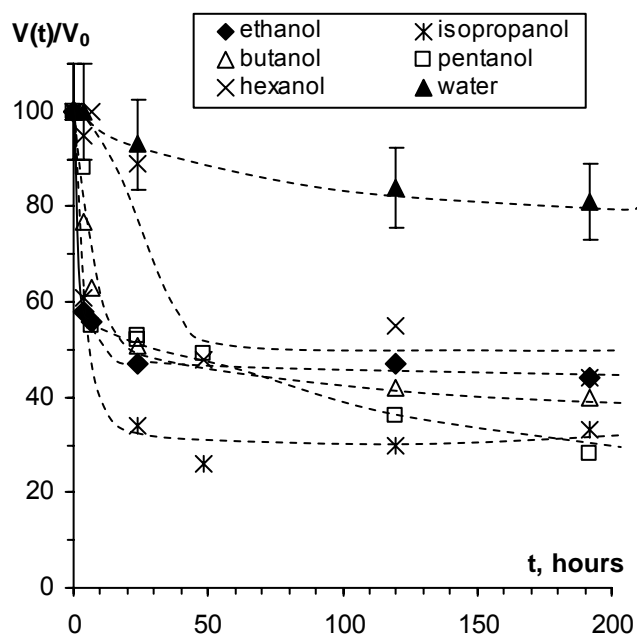


Figure III.11: Reduction of 5%Avicel-7.6%NaOH-water sample volume in regenerating bath of different liquids. Lines are given to guide the eye

Due to the fact that samples were strongly contracting, the application of Fick approach was impossible. Thus general thermodynamic reasoning will be used for the analysis of the contraction of Avicel-NaOH-water gels in alcohol regenerating baths.

When Avicel-7.6%NaOH-water gel is placed in a regenerating bath, cellulose coagulates due to the phase separation leading to a swollen-in-non-solvent cellulose sample. The degree of swelling of cellulose depends on the miscibility of cellulose with a given liquid. The notion of a solubility parameter can thus be used to explain cellulose sample contraction. The solubility or Hildebrand parameter δ describes the attractive strength between the molecules of the material. For a polymer-solvent system, the simplest way to predict polymer miscibility is to compare its solubility parameter with the one of the solvent. A rule of thumb says that the closer are solubility parameters, the better is polymer miscibility in a given liquid. Being very rough, this approach gives a certain overview of the dissolution and/or swelling of a polymer in a solvent. In our case, the solubility parameters of water and alcohols will be compared with the one of cellulose.

The solubility parameters of cellulose, water and alcohols are summarised in Table III.4³⁷. Figure III.12 shows the value of sample reduced volume at equilibrium $(V/V_0)_{eq}$, taken from Figure III.11, as a function of the solubility parameters difference $\Delta\delta = \delta_{cell} - \delta_{bath}$, where δ_{cell} and δ_{bath} are cellulose and regenerating liquid solubility parameters, respectively. The smallest $\Delta\delta$ corresponds to cellulose/water system; indeed the sample volume is decreased less than 15%. Larger is the solubility parameter difference, higher is the volume reduction. If plotting

the reduced volume at equilibrium as a function of molar mass of regenerating liquid (see inset Figure III.11), the trend is not that clear (except that in water the contraction is the lowest). It is the cellulose-liquid miscibility and thus the solubility parameter that governs cellulose swelling in a regenerating bath.

Material	Solubility parameter ³⁷ $\delta_{\pm 1}$, MPa ^{0.5}	Molar mass	Viscosity, $\times 10^{-3}$, Pa s
Cellulose	39.0		
Water	47.5	18	1.0
Ethanol	26.0	46	1.2
Isopropanol	23.9	60	2.27
Butanol	23.8	74	3.0
Penthanol	21.7	88	3.68
Hexanol	21.9	102	4.0

Table III.4: Solubility parameters, molar mass and viscosity of materials used, at 25°C

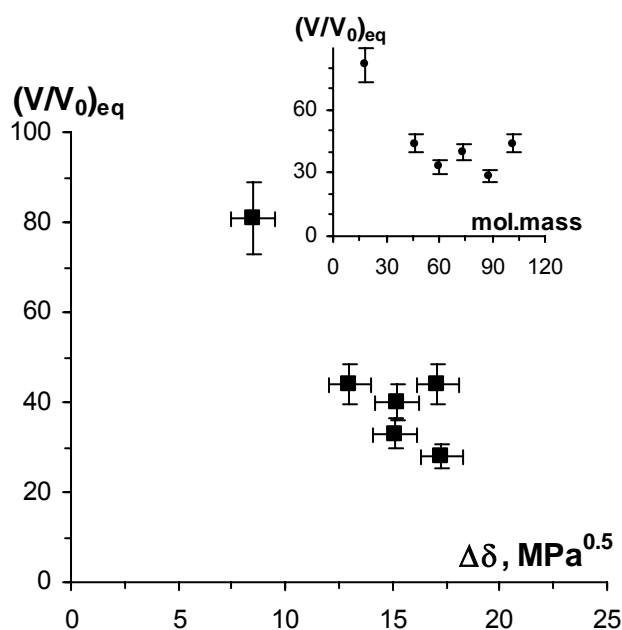


Figure III.12: 5%Avicel-7.6%NaOH-water gel contraction at equilibrium as a function of solubility parameter difference. Inset: the same as a function of regenerating liquid molar mass

The behaviour of Solucell-NMMO solutions in regenerating baths of different alcohols was also examined. The volume reduction of the samples was rather low, not more than 10-15%. Using refractometry, it was possible to measure the release of NMMO into regenerating bath, as described in Methods section, and to calculate the diffusion coefficients with Fick approximation. The results were compared with NMMO diffusion coefficients in pure liquids that were calculated using Stoke-Einstein formula 4 and knowing liquid viscosities, summarised in Table III.4. The results are presented in Figure III.13.

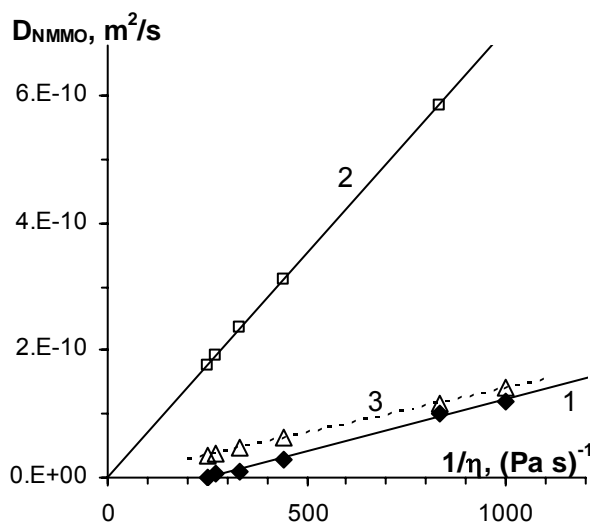


Figure III.13: NMMO diffusion coefficients, measured (dark points), from 3%Solucell-NMMO solution into different regenerating liquids and in the same pure liquids, calculated (2 and 3), as a function of inverse viscosity, at 25°C. Lines are least square linear approximations. See details in the text

As expected, the diffusion coefficient decreases with the increase of regenerating bath viscosity (Figure III.13). This was also predicted in ref. 19 for the regeneration of cellulose-NMMO solutions in different alcohol baths. The values of NMMO diffusion coefficients measured during regeneration are much lower than the ones calculated using formula 4 (line 2). This cannot be explained by the influence of cellulose concentration (measured – for 5%Solucell-NMMO and calculated – for $C_{cell} = 0$, i.e. diffusion of NMMO in pure liquids) because in Section III.2.2 it was shown that the diffusion coefficient practically does not vary for cellulose concentrations from 0 to 5% (see Figures III.3 and III.6). The reason of the difference in measured and calculated diffusion coefficients is the same as discussed in the first paragraph of Section III.2.2: in reality, NMMO concentration in the sample is high, but Einstein approach is valid for low solute concentration; thus the diffusion coefficient measured must be lower than the calculated one. D_{NMMO} obtained during regeneration of cellulose in water (Figure III.6) was five times smaller than calculated one as a diffusion of NMMO molecule in pure water, formula 4. It was interesting to check if the same ratio is valid for measured (during cellulose regeneration) and predicted (calculated with formula 4) NMMO diffusion coefficients in alcohols. To do this, the values of the D_{NMMO} predicted were divided by five; the result is shown by triangles and the corresponding line 3 in Figure III.13. These “new” diffusion coefficients are now much closer to the experimental results. This confirms the conclusion made in Section III.2: formula 4 is not applicable to predict D_{NMMO} at low cellulose concentrations during regeneration because NMMO concentration in the sample is high.

Conclusions

The diffusion of NaOH during regeneration of cellulose-NaOH-water gels in water and alcohols was studied and compared with the diffusion of NMMO from cellulose-NMMO solutions into the same regenerating liquids. At 5%-7% of cellulose, NaOH and NMMO diffusion coefficients are practically the same.

The analysis of the influence of cellulose concentration on NaOH diffusion coefficients shows that “porous membrane” (i.e. free volume or hydrodynamic approach) and not “hydrogel-obstruction” approach must be used for the understanding and interpretation of cellulose regeneration from cellulose-NaOH-water gels. The applicability of a free volume or hydrodynamic approach is caused by the phase separation process occurring during regeneration of cellulose from cellulose-NaOH gels placed in a non-solvent liquid. The interpretation of NMMO diffusion and thus of cellulose regeneration should also be with the “porous membrane” approach, but it is complicated by the high concentration of NMMO in the sample, by the presence of NMMO not linked to cellulose at low cellulose concentrations and the change of NMMO phase state during regeneration. An increase of the size of the diffusing entity due to NMMO dragging water molecules during diffusion should also be considered.

NaOH activation energy obtained from diffusion experiments coincides with the activation energy calculated from the rheological experiments for cellulose-NaOH-water and pure NaOH-water solutions. This result confirms the suggestion made in ref.5 that cellulose-NaOH-water solutions are in fact suspensions of NaOH hydrates with or without cellulose.

Finally, the swelling of cellulose in different non-solvents can be explained by the solubility parameter.

Acknowledgements

This work was supported by EC 6th PCRD, project “Aerocell” № NMP3-CT2003-505888. Authors are grateful to Gregor Kraft (Lenzing AG, Austria) for the preparation and characterisation of Solucell-NMMO solutions, to Thomas Rosenau (University of Natural Resources and Applied Life Sciences, BOKU, Vienna, Austria) for the calculation of NMMO radius using Density functional theory and to Patrick Navard (Ecole des Mines de Paris, CEMEF, France) for stimulating discussions.

References

1. Sobue, H., Kiesslig, H., Hess, K., *Z. Physik. Chem. B*, 1939, 43, 309
2. Kamide, K., Kowsaka, K., Okajima, K., *Polymer Journal*, **1985**, 17, 707
3. Isogai, A., Atalla, R.H., 1998, 5, 309.
4. Roy, C., Budtova, T., Navard, P., Bedue, O., *Biomacromolecules*, **2001**, 2, 687
5. Roy, C., Budtova, T., Navard, P., *Biomacromolecules*, **2003**, 4, 259
6. Laszkiewicz, B., *J. Appl. Polym. Sci.*, **1998**, 67, 1871
7. Zhou, J., Zhang, L., *Polymer Journal*, **2000**, 32, 866
8. Zhang, L., Ruan, D., Gao, S., *J. Polym. Sci. Part B: Polym. Phys.* **2002**, 40, 1521
9. Zhou, J., Zhang, L., Cai, J., *J. Polym. Sci. : Part B: Polym. Phys.* **2004**, 42, 347
10. Kunze, J., Fink, H.-P., *Macromol. Symp.*, **2005**, 223, 175
11. Yamashiki, T., Matsui, T., Kowsaka, K., Saitoh, M., Okajima, K., Kamide, K., *J. Appl. Polym. Sci.*, 1992, 44, 691
12. Ruan, D., Zhang, L., Zhou, J., Jin, H., Chen, H., *Macromol. Biosci.*, **2004**, 4, 1105
13. Zhou, J., Zhang, L., Cai, J., Shu, H., *J. Membrane Science*, **2002**, 210, 77
14. Ruan, D., Zhang, L., Mao, Y., Zeng, M., Li, X., *J. Membrane Sci.*, **2004**, 241, 265
15. Kuo, Y.-N., Hong, J., *J. Colloid and Interface Science*, 2005, 285, 232
16. Mao, Y., Zhou, J., Cai, J., Zhang, L., *J. Membrane Science*, 2006, article in press
17. Zhang, L., Mao, Y., Zhou, J., Cai, J., *Ind. Eng. Chem. Res.*, **2005**, 44, 522
18. Biganska, O., Navard, P., *Biomacromolecules*, 2005, 6, 1948.
19. Fink, H.-P.; Weigel, P.; Purz, H.J.; Ganster J. *Prog. Polym. Sci.* **2001**, 26, 1473
20. Crank, J., *The mathematics of Diffusion*, 2nd Edition, Clarendon Press, Oxford, 1975.
21. Laity, P.R., Glover, P.M., Hay, J.N., *Polymer*, **2002**, 43, 5827
22. *Handbook of tables for applied engineering science*, 2nd edition, CRC Press, 1983.
23. Amsden, B., *Macromolecules*, **1998**, 31, 8382
24. Yasuda, H., Lamaze, C.E., *J. Macromol. Sci. – Phys.*, 1971, *B5(1)*, 111
25. *Handbook of Chemistry and Physics*, CRC Press, Ed.D.R.Lide, 83rd edition, 2002-2003.
26. Zugenmayer, P. *Prog. Polym. Sci.*, 2001, 26, 1341
27. Tsai, D.S.; Streider, W. *Chem. Eng. Commun.*, **1985**, 40, 207
28. Phillips, R.J.; Deen, W.M.; Brady, J.F. *AIChE J.* **1989**, 35, 5(11), 1761
29. Clague, D.S., Phillips, R.J. *Phys. Fluids* **1996**, 8, 1720
30. Ogston, A.G. *Trans. Faraday Soc.* **1958**, 54, 1754
31. Cukier, R.I. *Macromolecules*, **1984**, 17, 252
32. Lustig, S.R.; Peppas, N.A. *J. Appl. Polym. Sci.* **1988**, 36, 735
33. Liu, R.-G.; Shen, Y.-Y.; Shao, H.-L.; Wu, C.-X.; Hu, X.-C. *Cellulose*, **2001**, 8, 13
34. Blachot, J.-F.; Brunet, N.; Navard, P.; Cavallé, J.-Y. *Rheol. Acta* 1998, 37, 107
35. Eckelt, J.; Wolf, B.A. *Macromol. Chem. Phys.* **2005**, 206, 227
36. Jie, X.; Cao, Y., Qin, J.-J., Liu, J.; Yuan, Q. *J. Membrane Sci.* **2005**, 246, 157
37. *Handbook of Solubility Parameters and Other Cohesion Parameters*, 2nd edition, A.F.M.Barton, CRC Press, 1991.

Chapter IV: Microstructural properties of Aerocellulose

Introduction

Chapter IV is dedicated to the microstructural study of Aerocellulose. Indeed, as far as the goal of the project is to create ultra light and highly porous cellulose material, the knowledge of its porous structure is very important. Porosity strongly determines many physical properties of materials such as permeability, adsorption properties, mechanical strength, durability, etc and allows predicting their behaviour in different applications.

This chapter concerns the fourth stage of Aerocellulose preparation: the study of porous structure of samples after CO₂ supercritical drying.

Porosimetry experiments as nitrogen adsorption and mercury intrusion were performed in Fraunhofer Institute for Applied Polymer Research, (Institut Angewandte Polymerforschung - FhG IAP in the following), Potsdam, Germany, on various types of Aerocellulose. The results obtained give useful information about the pore size distributions, pore volumes, and surface areas of the materials. Generally, these two methods are suitable and complementary for the characterisation of accessible open pores of a wide range of pore dimensions ranging from one nanometre to hundred microns, which correspond to the large pore size distribution of Aerocellulose.

Electron microscopy is an essential characterisation technique when dealing with porous materials providing information about pores shape, size, and general sample morphology. In our investigations two types of electron microscopy techniques were used: scanning electron microscopy (SEM) and transmission electron microscopy (TEM). SEM is used to determine the morphology and the pore size. TEM produces images of the micro porous and mesoporous material revealing the nanostructure of Aerocellulose. Some SEM images were made in FhG IAP.

The chapter is divided into two main parts. The materials used, the preparation of Aerocellulose, four techniques dedicated to the study of the porous structure cited above and the method of CO₂ supercritical drying are briefly presented in the first part of this chapter. In the second part the influence of various parameters like cellulose concentration, pulp origin, surfactant concentration, regenerating bath temperature and nature on the final morphology and microstructure of Aerocellulose samples was investigated.

1 Materials and Methods

1.1 Materials

1.1.1 Cellulose solutions and gels

Cellulose/7.6NaOH/water solutions were prepared as described in section II.2.1. Different types of native cellulose pulp were used: microcrystalline cellulose Avicel, fibrous Solucell and steam-exploded Borregaard with DP values of 170, 307 and 500, respectively. Each pulp is described in section II.1.1.

Solutions were gelled at different temperatures for several hours in cylindrical moulds with approximate diameter 3 cm and height 4.5 cm; the physical gels once formed (see details in Chapter II) were cooled down to room temperature and then immersed in regenerating bath. Cellulose concentration, gelation temperature and time will be precise for each case.

In one case Aerocellulose was prepared not from gels, but by dropping Avicel/NaOH/water solutions in regenerating bath to form cellulose beads. This was performed in the R&D laboratory of Genialab GmbH, Braunschweig, Germany.

Cellulose/NMMO/water solutions were prepared in the R&D laboratory of Lenzing AG, Austria. The pulp used was Solucell 1175 with DP 950, from eucalyptus. The proportions between the components are 3% cellulose-82% NMMO-15% water, called 3 Solucell 1175/NMMO solutions in the following. Solucell/NMMO/water solutions were in a crystalline state at room temperature. Two ways of Aerocellulose preparation were used:

- 1) Solucell /NMMO solution was melted at 70°C and the hot solution was pored into regenerating bath.
- 2) Solucell/NMMO was poured into the same mould as used for Avicel/NaOH/water solutions, cooled down to room temperature and, as a result, solid cylindrical samples were obtained. They were then immersed into regenerating bath.

1.1.2 Additives

In order to lighten the final material, the alkyl polyglycoside surfactant, Simulsol SL8, manufactured by Seppic, Inc., Fairfield, United-States, was used. This surfactant was added at various concentrations 0.1%, 0.5% and 1% in weight to the ready cellulose/NaOH/water solution. The mixture was stirred at 1000 revolution per minute for five minutes at +5°C, then immediately gelled at 50°C for two hours in order to “freeze” the foamed structure. Simulsol dissolved in water during the regeneration step.

1.1.3 Regenerating bath

Regeneration of cellulose consists in the release of cellulose solvent, sodium hydroxide or NMMO, from cellulose gels or solutions, and in the penetration of the non-solvent into cellulose samples resulting in the formation of a wet three-dimensional object, a sort of cellulose “network”. The influence of regenerating bath type and conditions on the structure and morphology of Aerocellulose was investigated.

Cellulose/NMMO/water solutions were regenerated in water and various alcohols: ethanol, isopropanol and pentanol at ambient temperature. Cellulose/NaOH/water solutions were

regenerated in water and in sulphuric acid solutions of various concentrations 0.02M, 0.2M and 1M. The influence of water temperature on the morphology of Aerocellulose was also investigated for both types of solutions. Cellulose solutions were regenerated in water at different temperature: 25°C, 50°C and 70°C.

Acetone and ethanol of analytical grade were used as a second regenerating bath because water is not compatible with supercritical CO₂ that is then used for samples drying. Carbon dioxide was delivered by Air Liquide, France for supercritical drying performed at CEP, Ecole des Mines, Sophia-Antipolis, France.

1.2 Methods

1.2.1 CO₂ supercritical drying

As we have seen in the first chapter, supercritical drying should be used in Aerocellulose preparation in order to replace solvent with air. This specific drying avoids the pores collapse due to the liquid surface tension and keeps intact the initial nanostructure.

After the regeneration step, cellulose is swollen in water. As it was mentioned in section I.2.3, water should be replaced by a liquid that is compatible with supercritical CO₂, like acetone or ethanol. After washing the swollen-in-water cellulose in one of these liquids, a swollen-in-acetone (or ethanol) cellulose is obtained. The sample is ready for the supercritical drying which is the final step of Aerocellulose preparation.

The supercritical fluid used in our study to dry samples is supercritical CO₂ (“sc CO₂” in the following) mainly because its critical point is easily obtainable (pressure P=73.8bar and temperature 31.1°C).

CO₂ supercritical extraction was performed at laboratory scale in CEP, Ecole des Mines, Sophia-Antipolis, France or at pilot plant scale by Natex, Ternitz in Austria. The two experimental techniques are briefly described below.

Laboratory scale set-up in CEP, Ecole des Mines, France:

To realise the supercritical drying, swollen cellulose samples were placed in a 1 litre-autoclave (Figure IV.1) containing some acetone in order to avoid the phenomena of evaporation during the autoclave closing. The system was closed and pressurized to 50 bars with gaseous CO₂, then heated to 37°C. The excess of acetone was purged, maintaining pressure and temperature constant with gaseous CO₂. When the excess of acetone was recovered, the system was pressurized with sc CO₂ (85 bars and 37°C) until the operating conditions were reached (80 bars and 35°C). Supercritical CO₂ solubilises the interstitial liquid acetone. After thermodynamic equilibrium was reached, the liquid phase contained in the pores of the sample was exchanged with sc CO₂ through a dynamic washing step (80 bars, 37°C, 5 kg CO₂ per hour) over approximately seven hours.

The greatest amount of acetone is recovered at the beginning of the drying while the release of acetone trapped in nanopores requires more time. When the total amount of the interstitial liquid was considered to be removed, the system was slowly and isothermally depressurised overnight (4 bars/h at 37°C) to avoid the condensation of liquid CO₂ and the phenomenon of cracking linked to the low permeability of samples. Once atmospheric pressure was reached, the system was cooled down to the ambient temperature and the autoclave was opened.

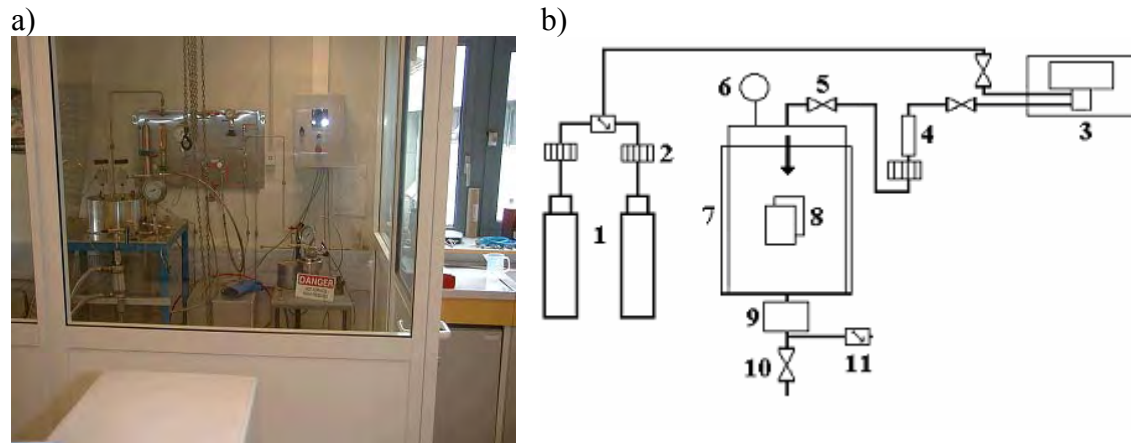


Figure IV.1: Laboratory-scale supercritical drying apparatus of CEP a) View of direct supercritical lab-scale drying loop b) Schematic representation of the lab-scale supercritical drying loop: (1) gaseous CO₂, (2) Heater (3) Air Compressor, (4) Buffer, (5) Feeding valve, (6) Pressure Gauge, (7) Autoclave (1 litre), (8) samples, (9) Pneumatic depressurisation valve, (10) Security valve, (11) Pressure reducer. Photo courtesy of CEP.

Pilot supercritical drying set-up in Natex, Austria.

The samples were put into a 5 litres autoclave (Figure IV.2) and covered with acetone to avoid a fast drying of the samples during pressurisation. During the pressurisation the outlet valve of the extractor was closed and no acetone could leave the extractor. Afterwards the system was pressurised by means of sc CO₂ between 80 and 200 bars. The temperature was fixed to 60°C. The CO₂ mass flow was adjusted to 25 kg/h. Through this dynamic supercritical washing step, the sc CO₂ removes all the organic solvent. In the separator, the solvent is separated from the CO₂, the latter is then re-circulated. After 4 hours dynamic extraction the pressure in the autoclave is decreased to the atmospheric pressure. Depressurisation time was optimised with 50 minutes.



Figure IV.2: Pilot plant scale supercritical drying apparatus of Natex, Austria. Photo courtesy of Natex.

With the window in the autoclave it was possible to follow the supercritical CO₂ drying process and the shrinkage of the sample during drying (see Figure IV.3: a –initial state, b –in the course of drying). The shrinkage of Aerocellulose sample from cellulose/NaOH/water gels after supercritical drying observed at Natex was in the same range of the one observed at CEP laboratory: lower than 20%.

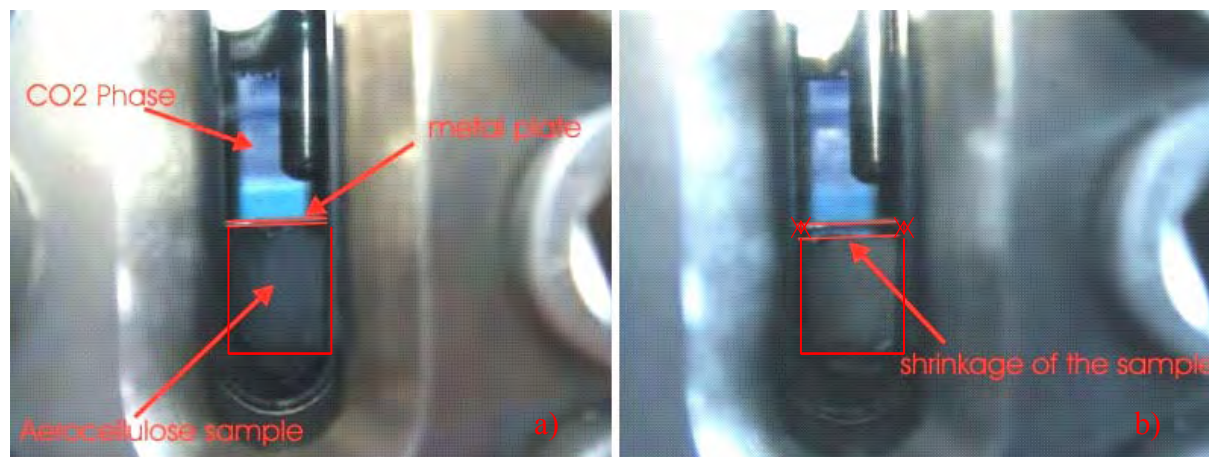


Figure IV.3: Shrinkage of the sample during supercritical drying a) before drying b) in the course of drying, pilot set-up in Natex, Austria. Photos courtesy of Natex.

In comparison to the evaporation process at ambient temperature which results to a volume contraction higher than 90%, supercritical dryings in Natex and in CEP lead to a volume shrinkage of cellulose sample lower than 20%. In the best conditions the volume shrinkage observed after supercritical drying was around 10%. Figure IV.4 shows the cellulose samples obtained by evaporation at ambient temperature and by CO₂ supercritical drying, Aerocellulose.

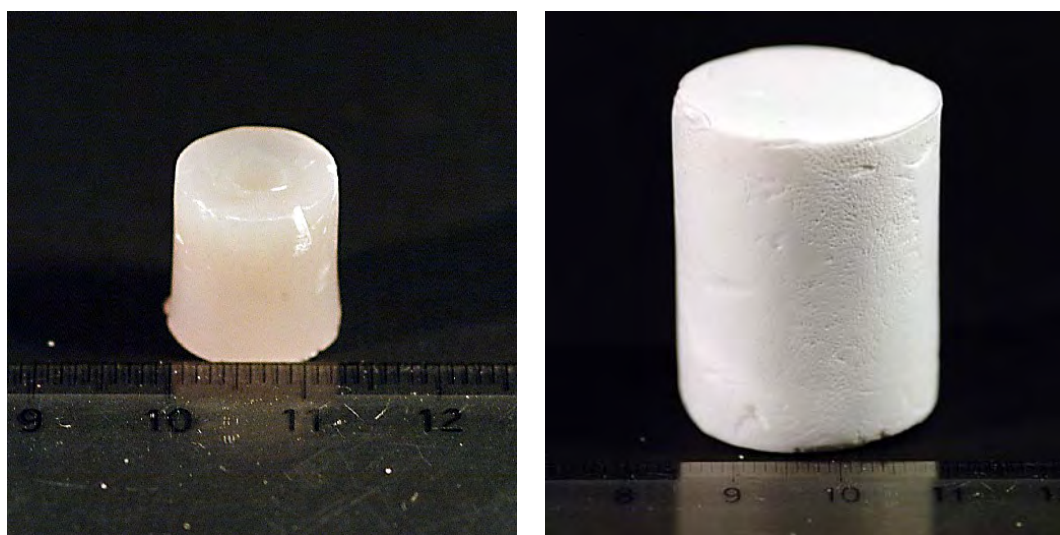


Figure IV.4: Dense cellulosic material dried at ambient temperature and Aerocellulose obtained by CO₂ supercritical drying

Owing to supercritical drying, we obtained dry, white and ultra light pure cellulose material – Aerocellulose- with approximate density (measured by dividing the mass by the volume) varying from 0.06 g.cm⁻³ to 0.25 g.cm⁻³.

1.2.2 Measurements of the porosity: a brief review of methods and theoretical approaches

1.2.2.1 Basic definitions

To understand the microstructure of Aerocellulose, some general definitions concerning the porosity of the material are given in this paragraph.

The word “pore” comes from the Greek word Πορος, which means “passage”. This implies that the pore acts as a passage between the external and the internal surfaces of a solid allowing material, such as liquids and gases, to pass through the solid.

Porosity can be described as the proportion of the non-solid volume to the total volume of material, and is defined by the ratio:

$$\rho = \frac{V_t}{V_m}$$

where V_t is the non-solid volume and V_m is the total volume of the material. Porosity is a fraction between 0 and 1, typically being higher than 0.7 for aerogel materials.

We can distinguish open and closed pores. Closed pores to the contrary of open pores are not open to the surface, and hence not accessible to gas or liquid. In the open type pores, there are blind pores (B – pores with a single connection to the surface), through pores (T – pores open on both sides of the particle) or interconnected pores (I – pores which communicates with other pores). Figure IV.5 shows the different pores observed in porous material.

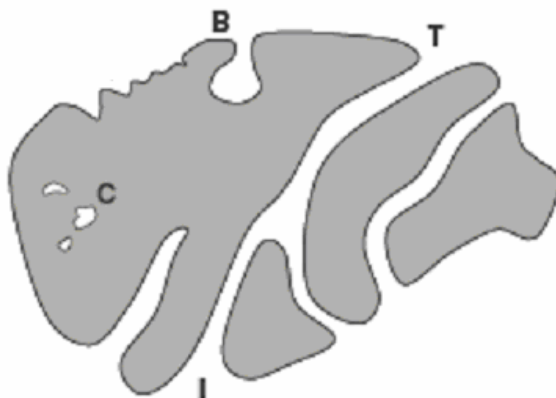


Figure IV.5: Cross-section of a hypothetical porous sample showing various type of pores: closed (C), through (T), interconnected (I). [Rouquerol et al, 1999]

The total pore volume is essentially the sum of two fractions:

$$V_t = V_o + V_c$$

where V_t is the total pore volume, V_o is the pore volume due to the open porosity in the solid, including transport and blind pores, and V_c is the closed pore volume.

The recommended I.U.P.A.C. classification of porous material is divided in three main groups depending on the pore size:

- *Micropores* are pores of internal width less than 2 nm
- *Mesopores* are pores of internal width between 2 and 50 nm
- *Macropores* are pores of internal width greater than 50 nm

There is no upper limit of the diameter of the macropores but it is usually 1-2 mm. It is possible to observe macro porosity by optical and scanning electron microscopy as they are larger than 50 nm. Using nitrogen adsorption technique, pore diameter in the range of 0.3-300 nm, i.e. micropores, mesopores and macropores are measurable. Using mercury porosimetry, pore diameters ranging from 6 nm to 100 μm can be detected.

Specific pore volume

The specific pore volume is the internal void space in a porous material. It can be measured by porosimetry experiments as mercury intrusion or nitrogen adsorption. It is expressed as a void volume (in cc or ml) divided by a mass unit (g).

Pore size distribution

Generally, the pore size distribution is represented as the relative amount of the pore volume (as a percentage or a derivative) as a function of the pore size.

Specific surface area

The specific surface area of a solid material is the total surface of the sample that is in contact with the external environment. It is expressed as square meters per gram of dry sample. It is obtained by measuring the amount of adsorbate gas corresponding to a monomolecular layer on the surface.

Adsorption

Adsorption is a process that occurs when a liquid or gas accumulates on the surface of a solid called adsorbent, forming a molecular or atomic film, called the adsorbate.

Adsorption is divided into two sub-categories: physical adsorption (physisorption) and chemical adsorption (chemisorption). Physisorption is applicable to all adsorbate-adsorbent systems in appropriated conditions of pressure and temperature whereas chemisorption may only occur if the adsorbate is capable of forming chemical bonds with the adsorbent. The process of adsorption is always exothermic due to the increased ordering of the adsorbate on the adsorbent surface, reducing the entropy.

Chemical Adsorption (Chemisorption)

Chemisorption involves the transfer of electrons between the adsorbent and the adsorbate resulting in the formation of chemical bonds. During the process, the chemical reaction between the two species causes adhesion of the adsorbate molecules onto adsorbent.

Physical Adsorption (Physisorption)

The attraction between the adsorbate and adsorbent is created by the formation of intermolecular electrostatic, such as London dispersion forces, or Van der Waals forces from induced dipole-dipole interactions. Physisorption occurs at any environmental condition (pressure and temperature) but it becomes measurable only at very low temperature. Gases such as argon or CO₂ can be used for adsorption, but nitrogen adsorption has become generally accepted as the standard method. Physisorption experiments are performed at very low temperature, usually at the boiling temperature of liquid nitrogen, -196°C, at atmospheric pressure. Due to the weak bonds formed between gas molecules and the surface (less than 15 kJ/mole), adsorption is a reversible phenomenon. Gas physisorption is considered non-selective, thus filling the surface step by step (or layer by layer) depending on the available solid surface and the relative pressure. Filling the first layer enables the measurement of the surface area of the material, because the amount of gas adsorbed when the monolayer is saturated is proportional to the entire surface area of the sample. The complete adsorption/desorption analysis is called an adsorption isotherm.

1.2.2.2 Classification of adsorption isotherms

Adsorption isotherms are conventionally plotted as the amount of gas adsorbed and desorbed as a function of relative pressure, P/P_0 where P and P_0 are the equilibrium and the saturation pressure of nitrogen at the temperature of adsorption.

The experimental procedure involves the use of partial pressure, where the actual pressure is expressed with respect to the saturation vapour pressure at a constant temperature of adsorption, hence the process is isothermal. Isotherms provide a significant amount of information about the adsorbent studied and its interaction with the adsorbate. The six IUPAC standard adsorption isotherms, first classified by Brunauer, Deming, Deming and Teller (B.D.D.T. system) are shown below, they differ by the different gas/solid interactions.

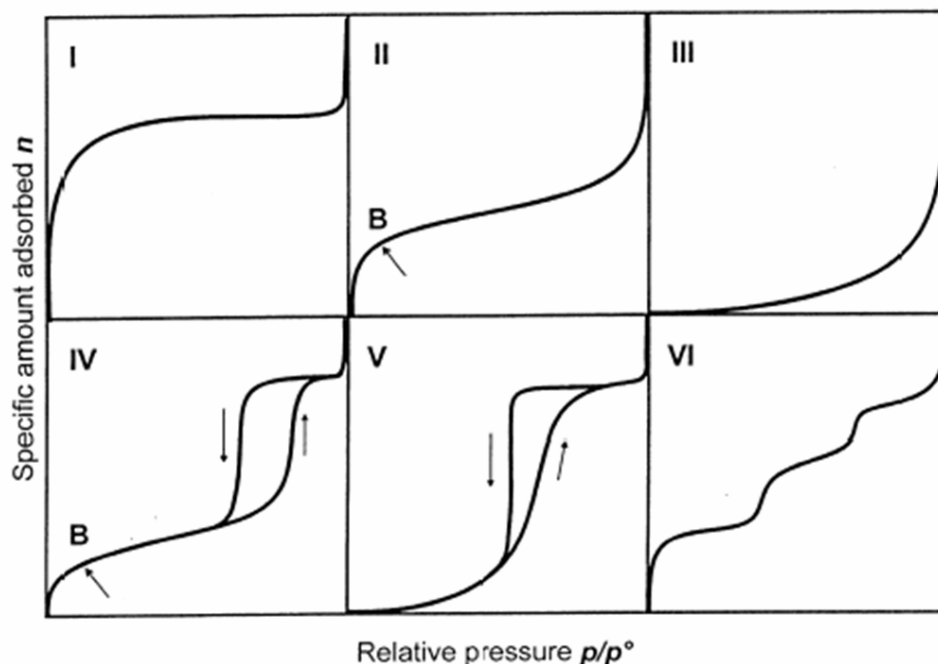


Figure IV.6: Schematic representation of isotherm classification [Rouquerol et al, 1999]

Type I Isotherm: The plot is typical for microporous solids, as the majority of micropore filling will occur at relative pressures below 0.1. The type I isotherm rises sharply at low relative pressures and then reaches a plateau. The initial increase of the amount adsorbed at low partial pressures is an indication of micropore adsorption. The appearance of a nearly horizontal plateau indicates a saturation of the monolayer and a very small external surface area.

Type II Isotherm: The plot is concave to P/P_0 axis, then almost linear and finally convex to the P/P_0 axis. Physical adsorption of gases by non-porous or macroporous solids is typical to this class of isotherm. The first change of curvature, point B, shows the moment when the first monolayer is almost complete. Monolayer coverage is followed by multilayering at high relative pressures. Carbons with mixed micro- and meso-porosity produce Type II isotherms.

Type III Isotherm: The plot obtained is convex to the relative pressure axis. This class of isotherm is characteristic of weak adsorbate-adsorbent interactions and is most commonly associated with both non-porous and microporous adsorbents. The interactions between the adsorbate and the adsorbent are lower than the interactions adsorbate-adsorbate that result in accelerated uptake at higher relative pressure.

Type IV Isotherm: The plot exhibits a hysteresis loop, which is usually associated with the filling of mesopores by capillary condensation. At low relative pressures monolayer coverage occurs followed by formation of further layers. The mesopores are filled in the final stages of the isotherm by multilayer formation and a cylindrical meniscus is formed. The adsorbed layer acts as a nucleus upon which capillary condensation may take place. The shape of the hysteresis loop is unique to each adsorption system. This type of isotherm is most valid for mesoporous materials.

Type V Isotherm: These isotherms are convex to the relative pressure axis and are characteristic of weak adsorbate-adsorbent interactions. These isotherms are indicative of

microporous or mesoporous solids. The reasons behind the shape of this class of isotherm are the same as those for Type III and type V isotherms and are typical for water vapor adsorption on hydrophobic materials.

Type VI Isotherm: The shape of this isotherm is due to the complete formation of monomolecular layers before progression to a subsequent layer. One example known is the adsorption of krypton on carbon black (graphitised at 3000° K) at 90° K. This type of isotherm is quite rare.

1.2.2.3 Nitrogen adsorption method

The porosity of Aerocellulose obtained with nitrogen adsorption method was measured in the FhG IAP. Experimental data were kindly provided to us for the further analysis. The Sorptomatic 1990 apparatus manufactured by ThermoQuest was used. Liquid nitrogen was used for adsorption as it does not alter the internal structure of the material under investigation. The adsorption experiments were done at -196°C, boiling temperature of liquid nitrogen under atmospheric pressure, and the molecular area of the nitrogen adsorbate is equal to 0.162nm², estimated through the average distance of molecules in liquid nitrogen. These measurements allow the quantification of the specific surface area, the pore volume and the pore size distribution within the limits of the technique (pore diameters from 2 nm to 100 nm). Prior to measurement, all samples were dried at 90°C for 16 hours. Adsorption and desorption isotherms over a range of relative pressures (P/P_0) from 0.01 to 0.95 were collected for all samples. Surface areas were determined from the Brunauer-Emmett-Teller (BET) equation within the relative pressure range between 0.01 and 0.1. Pore volumes and pore size distributions were determined using the Barrett-Joyner-Halenda (BJH) model. The BET theory and the BJH model are briefly described in the following paragraphs.

1.2.2.4 BET theory

In 1938 Stephan Brunauer, Paul Emmett and Edward Teller developed the BET theory named after the initials of its creators. This theory is based on the Langmuir adsorption theory, but, while Langmuir assumed that the gases form only one monolayer on the solid, Brunauer, Emmett and Teller suggested a multilayer adsorption mechanism (Figure IV.7).

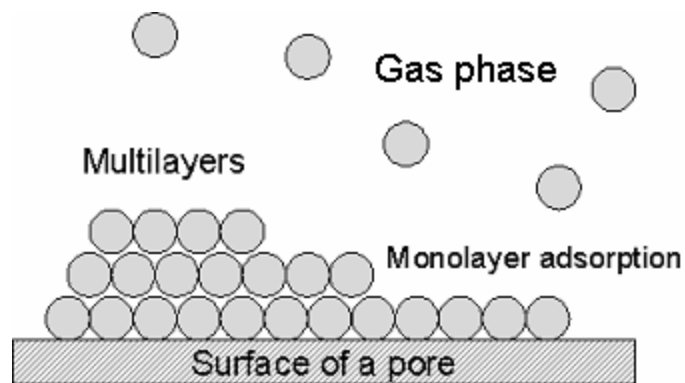


Figure IV.7: Adsorption phenomenon at pore surface

The BET theory is based on the hypothesis that the initial formation of the first adsorption monolayer is followed by the development of multilayer. As the pores are filled, there is no interaction between each adsorption layer and there is only one type of adsorption site. The resulting BET equation is expressed by:

$$\frac{1}{V[(P_0/P) - 1]} = \frac{1}{cV_m} \left(\frac{P}{P_0} \right) + \frac{1}{V_m} \quad (\text{IV.1})$$

where V is the volume of gas adsorbed at pressure P, V_m is the quantity of the adsorbed gas in the monolayer, P/P₀ is the relative pressure of adsorbate at the temperature of adsorption and c is the BET constant, which is expressed as follows:

$$c = \exp\left(\frac{E_1 - E_L}{RT}\right) \quad (\text{IV.2})$$

where E₁ is the heat of adsorption for the first layer, and E_L is that for the second and higher layers and is equal to the heat of liquefaction, R is gas constant and T is temperature. The BET adsorption isotherm can be plotted in coordinates [1/V [(P₀/P) - 1] versus [P/P₀]. This plot is called a BET plot; V and V_m are then easy to determine. The linear relationship of this equation is maintained only in the range of 0.05 < P/P₀ < 0.3. The theory of Brunauer, Emmett and Teller (BET) enables the calculation of the specific surface area, the pore size and the cumulative volume from the adsorption/desorption data. The relations between measured V and V_m and pores characteristics are given below.

The specific surface area

The specific surface area, S_{BET} is calculated from V_m the volume of monolayer by the following equation:

$$S_{BET} = \frac{V_m N_A a_m}{m V_L} \quad (\text{IV.3})$$

where N_A is the Avogadro constant, a_m is the cross section occupied by each nitrogen molecule (0.162 nm²), m is sample weight, V_L is the molar volume of nitrogen gas (22141 cm³) and V_m is the volume of monolayer.

Surface area of adsorbents depends on their structure. This parameter is strongly related to the pore size and the pore volume, i.e., the larger the pore volume the larger the surface area and the smaller the pore size the higher the surface area.

1.2.2.5 The BJH model

The Barrett-Joyner-Halenda (BJH) model is used to determine the pore size distribution. It is based on a cylindrical pores model. It is based on capillary condensation of nitrogen in the mesopores, which occurs at pressure less than saturated vapor pressure of the adsorbate forming a hemispherical liquid-vapour meniscus. It uses the classical Kelvin law, derived from the Laplace equation as following:

$$\ln \frac{P}{P_0} = \frac{2\gamma V_L}{rRT} \cos \theta \quad (\text{IV.4})$$

where P is the equilibrium vapor pressure of a liquid in a pore of radius r , P_0 the equilibrium pressure of the same liquid on a plane surface, γ is the surface tension, V_L the molar volume of the adsorbed liquid and θ the contact angle between the liquid and the pore wall, R the gas constant and T the absolute temperature.

Applying this law to nitrogen at the temperature of -196°C , the following relation is found between radius and partial pressure:

$$r = \frac{-0.415}{\ln\left(\frac{P}{P_0}\right)} \quad (\text{IV.5})$$

Considering that with the nitrogen adsorption measurements we obtain the volume of nitrogen adsorbed/desorbed as a function of the partial pressure, it is possible to calculate the pore volume as a function of the pore size and hence the pore size distribution of the material.

The calculation is generally done using the desorption curve.

1.2.2.6 The Dubinin and Radushkevich model

In order to determine the volume of micropores, the Dubinin and Radushkevich approach is frequently used. It is based on a semi-empirical theory developed by Dubinin and Radushkevich (DR) and is used to analyse the structures containing micropores. The process involved is micropore volume filling rather than layer-by-layer adsorption on the pore walls. The adsorbate volume V depends on adsorption potential A .

$$A = RT \ln\left(\frac{P}{P_0}\right) \quad (\text{IV.6})$$

and is expressed by the following equation (known as the Dubinin-Radushkevich equation):

$$\ln V = \ln V_0 - BA^2 \quad (\text{IV.7})$$

where the logarithm of the amount of the gas adsorbed is linearly proportional to the square of the adsorption potential (B is a constant). Writing this equation explicitly in terms of pressure, we obtain:

$$V = V_0 \exp\left[-\frac{1}{\beta E_0} \left(RT \ln \frac{P}{P_0}\right)^2\right] \quad (\text{IV.8})$$

where E_0 is called the solid characteristic energy, the parameter β is a function of the adsorptive only. The linear plot of $\ln V$ versus A^2 leads to determination of V_0 , which is the total micropore volume, and of βE_0 , which is the heat of adsorption.

1.2.3 Mercury Porosimetry

Mercury (Hg) porosimetry measurements were performed by FhG IAP. The experimental results were kindly provided to us for the further analysis. The Hg-intrusions were carried out by two mercury intrusion devices: the macropore unit “Pascal 140” and the mesopore unit “Pascal 440”.

Mercury porosimetry is based on the fact that mercury has a high surface tension, $480 \text{ mN}\cdot\text{m}^{-1}$ and is a strongly nonwetting liquid for most substrates. Mercury porosimetry is based on the capillary law governing liquid penetration into porous structure. In the case of a non-wetting liquid like mercury, this law is expressed by the Washburn equation:

$$D = 4\gamma\left(\frac{1}{P}\right)\cos\theta \quad (\text{IV.9})$$

where D is the pore diameter, P is the applied pressure, γ is the surface tension of mercury and θ is the contact angle between the mercury and the material (measured separately).

The Washburn equation assumes that all pores are cylindrical with circular cross-sections. Although pores are rarely cylindrical in reality, this equation provides a practical representation of pore size distribution.

Once the sample is immersed into mercury, a gradually increasing external pressure is applied to force mercury into the porous space. The volume of mercury V penetrating the pores is measured directly as a function of applied pressure P . As a result, an intrusion curve is obtained. This information provides the porous structure characterisation of the material.

The cumulative pore volume is the total introduced volume of mercury V_{tot} at the highest determined pressure. The total pore surface area is calculated using equation:

$$S = \frac{1}{\gamma|\cos\theta|} \int_0^{V_{\text{tot}}} p dV \quad (\text{IV.10})$$

The mean pore diameter is calculated using equation:

$$D_{\text{mean}} = 4 \frac{V_{\text{tot}}}{S} \quad (\text{IV.11})$$

The pore size is calculated for each pressure point. These measurements give the pore volume versus pore size distribution for the sample material. The volume pore size distribution, $D_v(d)$, is based on a model of cylindrical pores. It is defined as the pore volume per unit of pore diameter (d) by equation:

$$D_v(d) = \frac{p}{d} \cdot \frac{dV}{dP} \quad (\text{IV.12})$$

1.2.4 Electron microscopy

Two types of electron microscopy have been used to characterise our materials: scanning electron microscopy (SEM) and transmission electron microscopy (TEM). The specimen is bombarded with a high-energy electron beam, which leads to electron emission, which can either be transmitted or scattered.

1.2.4.1 Scanning electron microscopy

The SEM experiments were performed either in FhG-IAP, Potsdam; Germany, using a scanning electron microscope model JSM 6330JEOL F at an acceleration voltage of 5 kV or in CEMEF/Ecole des Mines, Sophia-Antipolis, France using a PHILIPS JEOL 35CF at an acceleration voltage of 10-15 kV.

The cryo-fractures were prepared after freezing the samples in liquid nitrogen and subsequent fracturing at -196°C . In order to avoid electrical charging during SEM investigations, thin layers of Platinum in FhG-IAP or of carbon in CEMEF were deposited by sputtering onto the surfaces of the cross sections.

In Scanning Electron Microscope (SEM), a fine beam of electrons is focused on the surface of the sample; different radiation types are emitted from the specimen and may be collected (see schematic presentation in Figure IV.8).

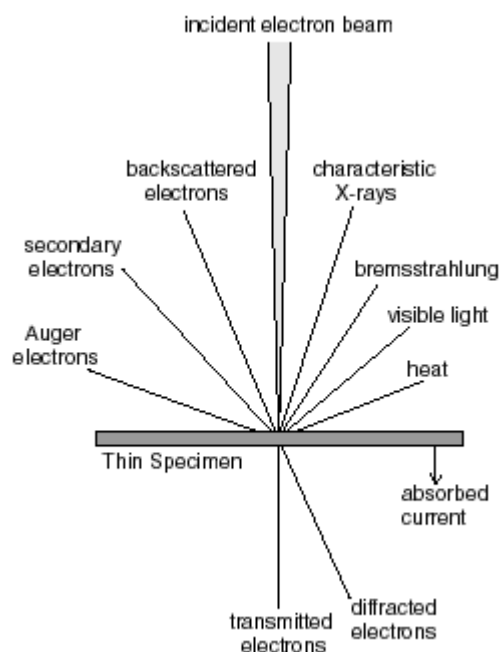


Figure IV.8: The radiations produced by electron bombardment of a material [Yao et al, 2005]

When an electron beam interacts with a bulk specimen, a variety of electron, photon, phonon and other signals can be generated. There are three types of electron that can be emitted from the specimen: secondary electron with energy lower than 50 eV, Auger electrons produced by the decay of the excited atoms, and backscattered electrons that have energies close to those incident electrons. All these signals can be used to form images of sample's surface. The electrons may be elastically reflected from the specimen, with no loss of energy. They may be

absorbed by the specimen and give rise to secondary electrons of very low energy, together with X-rays. They may be absorbed and give rise to the emission of visible light.

Secondary electrons are produced when the electron inelastically collide with the sample. The orientation of surface features influences the number of electrons that reach the secondary electron detector, which creates variations in image contrast that represents the sample's surface topography. Secondary electron mode was used in scanning electron microscopy observations.

Backscattered electrons are high-energy electrons produced by the elastic interactions between the sample's atoms and the incident electron beam. The production of backscattered electrons varies directly with the specimen's atomic number. The contrast of images is a function of composition - higher atomic number materials appear brighter than low atomic number materials.

X-rays can also be emitted by the specimen. X-ray detectors are used for examining the X-ray spectrum emitted by the sample under the influence of the electron beam and provide useful information on the elemental composition of the region of the sample.

Figure IV.9 illustrates a general scheme of SEM working principle:

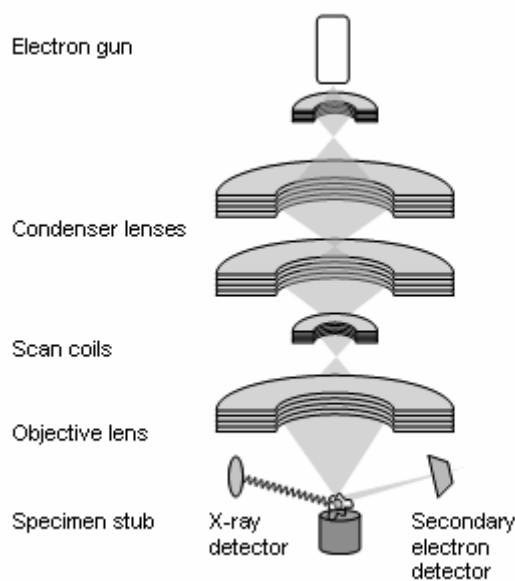


Figure IV.9: Schematic representation of a SEM [Web site 1]

In the SEM instrument, electrons from a tungsten filament in an electron gun are beamed at the specimen surface in a vacuum chamber. The electrons are accelerated due to a potential difference typically of the order of 5-15 kV. The electron beam is collimated by electromagnetic condenser lenses, focused by an objective lens, and scanned across the surface of the sample by electromagnetic deflection coils. When the energetic electrons hit the surface under investigation, secondary electrons are emitted. A detector collects secondary electrons produced from the sample-beam interaction and reports the information as an image on the cathode-ray-tube where a specimen image is mapped for observation. The secondary electron microscopy gives a resolution varying from 500 μm down to 500 nm.

1.2.4.2 Transmission electron microscopy

The TEM investigations were performed at the CEMEF, Sophia-Antipolis with a PHILIPS CM12 transmission electron microscopy at an acceleration voltage of 120 kV. The Aerocellulose is deposited on a copper grid. The grid is then placed into the chamber through an airlock and bombarded with a focused electron beam. The CM12 TEM is equipped with both a video-camera for real time imaging and a slow scan CCD camera for final images. The schematic presentation of TEM is shown in Figure IV.10.

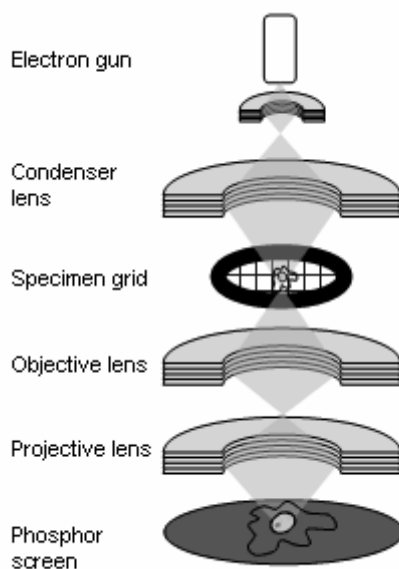


Figure IV.10: Schematic representation of a TEM [Web site 1]

In transmission electron microscopy, an electron beam is formed with an electron gun; it is accelerated by an electric field formed by a voltage difference of, typically, 120 kV. The microscope is comprised of several electromagnetic lenses, which mainly serve to focus the beam on one specific area of the sample. When excited electrons come into contact with the sample, three options can happen. The electrons can be undeflected (desired by TEM) or they can be elastically or inelastically scattered. At the bottom of the microscope the unscattered electrons hit a fluorescent screen, which gives rise to a "shadow image" of the specimen. The degree of darkness corresponds to the electron density. The image can be studied directly on a fluorescent screen or photographed with a camera.

The only major drawback of TEM is that it requires numerous observations to ensure that the image is representative of the bulk material and not of an artefact.

2 Results and discussion. Aerocellulose microstructure: influence of cellulose characteristics and preparation conditions

The influence of various parameters in Aerocellulose preparation was investigated on Aerocellulose final microstructure. They are listed below for cellulose/7.6NaOH/water and cellulose/NMMO/water systems. In our study we were varying one parameter and keeping all the others constant. However, because Aerocellulose is a new material never investigated before, it is not yet possible to draw a complete picture of the influence of each of the preparation parameters on material structure.

In the case of Aerocellulose obtained from cellulose/7.6NaOH/water solutions, the following preparation parameters were varied:

- Cellulose concentration: X= 3, 5, 6 or 7g in 100 g solution, in the Xcellulose/7.6NaOH/water solution
- Cellulose type: Avicel, Solucell I and Borregaard with respective DP 170, 307 and 500
- Additive (surfactant Simulsol) concentration: 0.1, 0.5 and 1% in weight of total to 5Avicel/7.6NaOH/water solution
- Regenerating bath conditions:
 - Water at various temperatures: 25, 50 and 70°C
 - Sulphuric acid at various concentration of 0.02M, 0.2M and 1M, at 25°C
- Supercritical drying were either performed in CEP, Ecole des Mines, France or in Natex, Austria.

With a few exceptions that will be specified, gelation of cellulose (Avicel or Borregaard)/7.6NaOH/water solution was performed at 50°C for 2 hours. In the case of Solucell I/7.6NaOH/water solution, the gelation was performed at 70°C for 2 hours as it was observed in section II.2.2.2. that gelation temperature for Solucell I was 55°C. After cellulose regeneration in water, water was exchanged with acetone and then cellulose samples were CO₂ supercritical dried in CEP, Ecole des Mines, France or in Natex, Austria.

In the case of Aerocellulose obtained from cellulose/NMMO solutions, cellulose concentration was 3% and type of cellulose was Solucell with DP950. The parameters bellows were changed:

- Regenerating bath conditions:
 - Water at various temperature: 25, 50 and 70°C
 - Alcohols: ethanol, isopropanol, pentanol, at 25°C
- Second exchange: water was either exchanged with ethanol or with acetone, both solvents compatible with supercritical CO₂
- Supercritical drying were either performed in CEP, Ecole des Mines, France or in Natex, Austria.

2.1 Example of Aerocellulose microstructure

In this section an example of the results obtained on the structure of a typical Aerocellulose sample is presented. Nitrogen adsorption-desorption and mercury intrusion were performed and SEM and TEM images were made. Different structural parameters like pores cumulative volume and specific surface area, pores size distribution, mean pore size and sample density were obtained. The influence of the preparation procedure and conditions on these parameters will be discussed in the forthcoming sections.

The Aerocellulose obtained from “5Avicel/7.6NaOH/water” solution is a typical Aerocellulose sample. The preparation of this representative Aerocellulose without any special treatment or additives used is described below.

5Avicel/7.6NaOH/water solution was gelled at 50°C for 2 hours. The formed gel was regenerated in water bath of 25 °C with further solvent exchange water→acetone and then was dried in CO₂ in supercritical conditions in CEP. The nitrogen adsorption-desorption isotherm for sample “5Avicel/7.6NaOH/water” is shown in Figure IV.11. The isotherm presents a hysteresis loop, typical for mesoporous materials, having the pores with a diameter of 2-50 nm. The reason for the hysteresis is the difference between the evaporation from the pore and the condensation within it. When gas condenses in a pore, the condensate moves on the walls inwards toward a central core of decreasing diameter. The decreased diameter retards the evaporation process and causes the decreasing portion of the loop to lag behind until all pores are emptied. Isotherms with this shape were typical for all samples studied.

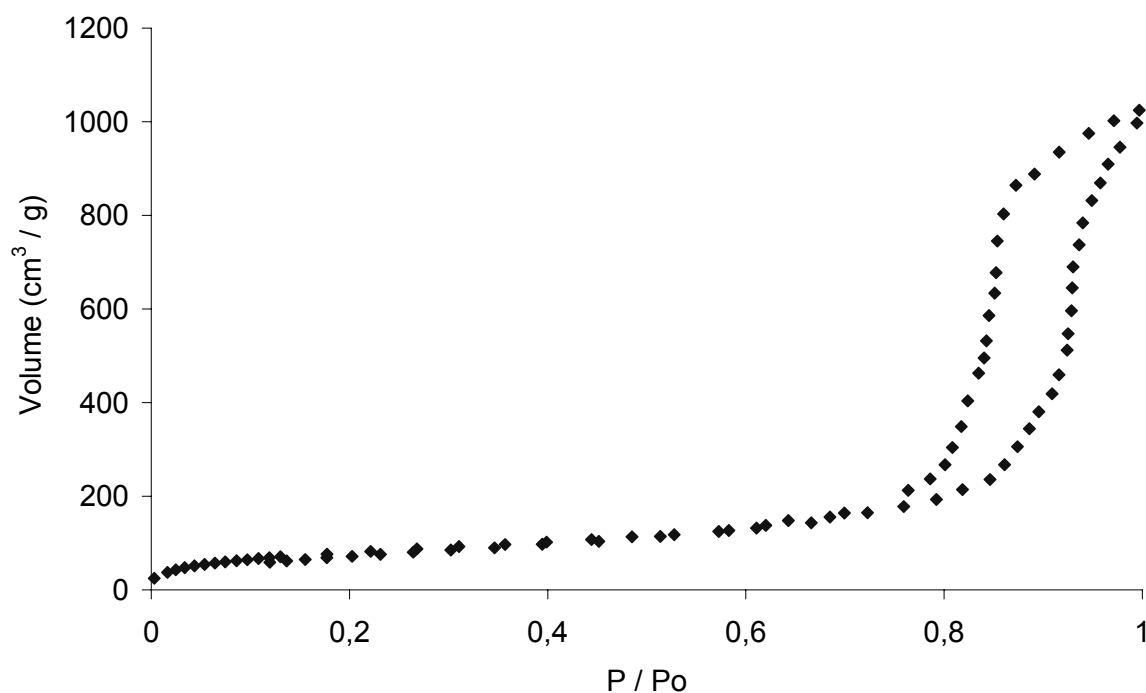


Figure IV.11: Nitrogen adsorption-desorption isotherm of Aerocellulose made from 5Avicel/7.6NaOH/water gel (gelation performed at 50°C for 2 hours) regenerated in water bath of 25°C, water exchanged by acetone, dried in CEP

The pores volume distribution deduced from nitrogen isotherm adsorption is represented in Figure IV.12.

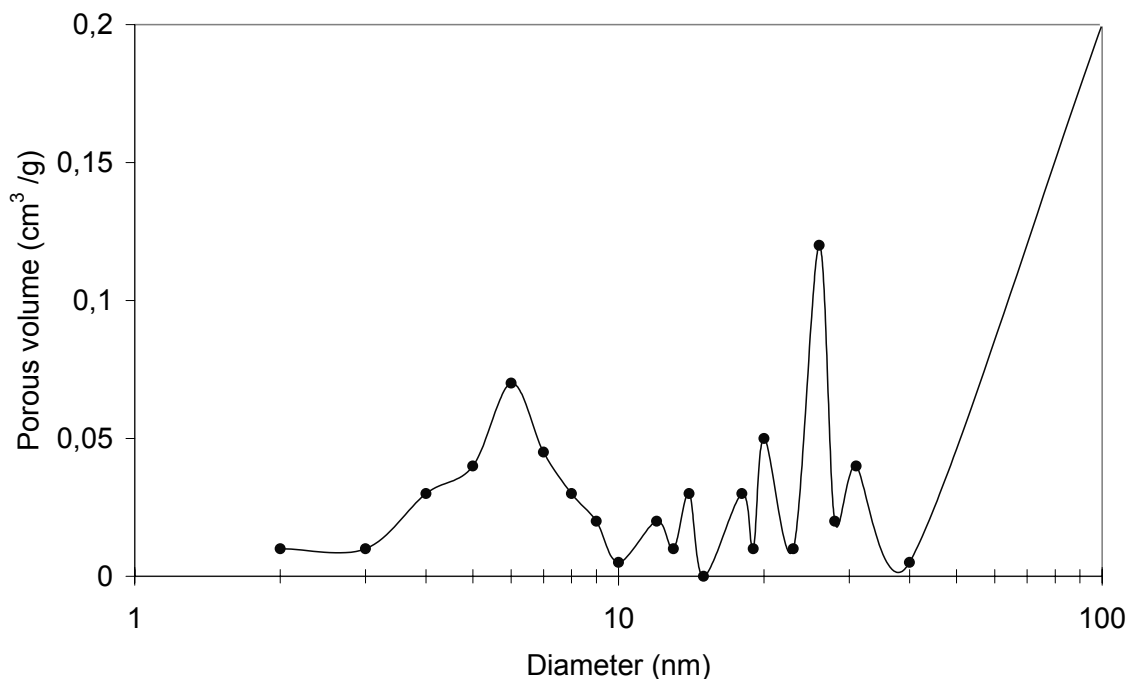


Figure IV.12: Porous volume distribution of the same Aerocellulose made from 5Avicel/7.6NaOH/water gel as in Figure IV.11, obtained from nitrogen adsorption measurements

This figure shows Aerocellulose porosity from 2 to 100 nm. It should be noted that nitrogen intrusion leads to a pore distribution with sizes lower than 100 nm. BJH model was used to determined the pore size distribution of all Aerocellulose materials.

With the mercury intrusion the volume caused by macropores can be estimated. Mercury intrusions analysis have shown that Aerocellulose have a macropores ranging in the size 2 nanometres up to 100 μm (Figure IV.13).

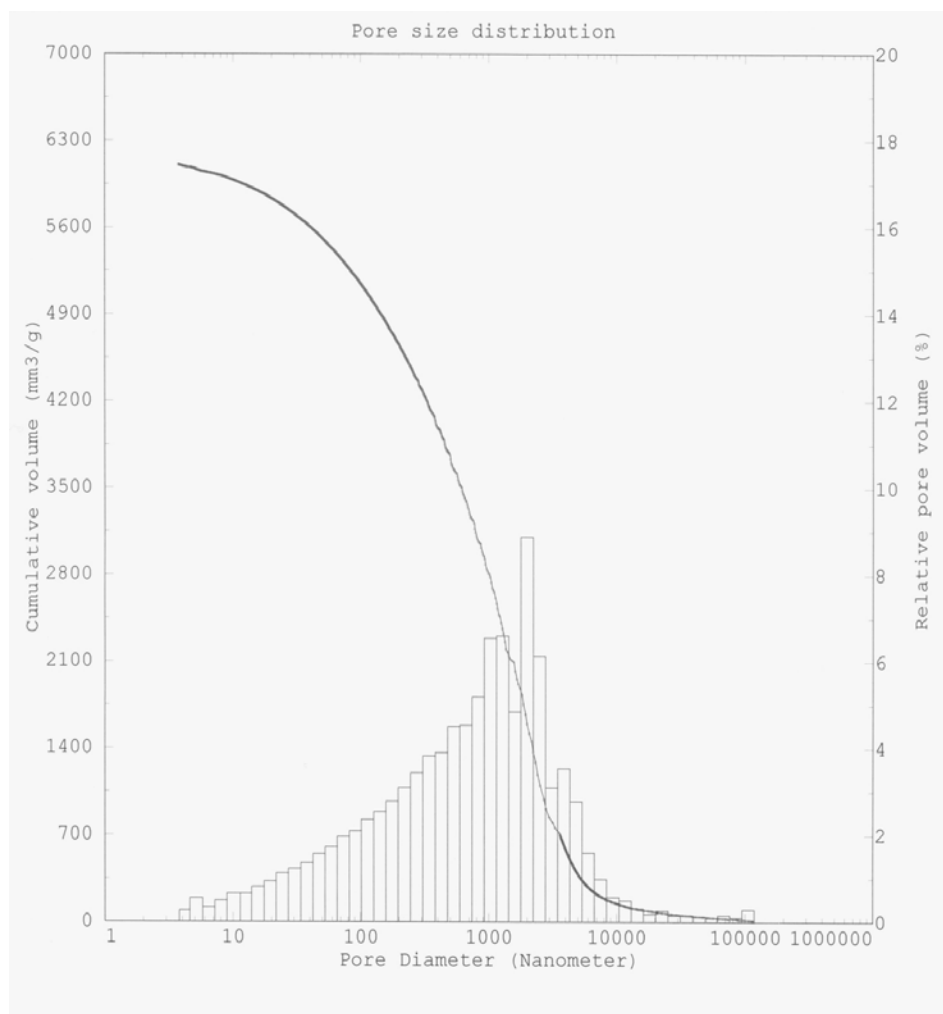


Figure IV.13: Pore size distribution of the same Aerocellulose made from 5Avicel/7.6NaOH/water gel as in Figures IV.11 and IV.12 but obtained from mercury porosimetry measurements

The pore size distribution shows Gauss distribution with a large range of pores from mesopores (2-50 nm) to macropores (pores with diameter over 50 nm). According to the mercury intrusion analysis the total porosity of this sample is of 96 %, the average pore radius is 450 nm and the total cumulative volume is 6.6 cm³/g. This high cumulative pore volume is due to the high number of large pores.

The specific pores surface of this sample obtained by the Hg intrusion (macro- and meso-pores) and by the N₂-sorption (BET, micro-pores) is shown in Figure IV.14.

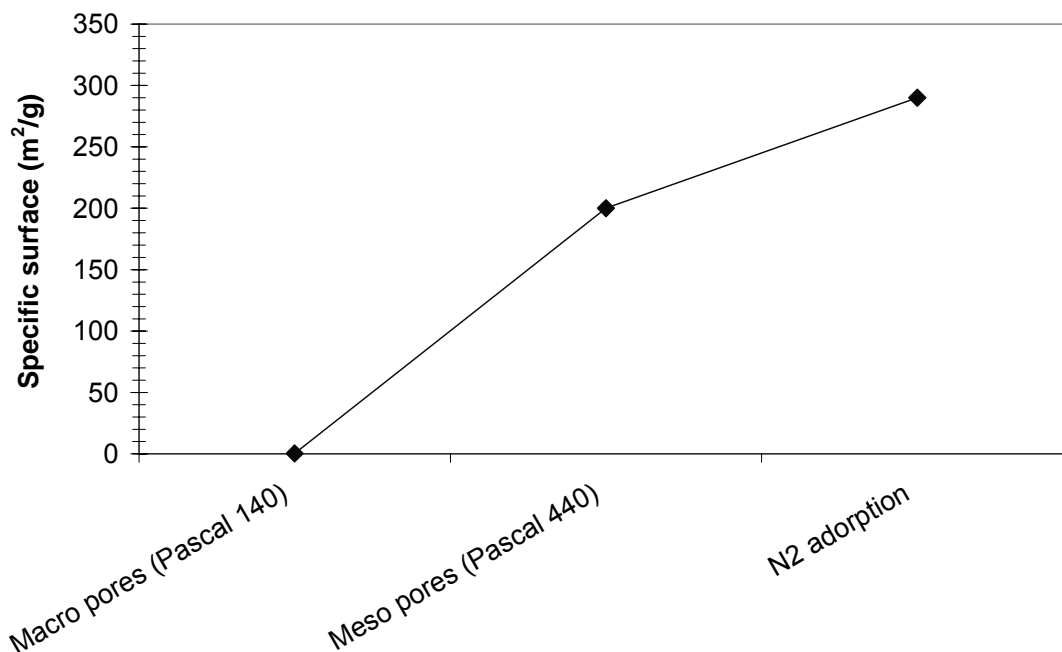


Figure IV.14: Specific surface of the Aerocellulose made from 5Avicel/7.6NaOH/water gel. The values were obtained by the Hg intrusion (macro- and meso-pores) and by the N₂-sorption (BET, micro pores)

It appears that the macropores do not contribute considerably to the surface area of the adsorbent, typically less than 1 m²/g. This contribution is rather low in comparison to the contribution of meso-pores (220 m²/g). The largest amount of the specific surface is contributed by micro-pores (300 m²/g).

The morphology of the same Aerocellulose was analysed with transmission and scanning electron microscopy. Figure IV.15 shows the SEM photographs at various magnitudes of the free surface and of the cross section of the typical Aerocellulose obtained from 5Avicel/7.6NaOH/water solution. The cross sections of the Aerocellulose were prepared by breaking the material under liquid nitrogen.

Macropores down to a diameter of 100 nm could be detected by this method. Micropores could not be detected by this technique; we suppose that these pores should be located inside the thin cellulose walls between the macropores.

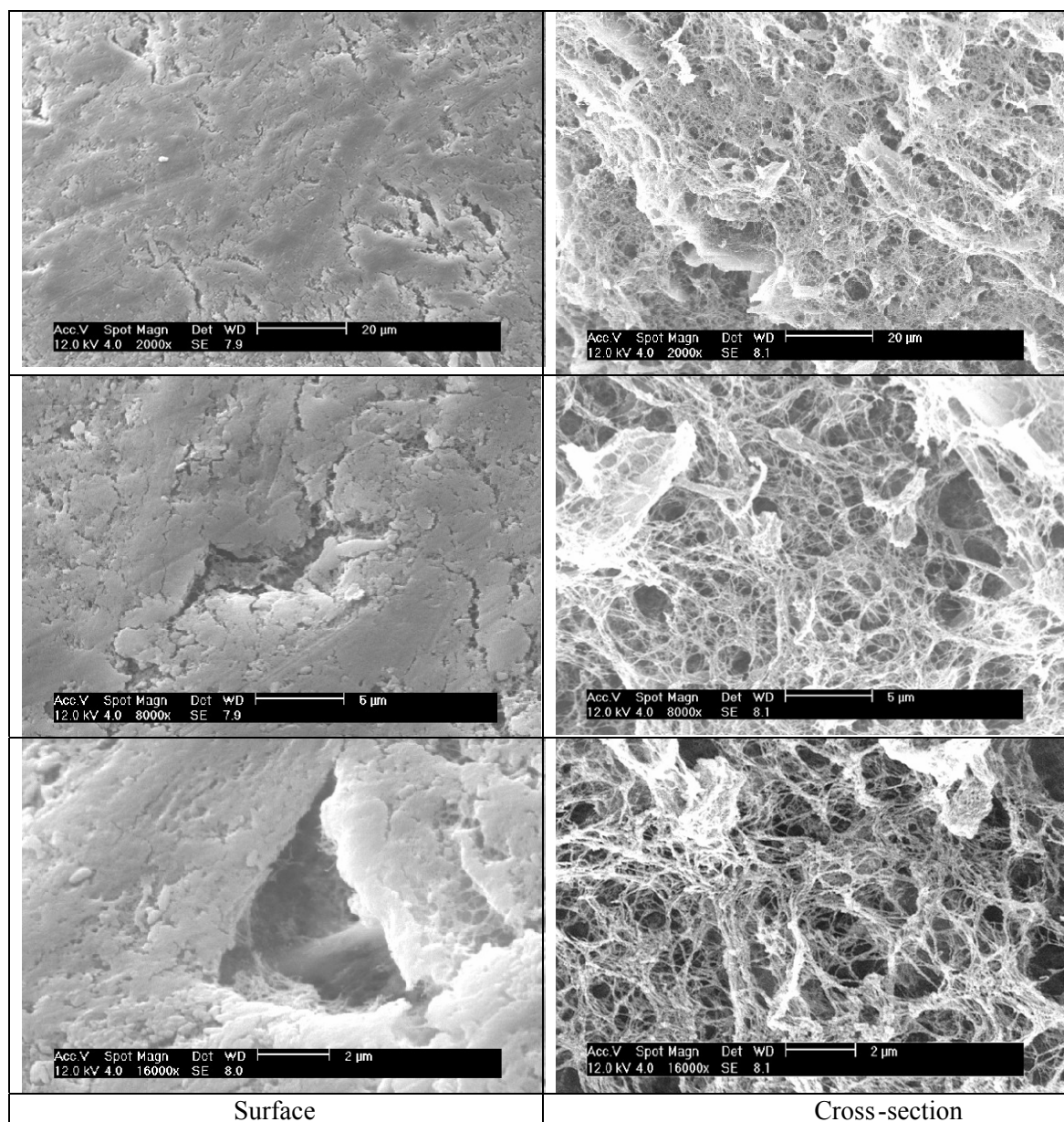


Figure IV.15: SEM micrographs of Aerocellulose made from 5Avicel/7.6NaOH/water gel

The Aerocellulose made from 5Avicel/7.6NaOH/water gel shows a quite dense surface. The skin thickness is lower than few hundreds nanometres. The formation of the skin may result from the increase of cellulose concentration stimulated by rapid solvent depletion from the top layer of the gel. In the inner areas, the sample displays a homogeneous porous structure. We can observe a large pore distribution from 10 μm to less than one micron. The thickness of the wall of large pores is around 100 nm.

Figure IV.16 presents the TEM images of Aerocellulose obtained from 5Avicel/7.6NaOH/water gel.

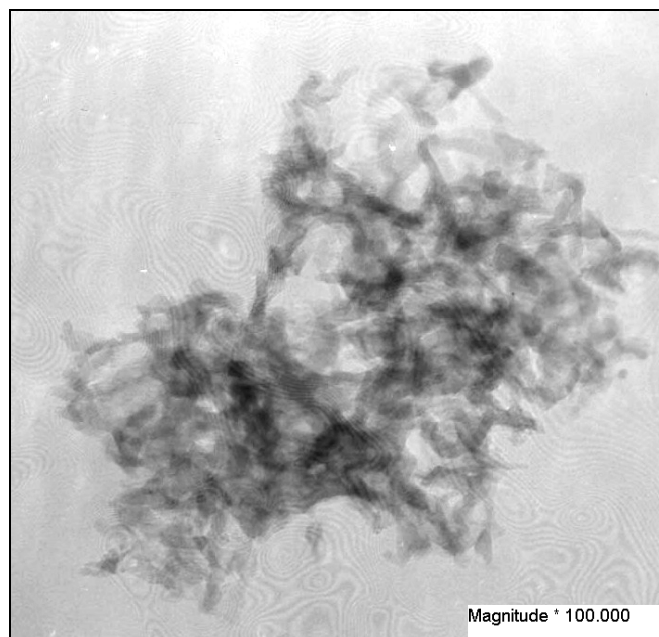


Figure IV.16: TEM image of Aerocellulose made from 5Avicel/7.6NaOH/water gel

TEM images provide further evidence of the homogeneous porous nanostructure of Aerocellulose formed by cellulosic fibrils superposed in layers.

2.2 Influence of gelation conditions

In order to check the influence of gelation conditions on Aerocellulose microstructure, we have compared the same initial solution, 5Avicel/7.6NaOH/water, either gelled at 50°C for two hours or at ambient temperature for 24 hours, then regenerated in water at 25°C, further solvent exchange water→acetone and then dried in CO₂ in supercritical conditions in CEP. The microstructural characteristics presents here and in the following as bulk density, mean pore diameter, specific surface, cumulative volume and porosity are the results obtained from mercury intrusion for mesopores and macropores. Table IV.1 summarises the microstructural characteristics obtained for these two samples.

Samples	Bulk density [g/cm ³]	Mean pore diameter [μm]	Specific surface [m ² /g]	Cumulative volume [cm ³ /g]	Porosity %
5 Avicel /7.6NaOH/water gelled at 25°C for 24hours	0.13	0.84	220	6.3	94.8
5 Avicel /7.6NaOH/water gelled at 50°C for 2hours	0.14	0.90	240	6.6	96

Table IV.1: Microstructural characteristics of Aerocellulose obtained from 5 Avicel /7.6NaOH/water solution with different gelation conditions

It appears that the gelation conditions affect very slightly the final microstructural characteristics of Aerocellulose. In the following each Avicel /7.6NaOH/ water solution was gelled at 50°C for 2 hours.

2.3 Influence of cellulose concentration

Table IV.2 presents the porous characteristics obtained by mercury intrusion of Aerocellulose from Avicel/7.6NaOH/water gels (gelation performed at 50°C for 2hours) of various cellulose concentrations: 5, 6 and 7g in 100 g solution and regenerated in water in the same standard conditions (water bath of 25°C, then water was exchanged by acetone) and then supercritical dried in CEP.

Samples	Cellulose concentration	Mean pore diameter [μm]	Cumulative volume [cm^3/g]	Specific surface [m^2/g]
5Avicel/7.6NaOH/water	5	0.90	6.6	216
6Avicel/7.6NaOH/water	6	0.72	6.1	220
7Avicel/7.6NaOH/water	7	0.70	6.0	198

Table IV.2: Porous characteristics of Aerocellulose obtained from XAvicel/7.6NaOH/water gels with X=5, 6 or 7 g in 100 g solution

It appears that the higher the cellulose concentration, the lower the pores mean diameter and thus the cumulative volume. This phenomenon was also observed by Jin and his co-workers, who have freeze dried solutions of cellulose of different concentrations [Jin et al, 2004] (see Figure I.23).

2.4 Influence of pulp properties

Table IV.3 summarises the micro-structural data obtained using mercury porosimetry for Aerocellulose made from different pulps using the same cellulose concentration 5cellulose/7.6NaOH/water prepared in the same conditions (gelation performed for 2 hours at 50°C for Avicel and Borregaard solutions and for 2 hours at 70°C for Solucell solution), regenerated in water at 25°C, water exchanged by acetone, dried in CEP.

Sample	Cellulose types	Bulk density [g/cm^3]	Mean pore diameter [μm]	Specific surface [m^2/g]	Cumulative volume [cm^3/g]	Porosity %
5cellulose/ 7.6NaOH/ water	Avicel, DP = 170	0.14	0.90	240	6.6	96
	Solucell, DP = 307	0.12	0.86	260	7.5	91
	Borregaard, DP = 500	0.13	0.92	280	7.2	94.7

Table IV.3: Microstructural characteristics of Aerocellulose obtained from different pulps from 5cellulose/7.6NaOH/water gels

There is practically no influence of the type of pulp used on micro structural properties: the density is $0.13 \pm 0.01 \text{ g/cm}^3$, the mean pore radius varies between $430 \pm 20 \text{ nm}$, the specific surface is $260 \pm 20 \text{ m}^2/\text{g}$ and the cumulative volume varies between 6.6 and 7.5. It seems that porosity is the highest for Aerocellulose from Avicel cellulose; this could be explained by better cellulose dissolution and thus the formation of a more fine structure. However, in order to make any adequate conclusion, more studies should be performed, for example, by keeping the same cellulose origin and treatment and varying only the DP.

2.5 Influence of surfactant addition

In order to lighten Aerocellulose material, the surfactant Simulsol SL8 was added at various concentrations: 0.1%, 0.5% and 1% in weight to 5Avicel/7.6NaOH/water solution. The idea was to create air bubbles during solution mixing with the surfactant and then to “block” them in the sample by immediate gelation. The gels obtained after 2 hours gelation at 50°C were regenerated in water at ambient temperature, water was exchanged by acetone and samples were dried in CEP in supercritical CO_2 conditions. Table IV.4 presents microstructural characteristics of Aerocellulose as a function of surfactant concentration.

Simulsol concentration	Mean pore diameter (μm)	Cumulative volume (cm^3/g)	Density (g/cm^3)
0%	0.9	6.6	0.14
0.1%	6.4	7.2	0.12
0.5%	28.1	8.6	0.10
1%	47.5	9.6	0.06

Table IV.4: Microstructural characteristics of Aerocellulose obtained from 5Avicel/7.6NaOH/water gels (gelation for 2 hours at 50°C) regenerated in water at 25°C , water exchanged by acetone, dried in CEP, for different Simulsol concentrations

With the increase of surfactant concentration, we observe an increase of cumulative volume. It corresponds to an increase of macropore formation in the material structure, which is revealed by the mercury porosimetry measurements. Higher is the surfactant concentration, higher are the pore diameter and the cumulative volume and as a result lower is sample density. The density is reduced by 30% by adding 0.5% of surfactant and twice by adding 1% of surfactant to the cellulose solution.

The Figure IV.17 presents the morphology obtained by scanning electron microscopy of the Aerocellulose obtained by adding 0.1% Simulsol SL8 to the initial cellulose solution.

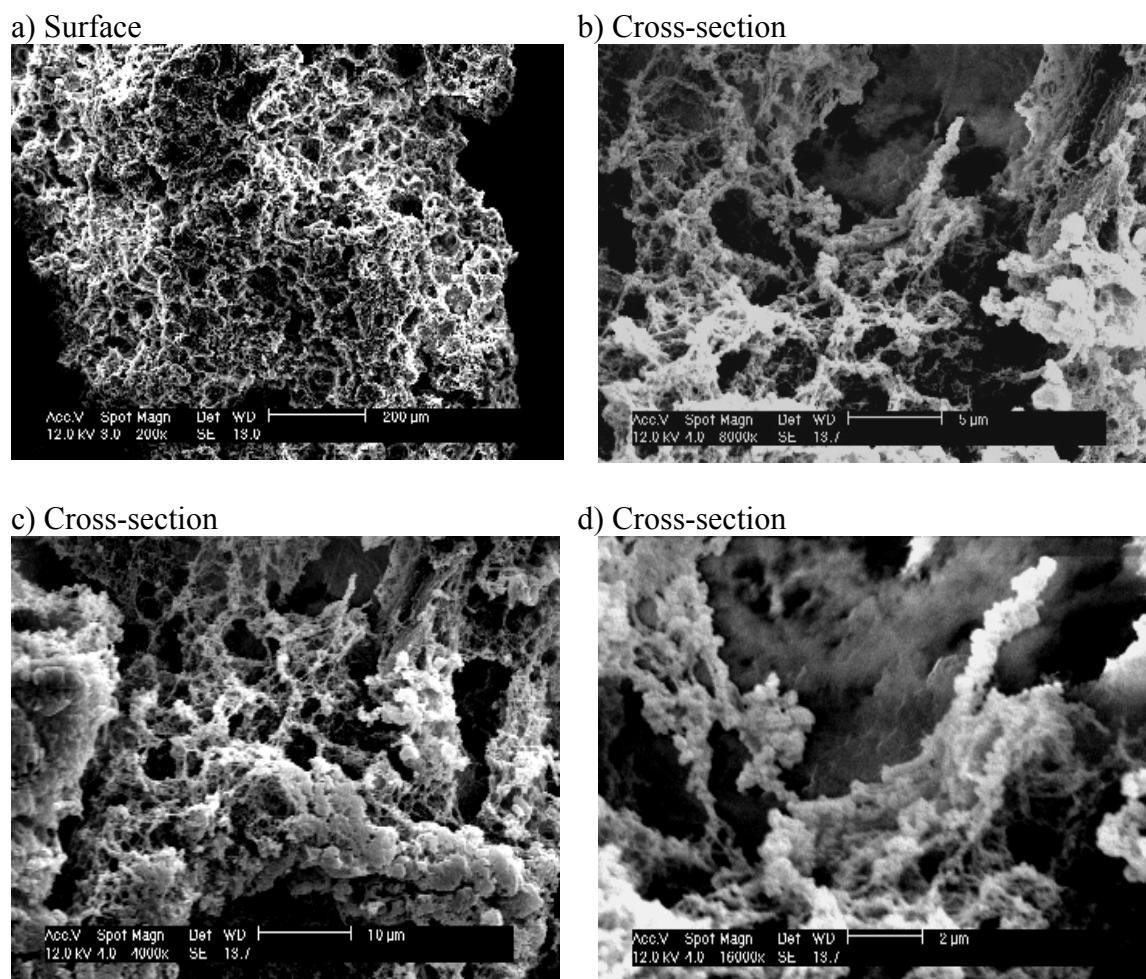
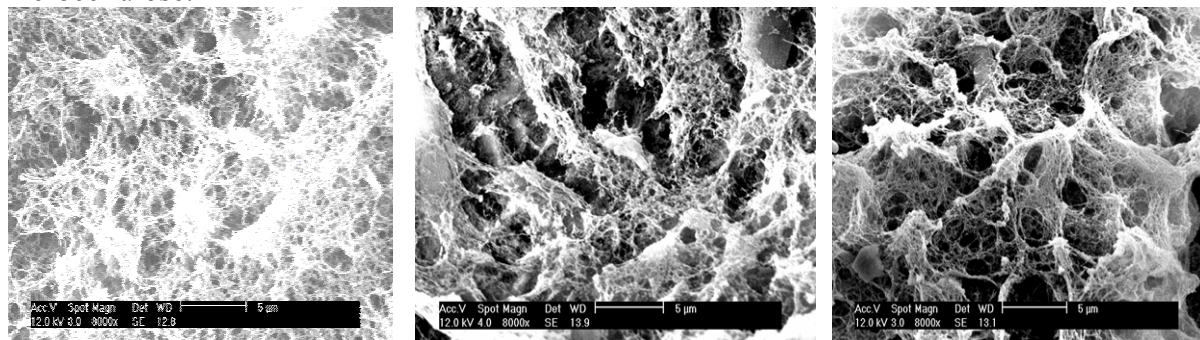


Figure IV.17: SEM micrographs of Aerocellulose obtained from 5Avicel/7.6NaOH/water gels (gelation for 2 hours at 50°C), regenerated in water at 25°, water exchanged by acetone, dried in CEP with 0.1% Simulsol added

The surface is quite dense with large pores of approximately 10 μm. The inner part is very porous with packed cellulose fibrils, as shown on the cross section images. Figure IV.18 presents the influence of various concentrations of surfactant on the morphology of Aerocellulose.



a) Aerocellulose without Simulsol

b) 0.5% Simulsol

c) 1% Simulsol

Figure IV.18: SEM micrographs of Aerocellulose obtained from 5Avicel/7.6NaOH/water gels a) without Simulsol b) with 0.5% Simulsol c) with 1% Simulsol added

These images show the increased amount of large pores that were created by air bubbles. The higher is the surfactant concentration, the higher is the pore size of macropores. The data obtained by mercury intrusion corroborates this result. As there are more macropores and thus more air in the material, the density decreases and the material is enlightened. The result obtained being rather predictable, it shows, however, an interesting and promising way of varying Aerocellulose porosity.

2.6 Influence of the regenerating bath

The next step in the preparation of Aerocellulose, after making cellulose solution and gel, is cellulose regeneration. (See scheme of Aerocellulose preparation on Figure 1.1). Solution or gel is placed into a bath of liquid that is cellulose non-solvent: solvent then leaves cellulose solution or gel and non-solvent enters the sample leading to cellulose “regeneration” that in fact is precipitation or coagulation. Phase separation occurs and as a result swollen-in-non-solvent cellulose is obtained.

It is known that regenerating conditions, like the type of non-solvent, strongly influences the properties of fibres regenerated from cellulose-NMMO solutions (see, for example Figure I.17, ref [Fink et al, 2001] where fibres of different morphologies were obtained by varying regenerating bath type). Here the influence of bath temperature in the case of water bath and of bath type (water and alcohols) is investigated. Aerocellulose prepared from cellulose/NaOH/water gels will be compared with the one made from cellulose/NMMO/water solutions. In the case when cellulose was regenerated in water, further exchange is needed to perform supercritical drying: water should be exchanged with a liquid compatible with sc CO₂. The influence of the second regenerating bath on Aerocellulose microstructure will also be checked.

2.6.1 Water regenerating bath: influence of temperature

We have investigated the influence of regenerating bath temperature on the final morphology of Aerocellulose. As we have seen in chapter 3, the higher water bath temperature, the faster the regeneration kinetics.

2.6.1.1 Case of Aerocellulose obtained from cellulose/NaOH/water gels

Figure IV.19 presents Aerocellulose obtained from 3Avicel/7.6NaOH/water gels regenerated in water at various temperatures: 25°C and 70°C, followed by exchanged with acetone and then supercritical dried.

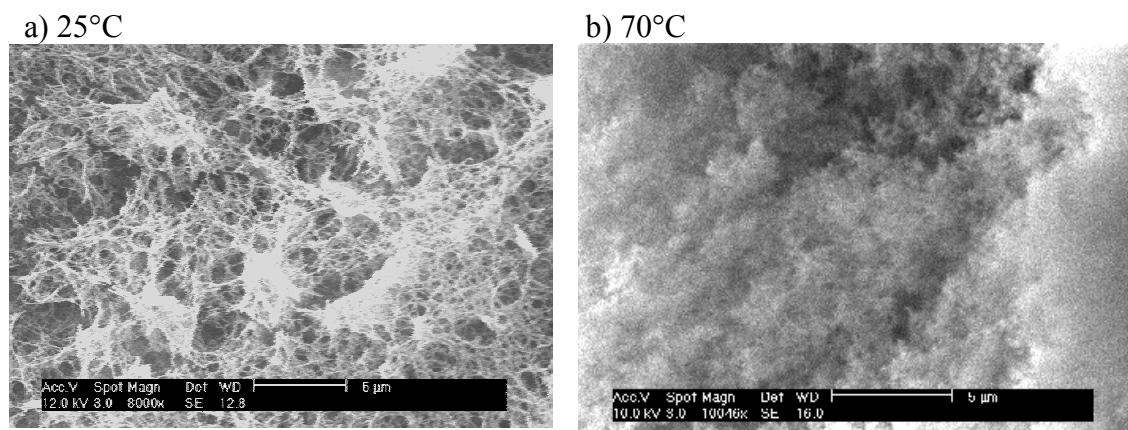


Figure IV.19: SEM micrographs of Aerocellulose obtained from 3Avicel/7.6NaOH/water gels (gelation performed at 50°C for 2hours) regenerated in water at ambient temperature (a) and at 70°C (b), exchange water→acetone and dried in CEP

Aerocellulose regenerated in water at ambient temperature shows a fibrillar structure while Aerocellulose regenerated in water at 70°C shows a « cloudy » structure. Higher temperature accelerates the diffusion of all components in the coagulating system. Probably because of this rapid precipitation cellulose chains have less time to “pack” and a cloudy structure is created.

Figure IV.20 presents an image at higher magnification of Aerocellulose prepared from 5Avicel/7.6NaOH/water gel regenerated in water at 50°C.

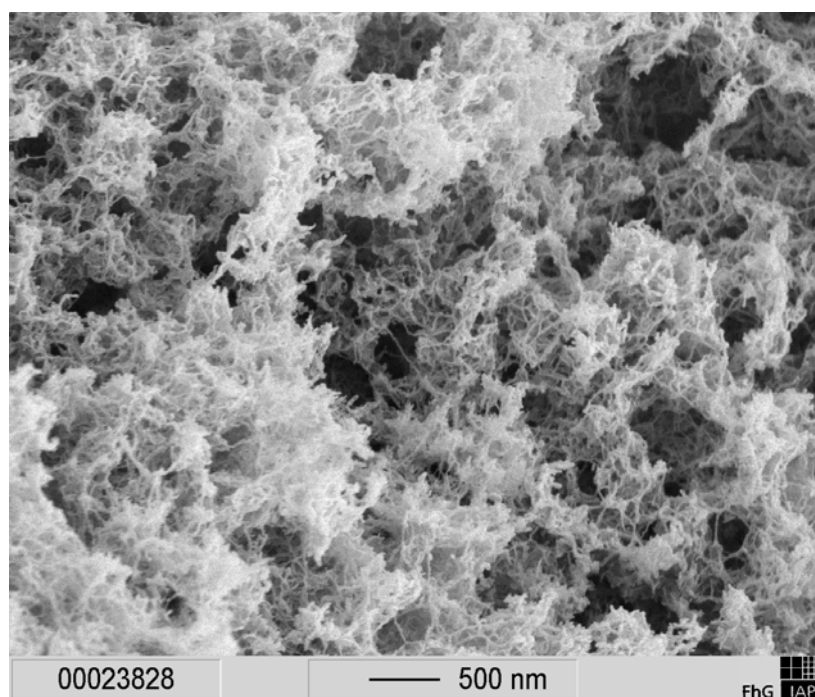


Figure IV.20: SEM micrographs of Aerocellulose prepared from 5Avicel/7.6 NaOH/water gel (gelation performed at 50°C for 2hours) regenerated in water at 50°C, exchange water→acetone and dried in CEP. Photo provided by FhG-IAP

Figures IV.21 and IV.22 show transmission electron microscopy images at different scales of the same sample prepared from 5Avicel/7.6NaOH/water gel regenerated in water at 50°C.

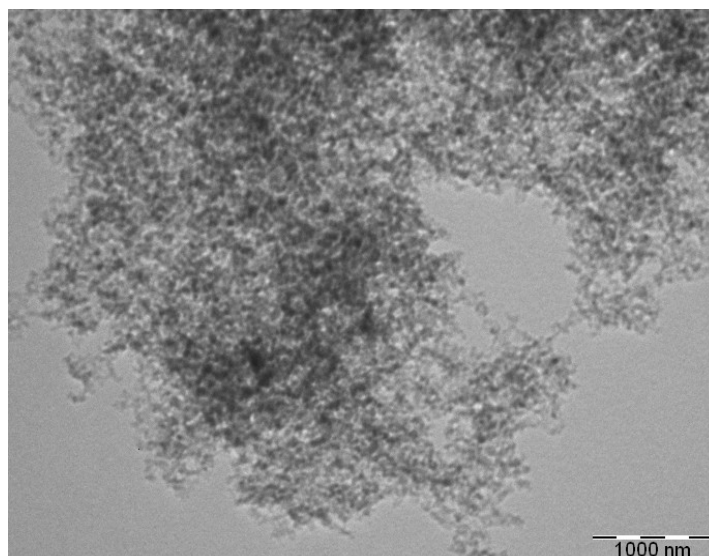


Figure IV.21: TEM image of the same Aerocellulose as in Figure IV.20 prepared from 5Avicel/7.6 NaOH/water gel (gelation performed at 50°C for 2hours) regenerated in water at 50°C, exchange water→acetone and dried in CEP

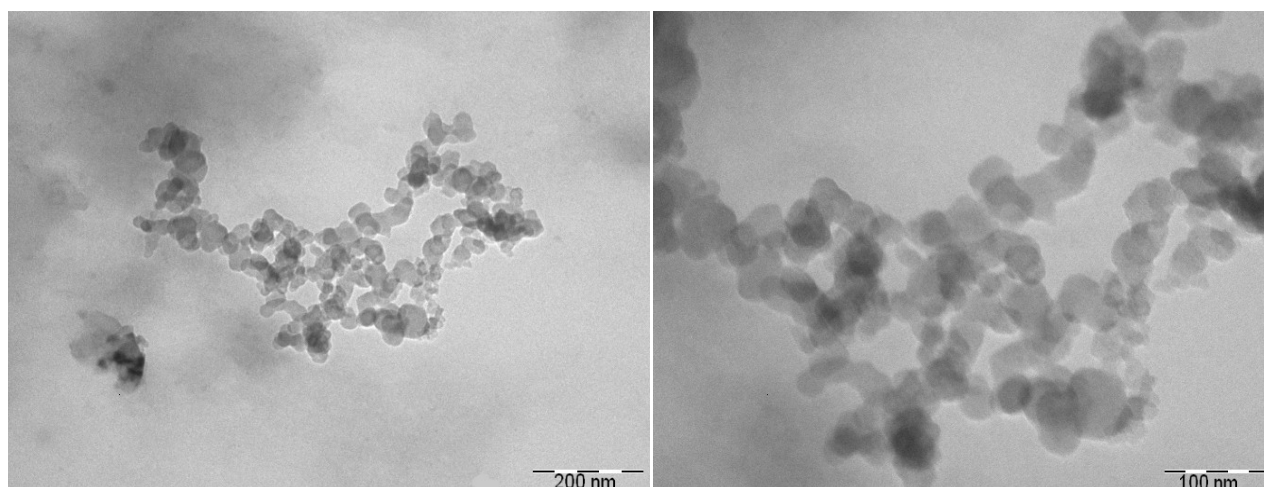


Figure IV.22: TEM image of the same Aerocellulose made from 5Avicel/7.6 NaOH/water gel regenerated in water at 50°C, as in Figures IV.20 and IV.21

Aerocelluloses regenerated in water at 50°C present a globular porous structure (Figures IV.21 and IV.22) intermediate between the one of sample regenerated at 25°C and 70°C (Figure IV.19).

Table IV.5 shows the influence of bath temperature on microstructural properties of Aerocellulose prepared from 5Avicel/7.6NaOH/water gels.

Water bath temperature	Bulk density [g/cm ³]	Mean pore diameter [μm]	Specific surface [m ² /g]	Cumulative volume [cm ³ /g]	Porosity
25°C	0.14	0.9	240	6.6	96
50°C	0.11	1.4	300	8.9	95

Table IV.5: Influence of bath temperature on microstructural characteristics of Aerocellulose obtained from 5Avicel/7.6NaOH/water gels

The increase in bath temperature has a strong impact on the structure of Aerocellulose: it creates larger pores, so it lightens the material and thus it reduces the density.

Another example of the influence of regenerating bath temperature is shown in Figure IV.23 for the case of Aerocellulose prepared from 5Borregaard/7.6NaOH/water gels (gelation at 70°C during two hours) and immediately regenerated in cold water at + 5°C, with further water→acetone exchange and dried in CEP.

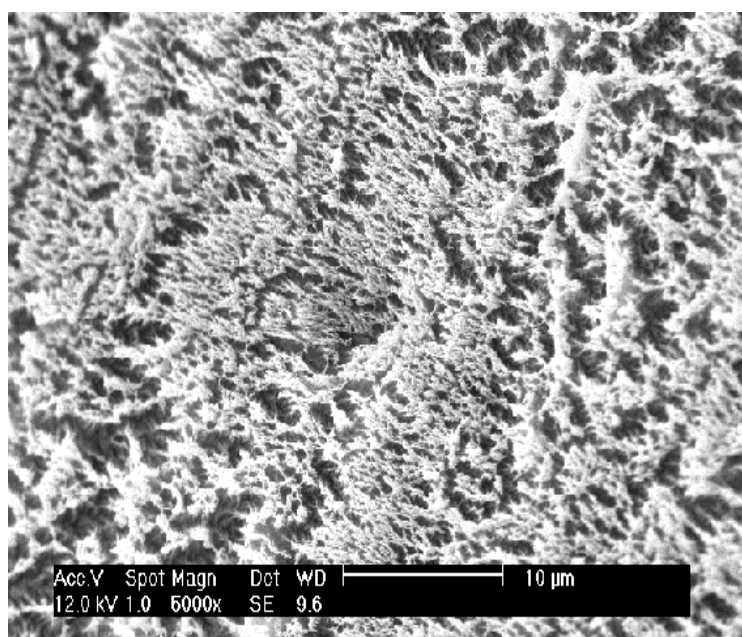


Figure IV.23: SEM micrographs of Aerocellulose prepared from 5Borregaard DP500/7.6NaOH/water gels (gelation at 70°C during two hours) regenerated in water at + 5°C, exchange water→acetone and dried in CEP

We can observe a sort of oriented structure probably due the strong flows caused by high thermal gradient between the hot aqueous sodium hydroxide solution that is released during regeneration and the cold water entering the sample.

2.6.1.2 Case of Aerocellulose obtained from cellulose/NMMO/water solutions

Different morphologies of Aerocellulose obtained from cellulose/NMMO solutions regenerated in water at various temperatures were observed. Figure IV.24 presents Aerocellulose prepared from molten 3% Solucell 1175/NMMO/water solution regenerated in water at 25°C with further water→acetone exchange and dried in CEP.

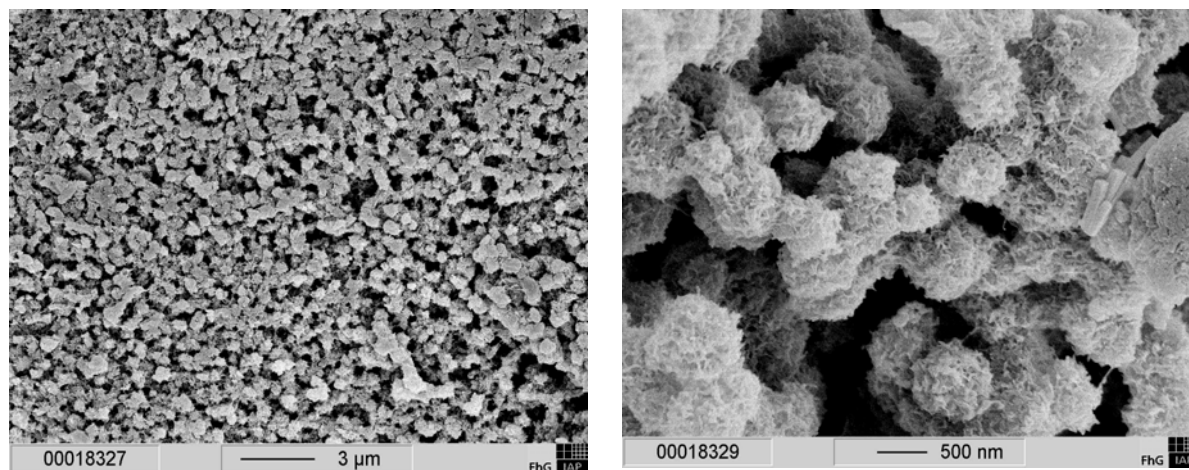


Figure IV.24: SEM micrographs of Aerocellulose prepared from molten 3% Solucell 1175/NMMO solution regenerated in water at ambient temperature, exchange water→acetone and dried in CEP. Photo provided by FhG-IAP

Aerocellulose presented in Figure IV.24 shows a particular morphology, it is a microporous globular structure formed by small spheres with a diameter around 1 μm. Because the spheres are of the same size, contacting each other, forming a slightly periodic structure and because cellulose is undergoing a clear phase separation from solution to precipitated state we can conclude that such a structure is a result of a spinodal decomposition.

The fact that the structure is composed of spheres is an advantage for some Aerocellulose application like electrochemical application or encapsulation application, which requires a high specific area.

No observation of Aerocellulose obtained from molten cellulose/NMMO solution and regenerated in hot water can be performed because molten cellulose solution disperse in the hot regenerating bath (no possibility to prepare an intact sample). The influence of regenerating bath temperature cannot be investigated for this way of preparation.

However the influence of water temperature could be observed on Aerocellulose prepared from crystalline cellulose/NMMO samples and regenerated in water baths. Figure IV.25 presents Aerocellulose prepared from crystalline 3% Solucell 1175/NMMO/water solution regenerated in water at temperature of 25°C and of 70°C with further water→acetone exchange and dried in Natex.

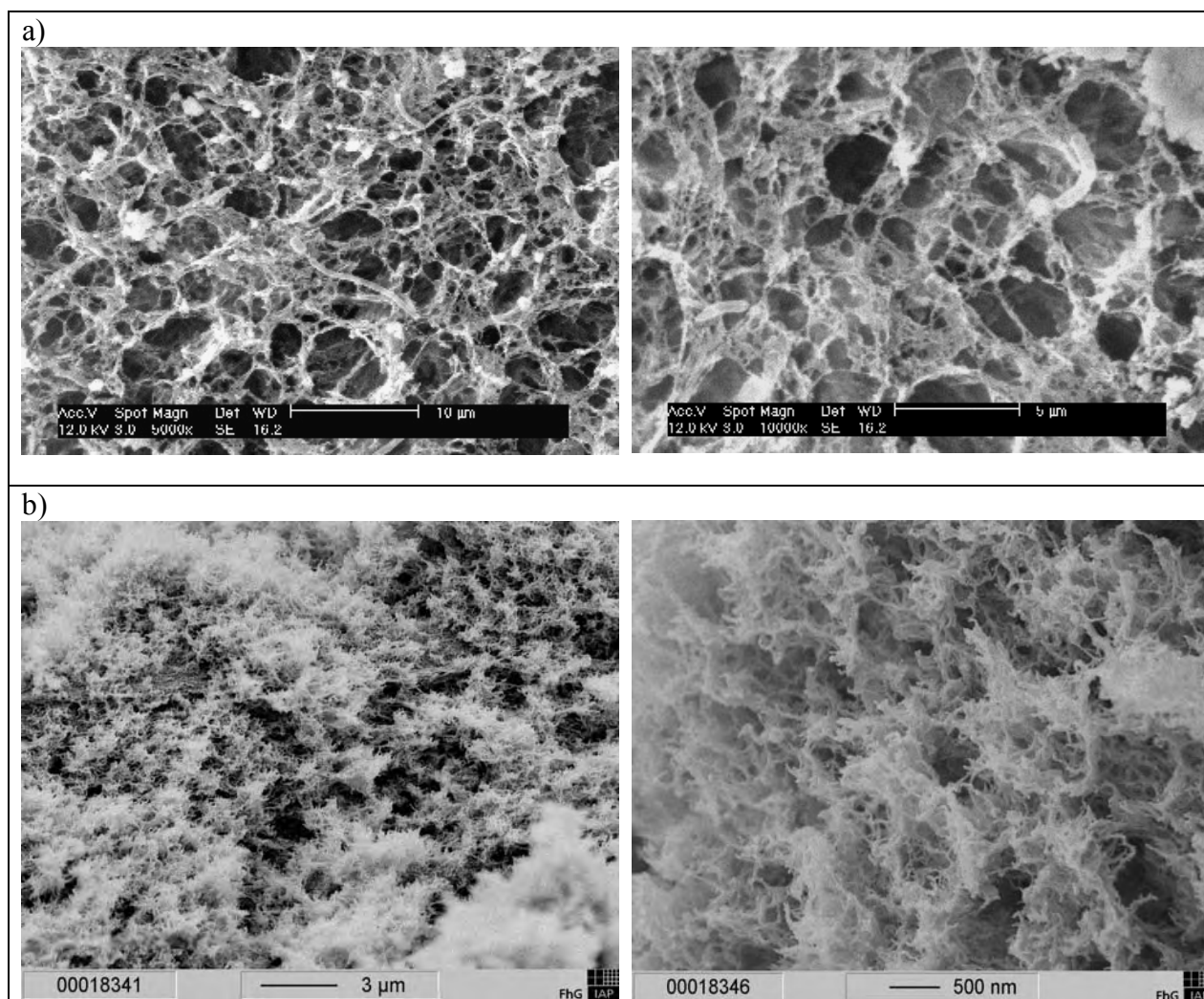


Figure IV.25: SEM micrographs of Aerocellulose obtained from crystalline 3% Solucell 1175/NMMO regenerated in water a) at 25°C and b) at 70°C, exchange water→acetone and dried in Natex, photo provided by FhG-IAP

From these SEM micrographs two observations can be made. First, we observe a totally different morphology as compared with the one observed for Aerocellulose obtained from molten cellulose/NMMO solution (Figure IV.24). It appears that the state of cellulose/NMMO solution, i.e. crystalline or molten (“molten” is in fact a real solution state), has a significant impact on final morphology of Aerocellulose. Indeed, when cellulose/NMMO is in solution state (“molten cellulose/NMMO”) and then placed into water, a phase separation cellulose/non-solvent takes place: water concentration becomes high and we are moving out of the region of cellulose dissolution on the phase diagram cellulose/NMMO/water (see Figure I.13). In this case the phase separation is governed by spinodal decomposition mechanism and regular spheres can be seen. When cellulose/NMMO is at room temperature (“crystalline cellulose/NMMO”), a phase separation between cellulose+linked NMMO and free crystalline NMMO had already occurred ref [Biganska et al, 2002]. During regeneration, water dilutes free NMMO leading to the appearance of large holes. A second phase separation occurs during which bound-to-cellulose-NMMO is removed from cellulose. Even if it occurs via spinodal decomposition mechanism, this is impossible to detect on the SEM image.

It is possible to make parallels with Aerocellulose structure obtained from cellulose/NaOH/water gels and cellulose/NMMO solution. The structure of Aerocellulose is very similar when cellulose is regenerated either from solid cellulose/NMMO or from cellulose/NaOH/water gel. In both cases solvent (NMMO or NaOH/water) are already separated from cellulose. Indeed, cellulose/NaOH/water solutions become opaque when gelling which is the indication of a phase separation. As it was mentioned in the previous paragraph, free NMMO is separated from cellulose + bound NMMO when the sample is in the solid state. Thus in both cases a porous structure with wide pore size distribution is obtained; it is due to the fact that water is first diluting regions with “free” solvent and thus making large pores and then “removing” the rest of the solvent from cellulose and making small pores. In the case of real cellulose/NMMO solution, cellulose and NMMO are homogeneously distributed all over the volume and a phase separation occurs in one step.

The second observation is if we compare Aerocellulose obtained from crystalline cellulose/NMMO solution regenerated in cold and hot water, we observe also a different morphology. Aerocelluloses prepared from samples regenerated in hot water present a “cloudy” structure; the same was obtained for cellulose/NaOH/water gels regenerated in hot water (Figure IV.19.b). In chapter 3, it was found that the higher water bath temperature, the quicker the regeneration kinetics. During the rapid regeneration, cellulose chains have less time to pack themselves and consequently cloudy disordered structure appeared.

2.6.2 Influence of the nature of the regenerating bath

2.6.2.1 Influence of bath acidity

The acidity of the bath was changed to check if this may influence Aerocellulose microstructure. 5Avicel/7.6NaOH/water gels were gelled for 2 hours at 50°C and were regenerated in sulphuric acid at a concentration of 0.02M, 0.2M and 1M, at ambient temperature followed by acid→ water and water→acetone exchanges and then cellulose samples were dried in CEP. The table IV.6 presents the porous characteristics obtained by mercury intrusion for these three samples.

H ₂ SO ₄ concentration	Ratio [H ₂ SO ₄]/[NaOH] inside the sample	Bulk density [g/cm ³]	Mean pore diameter [μm]	Cumulative volume [cm ³ /g]	Porosity [%]
0.02M	0.01	0.15	0.89	5.4	87.10
0.2M	0.10	0.17	0.80	5.1	81.40
1M	0.50	0.30	0.78	2.4	70.88

Table IV.6: Influence of bath acidity on microstructural characteristics of Aerocellulose obtained from 5Avicel/7.6NaOH/water gel regenerated in sulphuric acid at different concentrations at ambient temperature followed by water→acetone exchange and dried in CEP.

It appears that higher is the regenerating bath acidity, lower are the average pore diameter and the total porosity and thus the density.

The morphology of another Aerocellulose obtained from 5Avicel/7.6NaOH/water solution directly regenerated in acid bath was investigated. This sample was prepared in Genialab GmbH, Braunschweig, Germany, by dropping cellulose solution in 10% H₂SO₄ regenerating bath. As a result swollen cellulose beads in acid are formed. After an exchange of solvent acid to water and then water to acetone, cellulose beads were CO₂ supercritical dried in Natex. Using scanning electron microscopy, we have observed the formation of a skin on the surface of these beads (Figure IV.26).

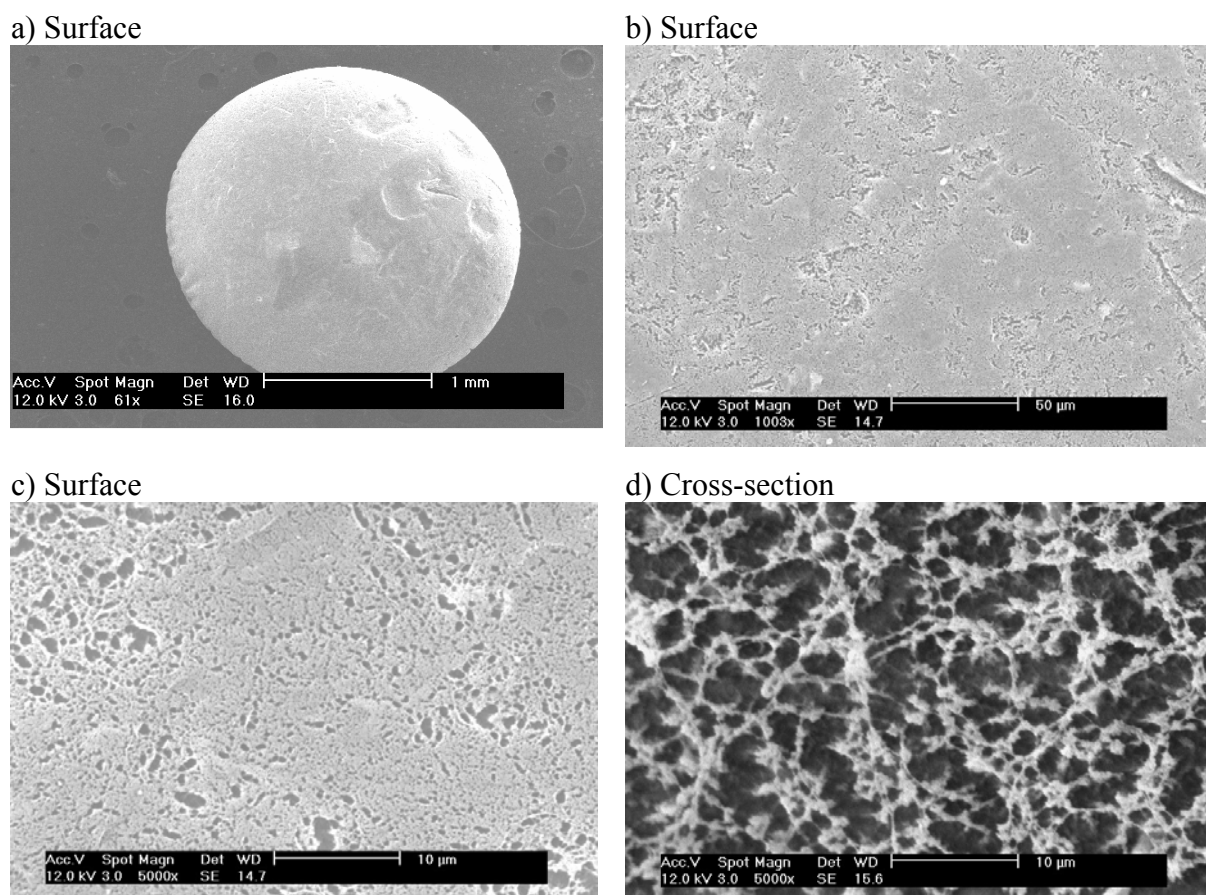


Figure IV.26 SEM micrographs of Aerocellulose from 5Avicel/7.6NaOH/water solutions regenerated in 10% H₂SO₄ bath, exchange acid→water, water→acetone and dried at Natex

The surface of the cellulose beads regenerated in sulphuric acid is very dense. At higher magnification we observe small pores on the surface, while inside the beads a highly porous “network” can be seen.

The appearance of a skin on the surface of the samples can be probably explained by the gradient of acid concentration during neutralisation process. Somehow the highest acid concentration is “received” by cellulose solution on its contact surface with the regenerating bath. During the regeneration course, acid is locally diluted by releasing in time NaOH. The higher the acid concentration, the more cellulose chains aggregate on the surface leading to the formation of a thick skin and thus to the decrease in the porosity and increase in density (see Table IV.6).

Table IV.7 presents microstructural characteristics of the Aerocellulose obtained from regeneration of 5Avicel/7.6NaOH/water solution in 10% H₂SO₄ water bath.

Sample	Bulk density [g/cm ³]	Mean pore diameter [μm]	Specific surface [m ² /g]	Cumulative volume [cm ³ /g]	Porosity
5Avicel/ 7.6NaOH/ water regenerated in 10%H ₂ SO ₄	0.27	0.2	250	2.9	77

Table IV.7: Microstructural characteristics of Aerocellulose beads obtained from 5Avicel/7.6NaOH/water regenerated in sulphuric acid at 25°C followed by exchange acid→water, water→acetone and dried at Natex

The porosity measurements revealed that regeneration in acid reduces porosity (77%), it decreases the pore size (0.2 μm) and it densifies (0.27 g/cm³) the material. This densification can be explained by the formation of a skin.

2.6.2.2 Influence of bath type

Because cellulose/7.6NaOH/water gels were strongly contracting in alcohol baths, it was not possible to elaborate Aerocellulose from cellulose/7.6NaOH/water gel regenerated in alcohol media, thus this case was not considered.

Nevertheless, as it was mentioned in Chapter III, the volume reduction during regeneration of Solucell/NMMO samples was rather low, not more than 15-20%. Solucell-NMMO samples were practically not contracting, thus the influence of the type of regenerating bath on Aerocellulose microstructural properties was investigated. Using refractometry, the release of NMMO into regenerating bath was measured and the diffusion coefficients were calculated with Fick approximation. It appears that the diffusion coefficients decrease when the molecular weight (and viscosity) of alcohols increase. Using scanning electron microscopy we have studied the final morphology of Aerocellulose samples prepared from crystalline 3% Solucell 1175/NMMO solution regenerated in various alcohol baths like ethanol or isopropanol, followed by exchange with acetone (Figure IV.27) and supercritical drying.

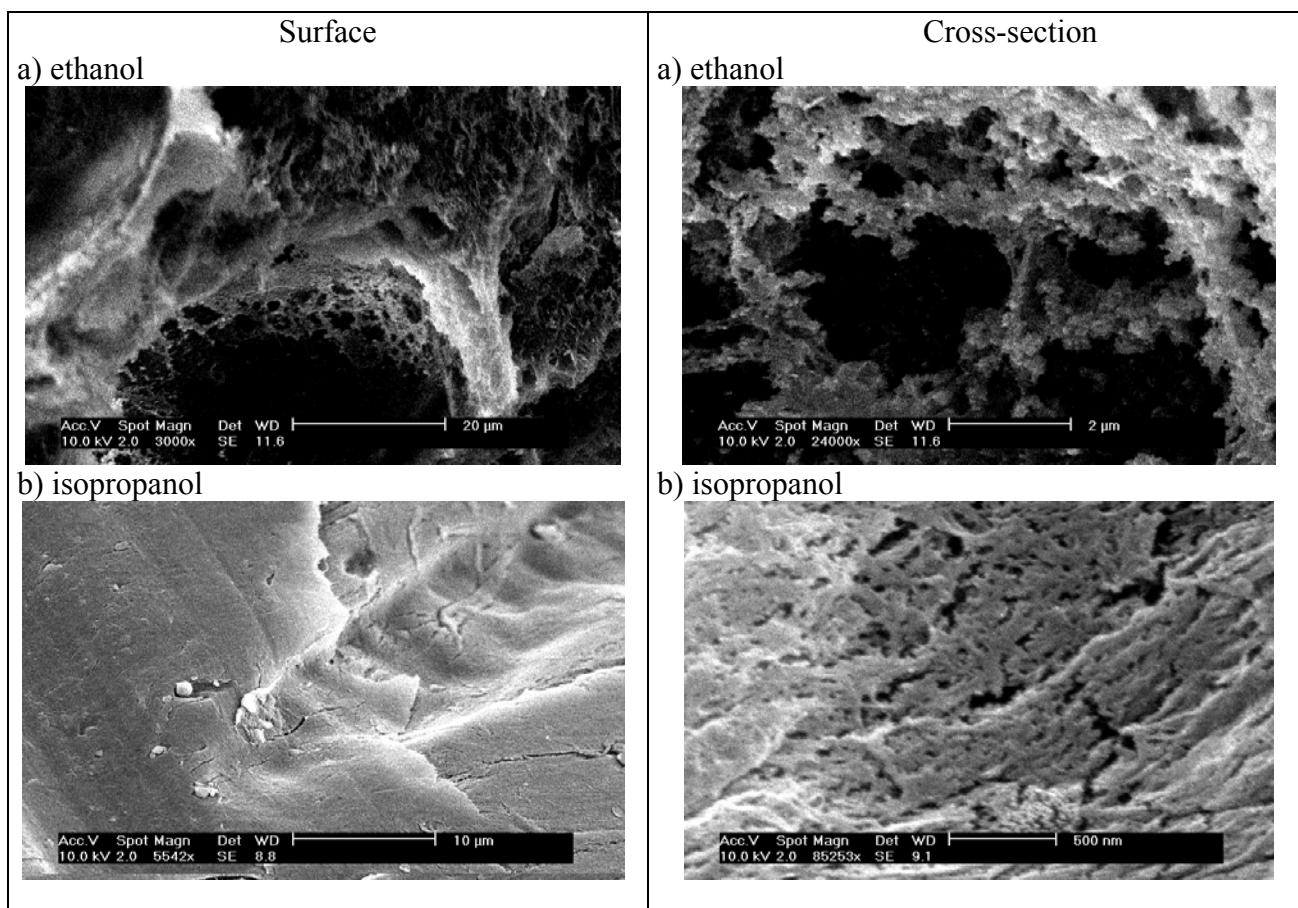


Figure IV.27: SEM micrographs of Aerocellulose prepared from crystalline 3% Solucell 1175/NMMO solution regenerated at ambient temperature in ethanol (a) and isopropanol (b), exchange alcohol→acetone and dried in CEP

The morphology of samples regenerated in alcohol baths is totally different as compared with the one regenerated in water (see Figure IV.25.a). It appears that ethanol is a better regenerating liquid than isopropanol in the sense that the final structure is more porous. After regeneration in ethanol the structure has the appearance of a lace while the structure obtained for isopropanol is more compact with a weak amount of nanopores. The two alcohols tested were not used as regenerating liquids in the following.

2.6.2.3 Influence of second regenerating bath

Because Aerocellulose is prepared via supercritical drying, the liquid in the sample should be compatible with liquid CO₂. It is known that acetone is well compatible with CO₂ thus in most of the cases water (or alcohol) was exchanged with acetone before drying the sample. Some other liquids, like ethanol, were used instead of acetone as far as ethanol is also compatible with CO₂ in the supercritical state.

An example for Aerocellulose obtained from molten (70°C) 3% Solucell 1175/NMMO solutions regenerated in water at ambient temperature and then either washed five times with acetone or with ethanol is shown in Figure IV.28 (a) and (b), respectively.

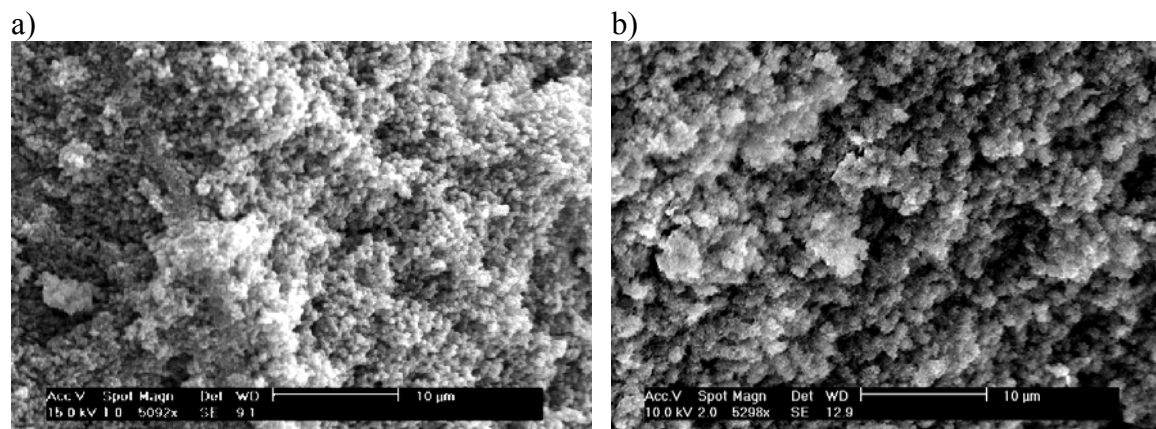


Figure IV.28: SEM micrographs of Aerocellulose prepared from molten 3%Solucell 1175-NMMO solution regenerated in water at ambient temperature with further exchange water→acetone (a) and water→ethanol (b), both at ambient temperature, and dried at CEP

We observe for both samples connected cellulose spheres, characteristic for the spinodal decomposition. It seems that the nature of the second bath does not influence much the morphology of final Aerocellulose. The most important step of Aerocellulose morphology formation is the first step of regeneration during which cellulose is coagulating, and the main parameters playing an important role in the formation of Aerocellulose structure are the bath nature and its temperature.

Conclusions

Aerocellulose is a new material that was made in the course of this PhD work. A lot of preparation parameters can be varied that influence or not the structural characteristics of the samples and their porosity. The study performed is a first step in the understanding of the correlation (preparation conditions)-Aerocellulose microstructure. Some trends that were observed are clear; some need further investigation. What can be said is that ultra porous and very light pure cellulose material, Aerocellulose, was obtained and we determined some correlations between the preparation conditions and the structural properties.

The microstructure of Aerocellulose was studied using porosimetry experiments such as nitrogen adsorption and mercury intrusion and the morphology of Aerocellulose samples was investigated using electron microscopy techniques: the scanning electron microscopy and the transmission electron microscopy.

The porosity is an open one with pores diameter varying from 2 nm to few hundreds of microns. The mean pore diameter is around 1 μm . The total porosity is higher than 90 % and density is around 0.1 g/cm^3 proving that Aerocellulose is a very light material. The specific surface is mainly due to the contribution of micropores and varies between 200 and 500 m^2/g . Almost all samples have a skin on the surface. This skin is created by the increase of cellulose concentration stimulated by rapid solvent depletion from the top layer of the sample.

The influence of various parameters was investigated. The following conclusions can be made:

- The gelation conditions of cellulose/NaOH/water solution have no influence on microstructural properties of Aerocellulose.
- Higher is cellulose concentration, lower is the pore radius.
- The type of cellulose pulp has very weak influence on the microstructure of Aerocellulose obtained from cellulose/NaOH/water gels, at least for the pulps studied: Avicel of DP 170, Solucell of DP 307 and Borregaard steam exploded of DP 500.
- The use of surfactant when preparing Aerocellulose from cellulose/NaOH/water gels decreases its density creating large macropores.
- The temperature of regenerating bath has a significant influence on the morphology and microstructure of Aerocellulose obtained from both routes, cellulose/NaOH/water gels and cellulose/NMMO solutions: the increase of temperature makes the structure cloudy, leads to density decrease and increases the specific surface.
- The nature of the regenerating bath liquid influences the microstructure of Aerocellulose. For example, for Aerocellulose obtained from NaOH route regenerated in acidic bath, it appears that higher is the acid concentration, lower is the diameter of pores. For Aerocellulose obtained from NMMO route regenerated in alcohol bath, higher is the molecular weight of the liquid, slower is the regeneration (obtained in Chapter 3) and more compact is the structure of the sample.
- The state of Aerocellulose precursor, i.e. a real solution or sample in a partly phase separated state, results in different Aerocellulose morphology. Connected cellulose sub-micron-size spheres appear when Aerocellulose is obtained from regenerated cellulose/NMMO solution; this is due to spinodal decomposition phase separation mechanism. A porous cellulose “network” with a wide pore size distribution is formed when Aerocellulose is obtained from the samples where a partial phase separation had already occurred: these are the cases of crystallised cellulose/NMMO solution or

gelled cellulose/NaOH/solution. The formation of large pores here are due to the quick removal of free solvent during regeneration (free NMMO crystals or NaOH/water solution); small pores are formed due to the second phase separation when solvent is completely detached from cellulose.

The microstructural properties of Aerocellulose sample obtained in different conditions are correlated to their mechanical properties in the next chapter.

References

[Biganska et al, 2002]	Biganska, O.; Navard, N.; Bedue, O.; Crystallisation of cellulose/N-methylmorpholine-N-oxide hydrate solutions Polymer, 43, (2002), pp 6139-6145
[Jin et al, 2004]	Jin, H.; Nishiyama, Y.; Wada, M.; Kuga, S.; Nanofibrillar cellulose aerogels Colloids and Surface A: Physicochemical Engineering., 240, (2004), pp 63-67
[Rouquerol et al, 1999]	Rouquerol, F.; Rouquerol, J.; K. Sing.; Adsorption by powders and porous solids Academic press, London, (1999)
[Yao et al, 2005]	Handbook of microscopy for nanotechnology Yao, N.; Wang, Z.L.; Kluwer academic Publishers, Boston, (2005)
[Web site 1]	http://www.steve.gb.com/science/electron_microscopy.html
[Fink et al , 2001]	Fink, H.; Weigel, P.; Purz, H.J.; Ganster, J.; Structure formation of regenerated cellulose materials from NMMO-solutions. Progress in Polymer Science, 26, (2001), pp 1473-1524

Chapter V: Mechanical properties of Aerocellulose

Introduction

Aerocellulose is a new type of ultra light cellulose material. It is not a conventional polymer foam, but is a special porous material with extremely high porosity on a micron scale. Because of its low density and cellular structure, Aerocellulose offers potential for energy adsorption in packaging. Their efficient use requires a detailed understanding of their mechanical behaviour and structure-properties relationships. The goal of this study is to determine the mechanical properties of Aerocellulose and to investigate the influence of various parameters of Aerocellulose preparation on its mechanical characteristics.

First part of this chapter gives a short bibliography on the mechanical properties of known porous materials: solid foams and aerogels. Second part presents the experimental results obtained from uniaxial compression tests performed on Aerocellulose prepared from NaOH and NMMO routes. From the compressive curves the mechanical characteristics as Young modulus, compressive yield strength and energy absorption were deduced. The influence of parameters of Aerocellulose preparation like cellulose concentration, pulp origin, bath regenerating temperature, influence of additives on the mechanical properties was investigated. Finally, the mechanical and microstructural relationships were studied using the deformation compressive models.

1 Bibliography: Mechanical properties of foams and aerogels

1.1 Mechanical properties of foams

A solid foam is a material which porosity exceeds typically 70% of total volume. It is an interconnected network of solid struts or plates that form the edge and the face of cells. The simplest cellular solid is the two-dimensional cellular solid with prismatic cells called honeycombs structure. More commonly three-dimensional cellular solid foams have a polyhedral structure.

If the material constituting the is contained in the cell edge only, the foam is said to be open-celled. If the solid material is distributed on the faces of the cells, the foam is said to be closed-celled.

In nature, cellular solid materials with a cellular structure are widespread. Examples of natural materials with prismatic, honeycomb-like cells include wood and cork (Figure V.1 a,b), while those with polyhedral cells are, for example, the inner core in plant stems and trabecular bone (Figure V.1 c,d).

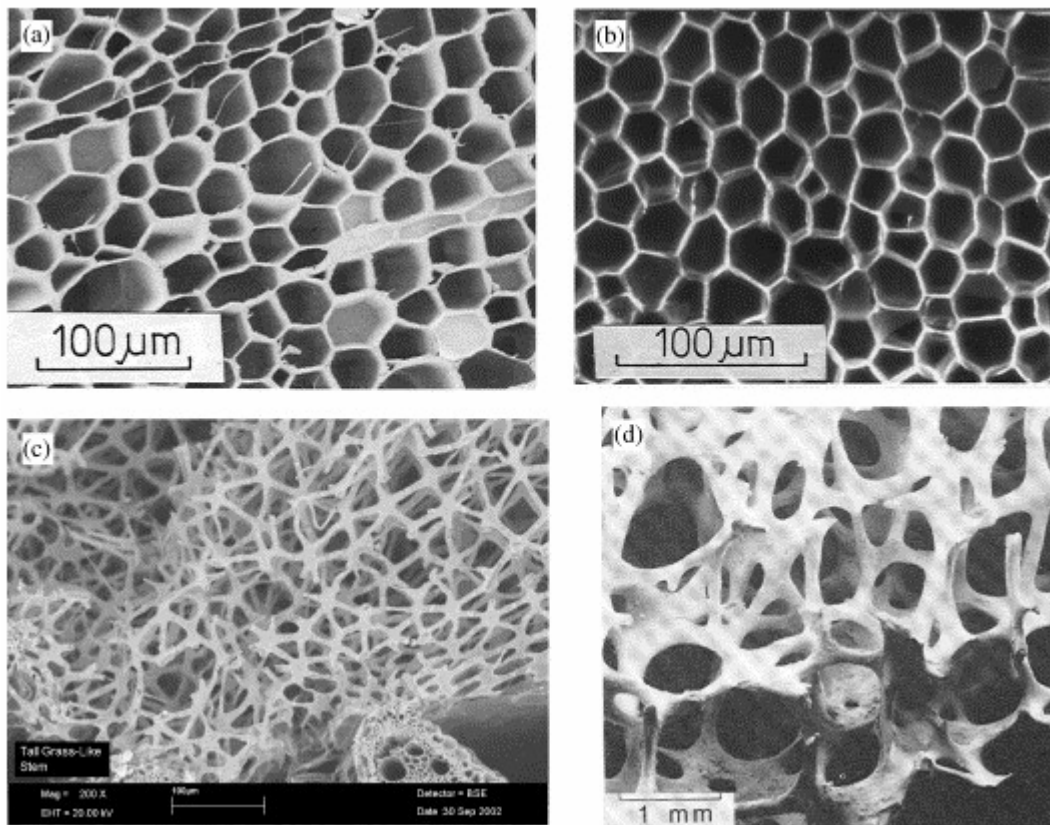


Figure V.1: Examples of cellular solids in nature: (a) balsa wood, (b) cork, (c) inner core of plant stem and (d) trabecular bone [Gibson, 2005]

An important feature of foam is its relative density, which is the density of the cellular solid ρ , divided by that of the solid it is made from, ρ_s , and is equivalent to the volume fraction of

solid. Higher is the wall thickness; higher is the density because the solid component of the foam occupies more space thereby shrinking the pore volume. Throughout this chapter, properties subscripted with “s” refer to the solid from which the foam is made (e.g. solid density: ρ_s); properties without the subscript “s” are those of the foam in total (foam density: ρ). Polymeric foams used for packaging and insulation have relative densities which are usually between 0.005 and 0.2, cork is about 0.15, and most of softwood are between 0.15 and 0.4. Commonly, cellular solids have a relative density lower than 0.3.

The mechanical properties of the foams are related to its structure and to the properties of the material of which the cell walls are made. The most important characteristics of the structure are the relative density ρ/ρ_s , the shape of the cell (isotropic or anisotropic) and the degree at which the cells are opened or closed.

Deformation mechanism in solid foams

Figure V.2 shows schematic compressive stress–strain curves for an elastomeric, an elastic-plastic and a brittle foam.

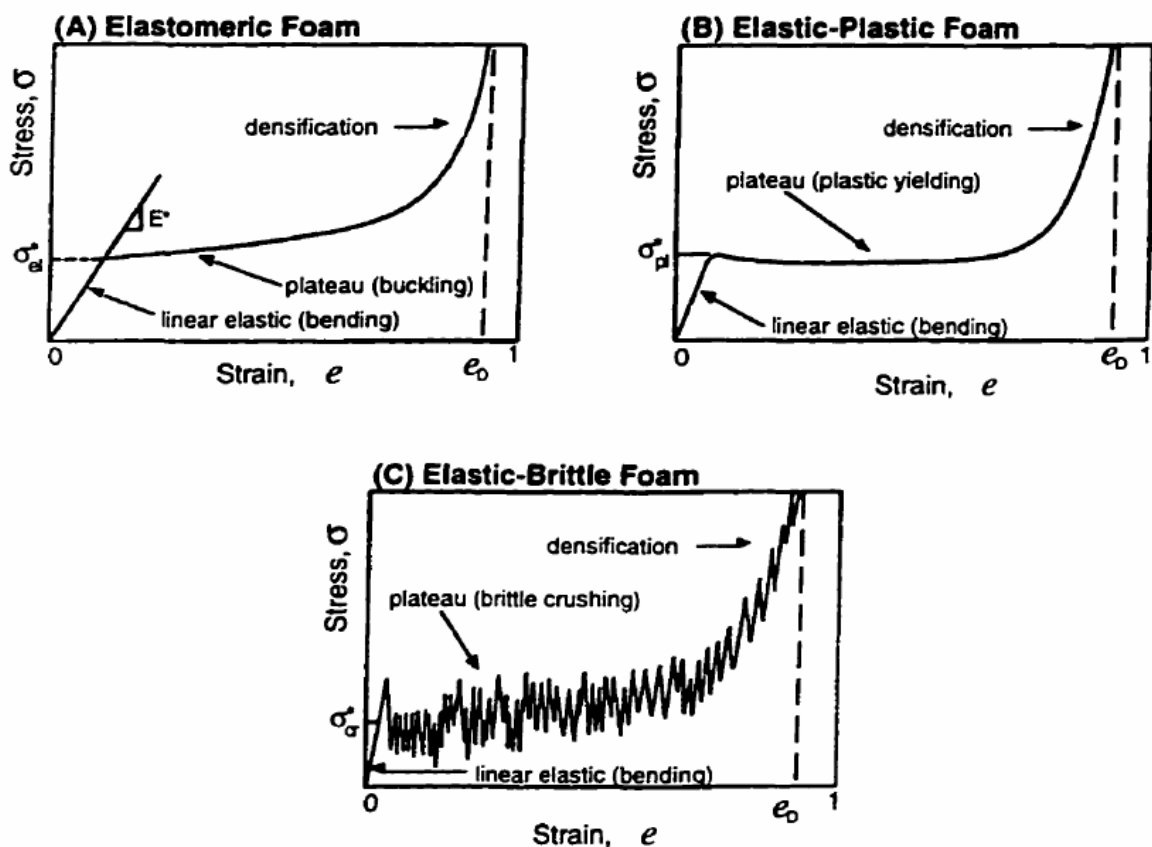


Figure V.2: Schematic uniaxial compressive stress–strain curves for (a) elastomeric foam, (b) elastic–plastic foam and (c) elastic-brittle foam [Gibson et al, 1997]

They are characterised by three regimes:

- A linear elastic regime at low stress, corresponding to cell edge bending. Young modulus, E , is the initial slope of the stress-strain curve.

- A stress plateau, corresponding to progressive cell collapse by elastic buckling, plastic yielding or brittle crushing, depending on the nature of the solid from which the foam is made.
- A densification regime, corresponding to the collapse of the cells throughout the material and subsequent loading of the cell edges and faces against one another. Many cellular materials have low relative densities (10–20%) so that they can be deformed up to large strains (70–80%) before densification occurs.

Elastomeric foam differs from plastic or brittle foam by the fact that at any deformation applied, the elastomeric foam is fully recoverable.

Theoretical relationships between the structure of cellular solids and their mechanical properties were published by Gibson and Ashby [Gibson et al, 1997].

Authors modelled open-cell foam as a cubic array of members of length l and square cross-section of side t (see Figure V.3), even if real cell shapes are more complex.

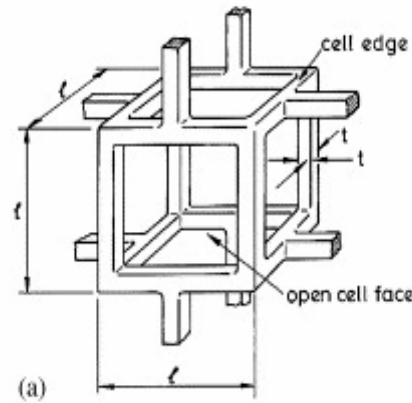


Figure V.3: A cubic model for an open-cell foam showing the edge length l , and the edge thickness t [Gibson et al, 1997].

The relative density of the foam is related to l and t by the following equation:

$$\frac{\rho}{\rho_s} = \left(\frac{t}{l}\right)^2 \quad (\text{V.1})$$

When a uniaxial stress is applied to the foam, each cell edge transmits a force F and edges bend (Figure V.4).

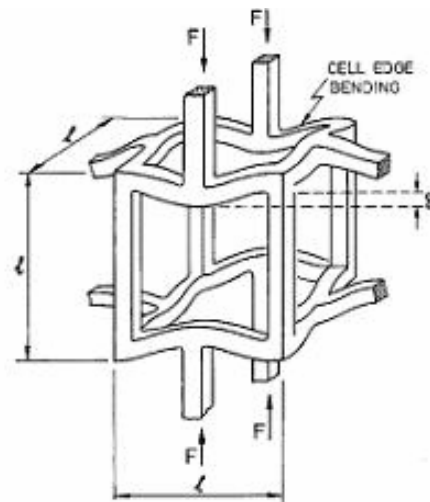


Figure V.4: Cell edge bending during linear elastic deformation [Gibson et al, 1997]

The Young modulus of the foam is given by equation:

$$\frac{E}{E_s} = C_1 * \left(\frac{\rho}{\rho_s} \right)^2 \quad (V.2)$$

Where:

E: Young Modulus of cellular solid

E_s: Young Modulus of dense solid

ρ: density of cellular solid

ρ_s: density of solid skeleton

C₁: constant depending on the microstructure of solid material. It is expected that the constant is close to unity, C₁~1.

Figure V.2 presents the three possible collapse mechanisms: buckling , yielding or crushing.

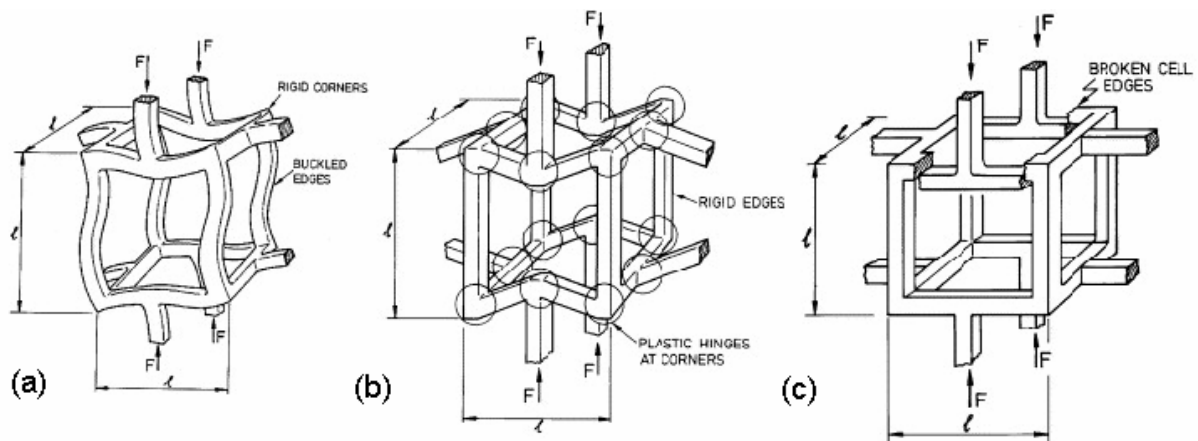


Figure V.5: Cell collapse by (a) elastic buckling, (b) plastic yielding, (c) brittle crushing [Gibson et al, 1997]

The stress at which elastic collapse stress occurs, σ_{el} , is given by the relation below:

$$\frac{\sigma_{el}}{E_s} = C_2 \left(\frac{\rho}{\rho_s} \right)^2 \quad (V.3)$$

Where:

σ_{el} : elastic collapse stress

C_2 : constant containing the constants of proportionality. It is expected that $C_2=0.05$.

In the case of plastic collapse, the plastic collapse stress, σ_{pl} is given by the relation V.4:

$$\frac{\sigma_{pl}}{\sigma_{y_s}} = C_3 \left(\frac{\rho}{\rho_s} \right)^2 \quad (V.4)$$

Where:

σ_{pl} : plastic collapse stress

σ_{y_s} : yield stress of dense material

C_3 : constant containing the constants of proportionality. It is expected that $C_3=0.3$

When a brittle foam is compressed, fracture of the edge happens at the brittle crushing stress σ_{cr} . The brittle crushing stress, σ_{cr} is given by the following relation:

$$\frac{\sigma_{cr}}{\sigma_{f_s}} = C_4 \left(\frac{\rho}{\rho_s} \right)^{3/2} \quad (V.5)$$

Where:

σ_{cr} : crushing stress,

σ_{f_s} : fracture strength of the dense material;

C_4 : constant containing the constants of proportionality. It is expected that $C_4=0.65$

In order to position Aerocellulose that is a new type of foam among other materials, the mechanical characteristics of various polymeric foams with the same low density were considered. Table V.1 presents different mechanical properties of these polymeric foams taken from literature, together with their density, Young modulus and compression strength.

[Reference]	[Saha et al, 2005]	[Thompson et al, 2003]	[Beverte, 2004]	[Zhou et al, 2005]
Material	PVC	PU	Polypropylene	Starch
Density (g/cm ³)	0.075	0.12	0.08	0.06
Relative density (g/cm ³)	0.06	0.1	0.09	0.04
Density of solid material (g/cm ³)	1.4	1.2	0.9	1.5
Young modulus (MPa)	38	22	29	0.022
Young modulus of solid material (MPa)	2400	2700	1130	30
Compression strength (MPa)	1.1	0.85	/	0.16

Table V.1: Polymeric foams and their mechanical properties

1.2 Mechanical properties of aerogels

Aerogels are a special class of ultra fine cell size (nanoporous), low-density foams. These materials have continuous porosity and a microstructure composed of interconnected colloidal-like particles or chains. Owing to their large pore volume, their strength properties are very low (less than 1MPa). Aerogels are fragile and brittle material like glasses or ceramics.

Scherer et al [Scherer et al, 1995] used mercury porosimetry to compress SiO₂ aerogel sample hydrostatically and used it as a mean to determine mechanical characteristics of aerogels. The shrinkage of aerogel under mercury pressure follows a buckling mechanism which links the pore size to the exerted pressure. Three distinct regions were noted on a pressure volume curve. For small increases in pressure, the volume of aerogel decreased in a linear way. As pressure was increased beyond a yield point, the aerogel began to deform plastically. Still greater increase in pressure caused the material to harden such the bulk modulus K changed with volume according to a power-law relationship:

$$K(V) = K_0 (V_0/V)^m \quad (V.6)$$

where K_0 and V_0 are the bulk modulus and sample volume at the point where the compression curve changes to upward concavity. Given the proportionality $K = E/3(1-2\nu)$ in which ν is the Poisson's ratio and assuming the independence of ν on the density, the scaling law applied to

E can also be applied to K with the same exponent m . They found that the bulk modulus of silica aerogels has a power-law dependence on density with an exponent of ~ 3.2 .

Gibson and Ashby [Gibson et al, 1997] proposed an open-cell foam model which predicts $m=2$. It has been known for over a decade (see Table V.2) that aerogels exhibit a scaling relationship of the mechanical properties (relative Young modulus and relative compressive strength) against relative density, ρ :

$$E \sim \rho^m, \sigma \sim \rho^n \quad (\text{V.7})$$

where m and n are the scaling exponents

Table V.2 illustrates some of the scaling exponents found for different aerogels and polymeric foams.

Material	Density (g/cm ³)	m	n	Reference
Silica aerogel	0.07-0.5	3.7 \pm 0.2	2.6 \pm 0.3	[Woignier et al, 1998]
Silica aerogel	0.035-0.188	3.05 \pm 0.05	/	[Pirard et al, 1996]
Silica aerogel	0.08-0.24	3.0 \pm 0.2	/	[Moner-Girona et al, 2001]
Resorcinol-Formaldehyde aerogel	0.04-0.3	2.7 \pm 0.2	2.4 \pm 0.3	[Pekala et al, 1990]
Starch foam	0.04-0.13	2.7	2.3	[Zhou et al, 2005]
PVC foam	0.075-0.3	/	1.4	[Saha et al, 2005]
PU foam	0.12-0.32	1.9	1.7	[Thompson et al, 2003]

Table V.2: Reported values of exponents m and n in equations (V.7) for different materials

Apparently, many aerogels exhibit much higher exponent than solid foam. A few attempts have been made to explain the higher than predicted scaling exponent from the aerogel structural features. The deviation of aerogels from the prediction developed for foams has been attributed to the abundance of dangling branches in the aerogel network. These dangling mass are clusters connected to the backbone of the aerogel network at only one point. These branches hang off the main skeleton of the network and do not bear the load and therefore the exponent is raising above 2.

According to Pirard et al [Pirard et al, 1996], a monodisperse distribution of pore size is not a realistic way of modelling aerogel. Aerogels are known to have a large range of pore size from 1nm to 1 μ m and thus require to be visualised by a sequence of cell size, L , variable from stage to stage. When a pressure P_n is applied to an aerogel during the mercury compression,

all pores with size above corresponding L_n , collapse and according to the buckling mechanism their volume reduces to zero. Authors proposed a mechanism based on the preferential buckling of the network around the large pores and relate m to the pore volume distribution. They found by this method m exponent value for silica aerogel equal to 3.05 ± 0.05 .

Ma et al [Ma et al, 2000] examined by the finite element method (FEM) the elastic properties of aerogels. Their simulation yields $m \sim 3.6$ for perfectly connected structure. These results suggest that the high exponent is largely because of the reduction in the connectivity of the material with decreasing density. Authors described the mechanical structure-property relationship in the aerogel by the “blob-and-link” model. The bonds (links) between the fractal clusters (blobs) are more sparsely distributed than those inside the clusters and therefore the strain energy is localised at the cluster boundaries during deformation.

In the aerogel model, only a small fraction of the bonds bears the strain energy when the network is deformed. Computer simulation of aerogel deformation shows that most of the stress is localised to the tenuous chains of particles connected in the fractal clusters, leaving the rigid blobs unload. In addition, fewer and fewer bonds are sharing the strain energy when the density decreases. This explains why the modulus of an aerogel drops sharply with decreasing density [Ma et al, 2001].

Mechanical compression tests were performed on Aerocellulose in order to determine the m and n scaling exponents and to determine if Aerocellulose mechanically behaves like a solid foam or aerogel.

2 Material and Methods

2.1 Materials

2.1.1 Aerocellulose from NaOH route

Cellulose-NaOH-water Aerocelluloses were prepared as described in section II.1.1. Different types of native cellulose pulp were used: microcrystalline cellulose Avicel, fibrous Solucell and steam exploded Borregaard, with DP values of 170, 307 and 500 respectively. Each pulp is described in section II.1.1. In order to have different densities of Aerocellulose three cellulose concentrations were studied: 5, 6 and 7 g in 100 g solution.

In order to lighten the final material, the surfactant Simulsol SL8 manufactured by Seppic, Inc., Fairfield, United-States was used at various concentrations: 0.1%, 0.5% and 1%. The preparation of this type of sample is described in section IV.1.1.2.

In order to reinforce Aerocellulose, fluff wood fibres, with DP value 1100, was added to cellulose-NaOH-water solution at 1 and 2 % concentration in weight of the total solution. The mixture was stirred for 5 minutes at 1000 revolution per minute at 5°C.

All cellulose solutions were poured in cylindrical mould and gelled at 50°C during 2hours. Then cylindrical cellulose gels were regenerated in distilled water.

The influence of water temperature on the mechanical properties of Aerocellulose was also investigated. Cellulose gels were regenerated in water at either 25°C or 50°C.

After the regeneration in water, water was exchanged with acetone. Finally, swollen cellulose in acetone were dried in CO₂ in supercritical conditions in CEP, Ecole des Mines, France or in Natex, Austria.

2.1.2 Aerocellulose from NMMO route

In case of NMMO route, the preparation and the regeneration of the cellulose-NMMO-water solutions was performed in the R&D laboratory of Lenzing AG, Austria. Three types of cellulose were used: Solucell 1175 (DP 950), Cotton Linter (DP 950) and Kappa (DP 1330) with cellulose concentration from 2% to 8%.

Cellulose-NMMO-water solutions were poured into cylindrical mould, cooled down to room temperature and, as a result, solid cylindrical samples were obtained. They were then immersed into water at ambient temperature. Water was exchanged with acetone of analytical grade. Cellulose samples were dried in CO₂ in supercritical conditions in Natex, Austria.

Since the mechanical properties were expected to be strongly dependent on the density, each Aerocellulose from NaOH and NMMO routes was weighted using an electronic balance and measured dimensionally using electronic callipers. Cylinder specimens prepared have proportion such as length/diameter = 1.5. The density varies from 0.05 g/cm³ to 0.26 g/cm³.

The density of the samples varies depending on supercritical drying conditions performed in Natex.

2.2 Methods

The universal testing machine, Dartec Testwell was used for the uniaxial compression tests and the designed software Workshop96 Dartec was used to record displacement and loading results. The compressive machine was equipped with a 50 kN load cell.

The specimens were inserted between two steel circular compression platens of the servo-hydraulic testing machine. The parallelism between the two platens was carefully adjusted through examination of the contact surface before the compression test. A displacement rate of 0.1 mm/s was applied on the top surface of each specimen as an external loading. Displacement rates from 0.1 to 10 mm.s⁻¹ were applied to study the influence of rate displacement on Aerocellulose mechanical properties. All specimens were loaded up to 70% of the deformation to obtain the whole compressive behaviour.

All measurements were made under ambient condition at about 20-22°C and 50-60% relative humidity.

3 Results and discussion: mechanical properties of Aerocellulose and influence of the preparation parameters

3.1 Examples of Aerocellulose mechanical properties

A series of photographs were taken during a compression test to observe the behaviour of Aerocellulose under compression on the Aerocellulose prepared from 5Avicel/7.6NaOH/water gel.

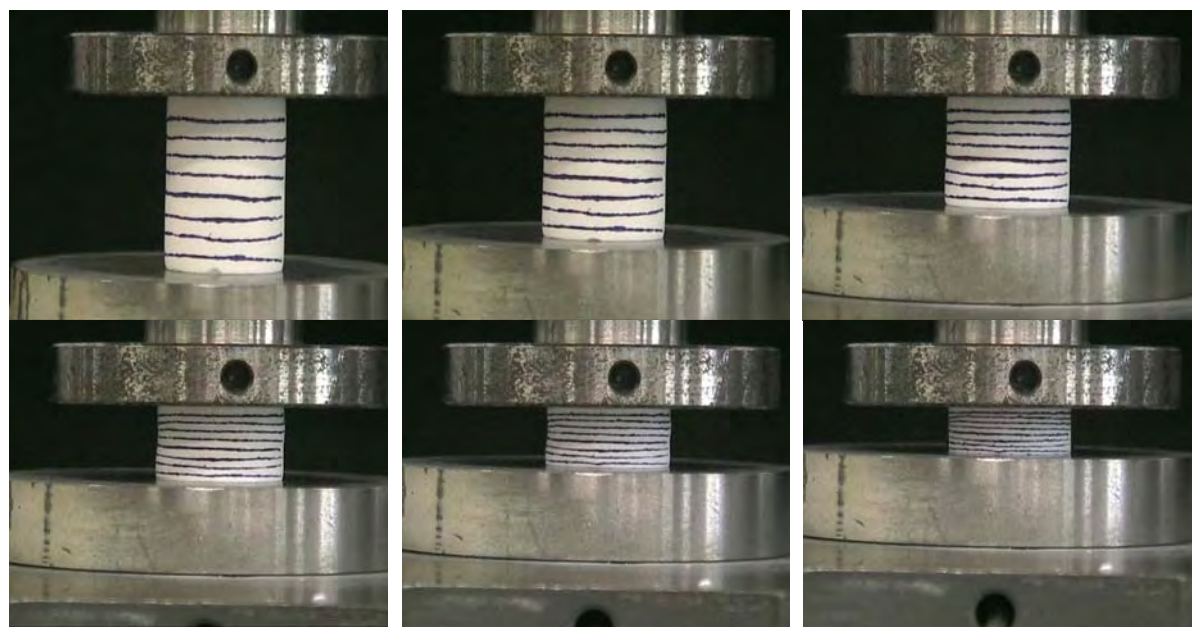


Figure V.6: Photographs taken at regular time interval (beginning at upper left) during compression test of Aerocellulose prepared from 5Avicel/7.6NaOH/water gel regenerated in water bath at 25°C, water exchanged by acetone, dried in CEP, with lines drawn to evaluate the deformation.

From the pictures we see that the compression is uniform and that the cross-section area does not change. These photos suggest that Aerocellulose compresses uniformly under loading.

As the cross-sectional area of the cylindrical Aerocellulose sample does not change significantly during compression, the stress $\sigma(t)$ (N/m²) is equal to the force $F(t)$ (N) per unit of the initial cross-sectional area A_0 (m²):

$$\sigma(t) = \frac{F(t)}{A_0} \quad (\text{V.8})$$

The deformation, ε , is defined as:

$$\varepsilon = \frac{h_0 - h(t)}{h_0} \quad (\text{V.9})$$

where h_0 and $h(t)$ are the initial height and the height at time t of Aerocellulose sample compressed.

Figure V.7 shows a typical uniaxial compression stress–strain curve obtained for Aerocellulose from 5Avicel/7.6NaOH/water solution gelled at 50°C for two hours, then regenerated in water at 25°C, further solvent exchange water→acetone and then dried in CO₂ in supercritical conditions in CEP. The stress is the force applied divided by the initial cross-section area, and the strain is the thickness variation of the specimen divided by the initial thickness.

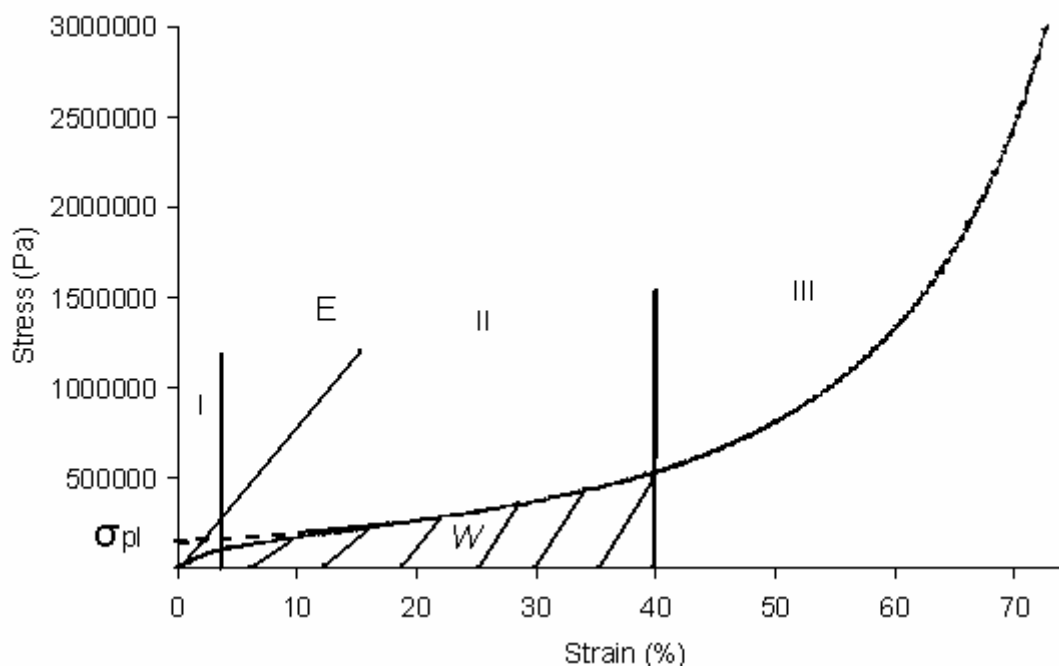


Figure V.7: Stress/strain curve for Aerocellulose made from 5Avicel/7.6NaOH/water gel as in Figure V.6

For each individual curve, three different regions can be identified (cf. Figure V.6). The first region at low stress ($< 2\%$) (I) is characterised by almost linear elastic behaviour. The region ends when the material starts to yield and reaches its compressive yield strength, σ_{pl} . The second region (II) of the compression curve is characterised by relatively horizontal plateau. The plateau region corresponds to the formation of local bands that multiply or propagate over the entire sample, up to the collapse of cell walls. This plateau region enables foams to absorb large amount of energy, W , without experiencing a large increase in stress. The third region (III) is characterised by a steep increase in the load–displacement curve corresponding to material densification. The cell walls come in contact one with another, causing an abrupt rise of stress.

From these compressive curves we can deduce the main mechanical characteristics: the Young modulus, the compressive yield strength (cf Figure V.7) and the energy of absorption.

The Young modulus was calculated from the linear elastic part of the stress-strain curve:

$$E = \left(\frac{\delta\sigma}{\delta\varepsilon} \right)_{\varepsilon \rightarrow 0} \quad (\text{V.10})$$

The plateau stress is determined by linear extrapolation of the initial linear increase in stress (region I) and of the plateau region (region II) of the compressive strain-rates curves (cf Figure V.6).

Finally, the energy absorption, W (J/m^3), is defined as the area under the stress-strain curve $S(x)$ up to any desired strain x .

$$W = \int S(x).dx \quad (\text{V.11})$$

Little energy is absorbed in the short linear elastic region; meanwhile the long plateau region allows large energy absorption. The level of this plateau depends on the material and the density of the foam. The energy absorption during the plastic deformation was obtained using the integration of the area under load-displacement curve up to 40% strain and was noted $W_{40\%}$.

The same types of curves were acquired for Aerocellulose obtained from NMMO route. Figure V.8 shows typical stress-strain curve for Aerocellulose from 8% Solucell 1175/NMMO/water solution regenerated in water at ambient temperature with further water → acetone exchange and dried in CO_2 supercritical conditions in Natex compared to the stress strain curve of Aerocellulose from 5Avicel/7.6NaOH/water gel presented in Figure V.7.

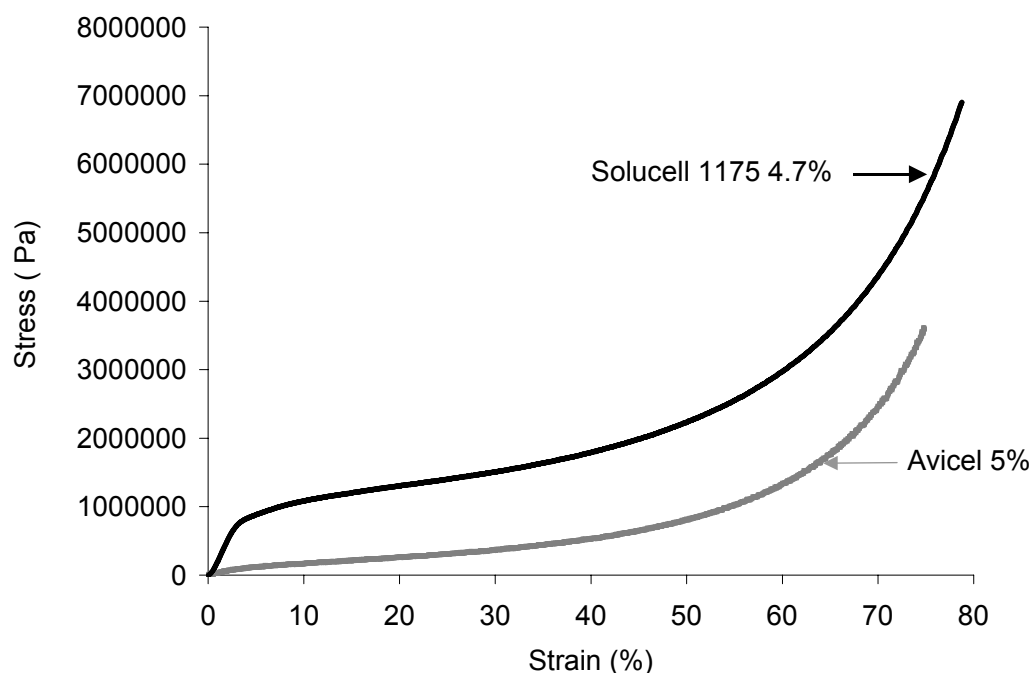


Figure V.8: Comparison of stress/strain curves for Aerocellulose made from 4.7% Solucell 1175/NMMO solution regenerated in water at ambient temperature with further water→acetone exchange and dried in Natex and made from 5Avicel/7.6NaOH/water gel as in Figure V.8

The stress-strain curves for Aerocellulose from NMMO route display the same behaviour than the curve obtained for Aerocellulose from NaOH route compression. Initial linear elasticity regime is followed by a plateau that corresponds to the breaking of the walls of the pores. The final stage of the curve in which the stress rises sharply corresponds to material densification. We can observe difference between the two routes of Aerocellulose preparation. The influence of pulp will be discussed in section III.4.

3.2 Effect of the displacement rate

Compressive experiments were performed at different displacement rates: $0.1\text{mm}\cdot\text{s}^{-1}$, $1\text{mm}\cdot\text{s}^{-1}$ and $10\text{mm}\cdot\text{s}^{-1}$, on Aerocellulose obtained from 6Avicel/7.6NaOH/water gels, regenerated in water at 25°C , with further exchange water-acetone and dried in Natex. Samples obtained have an average density of 0.19 g/cm^3 . This high density shows that a densification of the material probably occurs during supercritical drying. The resultant compressive stress-strain curves are shown in Figure V.9.

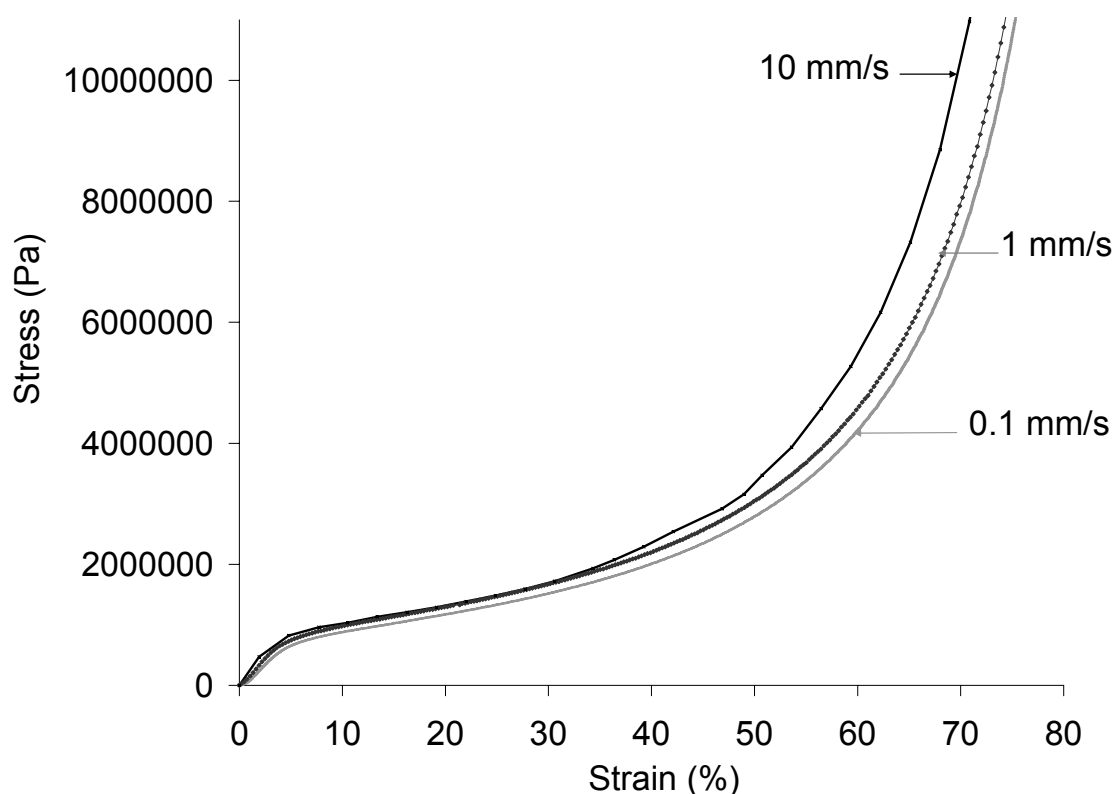


Figure V.9: Stress/strain curves for Aerocelluloses obtained from 6Avicel/7.6NaOH/water gel, regenerated in water at ambient temperature, with further water→acetone exchange and dried in Natex at various displacement rates

The stress-strain response of Aerocellulose at different displacement rates ($0.1-10\text{mm}\cdot\text{s}^{-1}$) shows a similar initial behaviour. Young modulus is of $17.4\text{ MPa} \pm 10\%$ and compressive yield strength is of $710000\text{ Pa} \pm 10\%$. When the densification of the material starts, in the third region, differences between the curves appear. This indicates that cell collapse increases and hence the energy absorption, which corresponds to the area under the stress-strain curve. This stress-strain measurement shows the slight dependence on the displacement rate. It is probable that Aerocellulose at higher displacement rates will absorb more energy. In the following all compressive test are performed at low displacement rate $0.1\text{mm}\cdot\text{s}^{-1}$ in order not to take into account the displacement rate effect.

3.3 Influence of cellulose concentration

Figure V.10 presents the compressive curves for Aerocellulose obtained from Avicel/7.6NaOH/water gels at various cellulose concentrations: 5, 6 or 7g, regenerated in water bath of 25°C , water exchanged by acetone and dried in CEP.

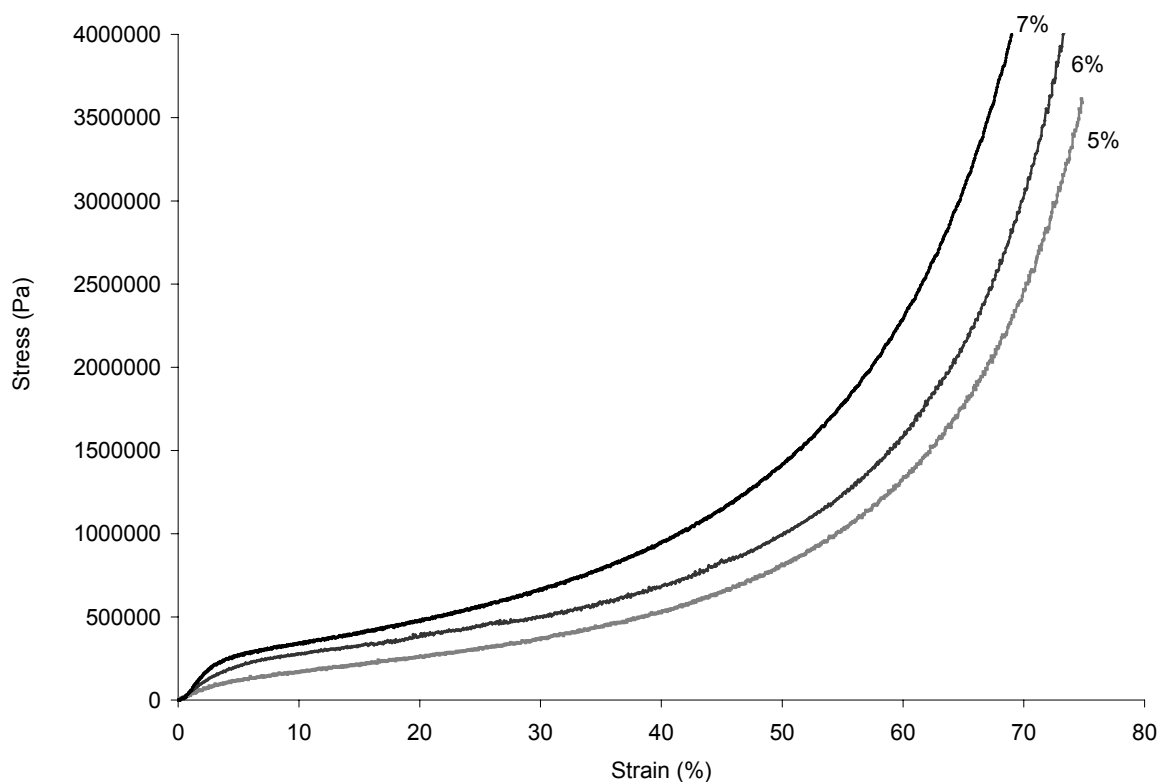


Figure V.10: Compressive curves for Aerocelluloses obtained from XAvicel/7.6NaOH/water gels with X=5, 6 or 7, regenerated in water bath of 25°C, water exchanged by acetone, dried in CEP

The compressive curves have the same profile, which is characteristic of porous materials with three separate regions: elasticity region at low deformation, plateau region followed by a densification of the material. As cellulose concentration and thus foam density increases, the stress plateau is extended and thus the strain at which densification started decreases whereas Young modulus and the plateau stress increases. The obtained average Young modulus and compressive yield strength are given in Table V.3.

Aerocelluloses obtained from XAvicel/7.6NaOH/water gels			
Cellulose concentration X (g)	5	6	7
Density (g/cm ³)	0.08	0.1	0.14
Young modulus (Pa)	2.7 10 ⁶	5.3 10 ⁶	9.2 10 ⁶
Yield strength (Pa)	1.2 10 ⁵	2.2 10 ⁵	2.6 10 ⁵
Energy absorption at 40% strain (kJ/m ³)	110	150	185

Table V.3: Young modulus, yield strength and energy absorption for Aerocelluloses obtained from NaOH route for different cellulose concentrations

As expected, higher cellulose concentration, higher Young modulus, yield strength and energy absorption. As it was seen in section IV.2.3, Aerocellulose with a higher cellulose concentration tends to have a lower pore size. It appears that denser Aerocellulose is able to better resist than lower density samples with higher pore size showing that the biggest pores are the first responsible of Aerocellulose collapse.

The influence of cellulose concentration was also investigated for Aerocellulose obtained from NMMO route. Figure V.11 shows the compressive curve obtained for Solucell 1175/NMMO/water solution, with cellulose concentration varying from 2 to 8%, regenerated in water at ambient temperature, with further water→acetone exchange and dried in Natex.

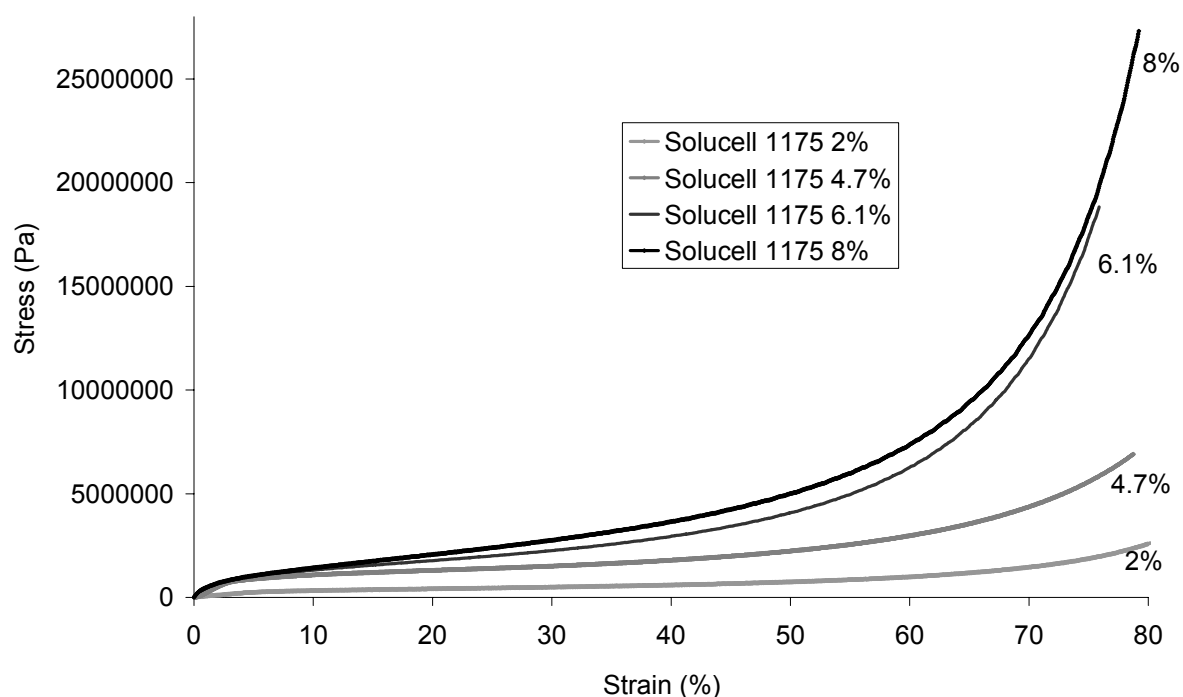


Figure V.11: Stress/strain curve for Aerocelluloses made from X Solucell 1175/NMMO solutions with X=2, 4.7, 6.1 or 8%, regenerated in water at ambient temperature with further water → acetone exchange and dried in Natex

We observe the same behaviour of compressive curve as the one obtained for Aerocellulose from NaOH route: the higher the cellulose concentration is, the higher the plateau level is but the shorter the stress plateau is. Table V.4 summarises the mechanical characteristics of the Aerocellulose obtained from NMMO route.

Aerocelluloses obtained from X Solucell 1175/NMMO/water solutions				
Cellulose concentration X (%)	2	4.7	6.1	8
Density (g/cm ³)	0.06	0.18	0.21	0.245
Young modulus (Pa)	4.8 10 ⁶	2.9 10 ⁷	4.10 ⁷	5.5 10 ⁷
Yield strength (Pa)	2.5 10 ⁵	8.5 10 ⁵	9.10 ⁵	9.2 10 ⁵
Energy absorption at 40% strain (kJ/m ³)	162	501	685	740

Table V.4: Young modulus, yield strength and absorbed energy for Aerocelluloses obtained from NMMO route as a function of cellulose concentration.

The mechanical properties of Aerocelluloses obtained from NMMO route are higher than the ones obtained for Aerocelluloses from NaOH route. This could be explained either by the difference of degree of polymerisation of pulp ($DP_{Avicel} = 180$, $DP_{Solucell} = 950$) or by the different route of preparation. However the second assumption is not valid because as it was mentioned in section I.V2.6.1.2, both NMMO and NaOH routes leads to the same type of morphology. Both routes are going first through the first phase separation before regeneration (gelation in NaOH route and crystallisation in NMMO route) and then final phase separation during regeneration. Aerocelluloses obtained from NMMO and NaOH routes have a Gaussian size distribution and their pores sizes are a few hundreds of nanometres. The influence of structure on mechanical properties will be discussed in section V.3.7.

3.4 Influence of pulp properties

The influence of cellulose pulp type on mechanical properties of Aerocellulose obtained from NaOH route was investigated. Figure V.12 shows compressive curves obtained for Aerocellulose prepared from different cellulose pulp: Avicel, Solucell and Borregaard with DP 180, 307 and 500, respectively, and with the same cellulose concentration: 7g for 100g solution.

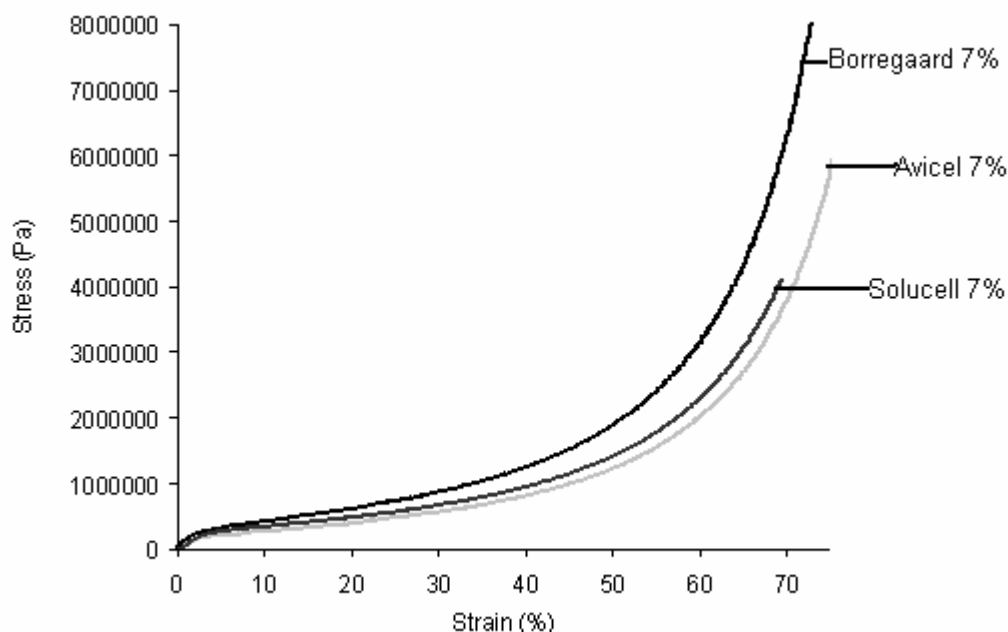


Figure V.12: Compressive curves for Aerocelluloses obtained from 7cellulose/7.6NaOH/water gels from different cellulose pulps, regenerated in water bath of 25°C, water exchanged by acetone, dried in CEP

The obtained average Young modulus and compressive yield strength are given in Table V.5.

Cellulose pulp	Avicel DP 180	Solucell DP 307	Borregaard DP 500
Density (g/cm ³)	0.14	0.145	0.16
Young modulus (Pa)	9.2 10 ⁶	1.22 10 ⁷	1.45 10 ⁷
Yield strength (Pa)	2.6 10 ⁵	2.9 10 ⁵	3.3 10 ⁵
Energy absorption at 40% strain (kJ/m ³)	185	220	310

Table V.5: Mechanical characteristics of Aerocelluloses obtained from 7cellulose/7.6NaOH/water regenerated in water at 25°C, water exchanged by acetone, dried in Natex, for different types of pulp.

There is a slight influence of pulp type on mechanical properties of Aerocellulose obtained from NaOH route that can be attributed to the difference in DP: higher the DP of the pulp is, higher the Young modulus and the compressive strength are.

Similar experiments were performed for Aerocelluloses obtained from NMMO route. The pulps were Solucell 1175, cotton linter and Kappa with DP 950, 950 and 1330, respectively, and with the same cellulose concentration: 2% (Table V.6).

Cellulose pulp	Cotton linter DP 950	Solucell 1175 DP 950	Kappa DP 1330
Density (g/cm ³)	0.06	0.06	0.052
Young modulus (Pa)	5.4 10 ⁶	4.8 10 ⁶	1.12 10 ⁷
Yield strength (Pa)	1.8 10 ⁵	2.5 10 ⁵	1.9 10 ⁵
Energy absorption at 40% strain (kJ/m ³)	120	162	94

Table V.6: Mechanical characteristics of Aerocelluloses obtained from 2cellulose/NMMO/water regenerated in water at 25°C, water exchanged by acetone, dried in Natex, for different types of pulp

It appears that Aerocelluloses obtained from cotton linter and Solucell 1175 pulps with the same DP 950 have almost the same Young modulus. At low stress, in the linear region, the Young modulus of Aerocellulose obtained from Kappa sample is higher than the one obtained from cotton linter or Solucell. However, Aerocelluloses obtained from Solucell have a higher plateau level and thus adsorb more energy than the two others Aerocelluloses tested.

3.5 Influence of additives

3.5.1 Influence of surfactant concentration

In order to lighten Aerocellulose material, the surfactant Simulsol SL8 was added at various concentrations: 0.1%, 0.5% and 1% in weight to 5Avicel/7.6NaOH/water solution. The gels obtained after 2 hours gelation at 50°C were regenerated in water at ambient temperature, water was exchanged by acetone and samples were supercritical dried in CEP. The compressive curves obtained for each Aerocellulose type with different surfactant concentrations are presented below (Figure V.13):

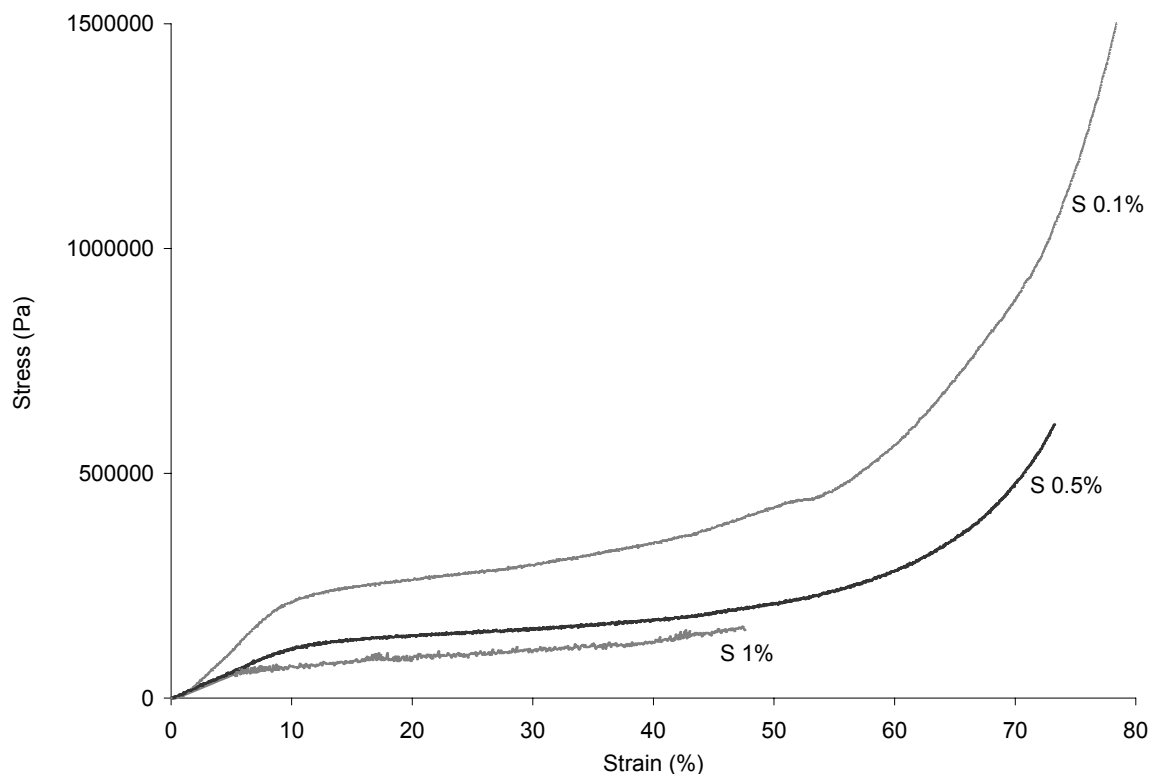


Figure V.13: Compressive curves for Aerocelluloses obtained from 5Avicel/7.6NaOH/water gels with surfactant, S, at various concentration: 0.1, 0.5 and 1%, regenerated in water bath at 25°C, water exchanged by acetone, dried in CEP

It appears that the higher the surfactant concentration is the more brittle is Aerocellulose. Aerocellulose obtained from 1% Simulsol/5Avicel/7.6NaOH/water solution fracture at a strain rate of 48%. Table V.7 presents mechanical properties as a function of surfactant concentration.

Simulsol concentration	0%	0.1%	0.5%	1%
Density (g/cm ³)	0.08	0.09	0.078	0.066
Young modulus (Pa)	2.7 10 ⁶	2.4 10 ⁶	1.5 10 ⁶	1.1 10 ⁶
Yield strength (Pa)	1.2 10 ⁵	2.1 10 ⁵	1.2 10 ⁵	6 10 ⁴
Energy absorption at 40% strain (kJ/m ³)	110	90	50	30

Table V.7: Mechanical characteristics of Aerocelluloses obtained from 5Avicel/7.6NaOH/water regenerated in water at 25°C, water exchanged by acetone, dried in CEP, for different Simulsol concentrations

We observe that more the surfactant concentration increases, more the mechanical properties of Aerocellulose (Young modulus, compressive strength and energy absorption) decrease. Figure V.14 compares the mechanical and the microstructural characteristics obtained from mercury porosimetry measurements (cf Table IV.4), which were provided by FhG-IAP for these Aerocelluloses

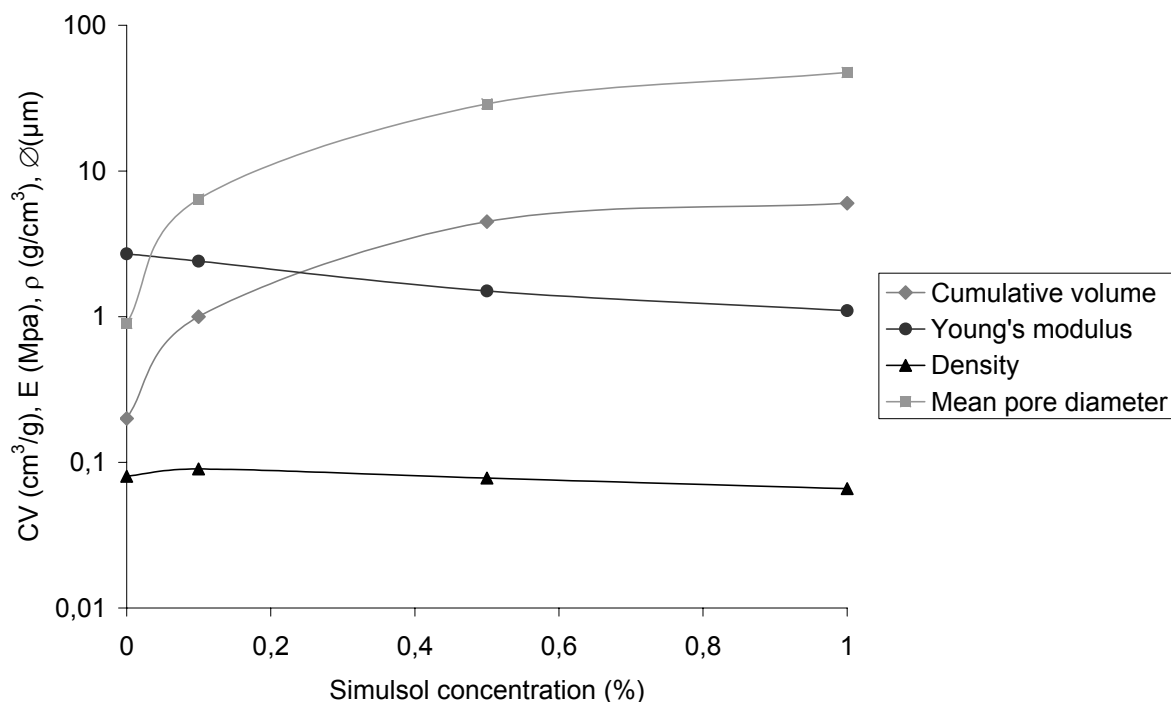


Figure V.14: Mechanical and microstructural properties of Aerocelluloses versus the Simulsol surfactant concentration

As it was shown in section IV.2.5, higher the surfactant concentration is, higher is the cumulative volume. This cumulative volume increase corresponds to an increase of the pore size of macropores created by air bubbles in the material structure. As there are more macropores and thus more air in the material, the density decreases and the material is enlightened. In fact the more Aerocellulose contain air the more brittle the material is. Thus, as expected, the addition of surfactant leads to a drop of Aerocellulose mechanical properties and a brittleness of the material.

3.5.2 Influence of fibres addition: attempts to reinforce Aerocellulose

In order to improve the mechanical properties of Aerocellulose, fluff fibres were added at 1 and 2% in weight concentration to 5Avicel/7.6NaOH/water solution. Solutions with fibres were gelled 2 hours at 50°C. Gels formed were regenerated in water at ambient temperature, water was exchanged by acetone and samples were supercritically dried in Natex. The compressive curves obtained for each Aerocellulose type with different fluff concentration are presented in Figure V.15:

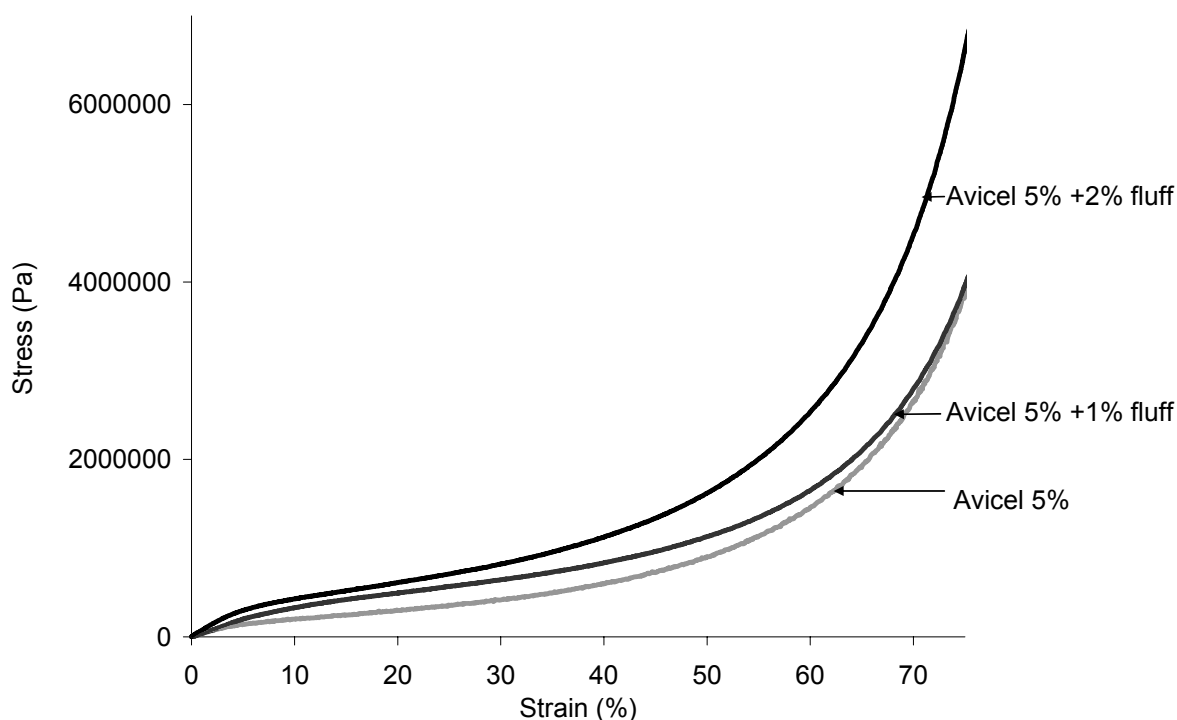


Figure V.15: Stress-strain curves for Aerocelluloses obtained from 5Avicel/7.6NaOH/water gels with fluff at various concentrations: 0, 1 and 2 %, regenerated in water bath at 25°C, water exchanged by acetone, dried in Natex.

When the fluff fibres are added, both collapse stress and plateau level increase. However, the difference between samples with 1 or 2% of fibres added is rather small. Table V.8 summarises the mechanical characteristics of these Aerocellulose samples.

Fluff fibres concentration	0%	1%	2%
Density (g/cm ³)	0.08	0.156	0.16
Young modulus (Pa)	$2.7 \cdot 10^6$	$4.4 \cdot 10^6$	$7.5 \cdot 10^6$
Yield strength (Pa)	$1.2 \cdot 10^5$	$2.5 \cdot 10^5$	$3 \cdot 10^5$
Energy absorption at 40% strain (kJ/m ³)	110	190	230

Table V.8: Mechanical characteristics of Aerocelluloses obtained from 5Avicel/7.6NaOH/water, regenerated in water at 25°C, water exchanged by acetone, dried in Natex

It appears that Young modulus; compressive strength and energy absorption are higher with fluff fibres addition. Thus fibres reinforcing increase the capabilities of load bearing and energy absorption during compression of materials, improving the mechanical properties of Aerocellulose. More rigid porous material can be produced which is able to absorb higher

impact energy and hence could be suitable for protecting heavy goods. More studies are needed to conclude on the optimal fibre concentration.

3.6 Influence of water regenerating bath temperature

The impact of water bath temperature on mechanical properties was tested on Aerocellulose obtained from NaOH route. Figure V.16 shows the typical stress-strain curve obtained for Aerocelluloses obtained from 5Avicel/7.6NaOH/water gels regenerated in water at 25 and 50°C, further solvent exchange water→acetone and then dried in CO₂ in supercritical conditions in CEP.

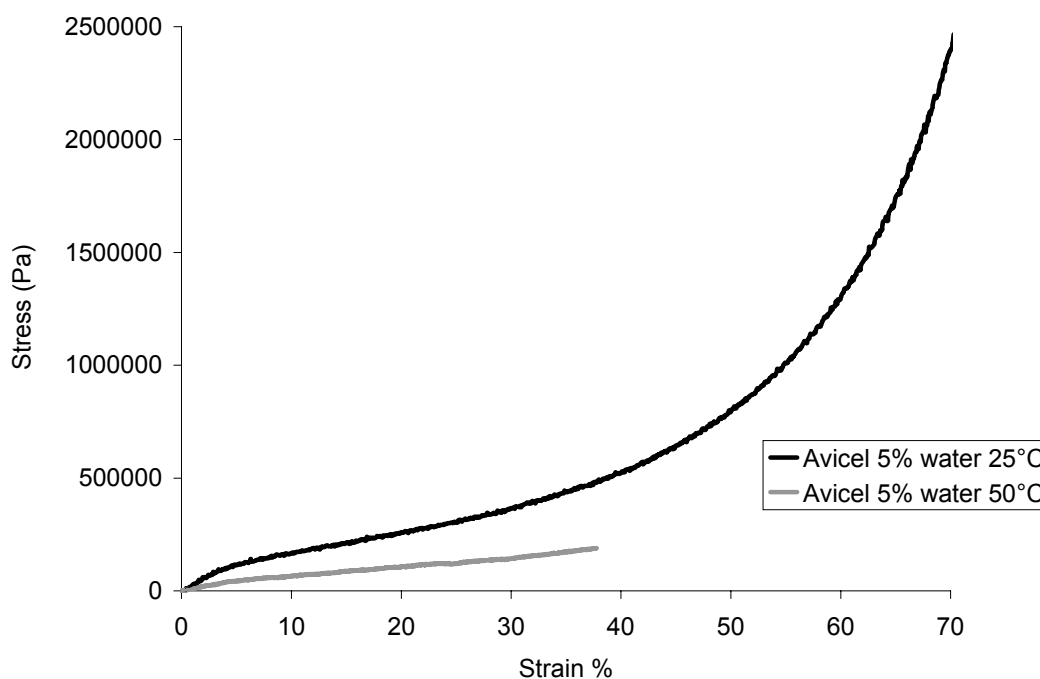


Figure V.16: Compressive curves for Aerocelluloses obtained from 5Avicel/7.6NaOH/water gels, regenerated in water bath at 25 or 50°C, water exchanged by acetone, dried in CEP

Aerocellulose obtained from 5Avicel/7.6NaOH/water gel regenerated in water at 50°C fractures around 38% of deformation. This can be explained by the microstructural characteristics of this type of sample and no densification was observed. Table V.9 summarises the mechanical and microstructural information concerning the influence of the bath temperature.

Bath water temperature	Young modulus (Pa)	Plateau stress (Pa)	Energy absorption at 40% strain (kJ/m ³)	Density (g/cm ³)	Total Porosity (%)	Macropores Porosity (%)	Mesopores Porosity (%)
25°C	2.7 10 ⁶	1.2 10 ⁵	110	0.08	96	7.1	88.9
50°C	1.2 10 ⁶	5 10 ⁴	45	0.07	94.8	23.3	71.5

Table V.9: Microstructural and mechanical characteristics of Aerocelluloses obtained from 5Avicel/7.6NaOH/water regenerated in water at 25°C or 50°C, water exchanged by acetone, dried in CEP

As it was demonstrated in section IV.2.6.1.1, the increase in bath temperature has a noticeable impact on the structure of Aerocellulose: it creates larger pores and so it lightens the material reducing its density. The porosimetry measurements performed at FhG-IAP reveal that a high percentage of macropores, 23% in sample that were regenerated in water at 50°C, as compared to 7.1 % for Aerocellulose regenerated at ambient temperature. It appears that the macropores collapse first and thus are responsible for the rapid fracture of Aerocellulose.

3.7 Structure-properties correlations

The relationships between mechanical and microstructural properties were studied for Aerocellulose samples obtained from NaOH and NMMO routes. It appears that the presence of macropores whatever is the way they were created – surfactant or bath temperature- has an important influence on the mechanical properties. More the quantity of macropores increases, more the density decreases and thus lower are the mechanical properties. This is valid for both NaOH and NMMO routes. The influence of the degree of polymerisation, DP, on the mechanical properties can be noted. Effectively, the mechanical properties of Aerocelluloses obtained from NMMO route are higher than the ones obtained for Aerocelluloses from NaOH route. This difference can be explained by the difference of degree of polymerisation of pulp: the DP of Avicel is 180; meanwhile the one of Solucell is 950.

Even if in the case of Aerocellulose the structure is far from ideal as the pore size shows a wide Gaussian distribution with a mean pore value around hundreds nanometres, we have used the Gibson and Ashby theory developed for the pores of the same size and we have correlated the relative Young modulus (E/E_s) and the relative compressive (σ/σ_s) strength with the relative density (ρ/ρ_s). Mechanical characteristics of cellulose are given below.

ρ_s (g/cm ³)	E_s (GPa)	σ_s (MPa)
1.5	25	350

Table V.10: Mechanical characteristics of cellulose [Ganster et al, 1996]; [Gibson, 1997]

Figures V.17 and V.18 present the relative Young modulus and the relative yield stress, respectively, versus the relative density for Aerocelluloses obtained from NaOH route.

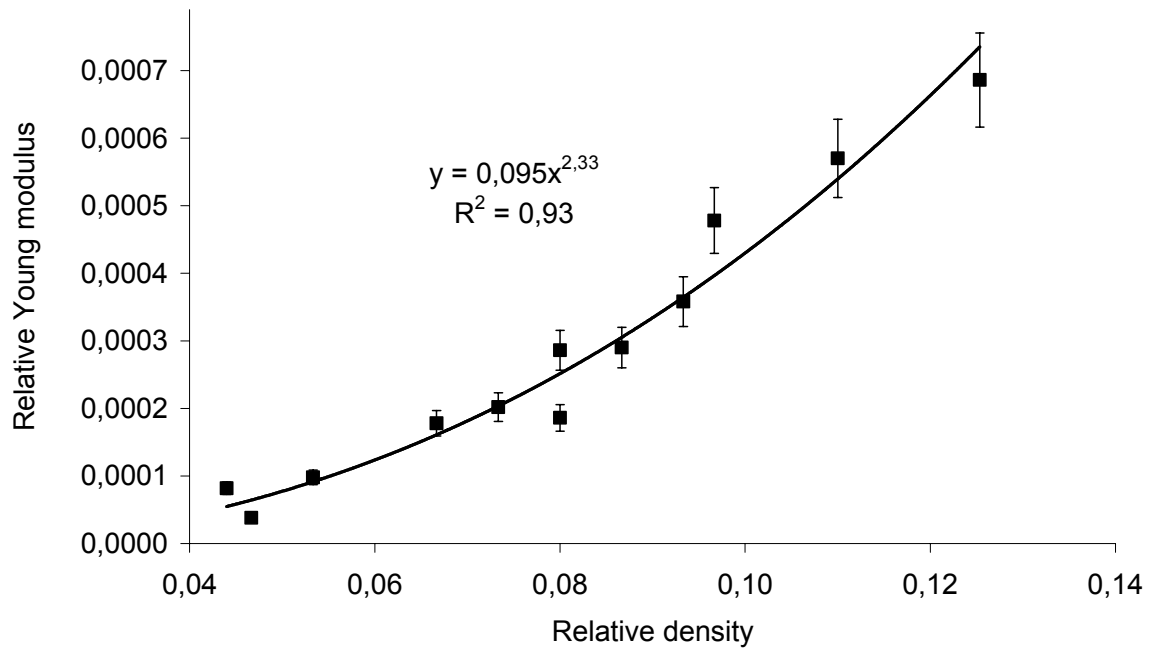


Figure V.17: Relative Young modulus versus the relative density for Aerocelluloses obtained from NaOH route.

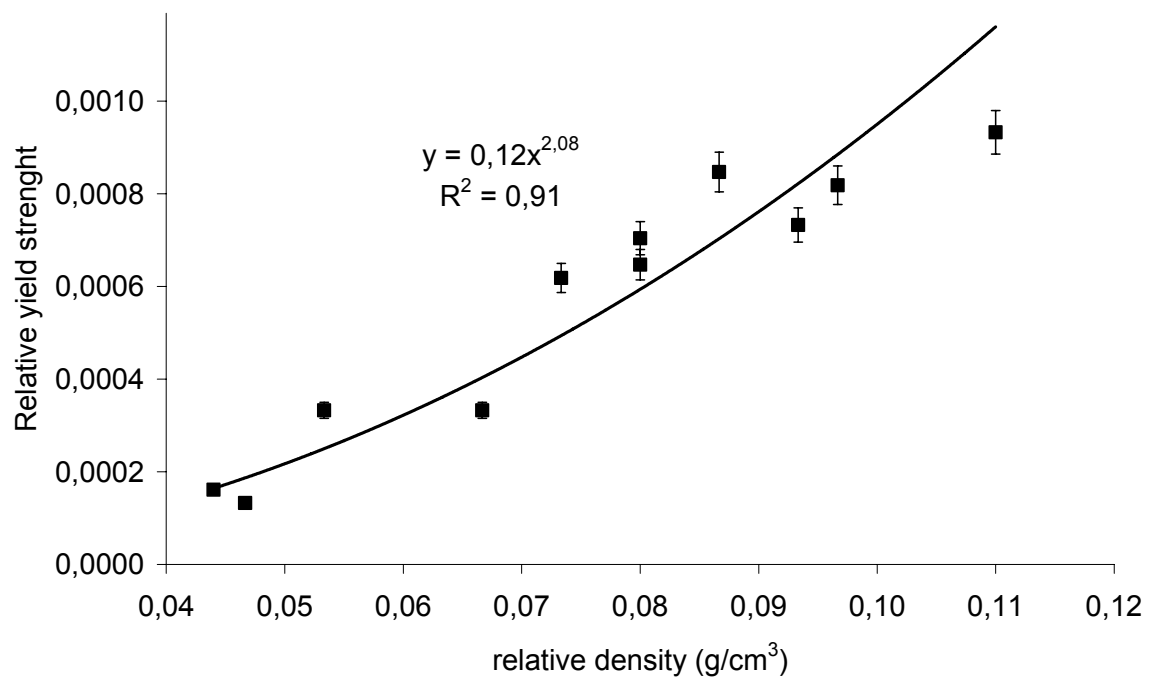


Figure V.18: Relative yield strength versus the relative density for Aerocelluloses obtained from NaOH route.

As can be seen there is a strong correlation between the relative elastic modulus, the relative compressive strength and the relative density. This suggests that the stiffness of Aerocellulose is dominated by the density of the porous material. Power laws were obtained for both relative Young modulus and relative yield strength values versus relative density. The values of scaling exponents n and m of equation V.6 are equal to 2.3 ± 0.2 and 2.08 ± 0.2 , respectively. As higher exponent values were not obtained, it appears that Aerocelluloses obtained from NaOH route mechanically behaves more like solid foam than like an aerogel.

We have compared the relationship between mechanical and microstructural properties for Aerocelluloses obtained from NaOH and NMMO routes. Figures V.19 and V.20 compare relative Young modulus and the relative yield stress respectively versus the relative density of both Aerocellulose samples.

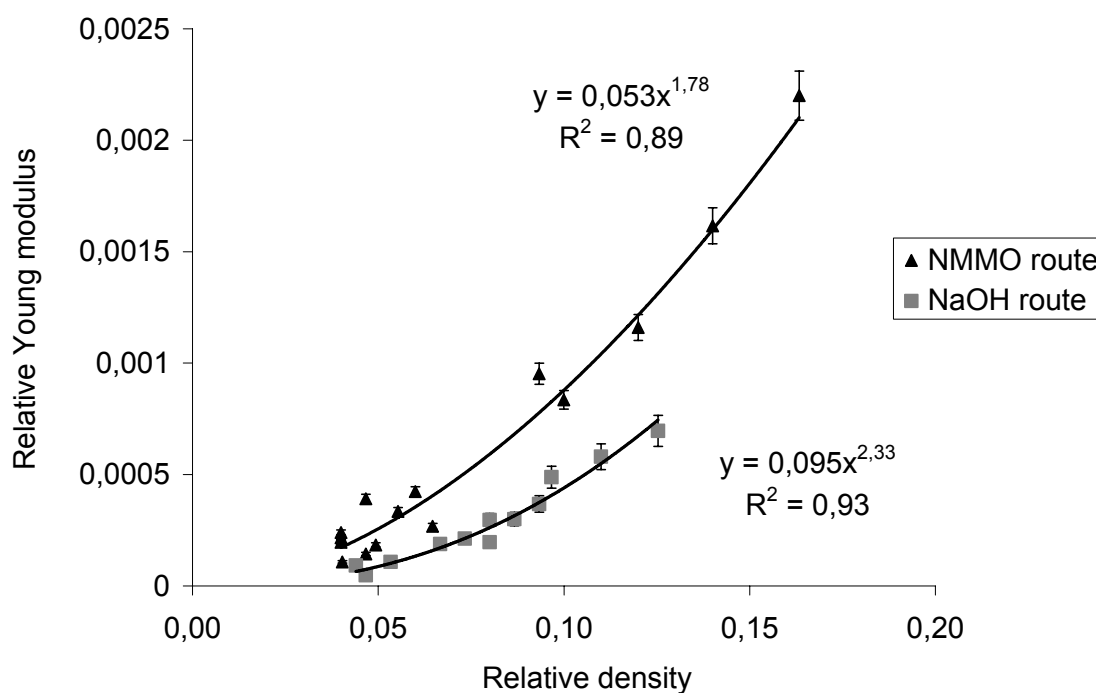


Figure V.19: Comparison of relative Young modulus versus the relative density for Aerocelluloses obtained from NaOH and NMMO routes

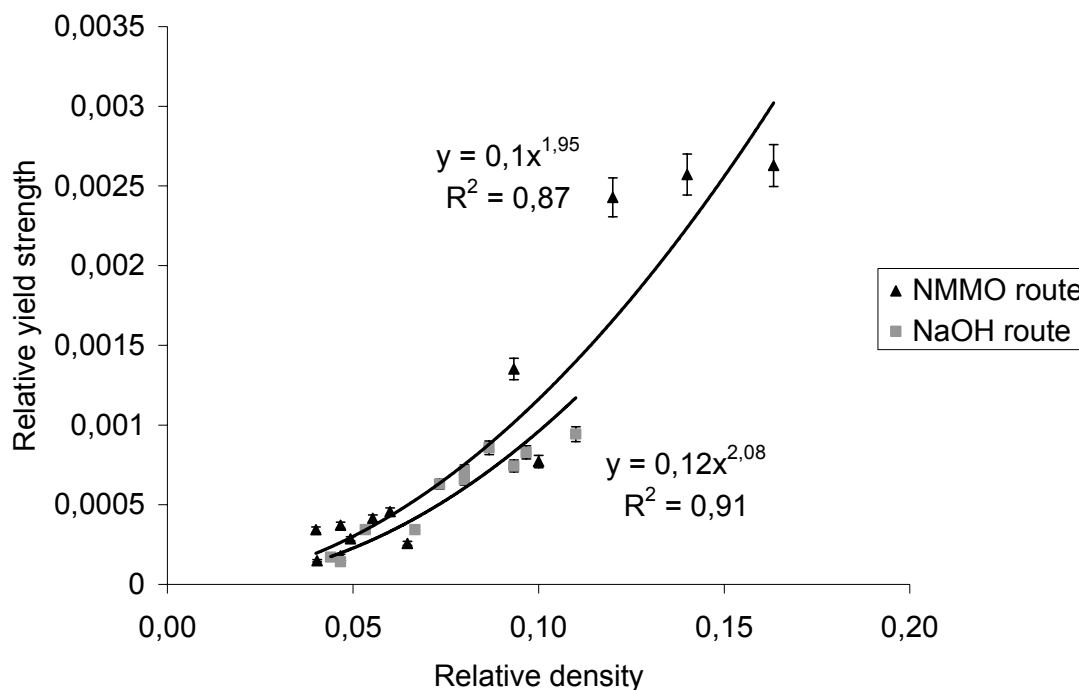


Figure V.20: Comparison of relative yield strength versus the relative density for Aerocelluloses obtained from NaOH and NMMO routes

Power laws were obtained for Aerocelluloses prepared from NMMO and the NaOH routes, the exponents are shown on the graphs. The curves shown in each figure have the same tendency with the dependences for NMMO samples being higher than the ones for NaOH samples. The difference between the two routes can be explained by the difference of cellulose DP, which is lower in the case of NaOH route. We obtain a good correlation with the Gibson and Ashby model of foam deformation under compression, particularly for the compressive plastic deformation, with an exponent of 2 ± 0.1 .

This confirms that our material mechanically behaves more like a foam than like an aerogel.

Finally, the energy absorption at 40% of strain is presented in Figure IV.21 for both NaOH and NMMO routes.

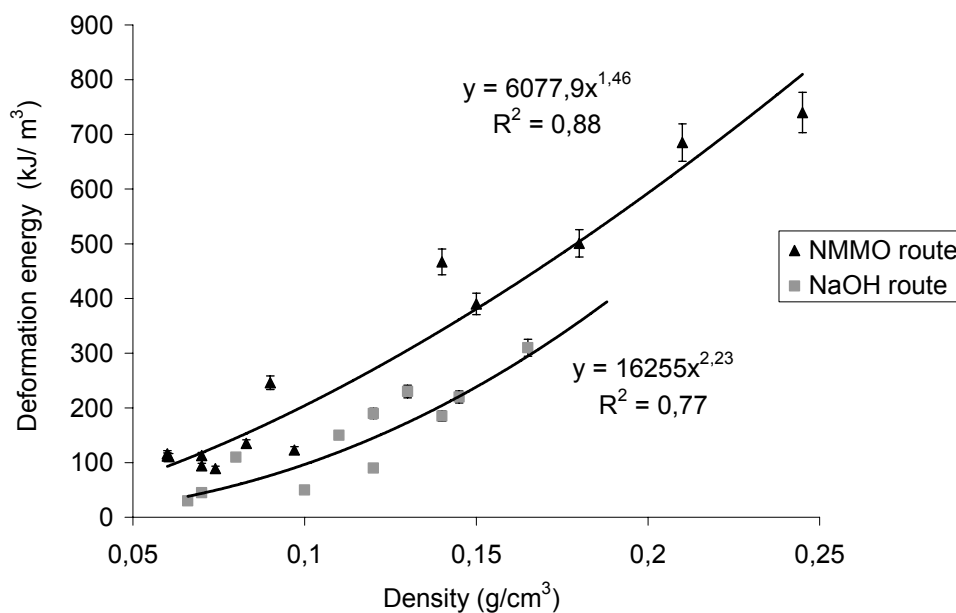


Figure V.21: Comparison of energy absorption versus the relative density for Aerocelluloses obtained from NaOH and NMMO route

The dependence of absorption energy on Aerocellulose density also obeys the power laws with an exponent of 1.46 and 2.23 for Aerocelluloses from NMMO and NaOH route, respectively. It appears that the absorption energy is higher for Aerocelluloses obtained from NMMO route than the one obtained from NaOH route. As previously, this could be explained by the difference of cellulose degree of polymerisation and thus of the rigidity of the initial cellulose forming the edges of the porous structure.

Conclusions

This study describes the first results on the mechanical properties of Aerocellulose obtained from NaOH and NMMO routes. Uniaxial compression tests were carried out to assess the mechanical characteristics such as Young modulus and compressive strength. The stress-strain behaviour of Aerocellulose was characteristic to the behaviour of cellular solid materials with three separate regions, elasticity region at low deformation, plateau region and densification of the material.

The influence of the preparation parameters of Aerocellulose on mechanical properties was investigated.

- The type of cellulose pulp has a slight influence on mechanical properties. It appears that the higher modulus and compressive strength values were observed for Aerocellulose with the higher cellulose degree of polymerisation.
- The influence of density is clearly reflected in the compressive properties of the Aerocellulose prepared for both routes. When the cellulose concentration and thus the density increases, Young modulus and yield stress increase, the stress plateau becomes shorter and thus the strain at which densification occurred starts to decrease.
- The impact of fibres used to reinforce the material was investigated. It appears that the fluff fibres addition at 1 or 2 % improves the mechanical properties of Aerocellulose.
- The addition of surfactant increases the number of macropores created by air bubbles in the material. As a result the material is enlightened, the density decreases and thus the Aerocellulose mechanical properties decrease.
- The same effect and for the same reason was noted when Aerocellulose was regenerated in a water bath of higher temperature: the density decreased and as a result the material is more fragile and fracture more rapidly.

Finally, the relationship between mechanical and microstructural characteristic was studied. Good correlations with the Gibson and Ashby model was observed for both relative Young modulus and relative yield stress versus the relative density. It appears that Aerocellulose from both routes, NaOH and NMMO, mechanically behave more like foams than aerogels. This could be explained by mean pore size around hundreds of nano-meters that is far from the micropore size scale of aerogels.

Among the physical properties of Aerocellulose, mechanical properties have an important impact on their practical applications. The mechanical characteristics of Aerocellulose are lower than commercial polymeric foams. For protective or cushion packaging, it is desirable that foams are able to absorb impact energy by compressing. The mechanical properties of Aerocellulose are strongly dependent on its structure and in particular, on its density. It was shown that it is possible to vary the mechanical properties of Aerocellulose through adjusting their formulation and the preparation parameters and thus there are ways to improve the response to mechanical stresses.

References

[Beverte, 2004]	Beverte, I.; Deformation of polypropylene foam neopolen® P in compression Journal of cellular plastics, 40, (2004), pp 191-204
[Ganster et al, 1996]	Ganster, J.; Blackwell, J.; NpH-MD Simulations of the elastic moduli of cellulose II at room temperature Journal of molecular modeling,2, (1996), pp 278-285
[Gibson, 2005]	Gibson, L.J.; Biomechanics of cellular solids Journal of biomechanics, 38, 3, (2005), pp 377-399
[Gibson et al, 1997]	Gibson, L.J.; Ashby, M.F.; Cellular Solids Structure and Properties (second Ed), Cambridge University Press, (1997)
[Liu et al, 2003]	Liu, Z.; Chuah, C.S.L.; Scanlon; M.G.; Compressive elastic modulus and its relationship to the structure of a hydrated starch foam Acta materiala, 51, (2003), pp 365-371
[Ma et al, 2000]	Ma, H-S; Roberts, A.P.; Prévost, J-H.; Jullien, R.; Scherer, G.W.; Mechanical structure-property relationship of aerogels Journal of non crystalline solids, 277, (2001), pp 127-141
[Ma et al, 2001]	Ma, H-S.; Prévost, J-H.; Jullien, R. ; Scherer, G.W.; Computer simulation of mechanical structure-property relationships of aerogels Journal of non crystalline solids, 285, (2001), pp 216-221
[Moner-Girona et al, 2001]	Moner-Girona, M.; Martinez, E.; Roig, A.; Esteve, J.; Molins, E.; Mechanical properties of silica aerogels measured by microindentation : influence of sol-gel processing parameters and carbon addition Journal of non crystalline solids, 285, (2001), pp 244-250
[Pekala et al, 1990]	Pekala, R.W.; Alviso, C.T.; LeMay, J.D.; Organic aerogels: microstructure dependence of mechanical properties in compression Journal of non crystalline solids, 125, (1990), pp 67-75

[Pirard et al, 1996]	Pirard, P.; Pirard, J.P.; Aerogel compression theoretical analysis Journal of non crystalline solids, 212, (1997), pp 262-267
[Saha et al, 2005]	Saha, M.C.; Mahfuz, H.; Chakravarty, U.K.; Uddin, M.; Kabir, M.E.; Jeelani, S.; Effect of density, microstructure and strain rate on compression behavior of polymeric foams Materials science and engineering A, 406, (2005), pp 328-326
[Scherer et al, 1995]	Scherer, G.W.; Smith, D.M., Qiu, X.; Anderson, J.M.; Compression of aerogels Journal of non crystalline solids, 186, (1995), pp 316 320
[Thompson et al, 2003]	Thompson, M.S.; McCarthy, I.D. ; Lidgren, L.; Ryd, L.; Compressive and shear properties of commercially available polyurethane foams Journal of biomechanical engineering, 125, (2003), pp 732-734
[Woignier et al, 1998]	Woignier, T. ; Reynes, J. ; Hafidi Alaoui, A. ; Beurroies, I. ; Phalippou, J. ; Different kinds of structure in aerogels : relationships with the mechanical properties Journal of non crystalline solids, 241, (1998), pp 45-52

Chapter VI: Application of Aerocellulose and of its carbonised form

Introduction

The objective in this chapter was to demonstrate the potential of the new porous cellulose materials for various applications. One example is Aerocellulose-inorganic particles composite prepared by encapsulating insoluble powders inside the Aerocellulose. Another example is the possibility to use carbonised Aerocellulose obtained from the pyrolysis of Aerocellulose for electrochemical purposes. After the pyrolysis of Aerocellulose, a highly porous nano-structured carbon materials is obtained, which could be used for energy conversion in fuel cells and energy storage in batteries. Indeed, carbon materials are often employed as electrode materials because of their good conductivity, large surface area and excellent corrosion resistance towards many electrolytes. Two applications of carbonised Aerocellulose are presented here: as an electrode material for primary lithium battery and as a catalyse support in Proton Exchange Membrane Fuel Cell electrodes.

1 Example of Aerocellulose application

The open-pore structure, high porosity and large surface area of Aerocellulose make it an ideal medium for preparing composite material. Our objective was to evaluate the wet Aerocellulose precursors and dry Aerocellulose as a matrix or carrier of different substances. Thus, we have encapsulated different insoluble powders into Aerocellulose beads. As a result, new cellulose-inorganic powder composites were elaborated. The preparation and the characterisation of Aerocellulose composite material are presented thereafter.

1.1 Preparation of Aerocellulose composite beads

Different types of powder, like metals or pigments, were encapsulated into Aerocellulose. The following powders were used in this study:

- Carbon black provided by Carbone Lorraine
- Copper provided by Baudier
- Iron provided by Prolabo
- Magnesium provided by Baudier
- TiO₂ provided by Merck
- Cosmenyl Blue AR12, a blue pigment, provided by Clariant

Aerocellulose composites were prepared as follow:

5Avicel/7.6NaOH/water solutions were prepared as described in section II.2.1. Insoluble powders were added to the ready solution at various concentrations in weight from 0 to 20%, in weight to the total solution. The mixture was stirred during 30 minutes at 5°C at 1000 revolution per minute. Then cellulose solution containing solid particles were placed in an ultrasound bath to homogenise the dispersion. Solutions with particles were pre-gelled in order to increase mixture viscosity and to avoid particles precipitation. Powder/5Avicel/7.6NaOH/water solution was dropped into water bath at 50°C by using a multi-channel micropipette, from Eppendorf, in order to form cellulose beads. Water was exchanged with acetone and dried in CO₂ supercritical condition in CEP, Sophia-Antipolis, France.

We have observed that the spherical shape of the beads is improved by increasing the viscosity of the solution, the cellulose concentration and the bath temperature.

1.2 Characterisation of Aerocellulose composite beads

1.2.1 Characterisation of powders

Before the characterisation of Aerocellulose composite beads, the powders particles were observed by scanning electron microscopy. Figure VI.1 shows the different powders studied.

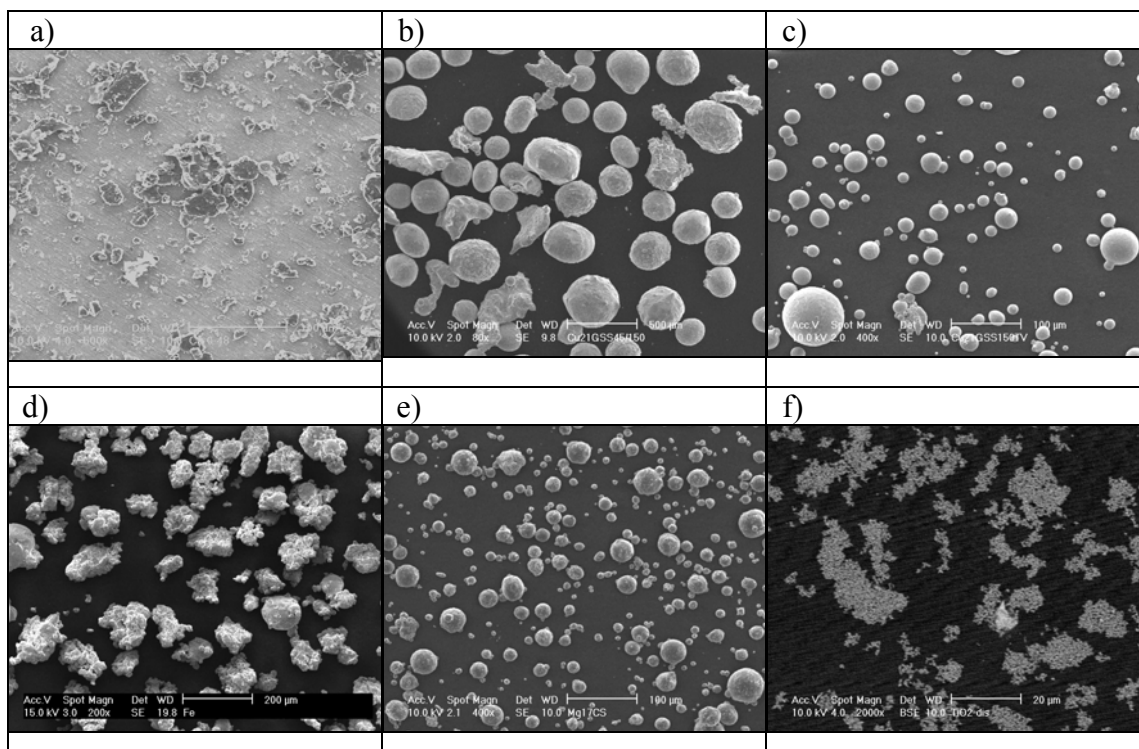


Figure VI.1: SEM micrographs of insoluble powders a) Carbon, b) and c) Copper with different particles sizes, d) Iron, e) Magnesium and f) TiO₂

From these images, we can observe different sizes and shapes of particles, some of them being spherical. We have analysed the particles size distribution of these powders using the image analysis software, Visilog. Based on the grey contrast, it allows the calculation of the surface and the particle diameter distribution of particles. Figure VI.2 presents an example of histogram found with Visilog from SEM micrographs of iron particles.

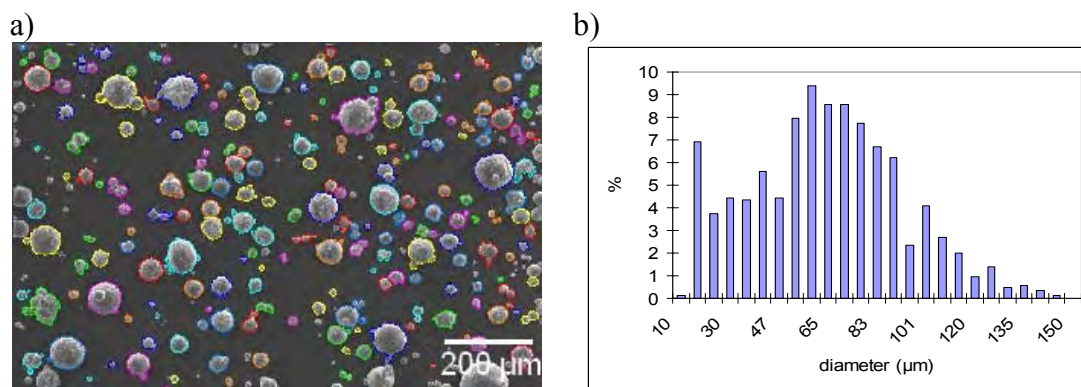


Figure VI.2: a) SEM micrograph analysed with Visilog and b) corresponding histogram of iron particles diameter distribution

The main diameter of iron particles is around 65 μm. Other powders were analysed by the same method. The mean diameters of magnesium and of the two copper particles are respectively of 10, 20 and 250 μm. Carbon black, TiO₂ and Cosmenyl blue particles were not analysed with Visilog due to the difficulty to disperse the powders homogeneously or due to a

bad grey contrast. Diameter particles distribution shows a large range from few micrometres to hundreds micrometres according to the powders studied.

1.2.2 Wet cellulose composite beads

During regeneration, no release of powder from the cellulose beads was observed in the time or when increasing powder concentration from 0 to 20%, except for carbon black powder. Figure VI.3 shows the photographs of composite cellulose beads after regeneration in water.

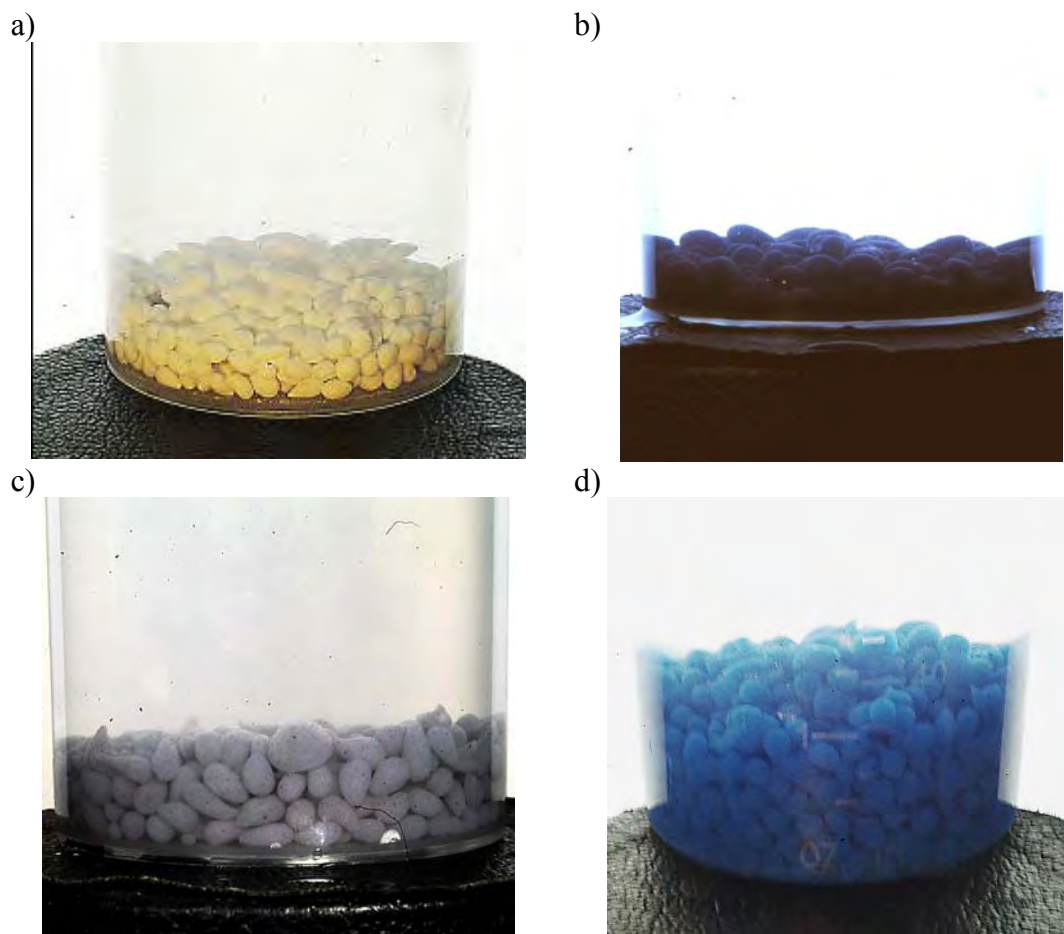


Figure VI.3: Photographs of cellulose beads in water with different powders encapsulated inside
a) 5% TiO_2 -cellulose beads, b) 10% Magnesium -cellulose beads, c) 5% Copper-cellulose beads,
d) 0.06% Cosmenyl blue -cellulose beads

The bead shape varies according to the powder encapsulated inside cellulose beads and its concentration. For instance, for the same concentration of particles, cellulose beads which contained TiO_2 particles are more spherical than the ones which contained copper particles. This could be explained by the difference of particles density ($d_{\text{TiO}_2} = 3.1$, $d_{\text{copper}} = 8.9$). One specific application is the encapsulation of iron particles which confers magnetic properties to wet Aerocellulose precursors and dried Aerocellulose. Figure VI.4 shows the magnetic properties of these beads, which are attracted by a magnet.



Figure VI.4: Photograph of 5% iron-cellulose beads in water with a magnet attracting the beads

Magnetic dispersed systems in polymeric biodegradable matrices constitute a new class of material, with potential applications in medicine or biochemistry. Recently, Correa and co-workers [Correa et al, 2005] have synthesized magnetic cellulose beads, using the emulsion method. Starting from a cellulose solution containing 2.8 wt% of cubic magnetic particles, authors have developed composite beads of 100 μm and used those as a vehicle in enzyme immobilization.

1.2.3 Aerocellulose composite beads

Figure VI.5 presents the composite Aerocellulose beads obtained after supercritical drying performed. The drying procedure described in section IV.1.2 was applied.

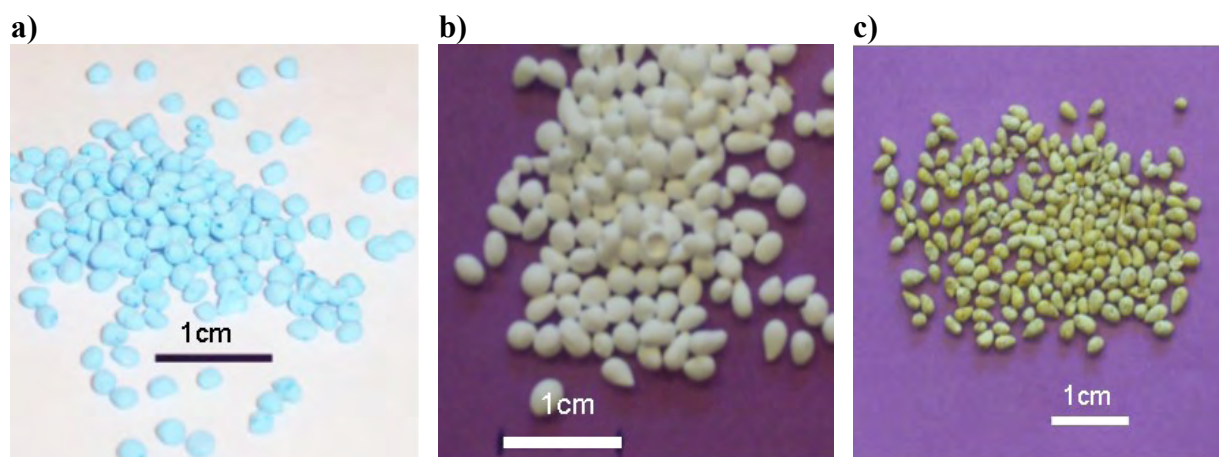


Figure VI.5: Photographs of composite Aerocellulose a): Cosmenyl Blue-Aerocellulose b) TiO_2 -Aerocellulose c) Iron-Aerocellulose

We have observed a slight shrinkage of the beads after drying, however no release of powder was noticed during the supercritical drying showing the beads resistance and the good encapsulation of inorganic powders.

Powders encapsulated in Aerocellulose beads were observed by scanning electron microscope. Figure VI.6 shows the surface and the inner part of iron-cellulose bead.

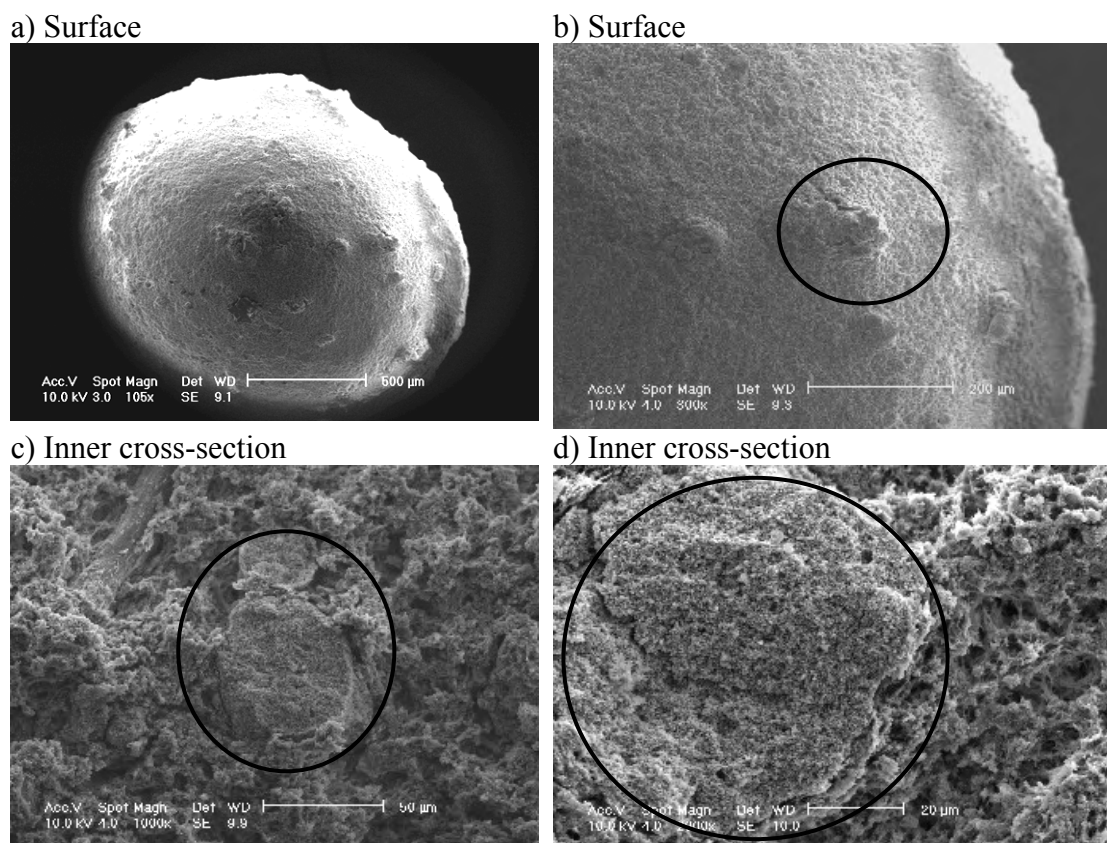


Figure VI.6: SEM photographs of iron particles encapsulated into Aerocellulose: surface a), b) and inside the bead c), d)

We observe a regular distribution of iron particles within the beads. Due to their large diameter (particle distribution from 10 to 150 μm), iron particles are trapped inside the porous structure. Figure VI.7 presents the inner part of TiO₂-cellulose bead.

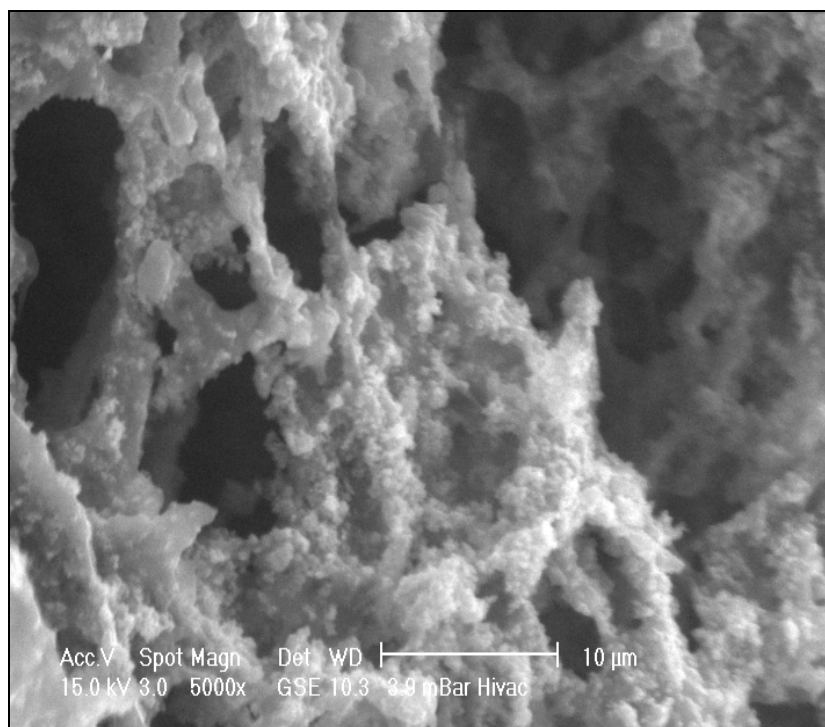


Figure VI.7: SEM photographs of inner cross section of TiO₂-cellulose beads

Contrary to iron particles, TiO₂ particles are not trapped inside the porous structure but they adhere on the fibres walls. White agglomerate particles of TiO₂ are detected on the fibres surface. According to the SEM photographs of TiO₂ powder (see Figure VI.1.f), the particles diameter is lower than one micrometre. It seems that TiO₂ particles are coating cellulose fibres. The impregnation of cellulose fibres by metal oxide has ever been reported by Kurokawa [Kurokawa et al, 1995] and by Nagaoka [Nagaoka et al, 2002]. The coating of cellulose fibres is due to coordination bonding between the hydroxyl group on pyranose rings and the polyvalent metal. This type of cellulose-metal oxide composite has widely been used as a substrate for reactants immobilization with many applications. Since in most cases these metal oxides are Lewis acids, new immobilized reactants on the oxide-coated cellulose can be envisaged. For instance, Dias et al, [Dias et al, 2002] have described the adsorption of porphyrin, a macromolecule which acts as a ligand for enzyme or metal, on cellulose/TiO₂ fibres.

To conclude, inorganic particles were encapsulated in Aerocellulose beads and a new type of material, porous cellulose composite was obtained. In most cases, no release was observed showing that these cellulose beads, either in a wet or in dry state, can be used as a biodegradable carrier of inorganic particles. Likewise, a wide range of inorganic particles can be dispersed in cellulosic matrix offering various properties as optical or magnetic properties to the new material and thus opening new applications in various fields as cosmetics, medicine, pharmaceuticals, etc.

2 Carbonised Aerocellulose and its applications

Another application of Aerocellulose is to pyrolyse the material and to use the resulting porous carbon for electrochemical purposes. The goal of this section is to describe the preparation of carbonised Aerocellulose and its microstructural properties and the electrochemical applications of this new material. The first part presents the preparation of carbonised Aerocellulose and the main microstructural results obtained. The second part is dedicated to the electrochemical applications of this new type of carbonised material as electrode for primary lithium battery and as a support material for Proton Exchange Membrane Fuel Cell (PEMFC).

2.1 Preparation and microstructural properties of carbonised Aerocellulose

2.1.1 Preparation of carbonised Aerocellulose

Before pyrolysing Aerocellulose samples, their thermal behaviour was investigated in order to determine the heating regime. The weight loss of cellulose on heating was determined using thermogravimetric analysis (TGA). TGA was performed on a TGA TA Instruments 2950 HR device at Central Analysis Service CNRS (Centre National de Recherche Scientifique), Vernaison, France. Aerocellulose obtained from 5Borregaard/7.6NaOH/water gels, regenerated in water at ambient temperature, water exchanged with acetone and dried in CO₂ supercritical conditions in CEP. Aerocellulose was heated with a heating rate of 4°C/min in a 90 mL/min inert nitrogen flow gas. Its weight was recorded as a function of increasing temperature from ambient temperature to 1000°C. Figure VI.8 shows the thermogram obtained for this Aerocellulose.

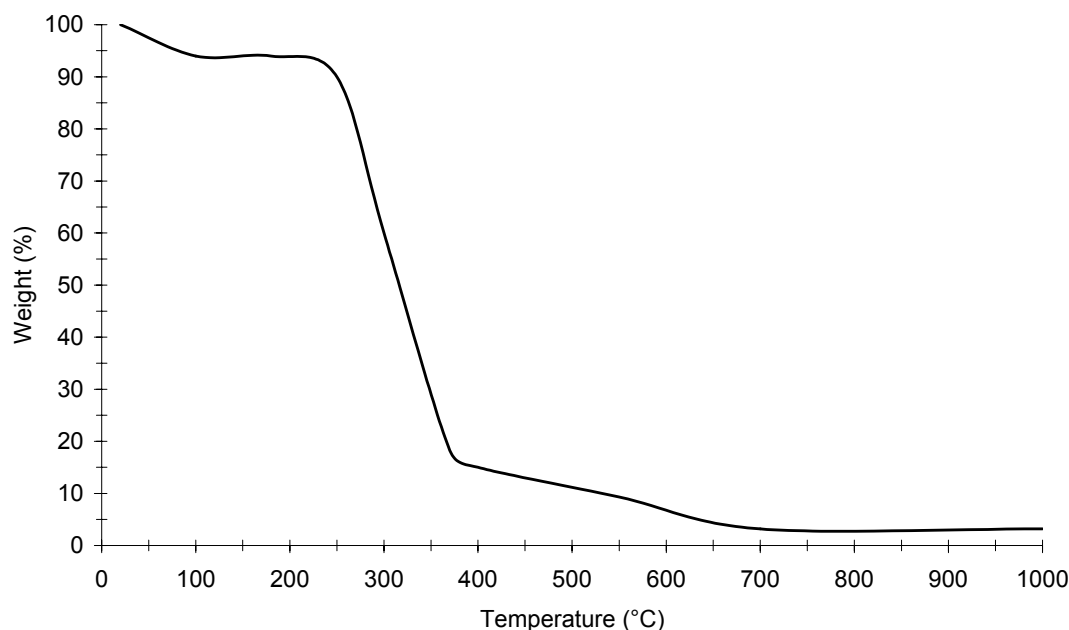


Figure VI.8: Thermogram of Aerocellulose

Table VI.1 presents the weight losses of Aerocellulose for various temperature ranges obtained from the thermogram.

	Amb- 160°C	160-370°C	370-550°C	550-1000°C	Total weight loss (%)
Weight loss (%)	4	77.8	8.9	6.1	96.8

Table VI.1: Weight loss as a function of temperature for Aerocellulose obtained from physical cellulose-NaOH-water gels

The first weight loss from ambient temperature to 160°C, 4%, corresponds probably to the water evaporation contained in the sample. The main weight loss occurs between 160 and 370°C. According to Banyaz, [Banyaz et al, 2001] this loss corresponds to the formation of volatile species such as CO, CO₂ and formaldehyde produced during the pyrolysis of cellulose. The total weight loss observed by TGA is 96.8%.

The Aerocellulose samples were pyrolysed using a laboratory furnace of CEP Ecole des Mines France (see Figure VI.9a). Schematic view of the furnace is depicted in Figure VI.9b. The pyrolysis was performed in a 5 L/min inert gas flow. The inert gas was either nitrogen or argon, of purity 99.995% and 99.999%, respectively, and was delivered by Air Liquid, France.

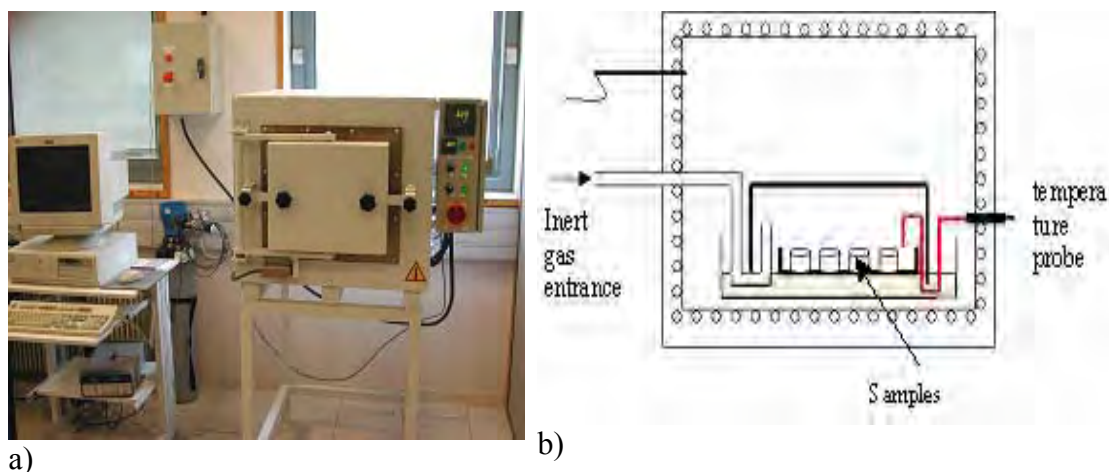


Figure VI.9: Photographs of CEP furnace used for samples pyrolysis (a) and schematic representation of pyrolysis device (b)

To take into account the TGA results and to limit the considerable weight loss, specific cycles of pyrolysis were performed. Two pyrolysis cycles, a short and a long one were investigated. They are composed of several steps.

- Cycle 1: First, a rise with a heating ramp at 2°C/mn from ambient temperature to 330°C, then a stationary plateau of one hour at this temperature, then a rise with a

heating ramp at 2°C/mn until 750°C, followed by a plateau of one hour and finally a decrease until ambient temperature

- Cycle 2: First a rise with a heating ramp at 4°C/mn from ambient temperature to 300°C which corresponds to the temperature range of major weight loss, then a stationary plateau of two hours at this temperature, then a rise with a heating ramp at 2°C/mn until 800°C, followed by a plateau of four hours at 800°C, and finally a decrease until ambient temperature.

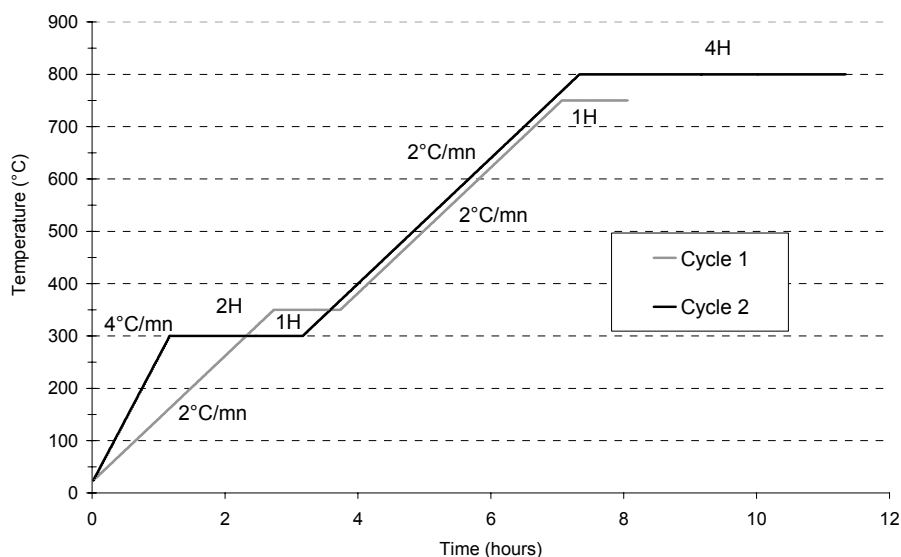


Figure VI.10: Pyrolysis cycles from ambient temperature to 800°C

For all Aerocellulose obtained from cellulose/7.6NaOH/water gels, the total weight loss was around $83 \pm 3\%$. No difference of weight loss within the experimental errors was observed between the two pyrolysis cycles. A total volume loss of 90% was observed by measuring the dimensions of Aerocellulose samples before and after pyrolysis. However, samples keep their monolithic initial shape after pyrolysis. One example of their shapes before and after pyrolysis is presented on Figure VI.11:



Figure VI.11: Photographs of Aerocellulose samples before and after pyrolysis

Elementary analysis of pyrolysed Aerocellulose was performed at Central Analysis Service CNRS (Centre National de Recherche Scientifique), Vernaison, France. The results are summarised in Table VI.2.

Elemental composition (%)	Initial Aerocellulose	Carbonised Aerocellulose with cycle 1	Carbonised Aerocellulose with cycle 2
% C	42.1	84.8	91
% O	51.7	12.7	7.9
% H	6.2	1.3	1.1

Table VI.2: Elemental composition of Aerocellulose obtained from cellulose/7.6NaOH/water gels before and after pyrolysis, in weight percentage

We observe that the increase of the duration of the two dwells at 350°C and 800°C in cycle 2 leads to a decrease of oxygen part and an increase of carbon part. In the following, all samples will be pyrolysed with cycle 2. According to [Babel, 2003], the part of oxygen in carbon fibres pyrolysed to 850°C is 3.7%. As our carbonised Aerocellulose with cycle 2 still presents high quantities of oxygen (7.9%), it seems that our carbonisation process is not totally completed.

2.2 Microstructural characterisations

2.2.1 Comparison of organic and pyrolysed Aerocellulose

The morphology of organic and carbonised Aerocellulose was investigated by microscopy observations and compared with the one of initial Aerocellulose. Figures VI.12 and VI.13 present the photographs obtained by scanning electron microscopy and by transmission electronic microscopy, respectively, for carbonised Aerocellulose obtained from 5Borregaard/7.6NaOH water gels, pyrolysed with cycle 1.

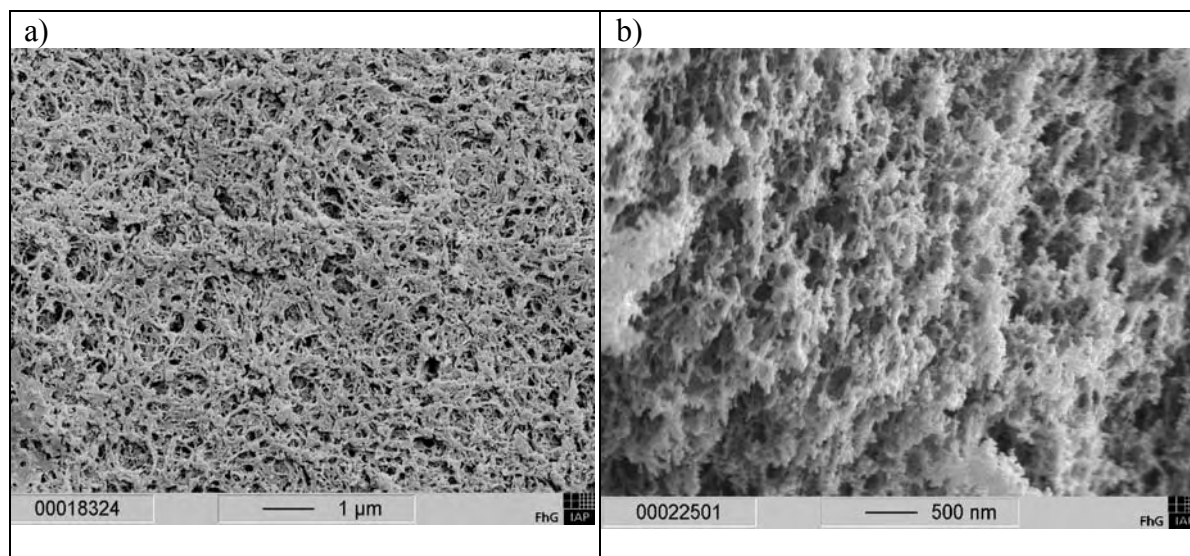


Figure VI.12: SEM photographs of Aerocellulose obtained from 5Borregaard/7.6NaOH water gels (a) and its pyrolysed form (b). Photo provided by FhG-IAP

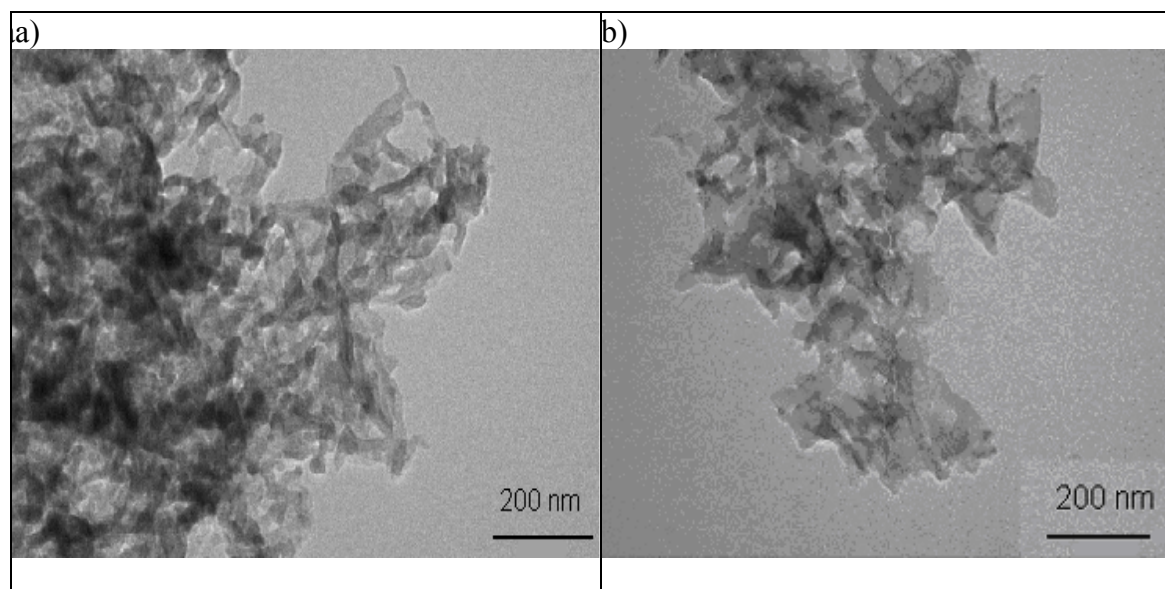


Figure V.13: TEM photographs of Aerocellulose and its pyrolysed form obtained from 5Borregaard/7.6NaOH water gels

We observe a preservation of the porous texture after pyrolysis. However, when looking at the SEM photographs, we can observe a denser structure for the pyrolysed Aerocellulose as compared with the initial Aerocellulose. Some kind of particles can be detected. No macropores are observed for this type of sample. We can notice for the pyrolysed Aerocellulose a dense porous structure with pores in the range of 10-100 nm.

Mercury porosimetry and nitrogen adsorption on organic and carbonised Aerocellulose obtained from 5Borregaard/7.6NaOH water gels were performed at FhG-IAP, Potsdam, Germany. Figure VI.14 shows the pore size distribution of the organic Aerocellulose obtained from 5Borregaard/7.6NaOH/water gels and its pyrolysed form.

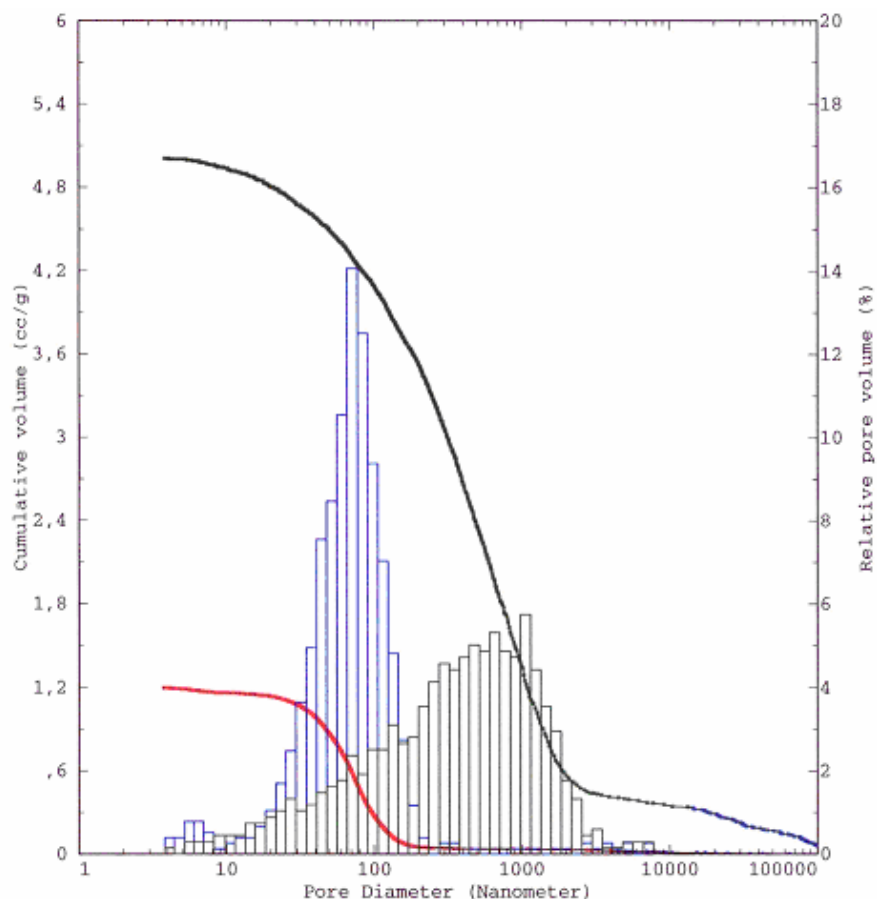


Figure VI.14: Comparison of pore size distribution of initial Aerocellulose obtained from 5Borregaard/7.6NaOH/water gels (in dark) and its pyrolysed form (in blue)

Obviously, the mean pore diameter is reduced by the pyrolysis and the distribution becomes narrower in the region of meso pores. The pore size distribution has a noticeable peak at 70 nm. The mean pore size is decreased by more than ten after the pyrolysis treatment. Table VI.3 summarises the microstructural characterisation of these initial and pyrolysed samples.

	Bulk density [g/cm ³]	Mean pore diameter [nm]	Specific surface BET [m ² /g]	Cumulative volume [cm ³ /g]	Porosity %
Initial Aerocellulose	0.13	920	280	7.2	94.7
Pyrolysed Aerocellulose	0.25	70	207	1.1	67

Table VI.3: Microstructural characteristics of Aerocellulose obtained from 5Borregaard/7.6NaOH/water gels and of its pyrolysed form

As a conclusion, the pyrolysis of Aerocellulose leads to a densification of the sample, to a decrease of the porosity and to a decrease of the mean pore size diameter.

2.2.2 Influence of Aerocellulose preparation and pyrolysis parameters on microstructural properties of carbonised Aerocellulose

The influence of Aerocellulose preparation parameters, such as cellulose concentration and the water regenerating bath temperature, on the microstructural properties of carbonised Aerocellulose was investigated. Mercury porosimetry and nitrogen adsorption on carbonised Aerocellulose were performed at SAFT, Bordeaux, France. Hg-intrusions and nitrogen adsorption were carried out on a Micrometrics Autosorb IV and BellSorb Mini II devices, respectively. Porosimetry techniques and model applied are described in section IV.1.2 and IV.1.3.

2.2.2.1 Influence of regenerating bath temperature

Aerocelluloses were obtained from 5Avicel/7.6NaOH/water gels regenerated at various water temperatures (25°C, 50°C and 70°C) followed by water→acetone exchange, dried in CO₂ supercritical conditions in CEP and pyrolysed with cycle 2 in CEP.

Figure VI.8 shows the pore size distribution of the pyrolysed Aerocellulose obtained from 5Avicel/7.6NaOH/water gels as a function of the water bath temperature: 25°C, 50°C and 70°C.

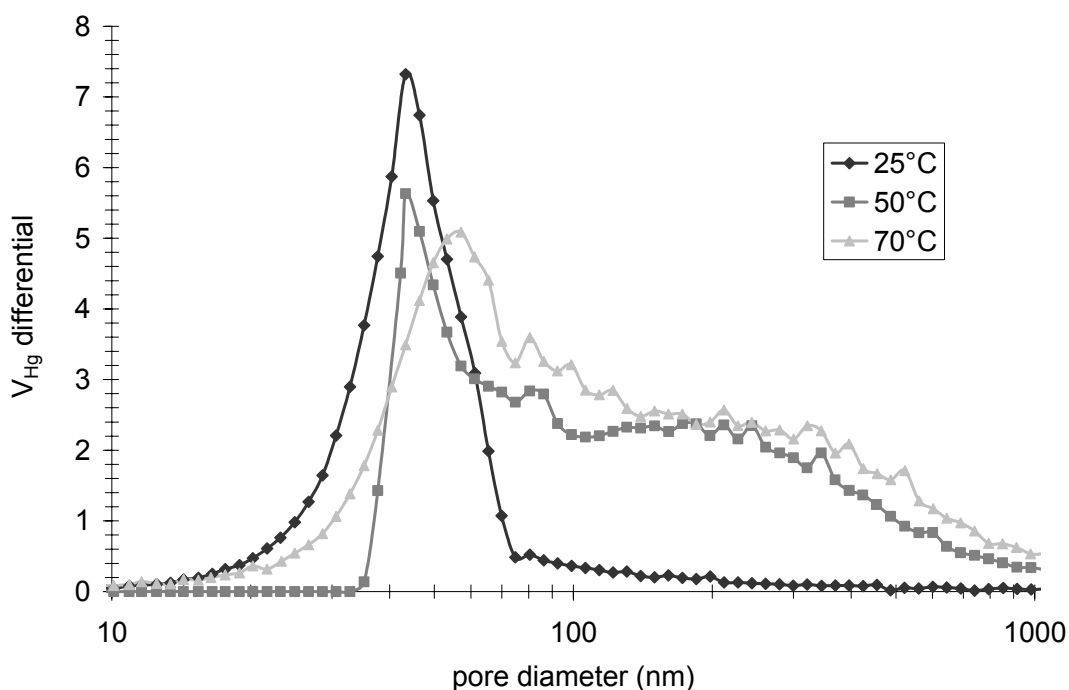


Figure VI.15: Influence of water regenerating bath temperature on pore size distribution of pyrolysed Aerocellulose

Table VI.4 summarises the microstructural characterisation of these pyrolysed samples.

Pyrolysed Aerocellulose obtained from 5Avicel/7.6NaOH/water gels regenerated in water of temperature:	Hg porosimetry			N ₂ adsorption	
	Cumulative volume [cm ³ /g]	Density [g/cm ³]	Mean pore diameter [nm]	Specific surface [m ² /g]	Micro pore Specific surface [m ² /g]
25°C	2.1	0.36	44	592	410
50°C	3.2	0.23	170-43	482	243
70°C	4.2	0.21	250-56	512	220

Table VI.4: Microstructural characteristics of pyrolysed Aerocellulose as a function of water regenerating water bath temperature

As it was described in section IV.2.6.1.1., the more the water regenerating bath temperatures increases, the more the density of initial Aerocellulose decreases. This observation remains true after the pyrolysis of these Aerocellulose. With the increase of bath temperature, pyrolysis creates a bimodal distribution of pore size around 50 nm and 200 nm. As there are fewer micropores in pyrolysed Aerocellulose, which were regenerated in hot water, the specific surface of these carbonised samples is lower than the one of samples regenerated in water at ambient temperature. When water regenerating bath increases, the macroporosity of pyrolysed Aerocellulose increases. As a result, the carbonised Aerocellulose are more brittle.

Figures VI.16 shows the morphology of pyrolysed Aerocellulose obtained from 5Avicel/7.6NaOH/water gels, regenerated at 50°C, then water exchanged with acetone, dried in CO₂ supercritical conditions in CEP and pyrolysed with cycle 2 in CEP.

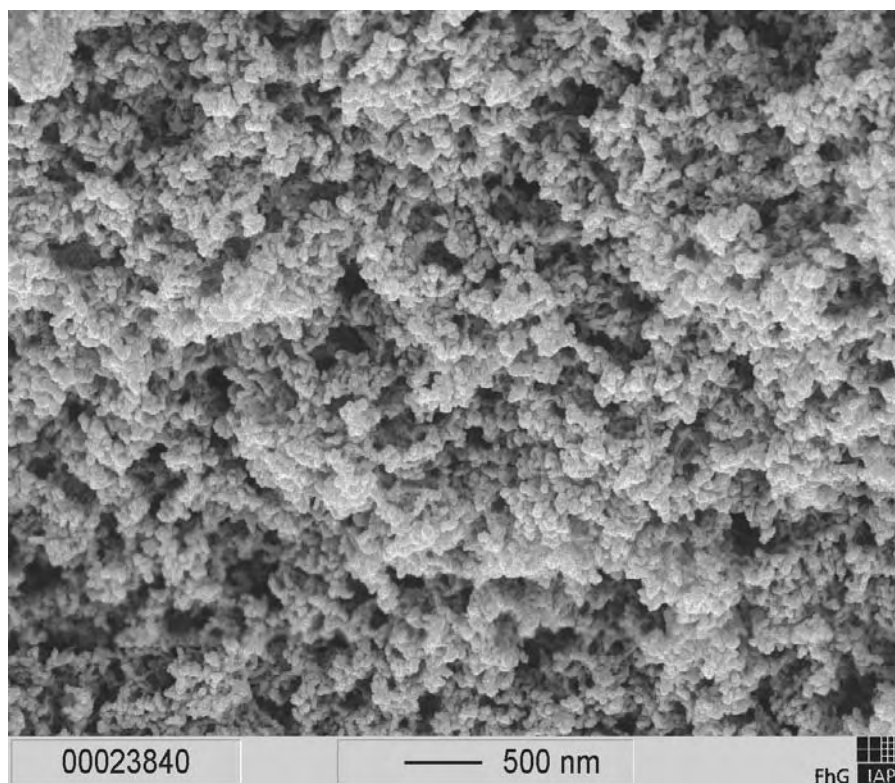


Figure VI.16: SEM photograph of pyrolysed Aerocellulose obtained from 5Avicel/7.6NaOH water gels, regenerated in water at 50°C, CO₂ supercritical dried in CEP and pyrolysed at CEP. Photo provided by FhG-IAP

We observe a globular texture with carbon spheres of a few nanometres. This structure differs from the one obtained from the carbonised form of Aerocellulose obtained from regeneration in water at ambient temperature and pyrolysed with short cycle 1 (see Figure VI.12b). This could be explained by a reorganisation of the carbonised Aerocellulose texture in the time. However, the formation of this special globular texture is still not thoroughly understood.

2.2.2.2 Influence of cellulose concentration

Aerocellulose obtained from 5Avicel/7.6NaOH/water and 7Avicel/7.6NaOH/water gels were regenerated at ambient temperature, then water exchanged with acetone, dried in CO₂ supercritical conditions in CEP and Natex, respectively, then pyrolysed with cycle 2 in CEP.

Figure VI.17 shows the pore size distribution of the pyrolysed Aerocellulose obtained from 5Avicel/7.6NaOH/water and 7Avicel/7.6NaOH/water gels.

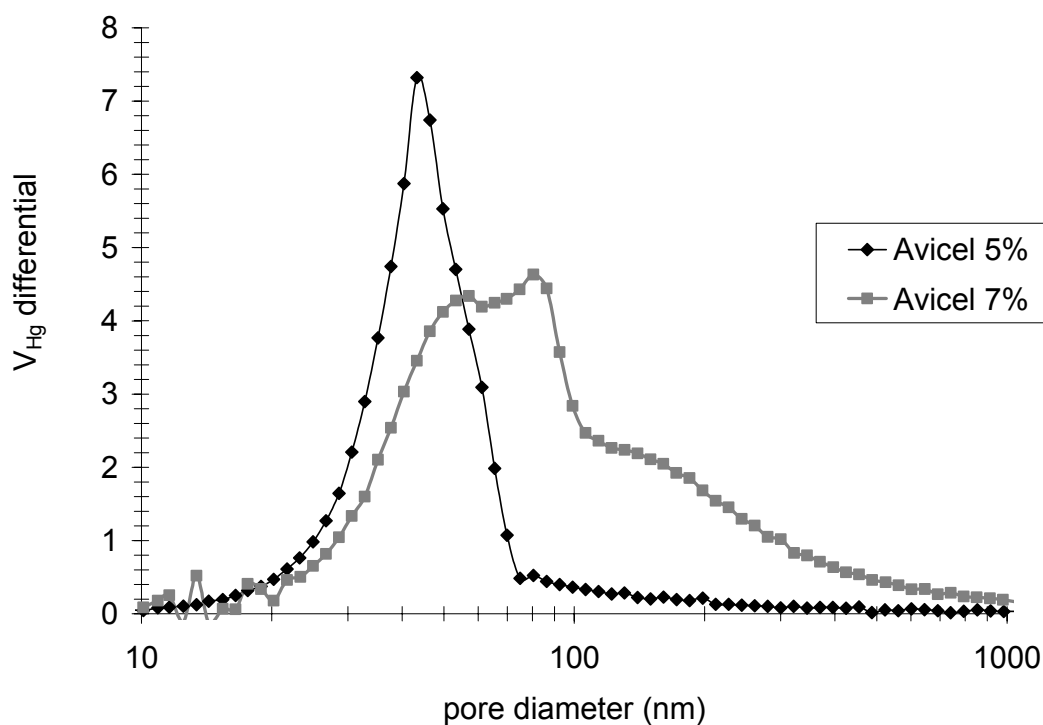


Figure VI.17: Influence of cellulose concentration on pore size distribution of pyrolysed Aerocellulose

Contrary to expectation, we observe that the pore size distribution of pyrolysed Aerocellulose from 7Avicel/7.6NaOH/water gel is wider than the one of carbonised Aerocellulose obtained from 5Avicel/7.6NaOH/water gel. Regarding the results obtained for initial Aerocellulose in section IV.2.3., it appears that the higher the cellulose concentration, the lower the pores mean diameter.

Table VI.5 summarises the microstructural characterisation of these pyrolysed samples.

Pyrolysed Aerocellulose obtained from:	Hg porosimetry			N ₂ adsorption isotherm	
	Cumulative volume [cm ³ /g]	Density [g/cm ³]	Mean pore diameter [nm]	Specific surface [m ² /g]	Micro pore Specific surface [m ² /g]
5Avicel/7.6NaOH/water solutions	2.1	0.36	44	592	410
7Avicel/7.6NaOH/water solutions	3.2	0.34	81	368	200

Table VI.5: Microstructural characteristics of pyrolysed Aerocellulose as a function of cellulose concentration

We observe an increase of the median pore diameter from 44 nm to 81 nm, and thus an increase of the cumulative volume. We can also notice a decrease of the micropores amount in the sample with the increase of cellulose concentration. However, because drying was performed not in exactly the same conditions, it is not possible to make an adequate

comparison. More data are needed to deduce the correlations between the structure and the preparation conditions.

2.2.2.3 Influence of the inert gas atmosphere

The influence of two inert gas flow, nitrogen and argon, on the microstructural properties of carbonised Aerocellulose has been investigated. No significant difference on mass loss has been observed after pyrolysis at 800°C in the two inert gases. The mass loss is around 82%±2%. Figure VI.18 shows the pore size distribution of the pyrolysed Aerocellulose obtained from 5Avicel/7.6NaOH/water gels as a function of the inert gas flow.

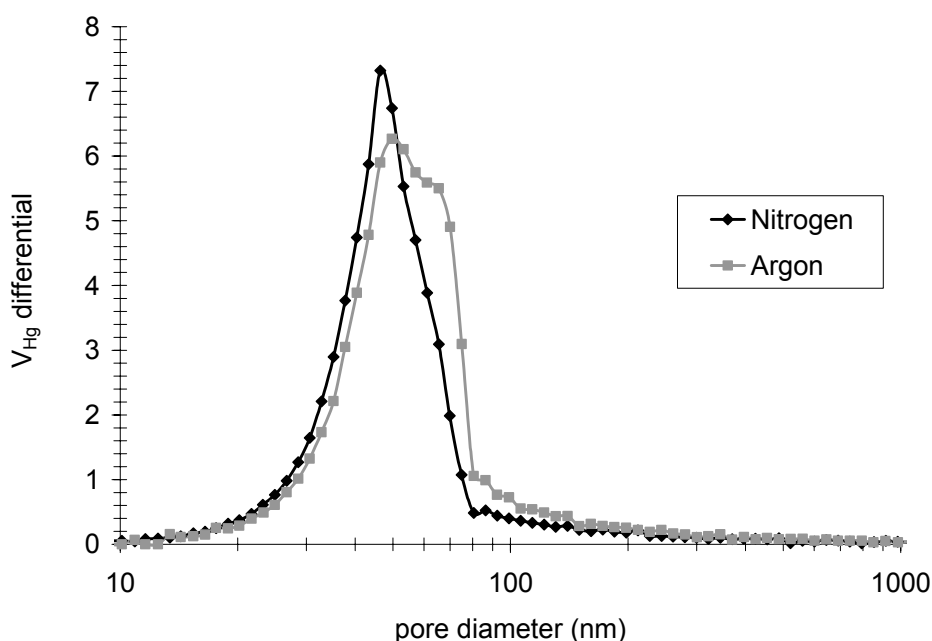


Figure VI.11: Influence of inert gas type on the pore size distribution of pyrolysed Aerocellulose

Table VI.6 summarises the microstructural characterisation of these pyrolysed samples.

Aerocellulose pyrolysed in inert gas :	Hg porosimetry			N2 adsorption isotherm	
	Cumulative volume [cm ³ /g]	Density [g/cm ³]	Mean pore diameter [nm]	Specific surface [m ² /g]	Micro pore Specific surface [m ² /g]
Nitrogen	2.1	0.36	44	592	410
Argon	2.3	0.34	52	652	450

Table VI.6: Microstructural characteristics of pyrolysed as a function of inert gas flow

The nature of the flow gas, argon or nitrogen, seems to have a negligible influence on the microstructure of carbonised Aerocellulose.

It appears that it is possible by varying the preparation parameters of carbonised Aerocellulose, such as the cellulose concentration or the regenerating bath temperature, to modify the properties of these materials and to adapt the porosity for required electrochemical applications.

2.3 Electrochemical applications

2.3.1 Carbonised Aerocellulose for primary lithium battery Li/SOCl₂

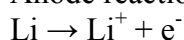
2.3.1.1 Generalities

The primary battery is a convenient, relatively inexpensive power source for portable electronics, lighting, toys and many other applications. The general advantages of primary batteries are good shelf life, high energy density, high operating cell voltage, a large operating temperature range and ease of use. It is called “primary” battery because it is a non-rechargeable battery. Primary lithium battery, Li/SOCl₂, has a very high energy density (about 500 Wh/kg) and an operating voltage of 3.3–3.5 V. The cell is generally a low-pressure system.

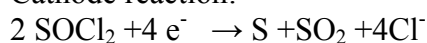
Lithium is the alkaline metal with the smallest molecular weight among this type of metals and has the highest standard potential of all the metals, over 3 V. For that reasons lithium as a material for negative electrodes allows a particularly high storage capacity. The reactivity of lithium metal in aqueous solutions requires the use of non-aqueous electrolytes for lithium batteries as thionyl chloride (SOCl₂), which is an inorganic solvent. Thionyl chloride when used in the lithium battery acts as both the electrolyte solvent and as the active cathode material. It is in liquid state between –105°C and +75°C, which allows the utilisation of the primary battery in a wide temperature range. During the discharge of a Li-SOCl₂ system, a decomposition reaction of the electrolyte on the carbon surface of the anode occurs, forming a passivation film, also called the solid electrolyte interface (SEI). It protects the lithium anode from reacting with the electrolyte and thus provides lithium cells with a long shelf life. This passivating layer conducts the lithium ions. It prevents further chemical reaction when not in use, thus preserving the cell's shelf life. The passivating layer conducts lithium ions.

Primary lithium battery Li/SOCl₂ is a liquid cathode concept, the reductant is metallic Lithium and the oxidant is the liquid electrolyte itself, SOCl₂, in contact with Li. The basic reactions in the Li/ SOCl₂ battery are given below:

Anode reaction:



Cathode reaction:



Cell reaction:



Figure VI.19 shows a schematic representation of primary lithium battery Li/SOCl₂.

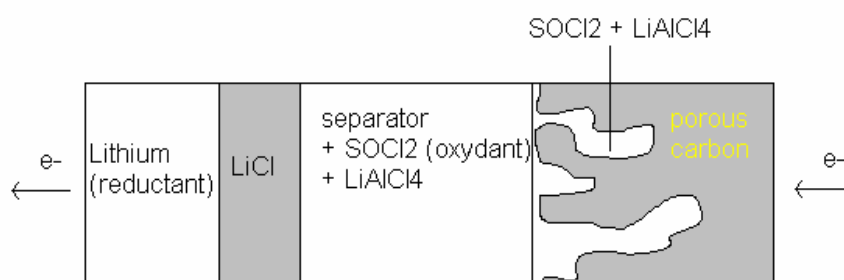


Figure VI.19: Schematic representation of primary lithium battery Li/SOCl₂

In a Li-SOCl₂ system, a spontaneous decomposition reaction occurs on the surface of the anode (Li). On the carbon surface, the thionyl chloride reduces to chloride ions, sulphur dioxide, and sulphur. The lithium and chloride ions then form lithium chloride. Sulphur and sulphur dioxide dissolve in the electrolyte, but at higher-rate discharges, SO₂ will increase the cell pressure. LiCl precipitates inside the porosity. Thus, cumulative porous volume and pores sizes of the carbon electrode play a key role on discharge time and voltaic capacity.

2.3.1.2 Button cell

The button cell was developed to miniaturise battery packs. Button cell can be found in watches, small electronics and memory backup. A schematic representation of button cell is shown in Figure VI.20.

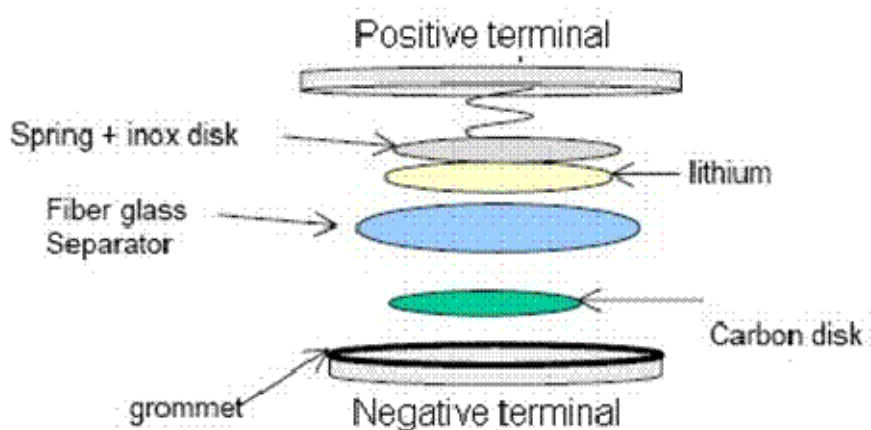


Figure VI.20: Button cells Li/C + SOCl₂ + LiAlCl₄

The cell consists of a lithium foil anode and a LiCl film, a separator (glass matting) and a porous carbon cathode support with the electrolyte being lithium tetrachloroaluminate (LiAlCl₄) salt dissolved in the thionyl chloride (SOCl₂). Electrolyte and lithium are in excess compared to carbon powder.

Our carbonised Aerocellulose, in disc shape, were tested as button cell. Three types of pyrolysed Aerocellulose were tested. Their preparation is summarised in Table VI.7.

Name	Cellulose concentration (g)	Water bath regenerating temperature (°C)	Supercritical drying	Pyrolysis cycle
Carbonised Aerocellulose 1	7	25	Natex	2
Carbonised Aerocellulose 2	5	50	CEP	2
Carbonised Aerocellulose 3	5	25	CEP	2

Table VI.7: Tested carbonised Aerocellulose of different preparation

Figure VI.21 presents the discharge curve of carbonised Aerocellulose tested at 0.1 mA. The massic capacity is the quantity of electricity delivered by the battery (mAh) divided by the weight of the carbon disc used.

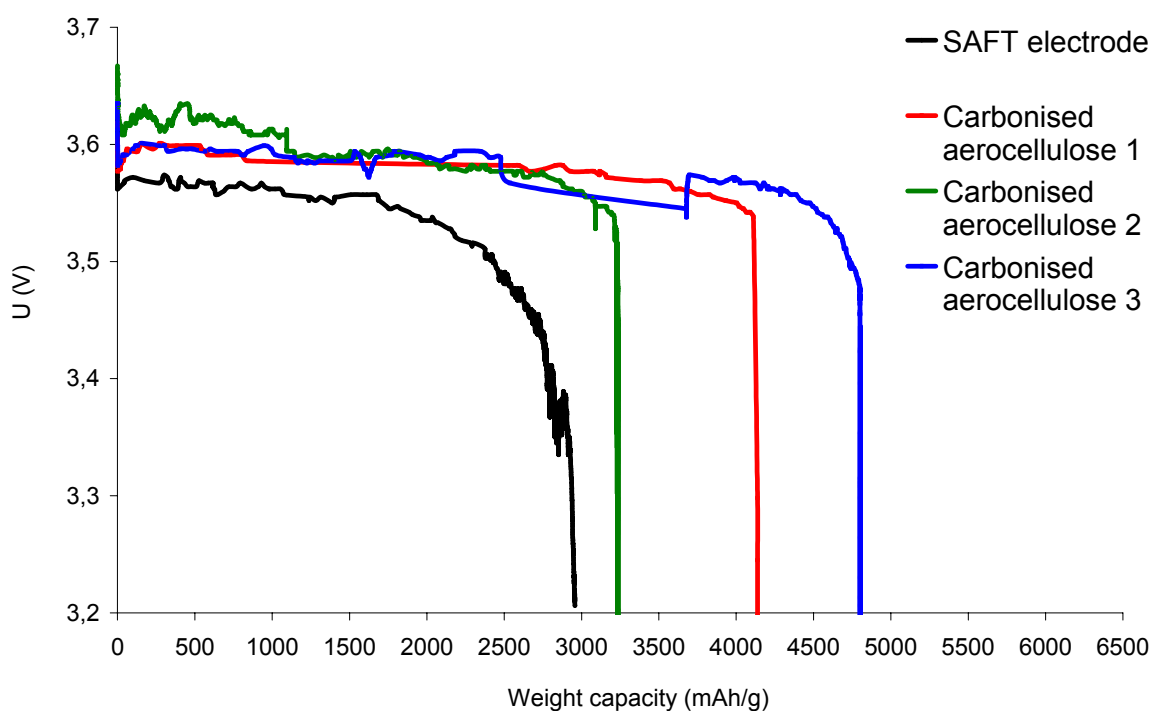


Figure VI.21: Comparison of massic capacity of button cell from SAFT reference electrode and different pyrolysed Aerocellulose

Table VI.8 sums up the microstructural properties and the massic capacity of the carbonised Aerocellulose and of the SAFT reference electrode.

Name	Cumulative volume [g/cm ³]	Density [g/cm ³]	Median Pore diameter [nm]	Specific surface [m ² /g]	Massic capacity [mAh.g]
SAFT carbon black reference	2.6	0.3	70	40	3000
Carbonised Aerocellulose 1	3.2	0.34	81	368	4200
Carbonised Aerocellulose 2	3.2	0.23	170-43	482	3200
Carbonised Aerocellulose 3	2.1	0.36	44	592	4800

Table VI.8 Characteristics of a reference carbon and of pyrolysed Aerocellulose used in button cell Li/SOCl₂

It appears that the electrochemical performances of carbonised Aerocellulose obtained from cellulose-NaOH-water gel used in button cell are superior to the one of reference electrode used by SAFT. As the amount of electrolyte and lithium are in excess in the button cell compared to the carbon cathode, it reveals that the capacity of carbonised Aerocellulose as limiting electrode is higher than the one of SAFT reference electrode.

2.3.1.3 Industrial cylindrical cell

A second application tested was the direct use of the cylindrical monolith of carbonised Aerocellulose as carbon element in industrial primary lithium battery. Figure VI.15 shows a schematic representation of industrial 14500 lithium/thionyl chloride (Li-SOCl₂) cylindrical AA-size cells.

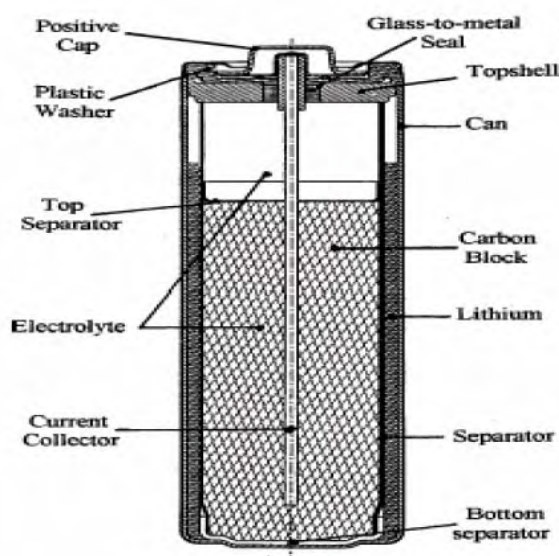


Figure VI.22: Drawing of an industrial 14500 cell

The block of carbon represents an important part of the cell. It is currently made by compression of carbon black powders with Teflon binder. The idea is to replace carbon black powder by carbonised Aerocellulose monolith. Carbon monoliths were obtained from pyrolysis of cylindrical Aerocellulose samples. More than 60 cylindrical Aerocellulose have been pyrolysed to obtain direct cylindrical carbon monoliths. Among them, carbonised samples 1 and 2, which preparation is described above (Table VI.7), were tested as carbon block in the industrial 14500 cell. Their cylindrical dimensions are the following: diameter= 14 mm and height= 25 mm. A nickel pin, collector of electron, was manually incorporated into the carbonised cylinder.

Figure VI.23 presents the discharge curve of carbonised Aerocellulose 1 and 2 performed at 1 mA, compared with the SAFT reference electrode.

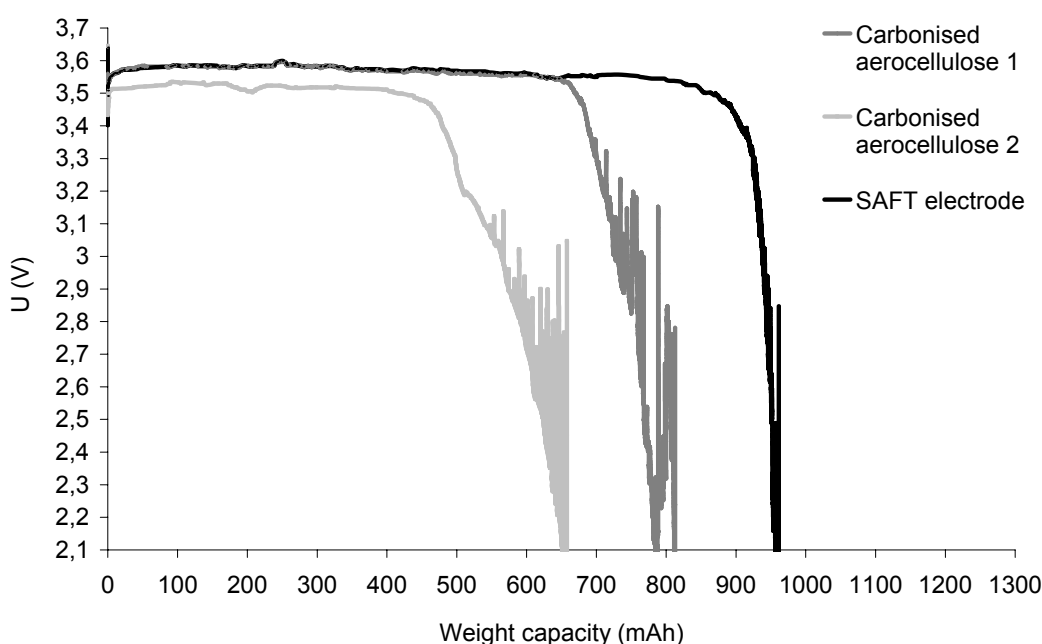


Figure VI.23: Comparison of massic capacity of industrial cell for SAFT reference electrode and carbonised Aerocellulose 1 and 2

We observe that the end of the discharge of carbonised Aerocellulose samples is noisy; this could be explained by the formation of micro cracks created during the drilling of sample to introduce the nickel pin or a loss of electrical contact. We obtain results inferior to the one of the reference cell showing that the scale change from button cell to industrial cell may produce some new troubles. However, these first results are not so far from the reference cell, which is promising for this type of application.

2.3.2 Proton exchange membrane fuel cell application

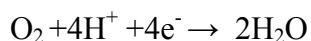
2.3.2.1 Generalities

The carbonised Aerocelluloses were tested as catalyst support for Proton Exchange Membrane Fuel Cell (PEMFC) electrode. PEMFC consists of a solid conducting membrane, an electrolyte such as perfluorosulphonic acid and polymer as Nafion[®] contained between two platinum impregnated porous electrodes. Nafion[®] due to its good chemical inertness and its mechanical stability is generally used as a proton conductor for proton exchange membrane fuel cells. PEMFC transforms the chemical energy liberated during the electrochemical reaction of hydrogen and oxygen to electrical energy. The hydrogen ions permeate across the electrolyte to the cathode, while the electrons flow through an external circuit provide power. Oxygen, in the form of gas, is supplied to the cathode and this combines with the electrons and the hydrogen ions to produce water. The electrochemical reactions occurring in a PEMFC are as follows:

At the anode: oxidation of hydrogen



At the cathode: reduction of oxygen



Total PEMFC reaction:

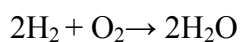


Figure VI.24 shows a schematic representation of a Proton Exchange Membrane Fuel Cell.

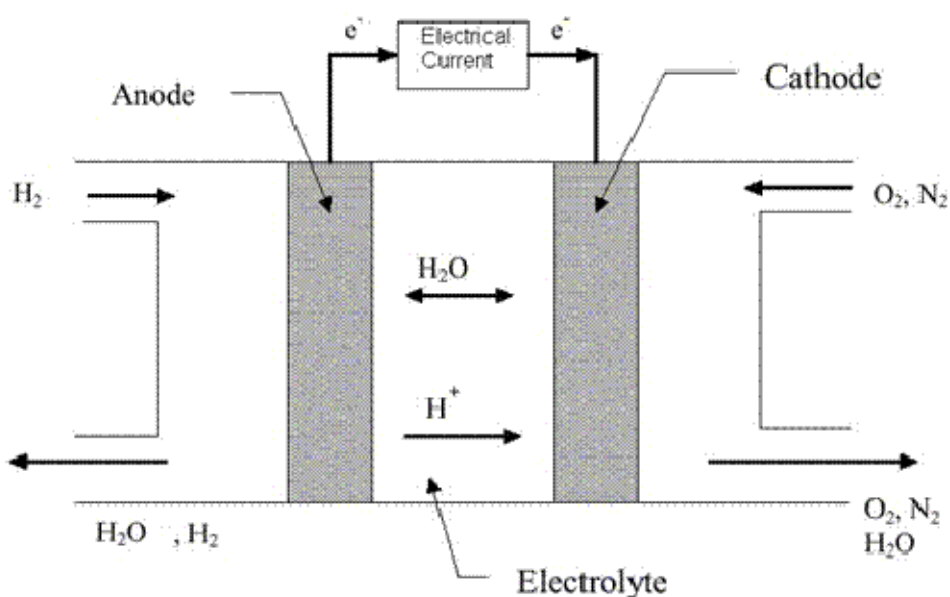


Figure VI.24: Schematic representation of PEMFC

PEM Fuel cells operate at low temperature of around 80°C. A catalyst, such as platinum (Pt), is often used to speed up the electrochemical reactions in the electrodes. At present, the majority of electrocatalysts consist of platinum nanoparticles deposited onto high-area carbon black particles, as Vulcan[®].

Carbonised Aerocellulose were tested for this specific application. They were obtained from cellulose/7.6NaOH water gels regenerated in water at various temperatures, then water exchanged by acetone, CO₂ supercritical dried at CEP, Sophia-Antipolis, France or at Natex, Ternitz, Austria and then pyrolysed at CEP, Sophia-Antipolis, France.

The electrochemical tests on carbonised Aerocellulose presented in this section were performed at the Laboratoire d'électrochimie et de physico-chimie des matériaux et des interfaces (LEPMI), Grenoble, France.

2.3.2.2 Preparation of cathodes for PEMFC

For fuel cell application, the preparation of a cathode from carbonised Aerocellulose is composed of several steps:

- 1) Activation: The carbonised Aerocellulose was crushed in an agate mortar during 15 minutes. Then the pyrolysed Aerocellulose was activated under controlled CO₂ atmosphere at 700; 800 and 900°C for one or two hours then cooled down to ambient temperature in CO₂ for one hour. The activation allows a better control of the carbon surface as it cleans the carbon substrate from oxygenated surface group. Such a thermal treatment opens up the micro porosity and removes some surface oxygenated species from the carbon. Its main goal is to "clean" the carbon substrate from oxide surface group in a reproducible way, so that the carbon samples all present the same state of surface before the platinum catalyst adjunction.
- 2) Platinum insertion. Carbon powder was suspended in a 0.1M H₂PtCl₆ aqueous solution for 48 hours under mechanical stirring at room temperature. Theoretically up to 20 wt% platinum should be loaded in the carbonised Aerocellulose. After impregnation, the platinum salt is reduced chemically in an excess of NaBH₄ solution in ultrasonic bath during 15 minutes. Then, the Pt/carbonised Aerocellulose powder was thoroughly washed to eliminate the traces of unreduced salt and unreacted NaBH₄ and filtered before being dried.
- 3) Deposit: An active layer was prepared by mixing carbonised Aerocellulose powder with water and isopropanol and Nafion[®], a sulfonated tetrafluorethylene copolymer which is protons conductor. The mixture is deposited on a glassy-carbon electrode for the electrochemical characterisation. The thickness of the porous active layer is 2-3 μm.

Figure VI.25 shows the Pt/carbonised Aerocellulose obtained before and after chemical reduction of platinum.

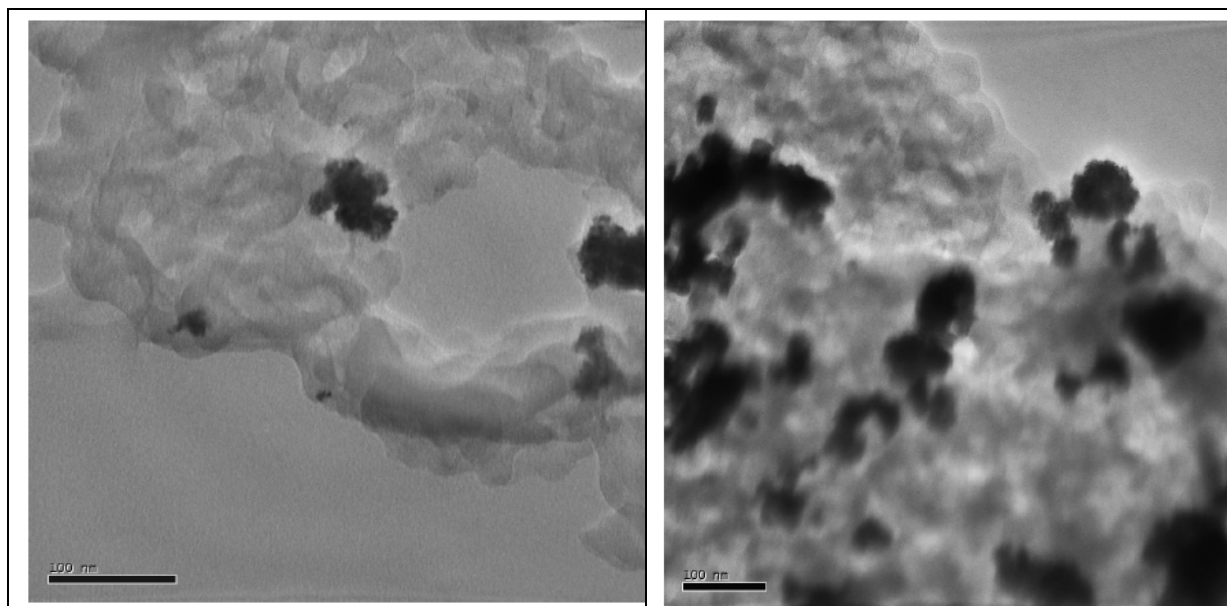


Figure VI.25: Transmission electron micrographs for carbonised Aerocellulose/Pt not activated (a) and chemically reduced (b) Photo provided by LEPMI

The activity of such electrocatalytic materials toward fuel cell reaction and more particularly oxygen reduction reaction were investigated. The active area of platinum was determined from CO-stripping coulometry. The electrochemical characterisation has been performed mainly using cyclic voltammetry in 1 M H_2SO_4 electrolyte at ambient temperature.

Figures VI.26 and VI.27 show the influence of activation procedure on platinum insertion in carbonised Aerocellulose. Pt/carbonised Aerocellulose was obtained from Aerocellulose made from 5Avicel/7.6NaOH/water gel, regenerated in water at 50°C, water exchanged with acetone, dried in Natex, pyrolysed with cycle 2 in CEP and finally Pt activated at various temperature during one hour and chemically reduced in 1M sulphuric acid solution at 20°C at 50 $\text{mV}\cdot\text{s}^{-1}$.

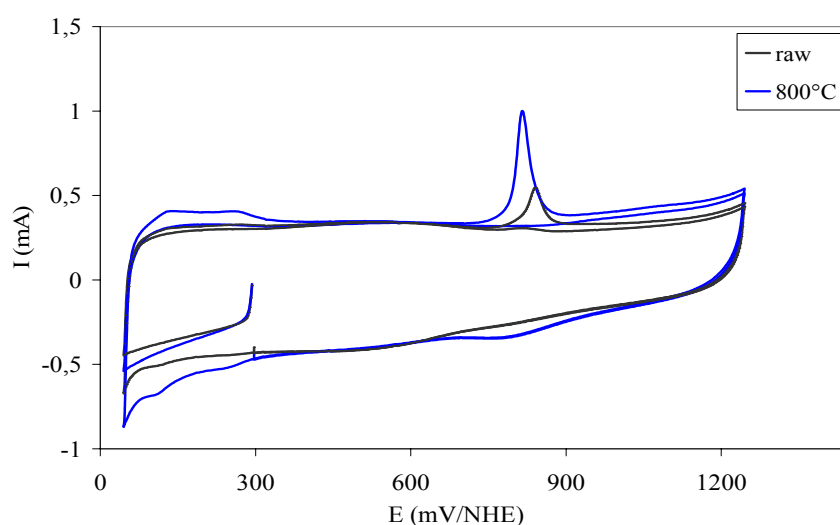


Figure VI.26: CO-stripping voltammogram for raw Pt /carbonised Aerocellulose and Pt/carbonised Aerocellulose activated at 800°C

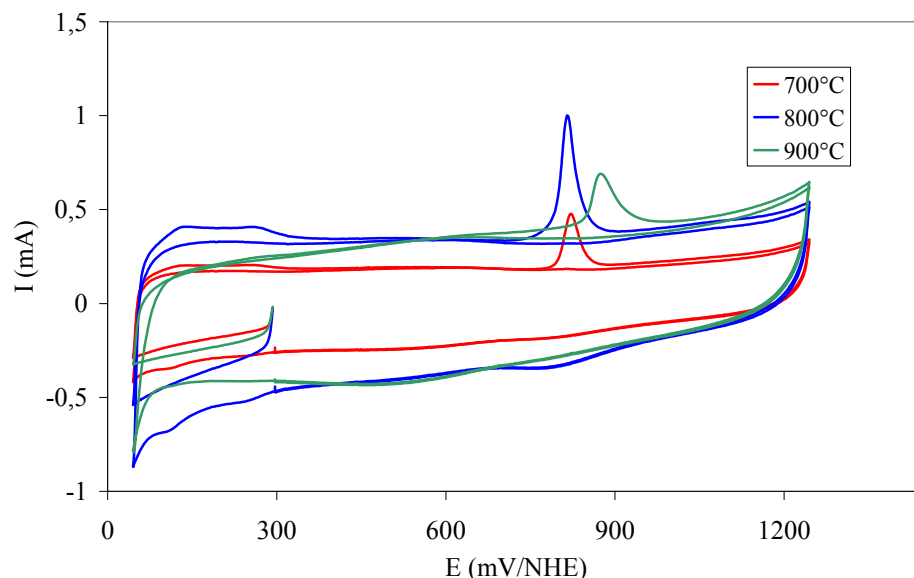


Figure VI.27: CO-stripping voltammogram for Pt/carbonised Aerocellulose activated at 700°C, 800°C and 900°C

The optimal activation temperature is 800 °C (i.e. the same as the pyrolysis temperature). Lower activation temperature does not clean enough the carbonised Aerocellulose surface from oxygenated surface groups that hinder the Pt insertion. Higher temperature yields too high mass loss and destruction of the carbonised Aerocellulose structure. In addition at 900 °C activation, the carbonised Aerocellulose becomes very hydrophobic.

2.3.2.3 Electrochemical characterisation of prepared electrodes

The Pt/carbonised Aerocellulose materials were tested regarding the oxygen reduction reaction (ORR) using the rotating disk electrode method from 500 to 2000 rpm. The obtained ORR current density, i_k , is related to the limiting current, i_l , by the equation:

$$i_k = \frac{i \times i_l}{i_l - i} \quad (\text{VI.1})$$

The voltage-current density relationship at the electrochemical interface is predicted by the Tafel equation:

$$\eta = a + b \log i_k \quad (\text{VI.2})$$

Where η is the voltage drop due to activation loss, i_k the current density, a and b are characteristic constants of the electrode system, called “Tafel constant” and “Tafel slope”, respectively.

The kinetics of oxygen reduction reaction ($\text{O}_2 + 4\text{H}^+ + 4\text{e}^- \rightarrow 2\text{H}_2\text{O}$) on cathode prepared from Pt/carbonised Aerocellulose are shown in Figure VI.28.

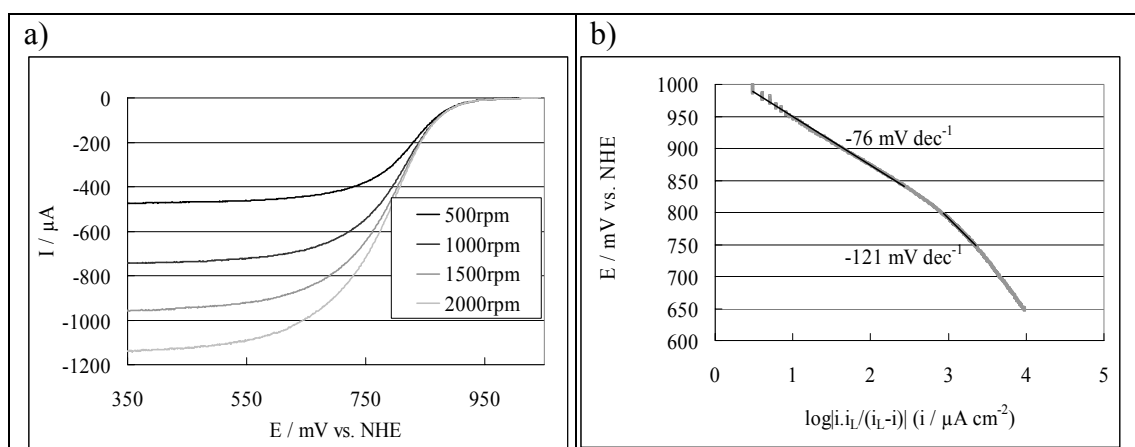


Figure VI.28: Quasi steady state voltammogram (a) related Tafel slopes for ORR on Pt/carbonised Aerocellulose prepared by impregnation/chemical reduction after 1 hour of activation at 800 °C

From these results, we can deduce the current density measured at 895 mV (i_{895}) and the Tafel slopes. Table VI.10 summarises their oxygen reduction reaction activity. Results are compared to the one of commercial Pt/Vulcan XC72R.

	$S_{Pt}^{CO} / \text{cm}^2$	Tafel slop (mV dec^{-1})	i_{895} ($\mu\text{A cm}^{-2} \text{ Pt}$)
Vulcan (20% Pt)	0.70	-77	-31
Raw Pt/Carbonised Aerocellulose	0.65	-85	-28
Pt/Carbonised Aerocellulose activated for 1h at 700 °C	0.62	-74	-35
Pt/Carbonised Aerocellulose activated for 1h at 800 °C	0.90	-76	-33
Pt/Carbonised Aerocellulose activated for 1h at 900 °C	1.40	-79	-36

Table VI.10: Physical properties and electrochemical activities for Pt/carbonised Aerocellulose activated at various temperatures

The ORR activities of Pt/carbonised Aerocellulose are close to the one of the commercial samples. Consequently, the carbonised Aerocellulose are promising substrate materials for the PEMFC electrocatalyst elaboration.

Conclusions

Two examples of Aerocellulose applications have been presented. First, we have investigated the encapsulation of insoluble powders in wet Aerocellulose precursors and dried Aerocellulose. Different types of powders, as metals or pigments, were encapsulated inside the Aerocellulose. In almost all cases, no release was observed in time or when loading the beads with powder. This demonstrates the good encapsulation of powder inside the beads. We have observed that powder particles are either trapped inside the porous structure if their particle diameter is higher than a few tens micrometres or adhere on the cellulose wall like in the case of titanium oxide particles. Wet Aerocellulose precursors and dry Aerocellulose can be used as a carrier of different insoluble substances. According to the powders used, different properties as coloured or magnetic beads were obtained. This new type of cellulose-inorganic particles composite open new applications in various fields as cosmetics, medicine, pharmaceuticals, etc.

Another application of the Aerocellulose was to use its pyrolysed form for electrochemical purposes. Therefore, we have pyrolysed the Aerocellulose samples in order to obtain carbonised porous structure. After pyrolysis, samples keep their monolithic initial shape. The weight loss was around $83 \pm 3\%$ whatever the pyrolysis cycle was. We have noticed after the pyrolysis of Aerocellulose a densification of the samples, a decrease of the porosity and a decrease of the mean pore size diameter from about one micron for the initial Aerocellulose to tens nanometres for carbonised Aerocellulose.

The influence of some preparation parameters, like water regenerating bath temperature or the cellulose concentration, on the microstructural properties of carbonised Aerocellulose was studied. The first results showed that it is possible to modify the properties of the carbonised Aerocellulose materials and to adapt the porosity for required electrochemical applications. However, more information is needed to deduce the correlations between the structure of carbonised Aerocellulose and the preparation conditions.

In the case of primary lithium battery, the interest of carbonised Aerocellulose compared to the conventional carbon materials in powder form like carbon black, relies on the possibility of both obtaining directly the monolithic shape desired for concerned application as industrial cell and of tailoring the porous structure by controlling the characteristics of the organic Aerocellulose precursors and its pyrolysis parameters. In the case of Proton Exchange Membrane Fuel Cell, carbonised Aerocellulose was tested with success as PEFMC electrode materials. A step of activation at the pyrolysis temperature improved the platinum insertion. Pt/carbonised Aerocellulose electrochemical activity is comparable with that of the commercial electrocatalysts. As a conclusion new “green” carbon have been developed thought pyrolysis of Aerocellulose and are suitable for electrochemical applications.

References

[Babel, 2003]	Babel, K.; Porous structure of cellulose carbon fibres during heating in the initial activation stage Fuel Processing Technology, 85, (2003), pp 75-89
[Banyaz et al, 2001]	Banyaz, J.L.; Li, S.; Lyons-Hart, J.; Shafer, K.H.; Gas evolution and the mechanism of cellulose pyrolysis Fuel, 80, (2001), pp 1757-1763
[Correa et al, 2005]	Correa, J.R.; Canetti, D.; Bordallo, E.; Rieumont, J.; Dufour, J.; Application of cubic magnetite to the synthesis of super paramagnetic cellulose beads for enzyme immobilization Proceeding in 8 th inter American congress of electron microscopy, La Habana, Cuba, September 2005
[Kurokawa et al, 1995]	Kurokawa, Y.; Hanaya, K.; Functionality of cellulose by impregnation of inorganic substances Carbohydrate Polymers, 27, (1995), pp 313-320
[Nagaoka et al, 2002]	Nagaoka, S.; Hamasaki, Y.; Ishihara, S.; Nagara, M.; Iio, K.; Nagasawa, C.; Ihara, H.; Preparation of carbon/TiO ₂ microspheres composites from cellulose/TiO ₂ microspheres composites and their evaluation Journal of molecular catalysis A: Chemical, 177, (2002), pp 255-263
[Dias et al, 2002]	Dias, S.L.P.; Gushikem, Y.; Ribeiro, E.; Benvenutti, E.V.; Cobalt(II) hematoporphyrin IX and protoporphyrin IX complexes immobilized on highly dispersed titanium (IV) oxide on a cellulose microfiber surface: electrochemical properties and dissolved oxygen reduction study Journal of Electrochemical Chemistry, 523, (2002), pp 64-69

General conclusions

The goal of this thesis was to prepare new ultra-light and highly porous material based on cellulose and to understand the relationships between its structure, properties and preparation parameters. Aerocelluloses obtained from NaOH route were compared with the ones prepared from NMMO route.

We have used cellulose dissolution in NaOH-water to prepare Aerocellulose. Different types of cellulose were dissolved in 7.6% aqueous sodium hydroxide solution at low temperature, -6°C. The rheological properties of cellulose-NaOH-water solutions have been investigated. Time, temperature increase leads to a decrease of solvent NaOH/water quality. Therefore, cellulose-cellulose interactions are favoured as compared to cellulose-solvent interactions. As a result, we observe an irreversible physical phenomenon of gelation. When adding urea, gelation of cellulose solution is delayed up to an optimal urea concentration and the solvent quality is increased. The rheological behaviour of solution depends on urea concentration and type of cellulose. Nevertheless, the mechanism of gelation is the same with or without urea. The exact action of urea on cellulose-NaOH-water solution remains an open question.

The kinetics of cellulose regeneration from cellulose-NaOH-water gels immersed in a non-solvent bath was investigated. The results were compared with the ones obtained for cellulose-NMMO-water solutions. Different theoretical models developed for the transport of solutes in hydrogels or in porous media were tested on the systems studied. It appears that the “porous membrane” approach must be applied for describing the NaOH and NMMO diffusion from the cellulose solution or gel to the non-solvent bath as a phase separation occurs during the cellulose regeneration step. We have established that the higher the bath temperature, the faster the cellulose regeneration. Using Arrhenius law, it is now possible to directly calculate the diffusion coefficient at each temperature. Moreover, we have observed that the higher the viscosity of alcohol used as regenerating bath liquid, the slower the cellulose regeneration.

We have revealed that the regeneration step is extremely important for the formation of the final structure of Aerocellulose. Temperature and nature of the regenerating bath and cellulose concentration have a significant effect on the microstructural properties of Aerocellulose. For instance, the increase of temperature makes the structure of Aerocellulose obtained from NaOH route cloudy, leads to density decrease and an increase of the porous volume. The state of cellulose solution, melted or crystalline in the case of cellulose-NMMO-water solution, and liquid or gelled in the case of cellulose-NaOH-water solution also plays a key role in the formation of Aerocellulose morphology. We have observed connected cellulose sub-micron-size spheres or porous cellulose “network” depending on whether cellulose-NMMO-water solution is melted or crystalline. All Aerocelluloses have an open porosity superior to 90%, with a pore diameter around a few hundreds nanometres. Their specific surface varies between 200 and 500 m².g⁻¹.

The influence of Aerocellulose preparation parameters on the mechanical properties of material was studied. The cellulose degree of polymerisation influences the mechanical properties of Aerocellulose. The higher the DP is, the better the mechanical characteristics are. Moreover, the higher the Aerocellulose concentration is, the higher the mechanical properties are. The presence of macropores whatever is the way they were created – surfactant or bath temperature increase - decreases the material density and thus lowers the mechanical properties. Using aerogel and foam deformation models, we have analysed the relationship between mechanical and microstructural characteristics. It appears that Aerocellulose from both routes, NaOH and NMMO, mechanically behave more like foams than aerogels. This could be explained by mean pore size of Aerocellulose around hundreds of nano-meters that is far from the micropore size scale of aerogels.

Finally, some examples of Aerocellulose applications have been presented. We have prepared Aerocellulose-inorganic particles composite by encapsulating insoluble powders inside the Aerocellulose. We have demonstrated that these composite cellulose beads, either in a wet or in dry state, can be used as a biodegradable carrier of different insoluble substances. We have pyrolysed the Aerocellulose in order to obtain highly porous nano-structured carbon materials. Significant weight loss, $83 \pm 3\%$, was noted. After pyrolysis, the mean pore size is decreased by more than ten from a few hundreds of nanometres to tens of nanometres. Two applications of carbonised Aerocellulose were targeted: as an electrode material for primary lithium battery and as a catalyst support in Proton Exchange Membrane Fuel Cell electrodes. The electrochemical results are in both cases comparable to the one of commercial carbon black. As a result, new interesting electrode from “green” material has been developed.

As a general conclusion, we have demonstrated that biomass and especially its principal constituent, cellulose, can be used in other than the traditional applications as fibres and paper. In the future, cellulose can substitute synthetic polymers and be transformed into new materials with high added value. Aerocellulose is such an example; it is a new material that responds to environmental requirements, it is renewable and biodegradable.

Perspectives

Aerocellulose being a totally new material, requires a lot of complementary studies since its preparation-structure-properties relationships are not fully understood. Indeed, we have observed that several Aerocellulose preparation parameters modify final properties of the material. For instance, the influence of the state of cellulose-NaOH-water solution, liquid or gel, regenerated in a non-solvent bath on the final morphology of Aerocellulose should be investigated. In addition, the influence of regenerating bath acidity on regeneration kinetics and final microstructure has to be studied and understood.

Regarding the rheological properties of cellulose-NaOH-water solutions with or without urea, a deeper study of the solution behaviour should be performed, in particular, varying cellulose polymerisation degree and origin. A phase diagram of cellulose-NaOH-urea-water should be built. Furthermore, a better understanding of physical phenomenon as the exact action of urea on gelation of cellulose solutions should enable to know precisely the role of urea and thus to optimise cellulose dissolution in these systems.

Finally, concerning the pyrolysed Aerocellulose used as electrode in primary lithium battery or as electrocatalyst support for Proton Exchange Membrane Fuel Cell electrode, interesting results have been found. However, their preparation and structure-properties relationships should be understood, better controlled and thus improved.